HAL
open science

Tectono-sedimentary and magmatic evolution of rifting and early seafloor spreading in the NW propagator to the South China Sea

Peng Chao

To cite this version:

Peng Chao. Tectono-sedimentary and magmatic evolution of rifting and early seafloor spreading in the NW propagator to the South China Sea. Earth Sciences. Université de Strasbourg, 2021. English. NNT : 2021STRAH005 . tel-03690852

HAL Id: tel-03690852

https://theses.hal.science/tel-03690852v1

Submitted on 8 Jun 2022

HAL is a multi-disciplinary open access archive for the deposit and dissemination of scientific research documents, whether they are published or not. The documents may come from teaching and research institutions in France or abroad, or from public or private research centers.

L'archive ouverte pluridisciplinaire **HAL**, est destinée au dépôt et à la diffusion de documents scientifiques de niveau recherche, publiés ou non, émanant des établissements d'enseignement et de recherche français ou étrangers, des laboratoires publics ou privés.

UNIVERSITÉ DE STRASBOURG

École Doctorale des Sciences de la Terre et de l'Environnement (ED413)

Institut Terre & Environnement de Strasbourg – ITES (UMR 7063)

THÈSE

présentée par :

Peng CHAO

Soutenue le : **12 octobre 2021**

Pour obtenir le grade de : **Docteur de l'université de Strasbourg**

Discipline/ Spécialité : Géophysique

Tectono-sedimentary and magmatic evolution of rifting and early seafloor spreading in the NW propagator of the South China Sea

THÈSE dirigée par :

Pr. Gianreto Manatschal	Université de Strasbourg, France
Dr. Pauline Chenin	Université de Strasbourg, France (Co-encadrant)

RAPPORTEURS :

Pr. Gwenn Péron-Pinvidic	NGU Trondheim, Norvège
Pr. Laetitia Le Pourhiet	Sorbonne Paris, France

AUTRES MEMBRES DU JURY :

Dr. Manuel Pubellier	ENS Paris/CNRS, France
Dr. Geoffroy Mohn	Cergy Paris, France
Dr. Daniel Sauter	Université de Strasbourg, France
Pr. Jianye Ren	China University of Geosciences, Wuhan, Chine
Dr. Cuimei Zhang	South China Sea Institute of Oceanology, Guangzhou, Chine

Table of Content

Extended abstract **7**

Résumé étendu **11**

Chapter I: Introduction **17**

1. Extensional systems in the Wilson cycle 17
2 Rifted margins 23
    2.1 Concepts and models 23
    2.2 Types of rifted margins 27
    2.3 Distribution of types of margins 32
    2.4 Rifted margins: ongoing research and open questions 34
3 The SCS: a natural laboratory to study rifting and breakup processes 36
    3.1 Geographical setting 37
    3.2. Geological setting and tectonic evolution 39
4. The study area 42
5. Open questions and aim of the thesis 45
    5.1 The syn-rift mega-sequence and its link to the tectono-magmatic evolution in a polyphase rift system: how to define, describe and interpret? 45
    5.2 From crustal separation to onset of seafloor spreading: how to define breakup? 48
    5.3 Crustal breakup: how does it propagate? 52
    5.4 The SCS: similarities and differences to Atlantic-type margins 56
6. Data, approaches and methods 56
    6.1 Data set used in the PhD 56
    6.2 Method and used approach 57
References 59

Chapter II: The tectono-stratigraphic and magmatic evolution of conjugate rifted margins: insights from the NW South China Sea **73**

Abstract 74
1. Introduction 74
2. Geological setting 78
    2.1. Geological evolution of the SCS 78
    2.2. Structure of the NW-SCS 79
3. Data, methods and terminology 80
    3.1. Data used and acquisition parameters 80
    3.2. Method 81

3.3. Terminology 82
4. Seismic interpretation 85
4.1. Main interfaces 85
4.2. First order crustal structure and rift domains 86
4.3. Intra-sediment reflections and stratigraphic units 88
4.4. Intra-basement reflections and fault structures 94
4.5. Magmatic additions 95
5. Kinematic restoration of section CGN-1: methodological approach 97
6. Discussion 101
6.1. Rift architecture, H block and upper- vs. lower plate 101
6.2. Kinematic restoration of section CGN-1: tectono-structural evolution 103
6.3. Time frame for rifting and related syn-rift tracts and magmatic units 107
6.4. Strain rates 108
6.5. The stratigraphic tape recorder of rifting: the Wheeler approach 109
6.6. Strain localization during rifting and individualisation and dismembering of the H-block 111
7. Conclusion 115
Acknowledgments 116
References 117

Chapter III: The transition from continental to lithospheric breakup recorded in proto-oceanic crust: Insights from the NW South China Sea 123

Abstract 124
1. Introduction 124
2. Geological setting 129
3. Data, methods, and terminology 130
3.1 Data used and acquisition parameters 130
3.2 Methods 131
3.3 Terminology 131
4. Seismic interpretation of the OCT 134
4.1. Seismic observations and location of the OCT 134
4.2. Sediment architecture in the OCT 142
4.3. Nature of basement in the OCT 144
4.4. Faults in the OCT 149
5. Discussion 150
5.1. Major characteristics of OCT and definition of proto-oceanic crust 150
5.2. The syn-breakup sedimentary record 152
5.3. From continental to lithospheric breakup: the link between faults, sediments and magma 154
6. Conclusion 158
References 160

Chapter IV: A 3D snapshot of crustal breakup deduced from seismic analysis of the tip of the NW South China Sea 165
Abstract 166
1. Introduction 166
2. Geological setting 169
3. Data, methods and terminology 171
3.1 Data used and acquisition parameters 171
3.2 Methods 172
3.3 Terminology and definitions used in this study 173
4. Reflection seismic lines: from observations to seismic interpretations 176
4.1. First-order seismic interfaces and rift domain boundaries 176
4.2. Sedimentary sequences 190
5. Mapping rift domains at the tip of the NW SCS 192
5.1. Mapping rift domains based on reflection seismic data 192
5.2. Nature of crust at the tip of the propagator: constraints from refraction seismic data 194
5.3. Comparison with existing OCB maps and potential field data 197
5.4. Distribution of sedimentary sequences at the tip of the NW SCS 199
6. Discussion 201
6.1. 3D crustal architecture at the tip of the NW SCS 202
6.2. Tectono-magmatic evolution during breakup at the tip of the SW SCS 205
6.3. Propagating vs retrograding: a new kinematic model for the NW SCS 207
7. Conclusion 209
References 211
Chapter V: Discussion 215
1. The syn-rift mega-sequence and its link to the tectono-magmatic evolution in a polyphase rift system: how to define, describe and interpret? 216
2. From crustal separation to onset of seafloor spreading: how to define breakup? . 224
3. Crustal breakup: how does it propagate? 229
References 234
Chapter VI: Conclusion 237
Chapter VII: Outlook 241
1. Time space correlations, unconformities and tectono-stratigraphic concepts 242
2. Evidence for a ridge jump in the NW SCS? 245
3. Sedimentation rates vs magmatic budget during rifting: towards a new classification 247
4. Lower crustal flow during crust necking 249
5. Extensional tectonic and crustal accretion at oceanic transform faults 250
6. From foreland basins to rifted margins: an example from the NE SCS 252
References 255

Extended abstract

Although the understanding of rifted margins, in particular of their most distal parts has significantly evolved in the last decades, the understanding of when, where and how continents rift, rupture and first oceanic crust forms remain unclear. Answering these questions is essential to improve our understanding of some of the most fundamental processes in Plate Tectonics, such as how continents rift apart, rift basins form and seafloor spreading initiates. In order to answer these questions, the access to the stratigraphic and magmatic tape recorder of rifted margins is fundamental. However, at present it is not only poorly understood but also barely documented, in particular in the most distal parts of rifted margins. The efficient record of syn-rift deformation in seismic data requires high sedimentation rates, which are however rare at distal margins. Moreover, most geophysical acquisitions and geological studies document only one margin, which makes it difficult to unravel the evolution of an entire conjugate rift system and associated breakup processes. Access to high quality seismic images of well-preserved pairs of conjugate rifted margins displaying high sedimentation rates during rifting and breakup is rare and exists only from a handful of examples, one of which is the South China Sea (SCS). This PhD aims to understand the processes controlling the transition from rifting to seafloor spreading through the analysis of a dense, high-resolution reflection seismic dataset located at the tip of the NW SCS propagator.

This study focuses on the tip of the NW-SCS propagator, where seafloor spreading propagated towards the Xisha Trough before it failed. In this region, numerous, high-resolution seismic reflection surveys provide a high-quality imaging of the sediment-rich and magma-poor conjugate margins, affording an excellent and rare opportunity to explore and describe the complete rift evolution. In addition, drill hole data of the International Ocean Discovery Program (IODP) Expeditions 367/368/368X drilled several sites at the Ocean–Continent Transition (OCT) approximately 200 km east of the study area. Thus, the high resolution, long-offset seismic and deep-water drill hole

data used in this PhD enabled the development of new concepts to explain crustal/lithospheric thinning, breakup and onset of seafloor spreading.

The approach used in this study aimed to: (1) provide a detailed description of the crustal architecture, define extensional domains as well as the margin architecture, (2) determine the tectono-sedimentary and magmatic evolution of conjugate rift systems; (3) understand the interplay between deformation, sedimentation and magmatic processes during rifting and breakup in 2D and 3D; (4) analyze and map the evolution of deformation through time and space by linking the tectono-stratigraphic evolution with the observed crustal thinning and synthesize it in a Wheeler diagram, and (5) quantify the amount of strain and strain-rate accommodated along conjugate margins/rift systems at the tip of a propagator. The study proposes qualitative and quantitative criteria that help to interpret the processes linked to two critical rift phases, which are the necking and crustal/lithospheric breakup phases. The main results of the PhD are presented in the form of three scientific papers.

Paper 1 is based on the description, interpretation and restoration of the CGN-1 reflection seismic section, which is one of the rare seismic lines imaging the complete tectono-sedimentary and magmatic architecture of a pair of conjugate rifted margins worldwide. The paper provides a detailed description of the crustal architecture, defines extensional domains, which are related to specific deformation phases, and determines the tectono-stratigraphic and magmatic evolution linked to rifting. This study includes a kinematic restoration relying on a systematic methodology that enables to quantify the amounts of extension and associated strain rates. We discuss the link between the kinematic evolution and the stratigraphic and magmatic record and illustrate it in a Wheeler Diagram. It is the first time such an approach is used to decipher the tectono-magmatic and sedimentary evolution of a complete syn-rift mega-sequence across conjugate rifted margins. Based on the identification and characterization of distinct stratal patterns and crustal architectures, this study proposes qualitative and quantitative criteria to interpret two critical rifting events, which are necking and hyperextension. These two events are linked to the individualization and subsequent dismembering of a so-called keystone, here referred to as H-block. The results

presented in this study challenge previous interpretations of correlative surfaces through the definition of different types of top basement and the distinction between syn- and post-tectonic packages within the syn-rift record. This approach leads to new interpretations for the tectono-stratigraphic and magma evolution of the NW SCS and has the potential to be used as a new approach to analyze, quantify and correlate events recorded in seismic sections across rifted margins.

Paper 2 investigates how new plate boundaries form and seafloor spreading initiates, which are two of the most important processes of Plate Tectonics. While former studies used to assume a sharp Ocean Continent Boundary (OCB) between continent and ocean, recent studies suggest a progressive Ocean Continent Transition (OCT) between unequivocal continental and oceanic crust. In the latter view, breakup is not instantaneous but a lasting breakup phase, which raises questions on the nature of: (1) the OCT basement; and (2) the processes operating between continental and lithospheric breakup. Based on detailed observations of high quality and yet unpublished reflection seismic data, we describe and interpret the characteristic structures of the NW-SCS OCT and their relationship with overlying syn-breakup sediments. The results show that the OCT displays a transition from fault-dominated rifting to magma-dominated seafloor spreading. On its continent-ward side, the OCT is made of hybrid crust where extensional thinning of continental crust is compensated by syn-extensional magmatic addition. Oceanward, this hybrid crust evolves into a fully magmatic but fault-dominated proto-oceanic crust, and finally turns into a mature Penrose-type oceanic crust. Relying on the growth structures of the syn-breakup sedimentary sequences and magmatic additions, we conduct a kinematic restoration of the breakup phase and propose that out-of-sequence flip-flop detachment faulting progressively decreasing in fault heaves was finally replaced by fully magmatic accretion. This restoration accounts for the observed switch from asymmetric fault-dominated- to symmetric and fully magmatic seafloor accretion.

Paper 3 investigates continental breakup and onset of seafloor spreading in 3D by documenting and mapping the OCT structure at the tip of the propagator in the NW-SCS. First the OCT is defined as located between the edge of the continental crust and

unequivocal oceanic crust. The basement of the OCT includes two types of crust, namely hybrid and proto-oceanic crust resulting from the complex interaction between crustal thinning along detachment systems and accretion of new syn-tectonic igneous rocks. Based on the results obtained in paper 3 it can be concluded that: 1) localization of deformation occurs simultaneous and perpendicular to the migration of magma-emplacement in front of a propagating spreading system, 2) the arrival of magma controls continental breakup, and 3) the final rifting stage and continental breakup phase are diachronous.

The results of this PhD show that rifting and breakup along the NW-SCS are, in many regards, different from classical Atlantic-type magma-poor or magma-rich margins. Neither evidence for exhumed mantle, nor emblematic seaward dipping reflections characterizing the magma-poor and magma-rich archetypes of rifted margins, respectively, have been found in the NW SCS. The occurrence of long-offset extensional detachment faults and their link to syn-breakup magmatic systems show complex interactions between extensional and magmatic systems during rifting and breakup. The results of this PhD shed some light on the spatial and temporal tectono-magmatic and sedimentary evolution of rift systems during final rifting, continental and lithospheric breakup and early seafloor spreading. The results of this PhD also lead to new questions such as the role of inheritance and the nature of the processes that control magma production and emplacement, both of which require further research.

Résumé étendu

Au cours des dernières décennies, la compréhension des marges riftées, en particulier de leurs parties les plus distales, a considérablement évolué. Cependant, les questions concernant la façon dont les continents se fissurent et se séparent, et la façon dont la première croûte océanique se forme restent en suspens. Répondre à ces questions est essentiel pour améliorer la compréhension de certains des processus les plus fondamentaux de la tectonique des plaques, tels que le rifting continental, la formation de bassins de rift et l'initiation de l'accrétion océanique. Pour répondre à ces questions, comprendre l'enregistrement stratigraphique et magmatique des marges riftées est fondamental. Cependant, à l'heure actuelle, cet enregistrement est non seulement mal connu, mais aussi peu documenté, en particulier dans les parties les plus distales des marges. Un enregistrement efficace de la déformation syn-rift dans les données sismiques nécessite des taux de sédimentation élevés, qui sont cependant rares dans les marges distales. De plus, la plupart des acquisitions géophysiques et des études géologiques ne documentent qu'une seule marge, ce qui rend la caractérisation de l'évolution des systèmes de rift dans leur ensemble et des processus de rupture qui leurs sont associés difficile. L'accès à des images sismiques de haute qualité de marges conjuguées dont les taux de sédimentation sont élevés pendant le rifting est rare et ne concerne qu'une poignée d'exemples, dont la mer de Chine méridionale (SCS). Cette thèse vise à comprendre les processus contrôlant la transition du rifting à l'accrétion océanique à travers l'analyse d'un réseau dense de données sismiques réflexion de haute résolution situé à la pointe du propagateur du nord-ouest de la mer de Chine méridionale (NW-SCS).

Cette étude se concentre sur la pointe du propagateur NW-SCS, où l'océanisation s'est propagée vers la Fosse de Xisha avant d'avorter. Dans cette région, de nombreux levés de sismique réflexion de haute résolution fournissent une imagerie de haute qualité de marges conjuguées riches en sédiments et pauvres en magma, offrant une excellente et rare opportunité d'explorer et de décrire l'évolution complète d'un système de rift. De plus, les données de forage des expéditions 367/368/368X du programme

international de découverte des océans (IODP) ont foré plusieurs sites à la transition entre océan-continent (OCT) à environ 200 km à l'est du site étudié. Ainsi, les données de forage en eau profonde et les données sismiques de haute résolution utilisées dans cette thèse ont permis le développement de nouveaux concepts pour expliquer l'amincissement crustal/lithosphérique, la rupture continentale/lithosphérique, et le début de l'accrétion océanique.

L'approche utilisée dans cette étude est basée sur l'interprétation de données de sismique réflexion de haute résolution dans le but de : (1) fournir une description détaillée de l'architecture de la croûte/des marges et définir les domaines de rift ; (2) déterminer l'évolution tectono-sédimentaire et magmatique du système de rift dans son ensemble ; (3) comprendre l'interaction entre déformation, sédimentation et processus magmatiques lors du rifting, aussi bien en 2D qu'en 3D ; (4) analyser et cartographier l'évolution de la déformation à travers le temps et l'espace en reliant l'évolution tectono-stratigraphique à l'amincissement de la croûte et synthétiser cette évolution dans un diagramme de Wheeler ; et (5) quantifier l'intensité et la vitesse de déformation le long de marges conjuguées situées à l'extrémité d'un propagateur. Cette étude propose des critères qualitatifs et quantitatifs permettant d'interpréter les processus liés à deux phases critiques du rifting, à savoir les phases d'étranglement et de rupture crustale/lithosphérique. Les principaux résultats de cette thèse sont présentés sous forme de trois articles scientifiques.

L'article 1 est basé sur la description, l'interprétation et la restauration de la section de sismique réflexion CGN-1, qui est l'une des rares lignes sismiques dans le monde à imager l'architecture tectono-sédimentaire et magmatique complète de marges riftées conjuguées. L'article fournit une description détaillée de l'architecture crustale, définit les domaines de rift liés à des phases de déformation spécifiques, et décrit l'évolution tectono-stratigraphique et magmatique liée au rifting. Cette étude propose également une restauration cinématique qui repose sur une méthodologie permettant de quantifier à la fois l'amplitude de l'extension et les taux de déformation associés. Nous y discutons le lien entre l'évolution cinématique et l'enregistrement stratigraphique et magmatique et l'illustrons dans un diagramme de Wheeler. C'est la première fois

qu'une telle approche est utilisée pour déchiffrer l'évolution tectono-magmatique et sédimentaire d'une méga-séquence syn-rift complète à travers des marges conjuguées. En se basant sur l'identification et la caractérisation des paquets sédimentaires et de l'architecture crustale sous-jacente, cette étude propose des critères qualitatifs et quantitatifs pour interpréter deux événements critiques de rifting, qui sont l'amincissement et l'hyperextension. Ces deux événements sont liés à l'individualisation et au démembrement ultérieur d'un bloc de croûte continentale, appelé ici le bloc H. Les résultats présentés dans cette étude remettent en question les interprétations précédentes des surfaces corrélatives en définissant différents types de toit de socle et en distinguant des ensembles syn- et post-tectonique au sein de l'enregistrement syn-rift. Cette approche novatrice conduit à de nouvelles interprétations de l'évolution tectono-stratigraphique et magmatique de la Mer de Chine occidentale et a le potentiel d'être appliquée plus largement pour analyser, quantifier et corréler les événements enregistrés dans les sections sismiques des marges riftées en général.

L'article 2 se concentre sur la formation de nouvelles limites de plaques et l'accrétion océanique, qui sont deux des processus les plus importants de la tectonique des plaques. Alors que les études antérieures supposaient une frontière abrupte entre le continent et l'océan (OCB), des études plus récentes suggèrent une transition progressive du continent vers l'océan (OCT). Dans ce dernier point de vue, la rupture n'est pas instantanée mais correspond à une phase prolongée, ce qui soulève des questions sur la nature : (1) du socle de l'OCT ; et (2) des processus opérant entre la rupture continentale et lithosphérique. Sur la base d'observations détaillées de données sismiques réflexion de haute qualité inédites, les structures caractéristiques de l'OCT de la mer de chine occidentale sont décrites et interprétées, ainsi que leurs relations avec les sédiments syn-tectonique sus-jacents. Ces résultats montrent que l'OCT enregistre une transition entre un rifting dominé par des failles et une expansion océanique dominée par le magma. Du côté du continent, l'OCT est constituée d'une croûte hybride où l'amincissement de la croûte continentale est compensé par des additions magmatiques syn-extension. Vers l'océan, cette croûte hybride évolue en

une croûte proto-océanique entièrement magmatique mais dominée par des failles, avant de se transformer finalement en une croûte océanique mature de type Penrose. En nous appuyant sur les structures de croissance des séquences sédimentaires et des additions magmatiques syn-rupture, nous effectuons une restauration cinématique de la phase de rupture et proposons que des failles de détachement hors séquence dont le rejet diminue progressivement vers l'océan sont finalement remplacées par une accrétion entièrement magmatique. Cette restauration explique l'évolution observée entre une extension asymétrique dominée par des failles et une accrétion symétrique et entièrement magmatique.

L'article 3 étudie la rupture continentale et le début de l'accrétion océanique en 3D en documentant et en cartographiant la structure de l'OCT à la pointe du propagateur dans la NW-SCS. Tout d'abord, l'OCT est définie comme étant située entre le bord de la croûte continentale et la croûte océanique univoque. Le socle de l'OCT comprend deux types de croûtes, à savoir les croûtes hybride et proto-océanique résultant de l'interaction complexe entre amincissement de la croûte le long de systèmes de failles de détachement et accrétion de nouvelles roches ignées syn-tectonique. Sur la base des résultats obtenus dans l'article 3, nous pouvons conclure que : 1) la localisation de la déformation se produit simultanément et perpendiculairement à la mise en place du magma dans un système de rift en propagation ; 2) l'arrivée du magma contrôle la rupture continentale ; et 3) la phase de rupture finale du rift est diachrone le long du propagateur.

Les résultats de cette thèse montrent que le rifting et la rupture continental/lithosphérique le long de la NW-SCS sont, à bien des égards, différents des marges classiques pauvres- ou riches en magma de type Atlantique. En effet, ni manteau exhumé, ni réflecteurs pentés vers l'océan (SDRs), qui sont respectivement emblématiques des archétypes de marges pauvres et riches en magma n'ont été trouvés dans la mer de chine occidentale. L'occurrence de failles de détachement extensives à fort rejet et leur lien avec les systèmes magmatiques syn-rupture démontrent l'existence d'interactions complexes entre les systèmes d'extension et les systèmes magmatiques pendant le rifting et la rupture continentale/lithosphérique. Les

résultats de cette thèse apportent un éclairage nouveau sur les évolutions tectono-magmatique et sédimentaire à la fois dans le temps et dans l'espace des systèmes de rift lors du rifting final, ainsi que sur les processus liés à la rupture continentale et lithosphérique et le début de l'accrétion océanique. Les résultats de cette thèse soulèvent également de nouvelles questions telles que le rôle de l'héritage dans les processus de production et de mise en place du magma. Ces nouvelles questions nécessitent cependant des recherches supplémentaires.

CHAPTER I

Introduction

1. Extensional systems in the Wilson cycle

The Wilson cycle, which builds on the Plate Tectonic paradigm, refers to the subduction–collision–collapse–rift–drift succession, a cycle that did not only occur repeatedly throughout the Earth history (Dewey& Burke, 1974) but that is also at the origin of the tectonic evolution of the South China Sea (SCS) (Ye et al., 2018; Sun et al., 2019; Li et al., 2018) (Fig. I.1). The idea of the Wilson cycle originates from the work of Wilson (1966), who first recognized that the distribution and evolution of paleo-faunal assemblages of North America and Northwestern Europe required the existence of a major ocean basin separating these continents during the lower and middle Paleozoic, whereas this ocean no longer existed from the late Paleozoic to the Late Mesozoic. Therefore, Wilson concluded that the North Atlantic had to open twice. Although Wilson's theory can capture the evolution from subduction to orogenic collapse, rifting and drifting, which is well described from the SCS, this theory did not describe how oceanic basins form in detail.

Rift systems and proto-oceanic domains, which are the main subjects of my PhD thesis, are common geological features. Examples are the Porcupine Basin and the Rockall Trough in the North Atlantic, the Red Sea and Gulf of Aden, the Gulf of California or the Woodlark Basin in Papua New Guinea. Fossil immature rifts and oceanic systems can also be found in collisional orogens emplaced during continental collision as for instance in the Alps (Sengör, 1991; Mohn et al., 2011), the Pyrenees (Boillot and Capdevila, 1977; Lescoutre and Manatschal, 2020) or the Variscides of Western Europe (Franke, 2006). Sengör (1991) and Chenin et al., (2017) suggested that narrow and immature oceanic basins experience an incomplete Wilson cycle different from that of wide oceans, where continental collision is preceded by long-

lasting subduction and the formation of arc systems (e.g., the Pacific subduction). This may explain why remnants of former rift systems and proto-ocean domains are better preserved in collisional orogenic systems such as the Alps or the Pyrenees than in Pacific-type ones. Research in these orogens enabled to investigate the nature of hyperextended rifted margins and proto-oceanic domains (Manatschal and Müntener, 2009; Lagabrielle et al., 2020) and to compare them with the structure of present-day rifted margins (Manatschal, 2004). In my PhD thesis, I focus on the extensional cycle recorded in the SCS, which can be subdivided in three major stages (Fig I.1): (1) the orogenic collapse stage; (2) the rifting stage; and (3) the drifting (oceanic) stage. Although I did not directly study the post-orogenic collapse in the SCS region, it is important to integrate this stage in the study of the SCS rift system since it controlled the characteristics of the initial lithosphere, in other words the *inheritance* to the subsequent rifting stage. Before focusing on the details of rifting and breakup of the continental crust and lithosphere that lead to the formation of rifted margins, I provide a short overview of the main three extensional stages within the Wilson cycle.

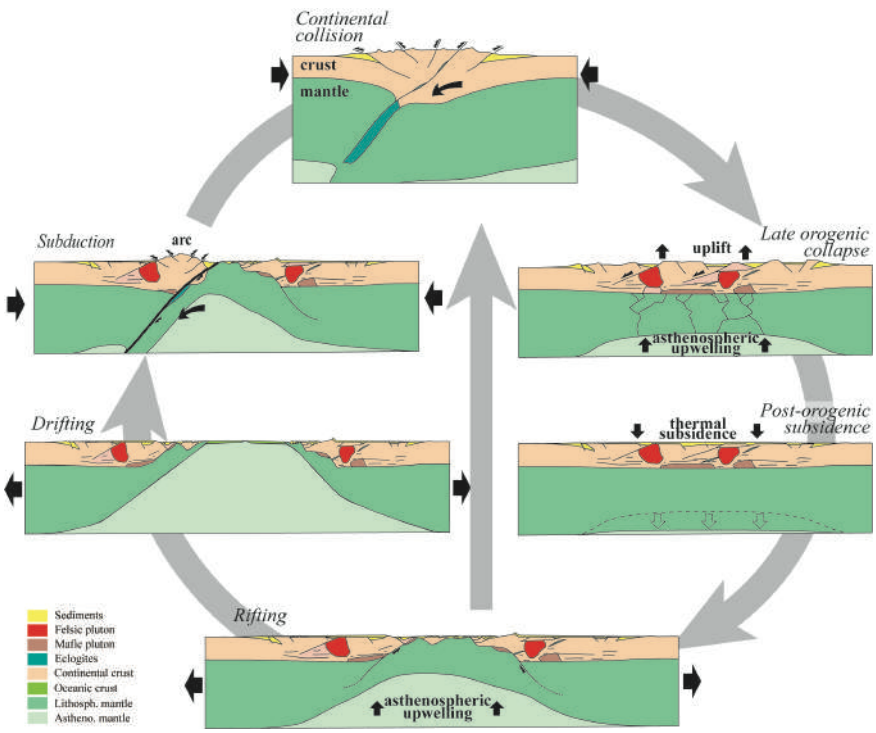

Figure I.1 *Simplified evolution model of the continental crust and the lithospheric mantle during a Wilson cycle. Figure modified after Malavieille et al. (1990) and Petri 2014.*

Orogenic collapse

The orogenic collapse stage is characterized by gravitational (i.e., topographic) re-equilibration of an over-thickened lithosphere and/or crust at the end of a collisional orogeny or a mature stage of subduction (Dewey, 1988; Rey et al., 2001). Orogenic collapse is commonly manifested by extension achieved via normal and/or (Searle, 2010) low-angle detachment faulting in high-elevated internal domains (over-thickened crust; e.g., Basin and Range (Wernicke, 1981) or Tibet (Searle, 2010)), while compression expressed as thrusting can continue in the lower elevated, more external parts of the orogenic system. Orogenic collapse can also include strike-slip faulting that can link the extensional and compressional systems (Dewey, 1988; Andersen, 1998). In many cases extensional structures reactivate former thrusts inherited from the orogenic stage (Peron-Pinvidic, 2020). In some cases, orogenic collapse is accompanied and/or followed by intense magmatic activity, as evidenced by widespread mafic to acidic intrusions. Examples are the Variscan in Western Europe, in the Basin and Range Province in the SW-USA and in the Canadian Cordillera (Costa and Rey, 1995; Vanderhaeghe et al., 1999; Reyet al., 2001; Petri et al., 2016). Magmatic underplating during orogenic collapse may be responsible for the flat Moho and the strong seismic layering of the lower crust, commonly observed to floor former orogenic domains (Bois et al., 1989; Rey, 1993; Vanderhaeghe, 2009). Mafic underplating results from the partial melting of the underlying mantle following slab break off and rise of the asthenosphere (Goodwin and McCarthy, 1990; Costa and Rey, 1995). The gabbroic underplated bodies are often related to sheared, formerly ductile or partially molten lower crust (Vanderhaeghe, 2009). However, orogenic collapse can also be devoid of extensive magmatic activity, as was, for instance, the collapse of the Caledonian range (Meissner, 1999; Fossen et al., 2014). Thus, orogenic collapse is linked to thermal heterogeneities that can be associated with the emplacement of magma and extension and exhumation processes. The thermal structure re-equilibrates over a few tens of millions of years (Jaupart and Mareschal, 2007) reaching a thermally equilibrated lithosphere. By contrast, most of the structural and lithological features inherited from orogenic collapse are preserved and create a compositional and structural inheritance that can control subsequent rifting events

(Manatschal et al., 2015). In contrast to Atlantic-type rifted margins, where rifting started within a thermally equilibrated lithosphere, the onset of rifting in the SCS is intimately linked to, and therefore difficult to distinguish from, the preceding orogenic collapse phase (Sun, 2016; Wang, 2019).

Rifting

Extension of the crust and lithosphere during rifting is usually achieved through a succession of deformation phases, which form a series of domains with relatively consistent and mappable characteristics (Péron-Pinvidic et al., 2013; Sutra et al., 2013; Chenin et al., 2017) (Fig. I.2). During an early stage of rifting, commonly referred to as *stretching stage* and preserved in the proximal parts of the final rifted margin, extension does not significantly modify the lithology of the crust or lithosphere (Picazo et al., 2016; Chenin et al., 2017) (Fig I.2). This contrasts with the stages of *necking* and *hyperextension*. During these stages of higher extension, crustal and mantle rocks can be severely hydrated and magma can form and interact with the subcontinental lithospheric mantle (Sutra et al., 2013; Doré and Lundin, 2015). Thus, it is important to note that, as extension progresses, the crust and the lithospheric mantle are increasingly modified by hydration reactions, thermal perturbations and/or magmatic additions, which make the description and understanding of the rifting more complex. Different inherited mantle composition (including fluid content) and/or geothermal gradient lead to different budgets of magma, resulting in either *magma-rich* or *magma-poor* rifting and rifted margins. These archetypes of rifted margins have been described from the northern- and southern North Atlantic, respectively (e.g., Péron-Pinvidic et al., 2013; Franke et al., 2013). Here I focus on the South China Sea (SCS), which has been defined as an *intermediate* type of rifted margins. I will further discuss this definition, as well as the characteristic evolution of the different types of rifting at the origin of the magma-poor, intermediate and magma-rich margin types in the core of this manuscript. The processes and models used to explain the structural and compositional variability (including magmatic budgets) observed along rifted margins will also be discussed in this thesis.

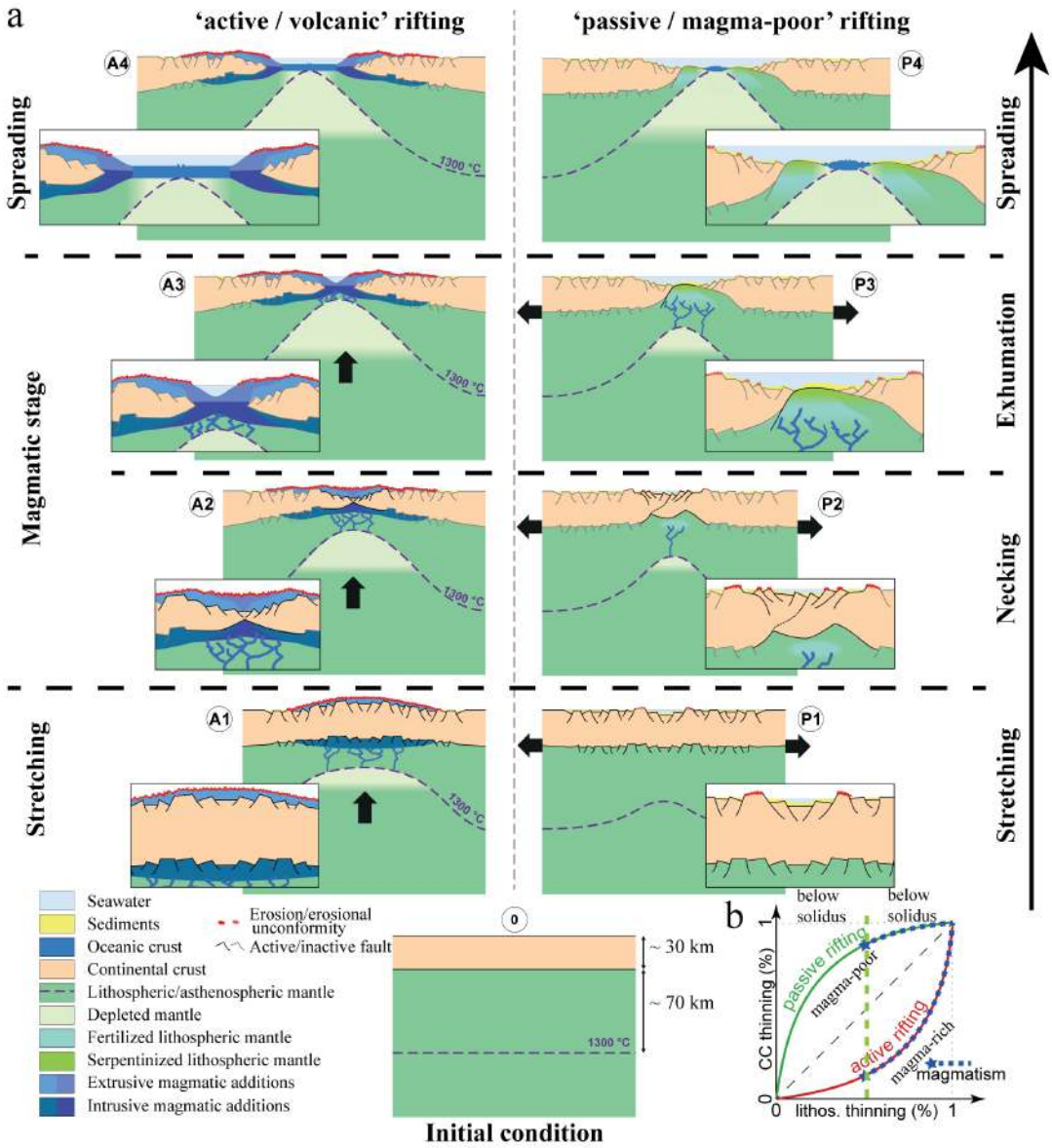

Figure I.2 *(a) Illustration of an active (left column) vs. a passive (right column) rift evolution. From bottom to top: initial stage (0) with an equilibrated lithosphere and crust (initial condition). A1 and P1: diffuse deformation phase (stretching): a large number of faults are active in the upper crust and the upper mantle. Possible onset of magma and uplift in the active system, slight subsidence in the passive system. A2 and P2: focusing phase (necking): most of the faults in the future proximal domain are abandoned while the deformation is focused in the future distal domain; crustal detachment faults allow significant thinning of the crust. A3: separation of the continental crust masked by the persistence of magmatic activity. P3: exhumation of the subcontinental mantle via one or more detachment faults. A4 and P4: stable oceanic accretion (spreading). (b) Schematic representation of the thinning of the continental crust (thinned. CC) as a function of lithospheric thinning (thinned. lithos.) during active (red curve) and passive (green curve) rifting. Magmatism begins (blue stars) approximately when the lithospheric thickness has been halved, i.e., much earlier in the case of active rifting than passive rifting. Modified after Chenin 2020.*

Breakup and onset of seafloor spreading

Ultimately, upwelling of the asthenosphere may trigger a self-sustaining spreading system at moderate to high seafloor spreading rates (Mutter and Zehnder, 1988; Huismans et al., 2001). In this case, a 6 to 7 km thick mafic oceanic crust with a remarkably homogeneous and characteristic magmatic composition, also referred to as Mid-Ocean Ridge Basalt (MORB) composition is formed (Bown and White, 1994; Dick et al., 2003; Gale et al., 2013). At the same time, the underlying mantle source is generally thought to evolve from an enriched lherzolite-dominated sub-continental mantle to a depleted harzburgite-dominated oceanic mantle that is genetically linked to the overlying oceanic crust (see Saunders et al., 1988). In this study I will investigate the processes of breakup in dip and strike sections across the propagator in the NW-SCS.

Evolution of extensional systems in a Wilson cycle

At Atlantic-type rifted margins, the classical evolution from orogenic collapse to rifting to seafloor spreading may take place over > 100 My (Caledonian N-Atlantic ~300 Ma; Variscan southern N-Atlantic ~150 Ma). As a consequence, rifting starts with a thermally equilibrated lithosphere (Manatschal et al., 2015). In the Atlantic, two archetypes of rifted margins have been identified, referred to as magma-poor and magma-rich rifted margins (Fig I.2) (Péron-Pinvidic et al., 2013; Franke et al., 2013; Doré and Lundin, 2015) that will be discussed below. It remains unclear if the different types of margins are the result of inheritance (e.g., mantle composition; Chenin et al., 2018), rates of extension (Bown & White 1995; see Lundin et al. 2018 for a review), or controlled by the occurrence or lack of plumes during rifting (Bown & White 1995; see Tomasi 2020 for a review). In the North Atlantic, rifting initiated after a stage of thermal equilibration, was *multistage* (i.e., comprised of several extensional events separated by a tectonic quiet phase and/or spatially offset) and *polyphase* (i.e., rifting was achieved through the succession of different deformation phases under a constant kinematic framework; Cadenas et al., 2020). Thus, the initial conditions and the age of rift onset with respect to the former orogenic event are relatively well known at Atlantic rifted margins (Chenin et al., 2015). In contrast, in the SCS, the time lag between

orogenic collapse and the onset of rifting was short (< 30 My). Consequently, the thermal state of the system at onset of rifting was not equilibrated yet, the age of rift onset is not well defined, and the duration of rifting was much shorter. Therefore, models previously developed for the North Atlantic cannot be used to describe the SCS.

2 Rifted margins

Improvements in seismic imaging, computing capabilities and analytical methods, as well as the increasing number of industry deep-water wells sampling distal offshore settings have underpinned new concepts for rifted margin evolution in the last two decades (Péron-Pinvidic et al., 2019). This concept evolution also benefited from studies of fossil rifted margins exposed on land (e.g., Alps and Pyrenees: Manatschal, 2004; Lagabrielle et al., 2020), which allowed significant progress in our understanding of extensional systems in general and rifted margins in particular. For example, the tectonic, sedimentary, and magmatic processes linked to the formation of rifted margins have been overhauled, giving rise to more quantitative approaches and new concepts. However, each of these processes cannot be understood by itself and requires to be considered as part of a whole in which inheritance and physical processes are integrated within a plate tectonic framework. Therefore, to understand these complex relationships, it is first necessary to understand the new concepts related to the formation of rifted margins, and how they can be introduced and used. In the following, I review the development of some of the concepts used in this study, which provides the foundation for the scientific questions I addressed in this PhD and the discussion of the results.

2.1 Concepts and models

Models of rifting trying to capture the evolution of rift systems have been developed along with the development of new techniques and the successive understanding of deeper and more distal parts of rifted margins. In the 1970^{ies} and 1980^{ies}, two types of rifting models were proposed. On the one hand, the depth-uniform, pure-shear model of McKenzie (1978) was inspired by physics and the North

Sea geology. On the other hand, the simple-shear model by Wernicke (1985) was inspired by field observations in the Basin and Range in the SW-USA. The “McKenzie” model suggests that extension results in symmetric thinning of the continental crust and leads to the formation of tilted blocks in the upper crust overlying a ductile lower crust. Thinning of the crust and lithosphere was proposed to be depth uniform and being inverse proportional to horizontal extension (Fig I.3a). The “Wernicke” model (Wernicke, 1985) proposes the existence of a lithospheric-scale detachment fault crossing the lithosphere and soling out in the asthenosphere. In this model crustal and mantle thinning do not occur at the same place. Exhumation of deeper crustal and mantle rocks is possible, and the isostatic and thermal response to extension is asymmetric (Fig. I.3b). Both models are based on the “conservation of mass”, i.e., that there are no magmatic additions, which enables to balance the pre-rift with the post-rift crustal surface. So-called non-conservational models where masses are allowed to be exchanged between the crust and mantle (e.g., creation of magma or hydration of mantle; Keen and Beaumont, 1990; Aslanian et al., 2009; Huismans and Beaumont, 2011 and references therein) are more difficult to restore and to model. A main limitation in the study of rifted margins, as shown in this study, is that it is difficult to distinguish between new magmatic and original continental crust using geophysical data only. This is due to the non-uniqueness of the density and velocities of rocks (Péron-Pinvidic et al., 2016; Tugend et al. 2020). This limitation also makes it difficult to test non-conservational models that include magmatic additions.

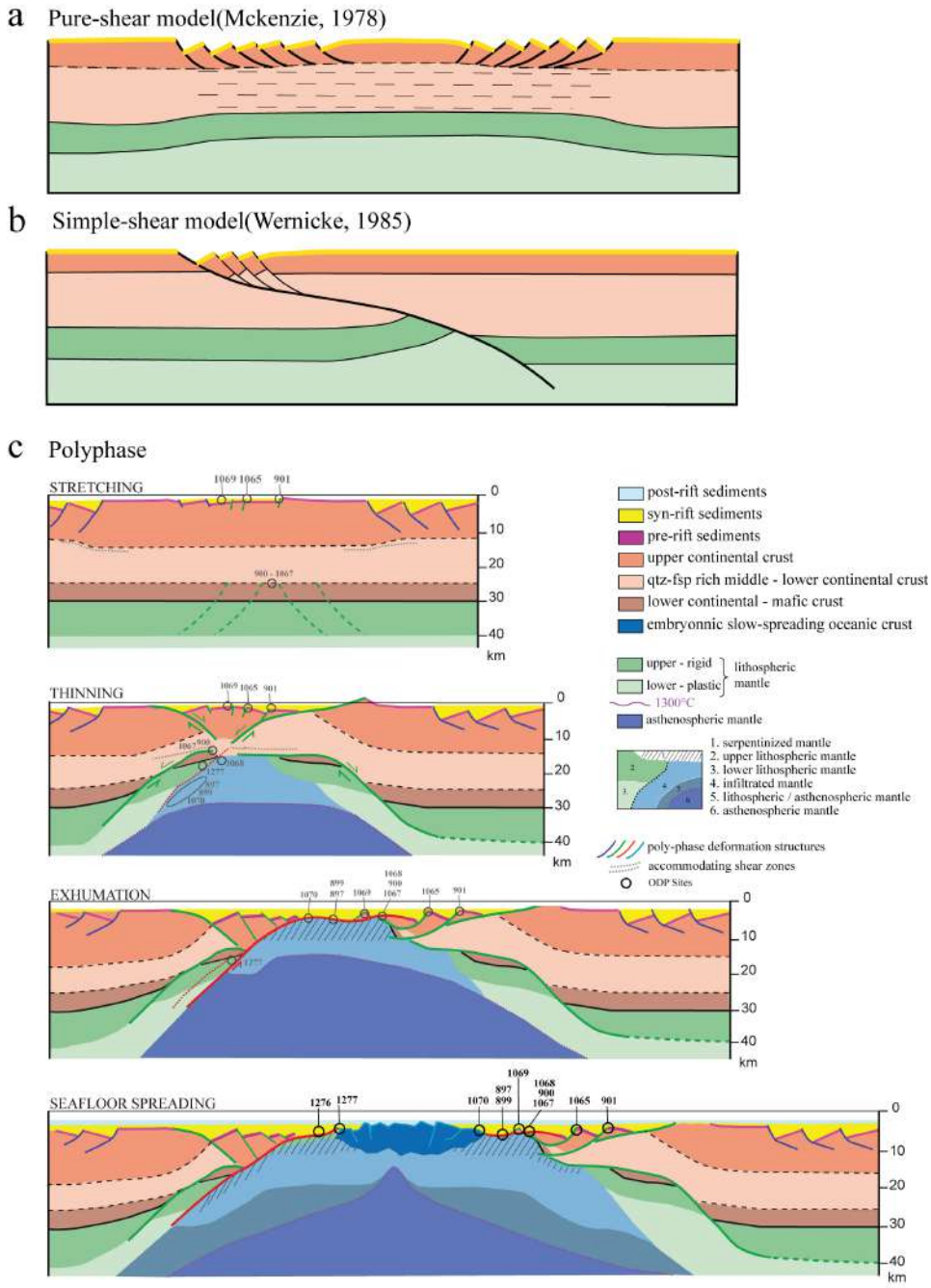

Figure I.3 *(a) Conceptual pure-shear model (modified after McKenzie, 1978). (b) Conceptual simple-shear model (modified after Wernicke, 1985). (c) Conceptual model of the evolution of a polyphase rift system including. A stretching mode characterized by high-angle normal faults associated with half-graben formation and subsidence. Continental crust may be slightly stretched, and sedimentary basins developed independently from each other. A thinning phase characterized by a conjugate decoupling system of detachment faults that accommodate exhumation of deeper crustal levels. Deformation goes from distributed to localized extension. An exhumation phase where detachment faults crosscut the embrittled crust and exhume serpentinized mantle rocks. A sea floor spreading phase during which oceanic crust is formed. Modified after Péron-Pinvidic and Manatschal (2009).*

It is important to note that initial models of rifting have been first developed to explain continental rifts (e.g., North Sea for the McKenzie model) or post-orogenic collapse extensional systems (e.g., Basin and Range for the Wernicke model). This is strongly linked to the way rifted margins have been investigated. Early studies of rifted margins focused on the proximal domains in shallow water and/or on intracontinental rift basins. Data acquisition concentrated on the sedimentary infill down to basement only in areas prospective for hydrocarbons, i.e., imaged the first few seconds using seismic reflection methods (e.g., Levell et al., 2010). More distal parts of the margins or deeper crustal and mantle configurations were not investigated, mainly due to the limited resolving power of the reflection seismic imaging technology available at that time. Consequently, models used to explain the formation of rifted margins assumed that the processes observed at continental rifts, described by either pure and/or simple shear models (McKenzie, 1978; Wernicke, 1985) (Fig. I.3a), could be applied to the whole rifted margin. Early studies, for example along the French Armorican margin produced predictive models of rift histories (Le Pichon and Sibuet, 1981). Although such models could partly explain the early evolution of rifted margins, including the formation of sedimentary basins and the addition of extension-related melt (i.e., magmatic additions in the White and McKenzie (1989) model), they were unable to predict the evolution of more mature rift systems approaching lithospheric breakup. The study of the more distal parts of rifted margins was hampered by the access to rocks and the difficulty to image the most distal parts of rifted margins and their transition to first oceanic crust. This became evident when industry and academics started to explore the distal margins with more powerful reflection and refraction seismic imaging methods and to drill the distal parts of rifted margins in the North Atlantic. The first sites were on the one hand the Norwegian-Greenland margins (ODP Legs 152 and 163; Saunders et al. (2007) and the Iberia-Newfoundland margins (ODP Legs 103, 149, 173, 210; Boillot et al., 1987, Sawyer et al., 1994, Whitemarsh et al., 1998 and Tucholke et al., 2007), which enabled to describe two archetype margins, referred to as volcanic and non-volcanic margins, later also referred to as magma-rich and magma-poor rifted margins.

Only from the 1980ies, and in particular the 1990ies onwards, models of rifting were further developed to explain the complete evolution of rifted margins, including the more distal parts and formation of first oceanic crust. The discovery was, however, that distal margins are very different from proximal margins and that the change between continental and oceanic crust is not a sharp limit but a transition (Manatschal et al., 2010). Until today, models explaining the complete rift evolution, including the rupture of continental lithosphere, are debated, and not calibrated. Although rifted margins have been investigated over many decades, the geological, geophysical, and rheological characterization of basement (crust and mantle), the extensional geometries and processes, the syn-rift stratigraphic architecture and magmatic products and their emplacement mechanism remain little understood. It remains to better understand how, when and where the crust and lithosphere thin and rupture, giving rise to the onset of seafloor spreading and the formation of a new plate boundary. Although many conceptual models (Péron-Pinvidic and Manatschal, 2009; Fig. I.3c) and dynamic models (Lavier and Manatschal, 2006; Huismans and Beaumont, 2011) have been proposed, these models are not yet calibrated and lack observational constraints, in particular in the distal parts of rifted margins. Thus, despite rifted margins contain some of the Earth's most voluminous sediment accumulations, host important energy and natural resources, and are a rich archive of global environmental and climate changes, they are yet little understood (e.g., Péron-Pinvidic et al., 2019). In this study, I focus on resolving when and where the crust and lithosphere thin and rupture based on an observational approach applied to some of the best seismic datasets that image rifted margins and their transition to oceanic crust in the propagator of the NW-SCS.

2.2 Types of rifted margins

Drilling of the North Atlantic distal margins during the different ODP Legs in the late 1980ies and in particular the 1990ies enabled to establish two main observations: 1) the occurrence of wide zones of exhumed subcontinental mantle linked to large offset normal faults and creation of new real estate in the southern North Atlantic (Boillot et al., 1980), and 2) the drilling of SDRs confirming that they formed as subaerial basaltic

flows in the northern North Atlantic. These observations set the stage for the subsequent subdivision of the margins into volcanic and non-volcanic (Boillot et al., 1987; Endholm et al., 1989), referred later as magma-poor or magma-rich (for reviews see Péron-Pinvidic et al., 2013; Franke et al., 2013). While the Iberia rifted margin became the archetype of a non-volcanic/magma-poor margin (Whitmarsh et al., 2001), the Norwegian-Greenland margins became the archetypes of volcanic/magma-rich margins (Eldholm et al., 1989). More recent drilling of the South China Sea (SCS) during IODP Legs 367/368, enabled to identify an *intermediate* type of rifted margin, which will be the focus of this study. Before concentrating on this new type and the SCS, I first provide an overview of the main three archetypes of rifted margins that are the magma-poor, magma-rich and transform margins.

Magma-poor margins

Magma-poor margins, as shown in Fig. I.4a, show broad zones of continental thinning, also referred to as crustal wedging, including faults and the formation of tilted blocks (Manatschal, 2004a, 2004b; Reston, 2007; Peron-Pinvindic et al., 2019). Hyperextended margins refer to margins where the continental crust is thinned to less than 10 km, the crust is embrittled and wedges out oceanward. Fluids hydrate the residual thin crust and underlying mantle, resulting in weak faults and a serpentinized uppermost mantle, which enable the development of long offset extensional detachment faults (Doré and Lundin, 2015; Tugend et al., 2015). Conjugate margins are often asymmetric: one margin is the footwall of the major detachment system, resulting in a significantly wider lower plate margin, and the other forms the hanging wall of the detachment system, resulting in a sharper upper plate margin (see Fig. I.3c; for original concept see Lister et al., 1991). At magma-poor rifted margins, crustal separation precedes magma-emplacement and formation of first mature oceanic crust, resulting in a wide zone of exhumed subcontinental mantle (Manatschal, 2004). Magma-poor rifted margins have been associated with slow extension (e.g., Bown and White, 1995; Perez-Gussinyé et al., 2006; Doré and Lundin, 2015), cold mantle (Boillot et al. 1987) or depleted mantle (Müntener and Manatschal, 2006; Chenin et al., 2018). Models for magma-poor margins include several stages comprising both pure-shear

and simple-shear phases (Fig. I.3c). Based on geophysical and geological observations from the West Iberian margin and geological mapping in the Alps, Whitemarsh et al. (2001) presented a conceptual model of magma-poor rifted margins that includes a phase of lithospheric necking and diffuse faulting, followed by a later phase of localization of rifting and the onset of seafloor spreading. Later models tried to explain the apparent discrepancy between displacement along the faults and the amount of extension through exhumation of mid-crustal and mantle rocks (Lavier and Manatschal, 2006; Mohn et al., 2012) or through a later phase of deformation after embrittlement of the crust (Reston, 2007; Gussinyer-Perez and Raneiro, 2010). Péron-Pinvidic and Manatschal (2009) proposed a conceptual model to explain the evolution of the margins, integrating most observations and ideas derived from the study of the Newfoundland-Iberian and Alpine Tethys margins. This model, shown in Fig. I.3c; describes a succession of modes, referred to as stretching, necking and hyperextension. These modes refer to the amount and style of crustal/lithospheric thinning (Sutra et al., 2013), where stretching is characterized by low ß values of < 1,5, necking is characterized by a thinning of the crust to ≤ 10 km and hyperextension starts when the crust has been stretched to full embrittlement, usually at a crustal stretching factor of ca. 3–4 (Perez-Gussinyé and Reston, 2001). Hyperextension ends either when subcontinental mantle starts to be exhumed or when magma is emplaced and leads to lithospheric breakup and steady-state seafloor spreading, as shown in this study.

Magma-rich margins

At magma-rich margins (Fig. I.4b) onset of magmatism resulting in the formation of Seaward Dipping Reflections (SDR) can bypass all extensional stages and force the lithosphere to breakup contemporaneously with the separation of the continental crust. At these margins, onset of magma formation occurs prior to crustal separation. In such examples mantle rocks are not exhumed and the transition between the continent and the first oceanic crust is characterized by large amounts of extrusive lavas forming thick SDR sequences and intrusives flooring the lower crust, often referred to as *high-velocity bodies* (e. g., Hinz et al., 1993; Eldholm and Grue, 1994; Thybo et al., 2013;

Franke., 2013; Geoffroy et al., 2015). Most magma-rich margins show crustal thinning prior to onset of the first magma, however, it remains yet unclear if crustal thinning continues after onset of magma (Tomasi et al., 2021), or alternatively if the crust is literally separated by the arrival of first magma, as suggested by Buck (2007). While in the latter case the contact between continental and fully magmatic crust is sharp and breakup is localized and fast in the former case crustal thinning can occur simultaneous to magmatic accretion resulting in a diffuse breakup including hybrid crust as observed in this study. For a discussion about the magmatic budget during breakup see also Tugend et al., (2020). Another debated question is if serpentinized upper mantle can occur underneath the SDR sequences on volcanic margins and if magma-rich rifted margins can start to evolve from a typical magma-poor margin (Lundin et al., 2018; Ros et al., 2017). Zhang et al. (2020) also showed that even in the absence of SDRs, large amounts of magma can pound in sediments forming syn-rift laccolith. Another question is related to the link between rifting and plume or hotspots. If rifts are associated with plumes (e.g., Tomasi et al. 2021), the emplacement of magma can happen before or during early stages of rifting and can force the breakup. Franke et al. (2013) proposed a link between rifting and plumes. Buiter and Torsvik, (2014) suggested that rifting precedes plume emplacement indicating a tectonic control. Thus, at present the understanding of magmatic processes at rifted margins is mainly hampered by the lack of the understanding of how magmatic systems interact with extensional systems, a subject that I will address in this study.

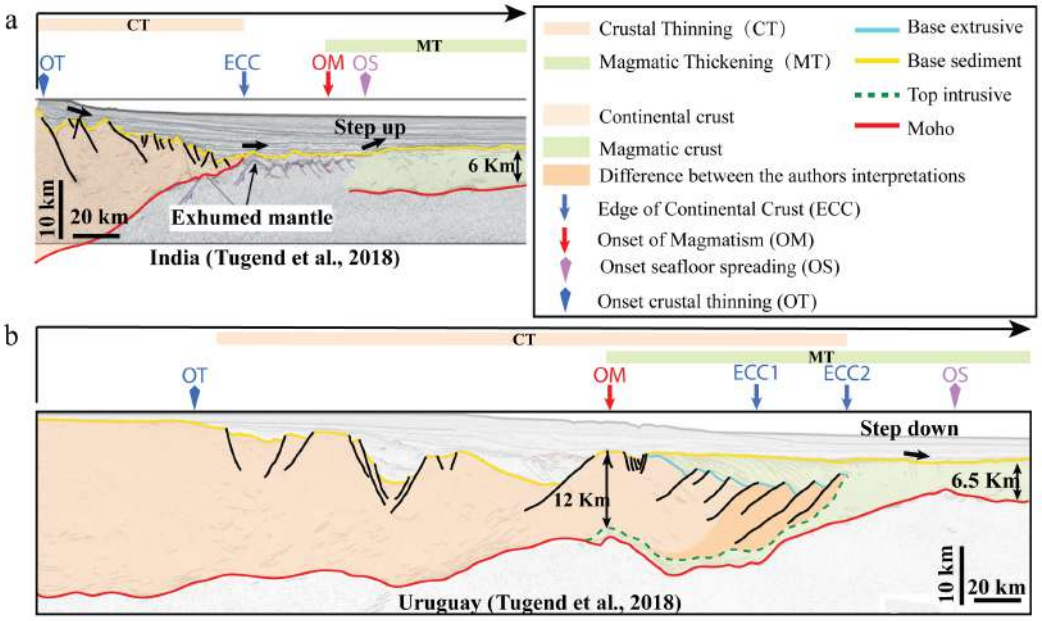

Figure I.4 *(a) Magma-poor rifted margin: seismic observations from the SE Indian rifted margin. (b) Magma-rich rifted margins: seismic observations from the Uruguayan rifted margin. Modified after Tugend et al. (2018) and Tomasi (2020).*

Transform margins

A third group of continental margins, of lesser importance for this study, are the so-called transform or highly oblique margins (for a review see Mercier de Lépinay et al., 2016). Transform/highly oblique rifting might be one of the most efficient ways to break-up continents since lower forces are required to break obliquely through cratonic crust (Lundin and Doré, 2019; Brune et al., 2012). The kinematic evolution of transform margins is suggested to include three stages (Mascle and Blarez, 1987): 1) the intra-continental transform fault stage such as for example the San Andreas and Dead Sea faults resulting in pull apart basins; 2) the active transform margin stage, when continental lithosphere slides against oceanic lithosphere; and 3) the passive transform margin, after the spreading center has passed along the margin and the transform margin becomes inactive. The length of a transform margin depends on three parameters: the obliquity between the regional trend and the relative plate motion, the width of the continental rift and timing of the deformation partitioning (Basile, 2015). One characteristic feature of many transform margins is the existence of marginal ridges parallel to the transform margin (Basile et al., 1996) and transform marginal plateaus that correspond to bathymetric highs at continental margins, situated at the

limit between oceanic basins of different ages (Loncke et al., 2020). Examples in the Atlantic Ocean are the Falkland, Demerara and Guinea plateaus (Schimschal and Jokat, 2018, 2019; Mercier de Lepinay, 2016; Parsiegla et al., 2008; Olyphant et al., 2017). Several hypotheses have tried to explain the existence of these marginal ridges such as: (1) crustal thickening from transpression in the intra-continental transform zone (e.g., Huguen et al., 2001); (2) thermal uplift due to heating of the continental lithosphere by the hotter oceanic lithosphere (e.g., Scrutton, 1979; Reid, 1989); and (3) flexural response of the lithosphere due to unloading by erosion (e.g., Basile and Allemand, 2002). Modern numerical studies hypothesize that most margin segments (more than 70%) do open in an oblique manner (exceed an obliquity of 20%) (e.g., Brune, 2014; Brune et al., 2014, 2018), an idea that can be tested in the propagator of the NW-SCS.

2.3 Distribution of types of margins

In the early 2000^{ies}, with the access to more and higher quality reflection seismic data, mainly from ION, TGS and other geophysical companies, the world margins have been classified as either non-volcanic, volcanic or transform margins (Fig. I.5). This enabled to show that there is approximately as many non-volcanic rifted margins as volcanic margins. The mapping was mainly based on two criteria: 1) the existence of SDRs forming smooth top basement dipping down onto oceanic crust, and 2) the occurrence of a structured top basement stepping up unto oceanic crust. While the former is characteristic of volcanic margins, the later qualifies a margin as non-volcanic (Fig. I.4). The distribution of volcanic margins appears to be linked to large igneous provinces and elevated potential mantle temperatures (Smallwood and White, 2002). However, the thermal influence of a hotspot is not well determined (Austin et al., 1990) and the relation between volcanic margins and the occurrence of hotspots is not straightforward (e.g., Franke et al., 2013). It is frequently suggested that non-volcanic margins result from slow extension, so it could be assumed that volcanic margins are associated with rapid extension. However, the South and Central Atlantic, which are both characterized by volcanic and non-volcanic segments, have been opening at ultra-slow to slow rates. At the North Atlantic margin, opening occurred at a rate of ca.

25 mm/yr half spreading rate, but subsequently half-spreading rates rapidly decreased to about 10 mm/yr (Le Breton et al., 2012). Other explanations for volcanic margins, apart from the mantle temperature during extension are the inherited fertile nature of the mantle. The relative ratio between extruded vs intruded magmatic additions, another little understood parameter in magmatic systems, may be controlled by factors such as magma composition, tectono-magmatic interactions, crustal rheology and composition and presence of fluids (e.g., Koopmann et al., 2014a; Tugend et al., 2020; Gouiza and Paton, 2019; Zhang et al., 2020).

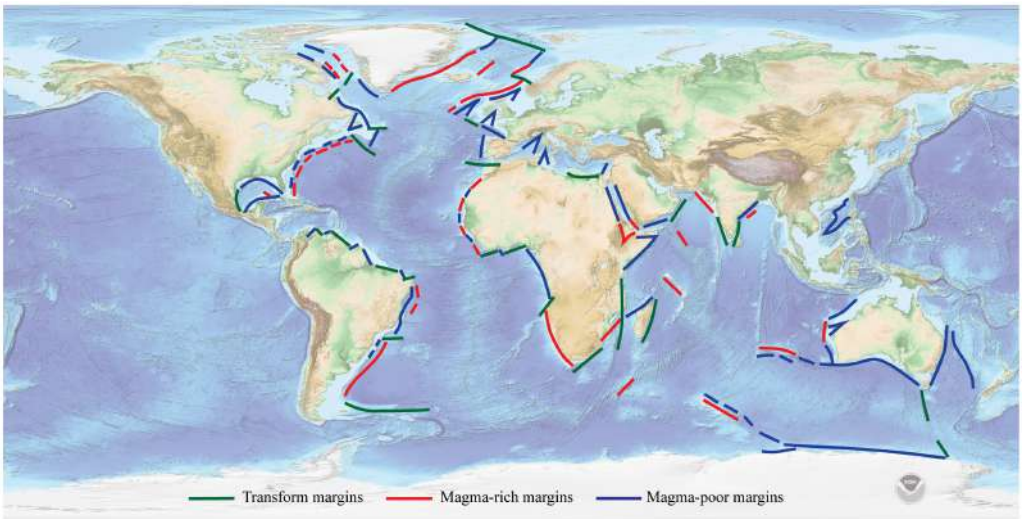

Figure I.5 *Bathymetric-topographic map of the world (map from National Geophysical Data Center) showing the distribution of magma-poor, magma-rich and transform margins. Transform margins can also be classified as magma-poor or magma-rich, however, the present state of knowledge about these margins is meager and prevent such a classification at the moment. Modified after Haupert et al. (2016).*

The present classification of magma-poor vs magma-rich rifted margins is mainly based on the contrasting magmatic budget identified at their distal settings. This binary view put the magmatic budget and the occurrence or absence of SDRs in the center of all studies, an evolution that continues until present. However, this way of looking rifted margins underscores the observation that all margins show magmatic additions as well as evidence for crustal thinning. Thus, the two-fold division may have been overly simplistic (Mutter, 1993). Müntener et al. (2010) demonstrated that at so-called magma-poor margins magma was produced during rifting but was not extracted, and therefore it is difficult to recognize. In contrast, the magmatic budget of volcanic

margins may have been overestimated (van Wijk et al., 2004; Tugend et al., 2020). Thus, the use of the more flexible terms “magma-poor” and “magma-rich” is more appropriate than that of non-volcanic and volcanic margins and it is likely that the full spectrum of margins between these end members may exist (e.g., Franke, 2013). The results of my PhD show that neither SDRs nor exhumed mantle domains exist in the NW-SCS, and that rifts can fail even after breakup, pointing out that rifted margins are far more complex than the commonly used binary view described above. While the magma-rich vs magma-poor classification appears to work for many present-day Atlantic rifted margins, it does not for the SCS. Thus, one of the aims of this study is to make detailed observations on high-resolution seismic sections from the NW-SCS Ocean Continent Transition (OCT) with the aim to provide additional observations to better characterize the nature of its rifted margins.

2.4 Rifted margins: ongoing research and open questions

The hydrocarbon industry and related service companies have undoubtedly been main drivers for the research at rifted margins. The improvement of reflection seismic imaging techniques and their global application enabled to better describe the architecture of rifts and rifted margins. The combination of new observations with the development of new modelling approaches and the study of margin remnants in collisional orogens enabled to develop a better understanding of the processes controlling the evolution of rift systems. The joint efforts between industry and academia made that at present we can explore and better understand the sedimentary archives of passive margins, which can help address some of the most pressing environmental issues presently faced by humanity. These include, for example, an understanding of rapid climate change and the link between slow and fast greenhouse gas cycles (methane and CO_2). More recent studies showed that, magma production during rifting and breakup has also been related to massive CO_2 production, which could explain natural excursions of methane and CO_2 in Earth history and may in turn explain climate change, such as the Paleocene-Eocene Thermal Maximum (PETM) that occurred simultaneous to the formation of the conjugate North Atlantic Volcanic margins ca. 55 Ma (e.g., Svensen et al., 2004; Brune et al., 2017b). Pinto et al., (2017)

and Abers et al. (2021) also suggested that mantle exhumation at magma-poor rifted margins and related serpentinization can account for substantial mass transfer of elements from the mantle into the hydrosphere, as well as the production of high volumes of methane and native hydrogen. Future research on rifted margins will be necessary to provide further details and confirm these results. However, a prerequisite for such studies is to understand how to interpret critical events such as magmatic breakup and/or serpentinization and to find the time equivalent deposits that may record these events.

Another challenge that the margin community is facing it the understanding of continental/lithospheric breakup. These studies have two main implications. A first one is linked to the opening of gateways that exerts a strong influence on the circulation of oceanic currents, and hence on the evolution and distribution of life (e.g., IODP Expedition 388). This evolution also controls the restriction of vast basins during rifting resulting in the formation of giant evaporite provinces favoring the preservation of organic material, as observed in many hyperextended rifted margins (e.g., South Atlantic, Gulf of Mexico, Central Atlantic) (Rowan, 2014). Thus, the formation of rifted margins, in particular during the stages preceding breakup, can have a fundamental impact on the paleo-climate, oceanography, and the redistribution of elements, gazes and source rocks in the Earth system. A second aspect of breakup relates to the tectono-magmatic processes that lead to plate separation and onset of seafloor spreading. While in the past the academic community was more focused on understanding the evolution of either rifts or mid ocean ridges, the breakup process has been less investigated. The fact that present-day rifted margins are not tectonically active makes it more difficult to image and understand the processes that are at the origin of crustal and lithospheric breakup. One of the aims of my PhD thesis will be to investigate the architecture of the OCT and the related processes controlling breakup.

A last, and more general theme of current research is the testing and generalization of existing rift models that have been mainly developed for magma-poor rifting in the North Atlantic to other rifted margins (Mjelde et al., 2002; Péron-Pinvindic et al., 2013; Tugend et al., 2018; Sapin et al. 2021). This leads to the fundamental

question of what controls rifting. Existing observations suggest a complex link between magmatic/asthenospheric and structural/lithospheric processes that cannot be easily predicted. The along strike spatial and temporal changes observed in the evolution of rift systems reflect the interplay between their inheritance (innate/"genetic code") and the physical processes at play (acquired/external factors) nicely documented in the example of the North Atlantic but difficult to generalize and apply to other margins such as those in the SCS. Thus, the aim of this study is to use long offset, high-resolution reflection seismic data to investigate the margins in the NW SCS and to compare the results with present-day models. Of key importance are the observation of the structural and magmatic variability along rifted margins and to link them with the stratigraphic record. In order to do so, I use a methodological approach to describe rifting evolution that will be further described in in section 1.6.

3 The SCS: a natural laboratory to study rifting and breakup processes

The processes controlling the formation of deep-water sedimentary basins, lithospheric breakup and first oceanic accretion are among the most fundamental processes in Earth tectonics. A prerequisite to understand these processes is to first describe the nature and structure of the basement (crust and mantle) and overlying sediments. However, only few examples exist where scientific drilling penetrated these zones or high-quality seismic data imaged their crustal structure. Among these few places are the Iberia-Newfoundland and Greenland-Norwegian margins in the North Atlantic that became the type localities of magma-poor and magma-rich margins, respectively. Studies on fossil margins exposed in orogens have been developed in the Alps and Pyrenees and provided some additional observations. However, at present rift models are biased due to the lack of studied examples where interpretations are data-driven rather than model-driven. From this perspective, the South China Sea (SCS) offers a unique opportunity. The International Ocean Discovery Program (IODP) implemented three and a half drilling expeditions (IODP 349, 367, 368, 368X) over the past 5 years to explore the processes of crustal and lithospheric breakup. The acoustic

basement was penetrated at 8 of the 12 drilled sites in early oceanic crust and the OCT, all in water depths exceeding 3700 m. This is the second largest drilling campaign at passive margins after the four Ocean Drilling Program (ODP) Legs (103, 149, 173 and 210) in the southern North Atlantic drilled in the 1990^{ies} and early 2000th (Tucholke et al. 2007). The access to new drilling results and the excellent seismic data available from the SCS attracted the interest of the global margin community, which is also evidenced by the numerous new publications. Thus, the choice of working in the SCS is strategic and not only enables to use one of the best natural laboratories to study rifting and continental breakup, but also to reinforce the interactions of the Strasbourg group with the Chinese margin community that is at the origin of my PhD project.

3.1 Geographical setting

The SCS is the largest marginal sea in the western Pacific, embracing an area of about 3.5 million km^2 and extending from the Tropic of Cancer to the equator, across over 20° of latitude (Fig. I.6). It is bordered on the NW by the Eurasian continent and by a series of islands, Taiwan, Luzon, and Palawan on the east and Borneo and Sumatra on the south. The deep basin, the continental slope, and the continental shelf, respectively, cover about 15%, 38%, and 47% of the total SCS area with an average water depth of 1140 m. The major feature of the SCS topography is the rhomboid-shape deep-water basin floored with an oceanic crust, extending from NE to SW. The deep basin has an average water depth of ~ 4700 m, with a maximum of 5559 m reported at its eastern margin (Wang et al. 2014, 2019).

The central deep basin is surround by continental and island slopes, topographically dissected and often studded with coral reefs. The northern slope with the Dongsha islands is separated by the Xisha Trough from the western slope with Xisha (Paracel Islands) and Zhongsha reefs (Macclesfield Bank), while the southern slope is occupied by the Nansha terrace, the largest reef area in the SCS. The Nansha Islands are scattered on a carbonate platform known also as “Dangerous Islands” covering a broad area of ~570,000 km^2. The eastern slope is narrow and steep, bordered by Luzon Trough and Manila Trench (Wang et al. 2014, 2019).

The continental shelf is best developed on the northern and southern sides of the SCS and becomes narrower towards the east. On the northern shelf, there are a number of submarine deltas developed off the Pearl and other river mouths, and fringing reefs are growing in the NW along the coasts of Leizhou Peninsula and Hainan Island. Exceeding ~ 300 km in width, the Sunda Shelf in the southwestern SCS is one of the largest shelves in the world. A number of submerged river valleys observed on the bottom of the Sunda Shelf are relict of a large river, drawn network (Wang et al., 2014).

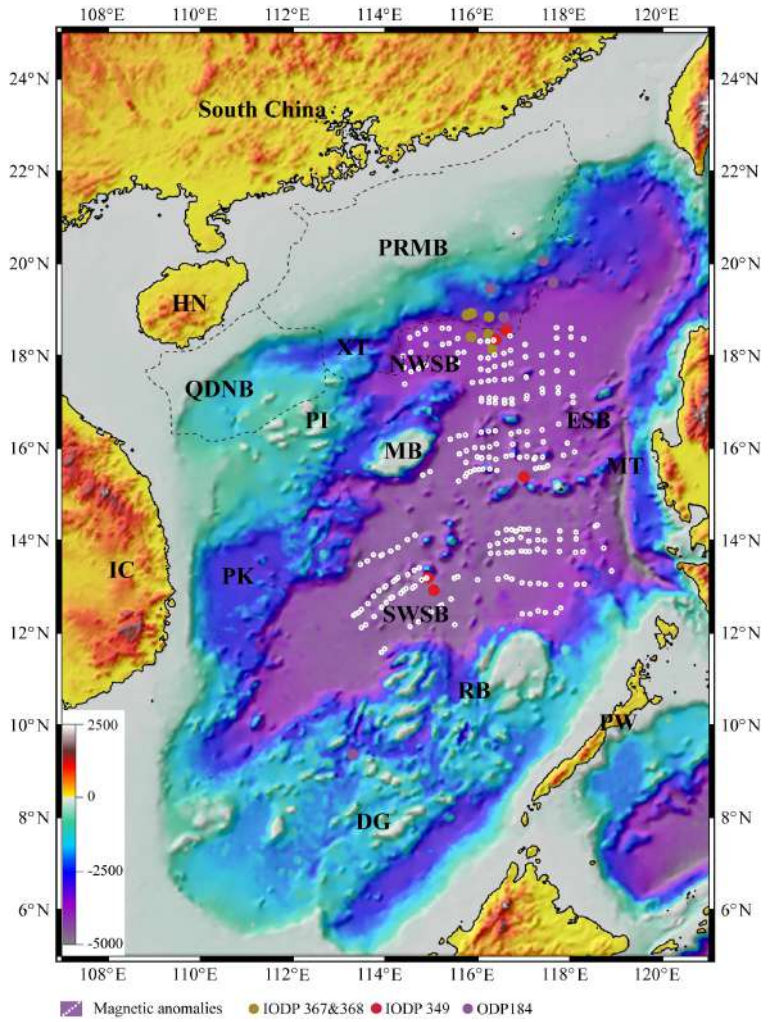

Figure I.6 *Regional bathymetric map of the South China Sea and surrounding areas and showing the location of the study area. Abbreviations of locations referred to in the text: MB, Macclesfield Bank; MT, Manila Trench; PRMB, Pearl River Mouth Basin; RB, Reed Bank; SB, Shuangfeng Basin; XT, Xisha Trough. The location of the IODP drill sites is based on Li et al. (2015) and Sun et al. (2018). The location of the magnetic anomalies is based on Briais et al. (1993). Modified after Gozzard et al. (2019).*

3.2. Geological setting and tectonic evolution

The SCS is bordered (Fig. I.7) on the north by a rifted continental margin, on the south by highly attenuated continental crust of the Dangerous Grounds, on the west by the attenuated continental crust offshore Vietnam deformed along a major strike-slip system that separates an extended and thinned curst from a normal thick crust flooring Vietnam (Fyhn et al., 2009; Savva et al., 2013). On its eastern side, the SCS subducts along the Manila Trench under the Luzon Arc (Ben-Avraham & Uyeda, 1973; Cardwell et al., 1980; Taylor & Hayes, 1980, 1983; Briais et al., 1993; Arfai et al., 2011). From a larger scale view the SCS is a marginal sea surrounded by subduction zones of the surrounding Pacific, Philippine Sea and Indo-Australian Plates located on its eastern and southern sides (Fig. I.7). The center of the SCS is made of a rhomb-shaped deep-water basin that bifurcates westwards, which allows to subdivide a SE and a NW subbasin (Fig. I.6), the latter corresponding to the study area.

Based on outcrop, drilling and magnetic data, rifting in the SCS is recognized to have started during the Late Cretaceous following the Mesozoic subduction of the paleo-Pacific plate and post-orogenic extension. Breakup and onset of seafloor spreading occurred in the Oligocene but were diachronous across the SCS (Sun 2019). Breakup initiated in the east at 33 Ma and lasted until 15.5 Ma in the northern sub-basin, while in the southwestern sub-basin it started at 23.6 Ma and stopped at 16 Ma (Li et al., 2014, 2015). A ridge jump from the northern basin to the south occurred at 25 Ma (Barchausen and Roeser 2004). When seafloor spreading stopped at about 15 Ma, eastward subduction of the SCS under the Manila Trench initiated (Zhao et al., 2019).

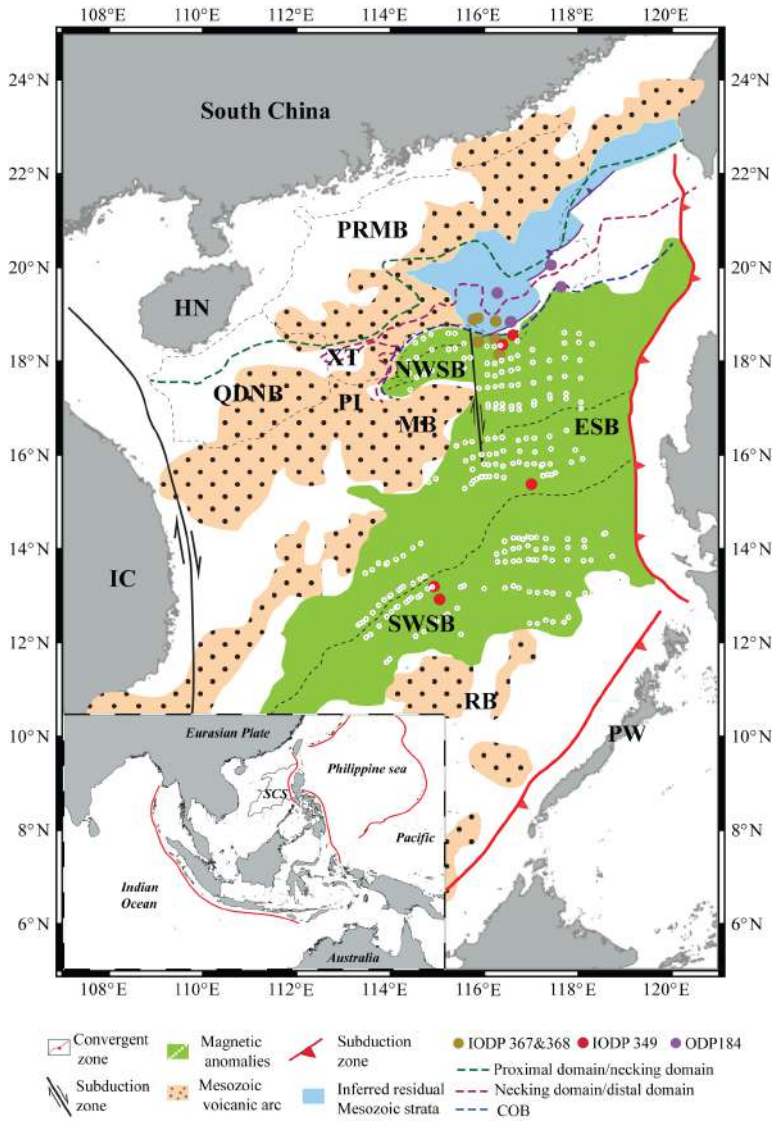

Figure I.7 *(a) The subduction zones surrounding the South China Sea. Modified after Sun et al. (2019). (b) Schematic map for the distribution of the Late Mesozoic arc and back-arc sedimentary basins in and around the SCS (Li et al., 2018 and Zhang et al., 2020). The location of the IODP drill sites is based on Li et al. (2015) and Sun et al. (2018). The location of the magnetic anomalies is based on Briais et al. (1993).*

A key difference to Atlantic-type margins is the coexistence of subduction zones and rifting, as well as the timing of rifting relative to the preceding orogenic collapse. In the Mesozoic, the Paleo-Pacific plate subducted northwestward beneath the southeastern Eurasian plate (Fig. I.8). At that time the study area was part of an Andean-type volcanic arc existing from Middle-Jurassic to Middle-Cretaceous time (Taylor and Hayes, 1983). During Late Cretaceous time, as a result of subduction slab rollback (e.g., Li and Li, 2007; Zhu et al., 2013), the crust which had been formed in the

convergence process was extended in front of the former subduction zone (Franke et al., 2014). This evolution is recorded by a series of NE trending Mesozoic volcanic activity. Igneous rocks extended from Japan through Southeast China into Southern Vietnam. Li et al. (2019) and Sun et al., (2019) suggested that the Mesozoic subduction hydrated and therefore weakened the lithosphere below the future SCS. Rollback of the Paleo-Pacific subduction is supposed to be responsible from the transition from convergence to divergence (Wang Pinxian, 2012). The Late Cretaceous is a key geological period with a transition to the subsequent Cenozoic rifting, which eventually resulted in the opening of the SCS (Hall, 2012; Ye Qing, 2018). However, it is difficult to define the transition from back-arc extension/orogenic collapse to rifting. It is also interesting to note that when rifting initiated in the future SCS domain, the Proto-SCS began to subduct beneath the northern Borneo and Sabah-Cagayan arc. Indeed, the subduction of the Proto-SCS is one possible geodynamic mechanism that may explain the onset of rifting and its transition into drifting in the SCS (Hall, 2002; Morley, 2002). During the early rifting stage, extension led to increasing decompression melting, which in turn led to increased diking and underplating during rifting (Zhang et al., 2020). From the late syn-rift to the early spreading stage, fertile mantle upwelling may have provided more high-magnesium magma and led to the high-velocity lower-crust underplating, diking and eruption during breakup (Sun, 2019; Zhang et al., 2019, 2020). At about 15 Ma, the SCS stopped spreading, contemporaneously with the onset of subduction of the SCS to the east under the Luzon arc.

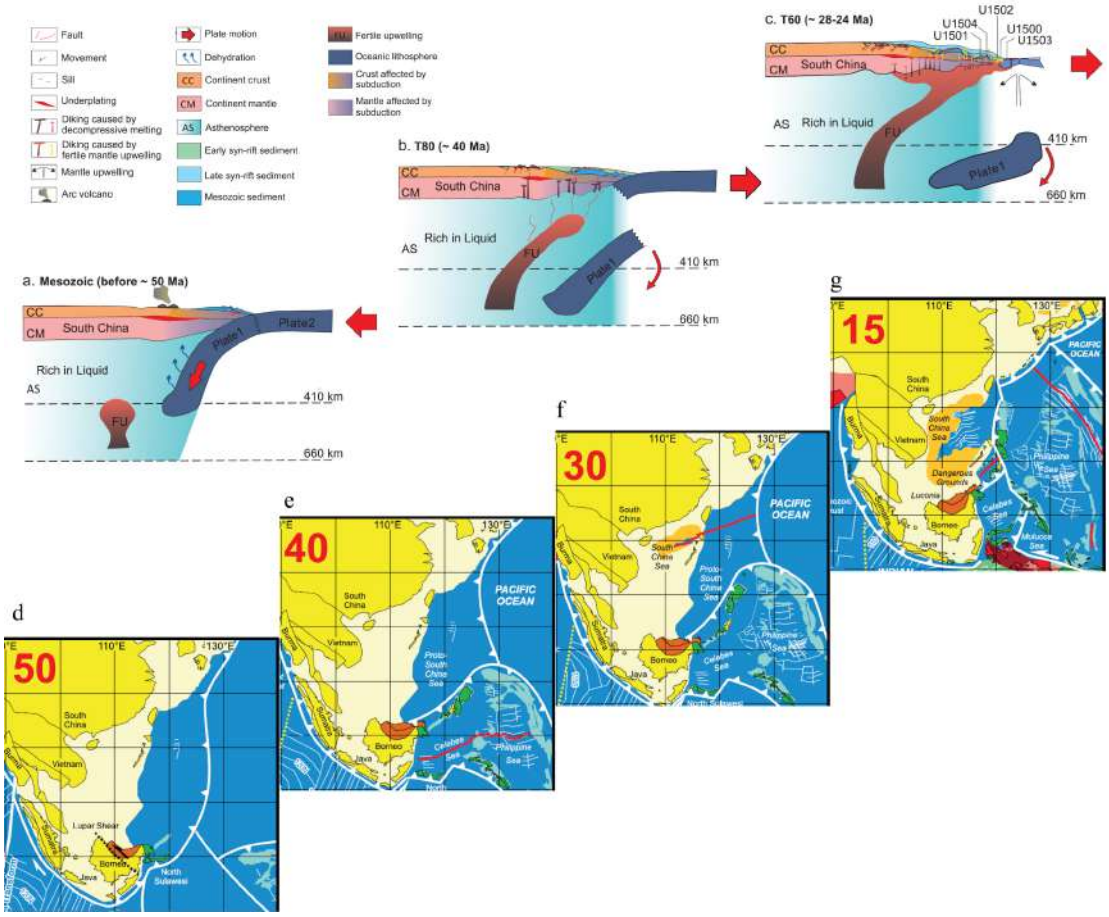

Figure I.8 *A conceptual mantle-scale model of the SCS showing the role of magmatic processes in rifting and breakup. (a) Mesozoic subduction of the paleo-Pacific below the South China block. (b) Slab breakoff supposed to occur during the early rifting stage, extension leads to decompression melting, which in turn results in diking and underplating that increases towards the area of breakup. (c) During the late syn-rift to early-spreading stage, fertile mantle upwelling may have provided more high-magnesium magma and led to the high-velocity lower-crustal underplating, diking and eruptions. Plates 1 and 2 might be the northern and southern slabs of the proto-South China Sea. (d) Paleogeographic reconstruction at 50 Ma. (e) Paleogeographic reconstruction at 40 Ma. (f) Paleogeographic reconstruction at 30 Ma. (g) Paleogeographic reconstruction at 15 Ma. Modified after Sun et al. (2019) and Hall et al. (2012).*

4. The study area

This study focuses on the propagator in the NW SCS, also referred to as the NW sub-basin (Fig. I.9). The study area separates the Macclesfield block in the south from the South China continental shelf in the north (Figs. I.6 and I.9). The area corresponds to a V shaped oceanic basin, which is surrounded by the Pearl River Mouth Basin in the north, the Xisha trough in the west and the Paracel Block (Zhongsha-Xisha) in the

south-west, and the Macclesfield Block in the south. The seafloor dips gently from SW to NE. The water depth is between 3000 and 3800 m. The Shuangfeng (double-peak) is a seamount located in the middle of oceanic basin. Sedimentary deposits in the basin are 1-2 km thick (Yao et al., 1999; Wu, 2012). The propagator has been traditionally classified as a non-volcanic margin and related to the southwestward movement of the Macclesfield–Paracel Block in the context of the opening of the SCS around 31–32 Ma (anomaly 11–12) (Taylor and Hayes, 1983; Ru and Pigott, 1986; Qiu et al., 2001; Shi et al., 2002). The propagating spreading center has been proposed to die out shortly before reaching the Xisha Trough in the west (~30 Ma;), commonly interpreted as an aborted rift (Taylor and Hayes, 1983; Shi et al., 2002). Qiu et al. (2001) analyzed the velocity structure of the continental crust on both sides of the Xisha Trough and showed that it is similar, suggesting a relatively homogeneous pre-rift continental crust.

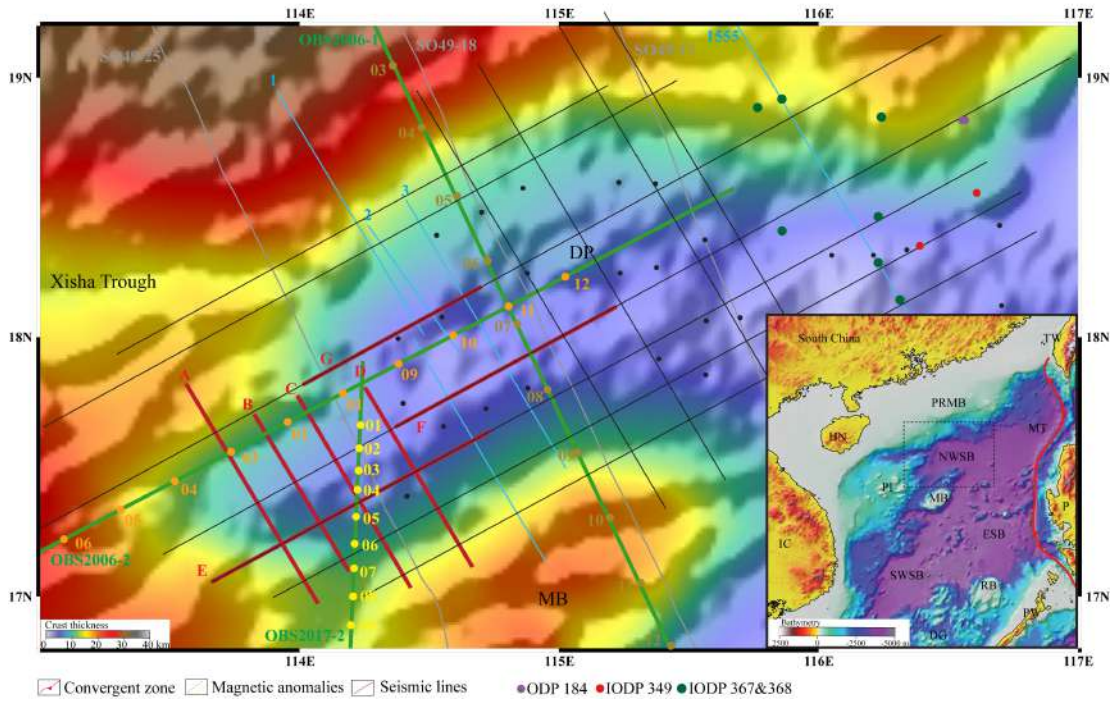

Figure I.9 *Crustal thickness map of the NW SCS (from Gozzard et al.; 2019) showing the location of the study area and the used datasets. Blue lines show in Paper1 and 2, red lines show in Paper 3. Green lines are OBS data (for references and details about data see chapters II to IV).*

The crustal thickness in the study area decreases from 21 km on the continental slope to 7.7 km in the oceanic basin (Wu et al., 2012; Gozzard et al., 2019). Ding et al., (2011) interpreted extensional and seafloor spreading structures in the NW-SCS at the northern edge of the Macclesfield Bank. Magnetic anomalies, together with seismic data and gravity anomalies, have been used to delimit the continental and oceanic domains, with special interest in determining the OCT position across the northern SCS margin (Taylor and Hayes, 1983; Briais et al., 1993; Nissen et al., 1995; Hsu et al., 2004; Hu et al., 2009; Franke et al., 2011). However, the proposed location varies significantly from study to study between the isobaths of 2500 and 3500 m outboard of the continental slope. The location of the OCT appears ill-defined in the narrow propagator, where magnetic lineations are unclear and the transition zone from mostly positive to negative free-air gravity anomalies is poorly defined (Cameselle et al.,2017). Wide-angle seismic data acquired across the NW-propagator (Ding et al., 2011), and parallel with our lines, have also been used to define the crustal domains in the propagator. However, even if the data have allowed interpreting oceanic crust under the deep-water area, the resolution of the data (OBS every 30 km or more) did not allow defining the boundary of the continental and oceanic domains accurately. The data used in this study cross this new proposed location of the OCT, as well as some linear gravity anomalies that occur on the eastern edge of the NW propagator. These linear anomalies may represent fracture zones with a strike parallel to the fracture zones offsetting the fossil spreading center, a point that needs to be further evaluated. It is also important to note that the orientation of these structures is close to the opening direction of the region. Wu et al. (2012) deduced, from refraction seismic data that no High Velocity Lower (HVL) crustal body can be found along the propagator in the OCT. This conclusion conflicts with the interpretation of Ding et al. (2012), Wang et al. (2020) and Li et al. (2021), who show that there are HVL in the lower crust of the OCT, suggesting a magmatic imprint during breakup and a sharp transition from thinned continental crust to oceanic crust within a width of 40 to 20 km (Wang et al., 2020). Frank et al. (2014) suggested that during the latest rifting stage one of the rift basin-bounding faults took the lead and penetrated into the mantle, suggesting coupling between the crust and the mantle. These authors assumed that the mantle

may have been exhumed in parts of the OCT along detachment faults. Cameselle et al. (2017) suggested that the NW-SCS breakup occurred abruptly by spreading center propagation rather than by thinning during continental rifting. Gao et al. (2016) proposed that onset of seafloor spreading, and the breakup of the mantle lithosphere may have occurred before crustal necking. This shows that different and competing interpretations exist for the study area. It is also important to note that none of the existing studies undertook a detailed description of the syn-rift sedimentary sequence. In previous studies, four post-tectonic sequences have been described: an Oligocene, an early-middle Miocene, a late Miocene and a Plio-Pleistocene sequences (Li et al., 2015). The lower Oligocene post-tectonic unit is easily discernable across the NW SCS because of its weaker seismic reflectivity compared to the Miocene and Plio-Pleistocene sequences above. One of the aims of my study is to investigate the syn-rift sequence and to link it to the extensional and magmatic evolution of the NW-SCS propagator.

5. Open questions and aim of the thesis

My thesis concentrated on the NW-SCS propagator and focused on four main questions: three of them are addressed in chapters II to IV and are the subject of three papers, one of which is submitted and the two others are ready for submission. The last question will be addressed in the outlook (chapter VII). In the following, I shortly introduce the main research themes and related questions that guided my PhD and which are going to be discussed in chapters II to IV.

5.1 The syn-rift mega-sequence and its link to the tectono-magmatic evolution in a polyphase rift system: how to define, describe and interpret?

Rifting is an extensional process during which accommodation space is created by both horizontal widening and vertical deepening and often linked to magma production. The sedimentary system and more particularly the syn-rift mega-sequence sensu Hubbard (1988) records the timing, location and type of tectonic deformation, the distribution of depocenters, the reorganization of sedimentary sources, as well as the evolution of water depths and paleoenvironments. Moreover, linking the extrusive

magmatic additions with the syn-rift stratigraphic record also enables to define when, where and how much magma is produced during rifting and breakup. While the syn-rift sequence is well defined at proximal margins, the distal parts of present-day rifted margins have remained largely inaccessible to exploration. Only a few locations exist, where the syn-rift mega-sequence has been drilled at distal deep water rifted margins, showing that the prediction of the syn-rift stratigraphic architecture, the sedimentary facies, and correlations with more proximal parts of the margin is difficult (Fig. I.10). Indeed, projection of timelines from proximal to distal parts of the margin and the definition of the syn-rift sequence are completely different in a classical rift model or a polyphase model. A major difference is the rift migration and localization resulting in a diachronous evolution of the syn-tectonic sequence. Another important difference is the occurrence of new real estate, i.e., a basement that is exhumed and topped by one or several detachment faults. Such surfaces coincide with the exhumation of lower crustal and mantle rocks in the distal margin (Fig. I.10). The improvement of seismic imaging methods, dating and modelling techniques enable at present to better define the characteristics of the syn-rift sedimentary sequence, to establish some first-order architectural characteristics, and to recognize correlative interfaces (e.g., Masini et al., 2013; Ribes et al., 2019; Pérez-Gussinyé et al., 2020; Chenin et al., subm). A major learning from the study of the syn-rift mega-sequence in the Iberia-Newfoundland and the Alpine Tethys is that stratigraphic horizons cannot be simply projected from proximal into distal domains (Ribes et al., 2019; Chenin et al., subm; see also Fig. I.10). This has major implications for the correlation from proximal to distal margins, interrogates concepts such as the validity of the breakup unconformity, and also asks to redefine the meaning of the term “syn-rift”. Indeed, one of the major problems is to understand how the change in the mode of extension both in time and across the margin impacts the stratigraphic tape recorder.

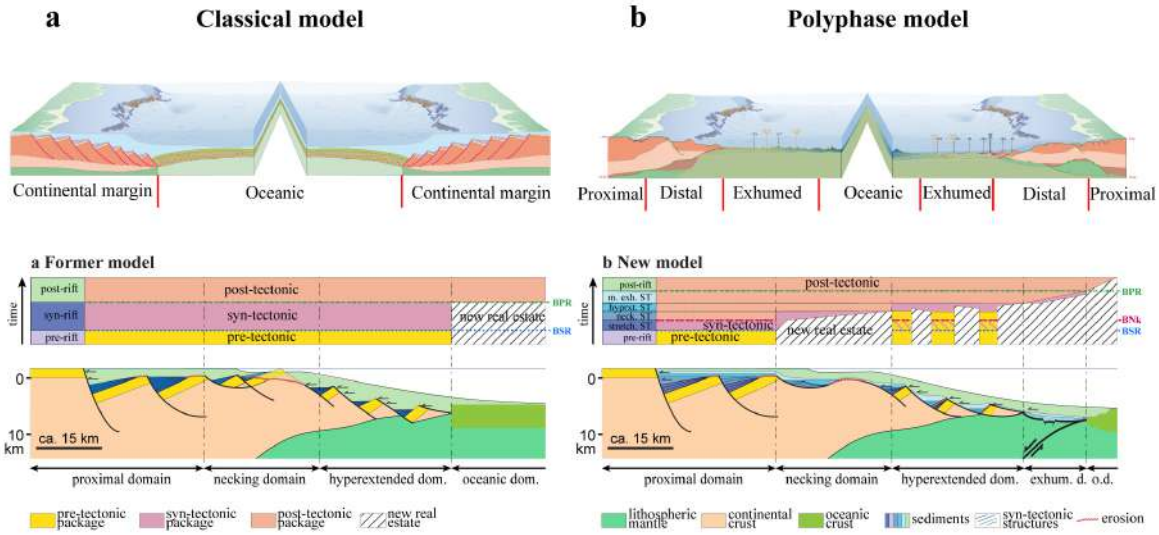

Figure I.10 *(a) The classical rifted margin model developed at the end of the 1970s and (b) the proposed polyphase margin model proposed after drilling the conjugate distal Iberian-Newfoundland conjugate amrgins. Modified from Péron-Pinvidic and Manatschal (2009) and Chenin et al. (subm.).*

Although some onshore and offshore studies investigated the stratigraphic record at distal margins, at present many questions remain, such as:

- How does the syn-rift megasequence record the tectono-magmatic rift evolution and how can the primary spatio-temporal evolution of active deformation during rifting and early seafloor spreading be defined?
- How to analyze the evolution of deformation through time and space by linking the tectonic and stratigraphic evolutions and how to quantify the amount of extension and strain-rate accommodated along conjugate margins?
- A subsidiary question is: does the tectono-stratigraphic record linked to different local sedimentary sources, depositional environments and sedimentation rates result in comparable first-order sedimentary architectures that are characteristic and enable to unravel the formation history of magma-poor rift systems?

Most of the more recent studies that tried to answer to these questions have been performed in the Alps and the North Atlantic margins. More recently, Xie et al. (2019)

and Lu et al. (2021) tried to apply the new concepts developed in the North Atlantic and the Alps to the SCS, aiming to propose correlations between proximal and distal parts of the margin. A prerequisite for such a study is to recognize the rift domains and the related tectonic structures acting during their formation and to link them to the stratigraphic record. Such studies require access to high-resolution seismic reflection data that cannot only resolve the sedimentary section, but also the architecture of the underlying basement. Moreover, high sedimentation rates during rifting are required, in order to resolve the syn-tectonic sedimentary architecture. The NW-SCS propagator fulfills all these requirements and can be considered as one of the best natural laboratories to answer to the questions listed above. In order to answer to the questions, I did a careful analysis of the dense, high-resolution seismic reflection dataset that images the conjugate margins at the tip of the NW-SCS propagator. The work includes: (1) a detailed description of the crustal architecture, (2) a definition of the extensional domains as well as the margin architecture, and (3) a determination of the tectono-sedimentary and magmatic evolution of the rift system via the study of conjugate rifted margins. This approach enabled me to understand the interplay between deformation, sedimentation and magmatic processes during rifting and breakup in 2D and allowed to analyze the evolution of deformation through time and space by linking the tectono-stratigraphic evolution with the observed crustal thinning. I synthesized these results in a Wheeler diagram and I quantified strain and strain rates for the whole rift duration along these conjugate margins. I proposed qualitative and quantitative criteria that help to describe the processes linked to two critical rift phases, which are the necking and hyperextension phases in the NW propagator of the SCS and to describe *when*, *where* and *how* accommodation space is created during specific periods of rifting. These results are presented in chapter II (paper 1) of my PhD.

5.2 From crustal separation to onset of seafloor spreading: how to define breakup?

The formation of a new plate boundary and creation of first oceanic crust, two of the most important Plate Tectonic processes, remain yet little understood. Indeed, the transition from rifting to seafloor spreading recorded in the crustal and syn-tectonic sedimentary and magmatic architecture of the OCT remains to be disentangled, in

particular its spatial and temporal transition (Fig. I.11). In the classical rift model (Figs. I.10a) the breakup process was considered to be an event where continental and lithospheric breakup occurred simultaneous and to produce a sharp boundary between continental and oceanic crusts, termed Ocean Continent Boundary (OCB). However, the drilling of exhumed, subcontinental mantle along the Iberia-Newfoundland conjugate margins (Whitemarsh et al., 2001; Tucholke and Sibuet, 2007; Péron-Pinvidic et al., 2007) showed that crustal separation occurred prior to onset of seafloor spreading and was separated by a transition zone, interpreted as the zone of exhumed subcontinental mantle, commonly named Ocean Continent Transition (OCT) (Fig. I.10b). In this view, *breakup* is not instantaneous but a lasting *breakup phase*. This new view raises questions on: (1) the nature of the *OCT* basement between unequivocal continental and oceanic crusts (Fig. I.11a); and (2) the nature of the processes operating between continental and lithospheric breakup. More recent observations suggest that breakup is complex, includes the interaction between detachment faulting and magmatic accretion that can change laterally along the margin, as shown by Zhang et al. (2021) and illustrated in Fig. I.11b to I.11d. These observations ask to redefine the process of breakup and related concepts such as that of breakup unconformity.

Recent studies along the Galicia margin (Dean et al., 2015; Davy et al., 2016), the Gulf of Guinea (Gillard et al., 2017), the E-India margin (Harkin et al., 2019), the Somalia margin (Mortimer et al., 2020) and the Labrador Sea (Gouiza and Paton, 2019), and at so-called young margins such as the Red Sea (Ligi et al., 2018), Gulf of Aden (Nonn et al., 2017), or Gulf of California (Lizarralde et al., 2007), also support the idea that the transition between the oceanward edge of the continent (location where the continental crust separates) and the location of first mature oceanic crust are separated by a transition zone (OCT). In such systems the main question remains where breakup occurred and how can it be defined.

At magma-rich margins the transition from the emblematic Seaward Dipping Reflection (SDR) to mature oceanic crust is often well imaged but little is known about the nature of the underlying lower crust (Geoffroy et al., 2015; Paton et al., 2017;

McDermott et al., 2018; Norcliffe et al., 2018). Therefore, the OCT in magma-rich margins is more difficult to define. More recent studies show that at magma-rich margins the interaction between tectonic and magmatic processes is complex and can result in the formation of hybrid crust, i.e., a composite crust made of continental crust with magmatic additions (Tugend et al., 2020; Tomasi et al., 2021). Such a crust is difficult to analyze and does neither belong to an unequivocal continental nor oceanic domain.

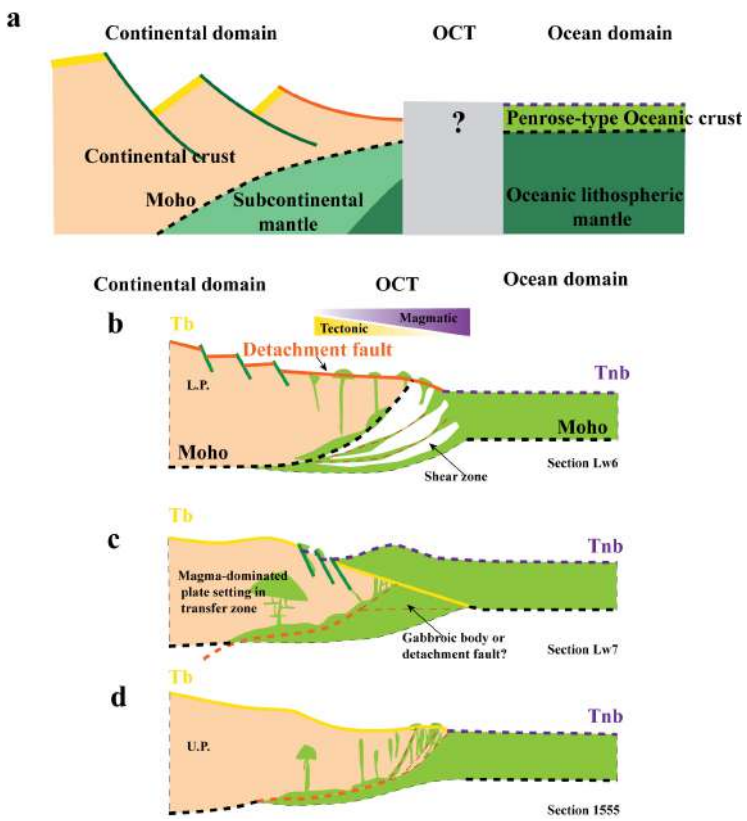

Figure I.11 *Schematic representation of the OCT located between unequivocal continental and oceanic crust and illustration of the lateral polarity change from a lower plate to an upper plate margin and the processes of breakup. Modified after Zhang et al (2021).*

In the SCS, the OCT has been drilled and imaged by high-quality seismic reflection surveys and it can be considered as the best place to describe the breakup process. Larsen et al. (2018), Ding et al. (2020), Zhang et al. (2021) and Nirregarten et al. (2020) presented a description of the OCT, based on an extraordinary data set. In these studies, the OCT is about 15 to 25 km wide. Larsen et al., (2018) and Ding et al.,

(2020) proposed that the transition between continental and oceanic crusts is rather sharp and resulted from a short and focused magmatic event at the end of rifting that triggered continental breakup and initiated seafloor spreading. In contrast, Zhang et al. (2020) proposed, in line with my work, that the first magma formed during crustal necking and that the magmatic budget steadily increased with time and progressively focused to the location of final lithospheric breakup. Implicit in this interpretation is that magma and extension interacted already during final rifting. Thus, the classical binary view that margins are either volcanic or non-volcanic is challenged by an increasing number of studies, which show that tectonic and magmatic activity interact during rifting (e.g., Tugend et al., 2020; Tomasi et al., 2021). Zhang et al. (2021) proposed for the central N-SCS, that breakup consists in a transition from detachment faulting to magmatic accretion occurring across a zone of some tens of kilometers width. Their study showed that there is a transition between crustal separation and onset of steady state seafloor spreading that is recorded in the OCT and includes hybrid crust. Implicit in this interpretation is that breakup includes a complex interaction between magmatic and extensional processes, which is also compatible with the observations reported by Quirk et al. (2014) from the OCT at the East Greenland margin in the North Atlantic. Gillard et al., (2015; 2019) proposed, based on the study of the Antarctica - South Australian conjugate margins and other examples, a model in which the breakup phase was dominated by flip-flop detachment faulting. However, in their studies the relationship between the extensional and magmatic structures and the syn-breakup sedimentary sequences were not clearly documented. In chapter III (paper 2), I will therefore try to answer to the following questions:

- How is the evolution linked to breakup and the formation of a new plate boundary recorded in the OCT?
- What is the crustal structure and related sedimentary architecture of the OCT domain and how can the OCT domain be defined?
- What are the processes at play between continental and lithospheric breakup?

- A subsidiary question is related to the validity of the “breakup unconformity” sensu Falvey (1974), a concept that has been widely used and abused in the literature to date breakup at global rifted margins.

Based on detailed observations of high quality and yet unpublished reflection seismic data and the high sedimentation rates during breakup, which provides an efficient tape recorder to document the breakup processes, I describe and interpret the characteristic structures of the OCT in the NW-SCS propagator. The study area is one of the few examples worldwide where the tip of an oceanic propagator is imaged by high-quality seismic data, where sedimentation rates are sufficiently high to record the syn-breakup tectono-magmatic evolution, and where these structures are not masked by magma and/or salt. Thus, the detailed investigation of the NW-SCS propagator allowed me to understand the spatial and temporal tectonic and magmatic evolution during the breakup phase and enabled me to discuss the processes leading to the formation of a mature oceanic spreading centre. The results of this study are presented in chapter III (paper 2).

5.3 Crustal breakup: how does it propagate?

Continental breakup and onset of seafloor spreading are singular events that are, unlike steady-state seafloor spreading or subduction processes, rare and cannot be directly observed at present. The best place to investigate how breakup propagates are V-shaped oceanic basins. There are a handful of examples, among which the best studied ones are the Woodlark basin (Taylor et al. 2009), the Gulf of California (Lizzaralde et al., 2007), the northern tip of the Red Sea (Ligi et al., 2018), and the Afar/western Gulf of Aden (Nonn et al., 2019). The development of three-dimensional modelling techniques enables to simulate and investigate how breakup propagates and what are the controlling processes (Le Pourhiet et al., 2018). However, it is important to note that observing and describing breakup is not trivial (see previous section and chapter III), and therefore analyzing the propagation is even more difficult. The problem is that breakup structures are complex and that underlying assumptions are in most cases not confirmed by observations or calibrated by drill hole data. Vink (1982) proposed a model for continental breakup with distortion, where oceanic basins are

formed by propagating rifts (Fig. I.12a). In this model, the region in front of the rift extends by continental faulting and crustal thinning, while the region behind the rift expands by seafloor spreading. Similar observations have been reported from the Woodlark basin (Taylor et al., 2009). The propagating rift model implies that large amounts of continental extension (up to 150 km) occur and that the continental boundaries are not isochrons and that the tip of the propagator is not an Eulerian pole (Le Pourhiet et al., 2018) as proposed by Martin et al. (1984) (Fig. I.12b). Nirrengarten et al. (2018) proposed a more complex model for the southern North Atlantic rift system, where extension is partitioned between different basins that occurs simultaneous to rift propagation (Fig. I.12c). However, the kinematic evolution of this area is not well constrained due to the lack of oceanic magnetic anomalies during the Cretaceous normal polarity super chron. Therefore, the rift and early seafloor spreading evolution (200–83 Ma) remains highly disputed due to contentious interpretations of the J magnetic anomaly on the Iberia-Newfoundland conjugate margins. However, the results of the study remain interesting and worth comparing to the SCS, despite the different tectonic settings and rheology, since it includes continental micro-block formation that enables the partitioning of the deformation between different rift segments. Neuharth et al. (2021) show, based on numerical modeling, that such continental micro-blocks may form through the linkage of rift segments. Luo et al. (2021) discussed the nature of the propagator in the SW-SCS and concluded that the partitioning of extension among different rift segments is the most compatible way to explain the seismic observations (see their Fig. 12c). In their model, partitioning between different segmented basins occur simultaneous to propagation of lithospheric breakup, which is also compatible with a long distant Eulerian pole during breakup, as defined by the magnetic anomalies (Briais et al., 1993). This model is also compatible with the study of Le Pourhiet et al. (2018) who showed that the SCS oceanic propagators cannot be explained by horizontal rotation around a Eulerian pole located at the tip of the oceanic propagator. However, this leads to the question of why the propagators were not able to break though the continent and stopped. Two possible explanations can be envisaged: 1) the far-field compression due to the west-to-east topographic gradient across the Indochinese Peninsula prevent continental breakup

propagation (Le Pourhiet et al., 2018), or 2) the inherited arc-crust trending NE-SW (Fig. I.7) was too strong and inhibited a successful breakup. In order to test the second possibility of the control of crustal inheritance, the recent study by Li et al. (2021) that complements the earlier work of Ding et al. (2012) and Wu et al. (2012) is important. It investigates the crustal structure below the Zhongsha Block (Macclesfield Block) and the adjacent abyssal basins. These authors propose based on refraction seismic studies, a crustal model for the NW-SCS that I integrate in my work. Previous studies by Cameselle et al. (2015, 2021) and Franke et al. (2014) interpreted the 3D structural variability and the narrow OCT as a consequence of the abrupt termination of continental rifting by the NE to SW propagation of a spreading center. Major disagreements exist between the evaluation of the magmatic budget. While Franke et al. (2014) assumed mantle exhumation, Cameselle et al. (2015) suggested that breakup occurred abruptly by spreading center propagation rather than by thinning during continental rifting. In my study, I analyzed sections across and along the tip of the NW-SCS propagator and come to different conclusions (see chapter IV). The results of this study provide answers to the following questions:

- How to identify, characterize and map the crust in the tip of an oceanic propagator?
- What is the 3D structural variability of the crust and how is it linked to the spatial and temporal changes along strike?
- How does breakup evolve at the tip of an ocean propagator and what are the processes controlling breakup?
- How do extensional and magmatic processes interact and how is this interaction documented in the sedimentary sequence?
- A subsidiary question is what controls the propagation and what can explain that it stalls?

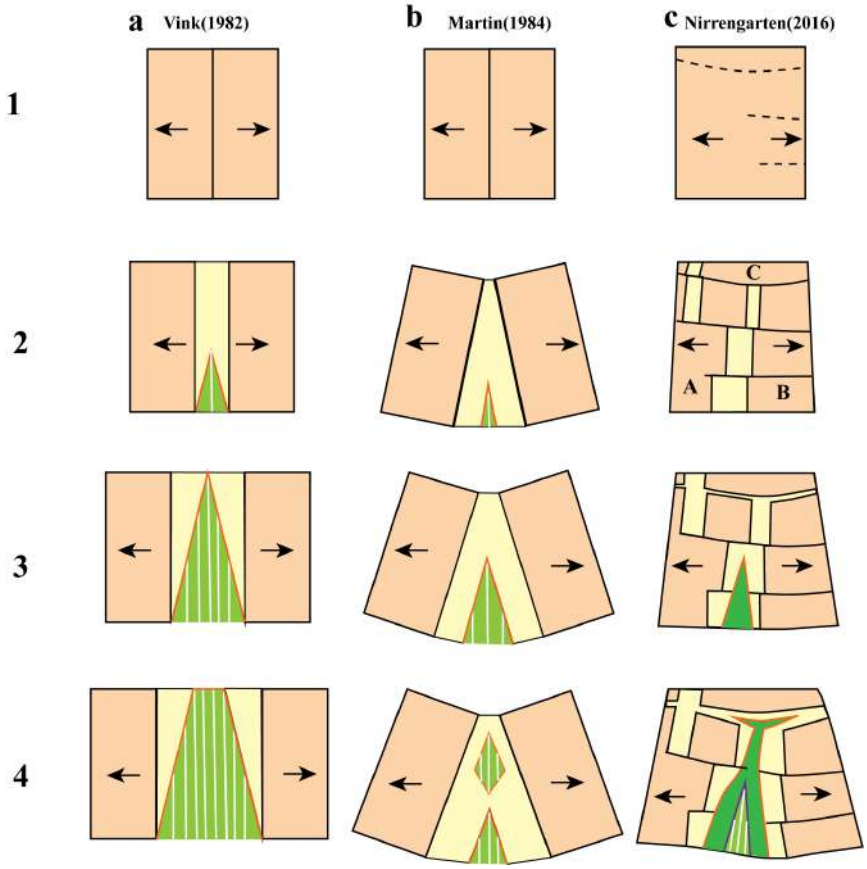

Figure I.12 *Rift propagation models: (a) model from Vink (1982), (b) model from Martin (1984), and (c) model of rift and seafloor spreading of a three-plate system modified from Nirrengarten et al. (2018).*

The advantage of investigating the tip of the NW-SCS propagator is that it enables to look at a snapshot of a propagating breakup system. In my study I undertook a careful analysis of high-resolution geophysical data that enabled me to describe the structures, magmatic additions and sediments formed during the breakup and to deduce where, when and how breakup occurred. The major advantage of the NW-SCS propagator is the excellent dataset, the limited volume of magmatic additions and the lack of salt, both of which can mask the crustal structure, the high sedimentation rates during breakup, and the proximity to IODP drill hole data, altogether making the study area one of the best places to investigate the propagation of a breakup system. The results of this part are presented in chapter IV of my thesis and are part of paper 3 that is in preparation.

5.4 The SCS: similarities and differences to Atlantic-type margins

Most of the new rift concepts, including the binary magma-rich vs. magma-poor classification of rifted margins are based on work made in the North Atlantic and have been used and adapted subsequently to the global rifted margins (Reston, 2009; Péron-Pinvidic et al., 2013; Franke, 2013). This classification is based on first-order characteristics such as crustal shapes, magmatic budgets and magmatic structures, top basement roughness and the observation whether the crust steps up or down onto oceanic crust (Tomasi, 2020). Yet recent observations at margins from where high-resolution reflection seismic and drill hole data are available show that the archetype margins can only describe first-order features of margins but cannot predict regional observations. Indeed, the magma-rich/magma-poor classification does not consider the relative timing of lithospheric vs. crustal thinning, while there is an intrinsic link between them and the final crustal shape of OCTs. In this respect, the SCS is a key example for investigating different types of rift evolutions that differ from the North Atlantic by their rheology, inheritance and the link to subduction zones. One of the original aims of my PhD was to compare the Atlantic-type evolution with that of the SCS, a plan that we did not follow, not only because of the lack of time, but also because the mapping of the OCT in the NW-SCS propagator was done at a scale that does not have an analogue on the North Atlantic. Therefore, I abandoned this plan. However, it is important to state here that although my study has initially been driven by the work done in the North Atlantic and the Alps, I was eventually able to recognize that, while some ideas previously developed at these sites may explain some of the observations in the NW SCS, others do not. Thus, a comparison requires reinspecting some of the observations done in the North Atlantic or in the Alps, which asks for new studies in these areas.

6. Data, approaches and methods

6.1 Data set used in the PhD

With permission of the China National Offshore Oil Corporation (CNOOC), I had access to a seismic data set of over 5000 km multichannel 2D airgun reflection seismic

profiles covering the NW SCS over an area of about 35,000 km² (Fig. I.9). All these lines are multichannel seismic (MCS) sections, which record down to 12 s Two-Way Travel Time (TWT) across the conjugate margins of the NW-SCS propagator. Data were acquired with a 7.5 km long streamer with 600 channels and group intervals of 12.5 m. Record length was 12s TWT at a sampling interval of 2 ms and shot interval of 37.5 m (Lei and Ren, 2016). All seismic profiles are oriented either NNW-SSE (about 20 km spacing) or ENE-WSW (about 15km spacing).

The seismic signal was generated using a Bolt Longlife Airgun (3850 in³ of volume), by means of compressed air (2000 psi). The record length and sampling rate were set at 11996ms TWT and 2ms, respectively. The acquired signals were recorded within 396 channels using a fold of 99, and lie in the frequency range of 40-60 Hz, allowing a vertical resolution up to 40 m. The data were processed through Omega V1.8.1 software, applying a bandpass filter (ranging from 6 Hz of low-cut frequency and 12 dB/s of low-cut slope to 136 Hz of high-cut frequency and 276 dB/s of high-cut slope), a de-noising and amplitude compensation and a post-stack time Kirchhoff migration. (Hui Chen 2021 MPG)

6.2 Method and used approach

It is important to state that, in the absence of drill hole data, which is for distal margins more the rule than the exception, there is a thin line between description and interpretation. Therefore, it is not always possible to distinguish between a seismic observation and an interpretation and it is important to be aware that seismic interpretations are non-unique. Therefore, my aim here is to provide a set of observations that enables to produce a coherent description of the architecture of the margin, OCT and oceanic crust across conjugate margins based on observed seismic geometries, seismic facies and structures. In order to do so, I subdivided the description in four successive steps that are increasingly more interpretative and that include: 1) identification of first-order seismic interfaces (seafloor, top acoustic basement, Moho), 2) definition of crustal architecture and related rift domains, 3) description of the relation between top acoustic basement and the sediment reflections, and 4) mapping of intra-basement structures and faults, including fault offsets, sealing

levels and decoupling levels and the identification of magmatic additions, which are inseparable from the tectonic structures.

This proposed approach enabled me to build a coherent interpretation, in which first-order and objective observations are first established, building the frame for subsequent, more subjective interpretations. Using the observations in the sedimentary sequence, I built a temporal and spatial framework that I linked with the structural and magmatic observations that enabled me to characterize the entire evolution of the OCT at the conjugate margins. The more detailed approaches and terminologies used are defined in each chapter of the manuscript/paper and are kept consistent throughout the study.

References

Albers, E., Bach, W., Pérez-Gussinyé, M., McCammon, C., & Frederichs, T. (2021). Serpentinization-Driven H2 Production From Continental Break-Up to Mid-Ocean Ridge Spreading: Unexpected High Rates at the West Iberia Margin. *Frontiers in Earth Science*, *9*, 673063. https://doi.org/10.3389/feart.2021.673063

Andersen, T. B. (1998). Extensional tectonics in the Caledonides of southern Norway, an overview. *Tectonophysics*, *285*(3), 333–351. https://doi.org/10.1016/S0040-1951(97)00277-1

Arfai, J., Franke, D., Gaedicke, C., Lutz, R., Schnabel, M., Ladage, S., et al. (2011). Geological evolution of the West Luzon Basin (South China Sea, Philippines). *Marine Geophysical Research*, *32*(3), 349–362. https://doi.org/10.1007/s11001-010-9113-x

Aslanian, D., Moulin, M., Olivet, J.-L., Unternehr, P., Matias, L., Bache, F., et al. (2009). Brazilian and African passive margins of the Central Segment of the South Atlantic Ocean: Kinematic constraints. *Tectonophysics*, *468*(1), 98–112. https://doi.org/10.1016/j.tecto.2008.12.016

Austin, J. A., Jr., Stoffa, P. L., Phillips, J. D., Oh, J., Sawyer, D. S., Purdy, G. M., et al. (1990). Crustal structure of the Southeast Georgia embayment-Carolina trough: Preliminary results of a composite seismic image of a continental suture(?) and a volcanic passive margin. *Geology*, *18*(10), 1023–1027. https://doi.org/10.1130/0091-7613(1990)018<1023:CSOTSG>2.3.CO;2

Barckhausen, U., & Roeser, H. A. (2004). Seafloor spreading anomalies in the South China Sea revisited. *Washington DC American Geophysical Union Geophysical Monograph Series*, *149*, 121–125. https://doi.org/10.1029/149GM07

Basile, C. (2015). Transform continental margins — part 1: Concepts and models. *Tectonophysics*, *661*, 1–10. https://doi.org/10.1016/j.tecto.2015.08.034

Basile, C., & Allemand, P. (2002). Erosion and flexural uplift along transform faults. *Geophysical Journal International*, *151*(2), 646–653. https://doi.org/10.1046/j.1365-246X.2002.01805.x

Ben-Avraham, Zvi., & Uyeda, S. (1973). The evolution of the China Basin and the mesozoic paleogeography of Borneo. *Earth and Planetary Science Letters*, *18*(2), 365–376. https://doi.org/10.1016/0012-821X(73)90077-0

Boillot, G., Grimaud, S., Mauffret, A., Mougenot, D., Kornprobst, J., Mergoil-Daniel, J., & Torrent, G. (1980). Ocean-continent boundary off the Iberian margin: A serpentinite diapir west of the Galicia Bank. *Earth and Planetary Science Letters*, *48*(1), 23–34. https://doi.org/10.1016/0012-821X(80)90166-1

Boillot, G., Recq, M., Winterer, E. L., Meyer, A. W., Applegate, J., Baltuck, M., et al. (1987). Tectonic denudation of the upper mantle along passive margins: a model based on drilling results (ODP leg 103, western Galicia margin, Spain). *Tectonophysics*, *132*(4), 335–342. https://doi.org/10.1016/0040-1951(87)90352-0

Boillot, Gilbert, & Capdevila, R. (1977). The Pyrenees: Subduction and collision? *Earth and Planetary Science Letters*, *35*(1), 151–160. https://doi.org/10.1016/0012-821X(77)90038-3

Bois, C., Pinet, B., & Roure, F. (1989). Dating lower crustal features in France and adjacent areas from deep seismic profiles. *Washington DC American Geophysical Union Geophysical Monograph Series*, *51*, 17–31. https://doi.org/10.1029/GM051p0017

Bown, J. W., & White, R. S. (1994). Variation with spreading rate of oceanic crustal thickness and geochemistry. *Earth and Planetary Science Letters*, *121*(3), 435–449. https://doi.org/10.1016/0012-821X(94)90082-5

Breton, E. L., Cobbold, P. R., Dauteuil, O., & Lewis, G. (2012). Variations in amount and direction of seafloor spreading along the northeast Atlantic Ocean and resulting

deformation of the continental margin of northwest Europe. *Tectonics*, *31*(5). https://doi.org/10.1029/2011TC003087

Briais, A., Patriat, P., & Tapponnier, P. (1993a). Updated interpretation of magnetic anomalies and seafloor spreading stages in the south China Sea: Implications for the Tertiary tectonics of Southeast Asia. *Journal of Geophysical Research: Solid Earth*, *98*(B4), 6299–6328. https://doi.org/10.1029/92JB02280

Briais, A., Patriat, P., & Tapponnier, P. (1993b). Updated interpretation of magnetic anomalies and seafloor spreading stages in the south China Sea: Implications for the Tertiary tectonics of Southeast Asia. *Journal of Geophysical Research: Solid Earth*, *98*(B4), 6299–6328. https://doi.org/10.1029/92JB02280

Brune, S. (2014). Evolution of stress and fault patterns in oblique rift systems: 3-D numerical lithospheric-scale experiments from rift to breakup. *Geochemistry, Geophysics, Geosystems*, *15*(8), 3392–3415. https://doi.org/10.1002/2014GC005446

Brune, S., Popov, A. A., & Sobolev, S. V. (2012). Modeling suggests that oblique extension facilitates rifting and continental break-up. *Journal of Geophysical Research: Solid Earth*, *117*(B8). https://doi.org/10.1029/2011JB008860

Brune, S., Heine, C., Pérez-Gussinyé, M., & Sobolev, S. V. (2014). Rift migration explains continental margin asymmetry and crustal hyper-extension. *Nature Communications*, *5*(1). https://doi.org/10.1038/ncomms5014

Brune, S., Williams, S. E., & Müller, R. D. (2017). Potential links between continental rifting, CO2 degassing and climate change through time. *Nature Geoscience*, *10*(12), 941–946. https://doi.org/10.1038/s41561-017-0003-6

Brune, S., Williams, S. E., & Müller, R. D. (2018). Oblique rifting: the rule, not the exception. *Solid Earth*, *9*(5), 1187–1206. https://doi.org/10.5194/se-9-1187-2018

Buck, W. R. (2007). Do Lava Flows Drive Caldera Collapse at Spreading Centers?, *2007*, T22E-08. Presented at the AGU Fall Meeting Abstracts.

Buiter, S., & Torsvik, T. (2014). A review of Wilson Cycle plate margins: A role for mantle plumes in continental break-up along sutures? https://doi.org/10.1016/J.GR.2014.02.007

Cadenas, P., Manatschal, G., & Fernández-Viejo, G. (2020). Unravelling the architecture and evolution of the inverted multi-stage North Iberian-Bay of Biscay rift. *Gondwana Research*, *88*, 67–87. https://doi.org/10.1016/j.gr.2020.06.026

Cameselle, A. L., Ranero, C. R., Franke, D., & Barckhausen, U. (2017). The continent-ocean transition on the northwestern South China Sea. *Basin Research*, *29*, 73–95. https://doi.org/10.1111/bre.12137

Cameselle, A. L., Ranero, C. R., & Barckhausen, U. (2020). Understanding the 3D Formation of a Wide Rift: The Central South China Sea Rift System. *Tectonics*, *39*(12). https://doi.org/10.1029/2019TC006040

Cardwell, R. K., Isaacks, B. L., & Karig, D. E. (1980). The Spatial Distribution of Earthquakes, Focal Mechanism Solutions, and Subducted Lithosphere in the Philippine and Northeastern Indonesian Islands. In *The Tectonic and Geologic Evolution of Southeast Asian Seas and Islands* (pp. 1–35). American Geophysical Union (AGU). https://doi.org/10.1029/GM023p0001

Chen, H., Stow, D. A. V., Xie, X., Ren, J., Mao, K., Gao, Y., et al. (2021). Depositional architecture and evolution of basin-floor fan systems since the Late Miocene in the Northwest Sub-Basin, South China Sea. *Marine and Petroleum Geology*, *126*, 104803. https://doi.org/10.1016/j.marpetgeo.2020.104803

Chenin, P., Manatschal, G., Lavier, L. L., & Erratt, D. (2015). Assessing the impact of orogenic inheritance on the architecture, timing and magmatic budget of the North Atlantic rift system: a mapping approach. *Journal of the Geological Society*, *172*(6), 711–720. https://doi.org/10.1144/jgs2014-139

Chenin, P., Manatschal, G., Picazo, S., Müntener, O., Karner, G., Johnson, C., & Ulrich, M. (2017). Influence of the architecture of magma-poor hyperextended rifted margins on orogens produced by the closure of narrow versus wide oceans. *Geosphere*, *13*(2), 559–576. https://doi.org/10.1130/GES01363.1

Chenin, P., Schmalholz, S. M., Manatschal, G., & Karner, G. D. (2018). Necking of the Lithosphere: A Reappraisal of Basic Concepts With Thermo-Mechanical Numerical Modeling. *Journal of Geophysical Research: Solid Earth*, *123*(6), 5279–5299. https://doi.org/10.1029/2017JB014155

Costa, S., & Rey, P. (1995). Lower crustal rejuvenation and growth during post-thickening collapse: Insights from a crustal cross section through a Variscan metamorphic core complex. *Geology*, *23*(10), 905–908. https://doi.org/10.1130/0091-7613(1995)023<0905:LCRAGD>2.3.CO;2

Davy, R. G., Minshull, T. A., Bayrakci, G., Bull, J. M., Klaeschen, D., Papenberg, C., et al. (2016). Continental hyperextension, mantle exhumation, and thin oceanic crust at the continent-ocean transition, West Iberia: New insights from wide-angle seismic. *Journal of Geophysical Research: Solid Earth*, *121*(5), 3177–3199. https://doi.org/10.1002/2016JB012825

Dean, S. L., Sawyer, D. S., & Morgan, J. K. (2015). Galicia Bank ocean–continent transition zone: New seismic reflection constraints. *Earth and Planetary Science Letters*, *413*, 197–207. https://doi.org/10.1016/j.epsl.2014.12.045

Dewey, J. F. (1988). Extensional collapse of orogens. *Tectonics*, *7*(6), 1123–1139. https://doi.org/10.1029/TC007i006p01123

Dewey, John F., & Burke, K. (1974). Hot Spots and Continental Break-up: Implications for Collisional Orogeny. *Geology*, *2*(2), 57–60. https://doi.org/10.1130/0091-7613(1974)2<57:HSACBI>2.0.CO;2

Dick, H. J. B., Lin, J., & Schouten, H. (2003). An ultraslow-spreading class of ocean ridge. *Nature*, *426*(6965), 405–412. https://doi.org/10.1038/nature02128

Ding, W., Li, M., Zhao, L., Ruan, A., & Wu, Z. (2011). Cenozoic tectono-sedimentary characteristics and extension model of the Northwest Sub-basin, South China Sea. *Geoscience Frontiers*, *2*(4), 509–517. https://doi.org/10.1016/j.gsf.2011.05.010

Ding, W., Schnabel, M., Franke, D., Aiguo, R., & Zhenli, W. (2012). Crustal Structure across the Northwestern Margin of South China Sea: Evidence for Magma-poor Rifting from a Wide-angle Seismic Profile. *Acta Geologica Sinica - English Edition*, *86*(4), 854–866. https://doi.org/10.1111/j.1755-6724.2012.00711.x

Ding, W., Sun, Z., Mohn, G., Nirrengarten, M., Tugend, J., Manatschal, G., & Li, J. (2020). Lateral evolution of the rift-to-drift transition in the South China Sea: Evidence from multi-channel seismic data and IODP Expeditions 367&368 drilling results. *Earth and Planetary Science Letters*, *531*, 115932. https://doi.org/10.1016/j.epsl.2019.115932

Doré, T., & Lundin, E. (2015). RESEARCH FOCUS: Hyperextended continental margins—Knowns and unknowns. *Geology*, *43*(1), 95–96. https://doi.org/10.1130/focus012015.1

Eldholm, O., Thiede, J., & Taylor, E. (1989). The Norwegian Continental Margin: Tectonic, Volcanic, and Paleoenvironmental Framework. https://doi.org/10.2973/ODP.PROC.SR.104.110.1989

Eldholm, Olav, & Grue, K. (1994). North Atlantic volcanic margins: Dimensions and production rates. *Journal of Geophysical Research: Solid Earth*, *99*(B2), 2955–2968. https://doi.org/10.1029/93JB02879

Fossen, H., Gabrielsen, R. H., Faleide, J. I., & Hurich, C. A. (2014). Crustal stretching in the Scandinavian Caledonides as revealed by deep seismic data. *Geology*, *42*(9), 791–794. https://doi.org/10.1130/G35842.1

Franke, D., Barckhausen, U., Baristeas, N., Engels, M., Ladage, S., Lutz, R., et al. (2011). The continent-ocean transition at the southeastern margin of the South China Sea. *Marine and Petroleum Geology*, *28*(6), 1187–1204. https://doi.org/10.1016/j.marpetgeo.2011.01.004

Franke, Dieter. (2013). Rifting, lithosphere breakup and volcanism: Comparison of magma-poor and volcanic rifted margins. *Marine and Petroleum Geology*, *43*, 63–87. https://doi.org/10.1016/j.marpetgeo.2012.11.003

Franke, Dieter, Savva, D., Pubellier, M., Steuer, S., Mouly, B., Auxietre, J.-L., et al. (2014). The final rifting evolution in the South China Sea. *Marine and Petroleum Geology*, *58*, 704–720. https://doi.org/10.1016/j.marpetgeo.2013.11.020

Franke, W. (2006). The Variscan orogen in Central Europe: construction and collapse. *Geological Society, London, Memoirs*, *32*(1), 333–343. https://doi.org/10.1144/GSL.MEM.2006.032.01.20

Fyhn, M. B. W., Boldreel, L. O., & Nielsen, L. H. (2009). Geological development of the Central and South Vietnamese margin: Implications for the establishment of the South China Sea, Indochinese escape tectonics and Cenozoic volcanism. *Tectonophysics*, *478*(3), 184–214. https://doi.org/10.1016/j.tecto.2009.08.002

Gale, A., Dalton, C. A., Langmuir, C. H., Su, Y., & Schilling, J.-G. (2013). The mean composition of ocean ridge basalts. *Geochemistry, Geophysics, Geosystems*, *14*(3), 489–518. https://doi.org/10.1029/2012GC004334

Gao, J., Wu, S., McIntosh, K., Mi, L., Liu, Z., & Spence, G. (2016). Crustal structure and extension mode in the northwestern margin of the South China Sea: CRUSTAL EXTENSION OF THE SOUTH CHINA SEA. *Geochemistry, Geophysics, Geosystems*, *17*(6), 2143–2167. https://doi.org/10.1002/2016GC006247

Geoffroy, L., Burov, E. B., & Werner, P. (2015). Volcanic passive margins: another way to break up continents. *Scientific Reports*, *5*, 14828. https://doi.org/10.1038/srep14828

Gillard, M., Sauter, D., Tugend, J., Tomasi, S., Epin, M.-E., & Manatschal, G. (2017). Birth of an oceanic spreading center at a magma-poor rift system. *Scientific Reports*, *7*(1). https://doi.org/10.1038/s41598-017-15522-2

Gillard, M., Tugend, J., Müntener, O., Manatschal, G., Karner, G. D., Autin, J., et al. (2019). The role of serpentinization and magmatism in the formation of decoupling interfaces at magma-poor rifted margins. *Earth-Science Reviews*, *196*, 102882. https://doi.org/10.1016/j.earscirev.2019.102882

Goodwin, E. B., & McCarthy, J. (1990). Composition of the lower crust in west central Arizona from three-component seismic data. *Journal of Geophysical Research: Solid Earth*, *95*(B12), 20097–20109. https://doi.org/10.1029/JB095iB12p20097

Gouiza, M., & Paton, D. A. (2019). The Role of Inherited Lithospheric Heterogeneities in Defining the Crustal Architecture of Rifted Margins and the Magmatic Budget During Continental Breakup. *Geochemistry, Geophysics, Geosystems*, *20*(4), 1836–1853. https://doi.org/10.1029/2018GC007808

Gozzard, S., Kusznir, N., Franke, D., Cullen, A., Reemst, P., & Henstra, G. (2019). South China Sea crustal thickness and oceanic lithosphere distribution from satellite gravity inversion. *Petroleum Geoscience*, *25*(1), 112–128. https://doi.org/10.1144/petgeo2016-162

Hall, R. (2012). Late Jurassic–Cenozoic reconstructions of the Indonesian region and the Indian Ocean. *Tectonophysics*, *570–571*, 1–41. https://doi.org/10.1016/j.tecto.2012.04.021

Harkin, C., Kusznir, N., Tugend, J., Manatschal, G., & McDermott, K. (2019). Evaluating magmatic additions at a magma-poor rifted margin: An East Indian case study. *Geophysical Journal International*. https://doi.org/10.1093/gji/ggz007

Hinz, K., Eldholm, O., Block, M., & Skogseid, J. (1993). Evolution of North Atlantic volcanic continental margins. *Geological Society, London, Petroleum Geology Conference Series*, *4*(1), 901–913. https://doi.org/10.1144/0040901

Hubbard, R. J. (1988). Age and Significance of Sequence Boundaries on Jurassic and Early Cretaceous Rifted Continental Margins1. *AAPG Bulletin*, *72*(1), 49–72. https://doi.org/10.1306/703C81C8-1707-11D7-8645000102C1865D

Huguen, C., Guiraud, M., Benkhelil, J., & Mascle, J. (2001). Synlithification deformation processes of the Cretaceous sediments of the Ivory Coast-Ghana transform margin: A

way to detail the margin history. *Tectonics*, *20*(6), 959–975. https://doi.org/10.1029/2001TC900015

Huismans, R., & Beaumont, C. (2011). Depth-dependent extension, two-stage breakup and cratonic underplating at rifted margins. *Nature*, *473*(7345), 74–78. https://doi.org/10.1038/nature09988

Huismans, R. S., Podladchikov, Y. Y., & Cloetingh, S. (2001). Transition from passive to active rifting: Relative importance of asthenospheric doming and passive extension of the lithosphere. *Journal of Geophysical Research: Solid Earth*, *106*(B6), 11271–11291. https://doi.org/10.1029/2000JB900424

Keen, C. E., & Beaumont, C. (1990). Geodynamics of Rifted Continental Margins. https://doi.org/10.1130/DNAG-GNA-I1.391

Koopmann, H., Brune, S., Franke, D., & Breuer, S. (2014). Linking rift propagation barriers to excess magmatism at volcanic rifted margins. *Geology*, *42*(12), 1071–1074. https://doi.org/10.1130/G36085.1

Lagabrielle, Y., Asti, R., Duretz, T., Clerc, C., Fourcade, S., Teixell, A., et al. (2020). A review of cretaceous smooth-slopes extensional basins along the Iberia-Eurasia plate boundary: How pre-rift salt controls the modes of continental rifting and mantle exhumation. *Earth-Science Reviews*, *201*, 103071. https://doi.org/10.1016/j.earscirev.2019.103071

Larsen, H. C., Mohn, G., Nirrengarten, M., Sun, Z., Stock, J., Jian, Z., et al. (2018). Rapid transition from continental breakup to igneous oceanic crust in the South China Sea. *Nature Geoscience*, *11*(10), 782–789. https://doi.org/10.1038/s41561-018-0198-1

Lavier, L. L., & Manatschal, G. (2006). A mechanism to thin the continental lithosphere at magma-poor margins. *Nature*, *440*(7082), 324–328. https://doi.org/10.1038/nature04608

Le Pourhiet, L., Chamot-Rooke, N., Delescluse, M., May, D. A., Watremez, L., & Pubellier, M. (2018). Continental break-up of the South China Sea stalled by far-field compression. *Nature Geoscience*, *11*(8), 605–609. https://doi.org/10.1038/s41561-018-0178-5

Lei, C., & Ren, J. (2016). Hyper-extended rift systems in the Xisha Trough, northwestern South China Sea: Implications for extreme crustal thinning ahead of a propagating ocean. *Marine and Petroleum Geology*, *77*, 846–864. https://doi.org/10.1016/j.marpetgeo.2016.07.022

Lescoutre, R., & Manatschal, G. (2020). Role of rift-inheritance and segmentation for orogenic evolution: example from the Pyrenean-Cantabrian system. *BSGF - Earth Sciences Bulletin*, *191*, 18. https://doi.org/10.1051/bsgf/2020021

Levell, B., Argent, J., Doré, A. G., & Fraser, S. (2010). Passive margins: overview. *Geological Society, London, Petroleum Geology Conference Series*, *7*(1), 823–830. https://doi.org/10.1144/0070823

Li, C. F., Lin, J., Kulhanek, D. K., & Expedition 349 Scientists (Eds.). (2015). *South China Sea Tectonics* (Vol. 349). International Ocean Discovery Program. https://doi.org/10.14379/iodp.proc.349.2015

Li, C.-F., Lin, J., Kulhanek, D. K., Williams, T., Bao, R., Briais, A., et al. (2015). Expedition 349 summary. In *Li, C.-F.; Lin, J.; Kulhanek, D.K.; Williams, T.; Bao, R.; Briais, A.; Brown, E.A.; Chen, Y.; Clift, P.D.; Colwell, F.S.; Dadd, K.A.; Ding, W.-W.; Hernandez Almeida, Ivan; Huang, X.-L.; Hyun, S.; Jiang, T.; Koppers, A.A.P.; Li, Q.; Liu, C.; Liu, Q.; ... (2015). Expedition 349 summary. In: South China Sea Tectonics. Proceedings of the International Ocean Discovery Program: Vol. 349 (pp. 1-43). International Ocean Discovery Program 10.14379/iodp.proc.349.101.2015 <http://dx.doi.org/10.14379/iodp.proc.349.101.2015>* (Vol. 349, pp. 1–43). International Ocean Discovery Program. Retrieved from https://boris.unibe.ch/68255/

Li, Chun-Feng, Xu, X., Lin, J., Sun, Z., Zhu, J., Yao, Y., et al. (2014). Ages and magnetic structures of the South China Sea constrained by deep tow magnetic surveys and IODP Expedition 349. *Geochemistry, Geophysics, Geosystems*, *15*(12), 4958–4983. https://doi.org/10.1002/2014GC005567

Li, F., Sun, Z., & Yang, H. (2018). Possible Spatial Distribution of the Mesozoic Volcanic Arc in the Present-Day South China Sea Continental Margin and Its Tectonic Implications. *Journal of Geophysical Research: Solid Earth*. https://doi.org/10.1029/2017JB014861

Li, Y., Huang, H., Grevemeyer, I., Qiu, X., Zhang, H., & Wang, Q. (2021). Crustal structure beneath the Zhongsha Block and the adjacent abyssal basins, South China Sea: New insights into rifting and initiation of seafloor spreading. *Gondwana Research*, S1342937X2100188X. https://doi.org/10.1016/j.gr.2021.06.015

Li Z.-X., & Li X.-H. (2007). Formation of the 1300-km-wide intracontinental orogen and postorogenic magmatic province in Mesozoic South China: A flat-slab subduction model. *Geology*, *35*(2), 179–182. https://doi.org/10.1130/G23193A.1

Ligi, M., Bonatti, E., Bosworth, W., Cai, Y., Cipriani, A., Palmiotto, C., et al. (2018a). Birth of an ocean in the Red Sea: Oceanic-type basaltic melt intrusions precede continental rupture. *Gondwana Research*, *54*, 150–160. https://doi.org/10.1016/j.gr.2017.11.002

Ligi, M., Bonatti, E., Bosworth, W., Cai, Y., Cipriani, A., Palmiotto, C., et al. (2018b). Birth of an ocean in the Red Sea: Oceanic-type basaltic melt intrusions precede continental rupture. *Gondwana Research*, *54*, 150–160. https://doi.org/10.1016/j.gr.2017.11.002

Lister, G. S., Etheridge, M. A., & Symonds, P. A. (1991). Detachment models for the formation of passive continental margins. *Tectonics*, *10*(5), 1038–1064. https://doi.org/10.1029/90TC01007

Lizarralde, D., Axen, G. J., Brown, H. E., Fletcher, J. M., González-Fernández, A., Harding, A. J., et al. (2007a). Variation in styles of rifting in the Gulf of California. *Nature*, *448*(7152), 466–469. https://doi.org/10.1038/nature06035

Lizarralde, D., Axen, G. J., Brown, H. E., Fletcher, J. M., González-Fernández, A., Harding, A. J., et al. (2007b). Variation in styles of rifting in the Gulf of California. *Nature*, *448*(7152), 466–469. https://doi.org/10.1038/nature06035

Loncke, L., Roest, W. R., Klingelhoefer, F., Basile, C., Graindorge, D., Heuret, A., et al. (2020). Transform Marginal Plateaus. *Earth-Science Reviews*, *203*, 102940. https://doi.org/10.1016/j.earscirev.2019.102940

Lundin, E. R., & Doré, A. G. (2019). Non-Wilsonian break-up predisposed by transforms: examples from the North Atlantic and Arctic. *Geological Society, London, Special Publications*, *470*(1), 375–392. https://doi.org/10.1144/SP470.6

Lundin, Erik R., Doré, A. G., & Redfield, T. F. (2018). Magmatism and extension rates at rifted margins. *Petroleum Geoscience*, *24*(4), 379–392. https://doi.org/10.1144/petgeo2016-158

Luo, P., Manatschal, G., Ren, J., Zhao, Z., Wang, H., & Tong, D. (2021). Tectono - Magmatic and stratigraphic evolution of final rifting and breakup: Evidence from the tip of the southwestern propagator in the south China sea. *Marine and Petroleum Geology*, *129*, 105079. https://doi.org/10.1016/j.marpetgeo.2021.105079

Manatschal, G., Sutra, E., & Péron-Pinvidic, G. (2010). The lesson from the Iberia-Newfoundland rifted margins: how applicable is it to other rifted margins? *Undefined*. Retrieved from https://www.semanticscholar.org/paper/The-lesson-from-the-Iberia-Newfoundland-rifted-how-Manatschal-Sutra/7b7b4d93f8c8cde9ad078060c37d4e10516f793b

Manatschal, Gianreto. (2004). New models for evolution of magma-poor rifted margins based on a review of data and concepts from West Iberia and the Alps. *International Journal of Earth Sciences*, *93*(3). https://doi.org/10.1007/s00531-004-0394-7

Manatschal, Gianreto, & Müntener, O. (2009). A type sequence across an ancient magma-poor ocean–continent transition: the example of the western Alpine Tethys ophiolites. *Tectonophysics*, *473*(1), 4–19. https://doi.org/10.1016/j.tecto.2008.07.021

Manatschal, Gianreto, Lavier, L., & Chenin, P. (2015). The role of inheritance in structuring hyperextended rift systems: Some considerations based on observations and numerical modeling. *Gondwana Research*, *27*(1), 140–164. https://doi.org/10.1016/j.gr.2014.08.006

Mascle, J., & Blarez, E. (1987). Evidence for transform margin evolution from the Ivory Coast–Ghana continental margin. *Nature*, *326*(6111), 378–381. https://doi.org/10.1038/326378a0

Masini, E., Manatschal, G., & Mohn, G. (2013). The Alpine Tethys rifted margins: Reconciling old and new ideas to understand the stratigraphic architecture of magma-poor rifted margins. *Sedimentology*, *60*(1), 174–196. https://doi.org/10.1111/sed.12017

McCarthy, A., Tugend, J., Mohn, G., Candioti, L., Chelle-Michou, C., Arculus, R., et al. (2020). A case of Ampferer-type subduction and consequences for the Alps and the Pyrenees. *American Journal of Science*, *320*(4), 313–372. https://doi.org/10.2475/04.2020.01

McDermott, C., Lonergan, L., Collier, J. S., McDermott, K. G., & Bellingham, P. (2018). Characterization of Seaward-Dipping Reflectors Along the South American Atlantic Margin and Implications for Continental Breakup. *Tectonics*, *37*(9), 3303–3327. https://doi.org/10.1029/2017TC004923

McKenzie, D. (1978). Some remarks on the development of sedimentary basins. *Earth and Planetary Science Letters*, *40*(1), 25–32. https://doi.org/10.1016/0012-821X(78)90071-7

Meissner, R., & Krawczyk, C. H. (1999). Caledonian and Proterozoic terrane accretion in the southwest Baltic Sea. *Tectonophysics*, *314*(1), 255–267. https://doi.org/10.1016/S0040-1951(99)00247-4

Mercier de Lépinay, J., Munschy, M., Géraud, Y., Diraison, M., Navelot, V., Verati, C., et al. (2016). Magnetic mapping around Les Saintes islands (Lesser Antilles, Guadeloupe) for structural interpretation, *2016*, GP34A-05. Presented at the AGU Fall Meeting Abstracts.

Mercier de Lépinay, M., Loncke, L., Basile, C., Roest, W. R., Patriat, M., Maillard, A., & De Clarens, P. (2016). Transform continental margins – Part 2: A worldwide review. *Tectonophysics*, *693*, 96–115. https://doi.org/10.1016/j.tecto.2016.05.038

Mjelde, R., Kasahara, J., Shimamura, H., Kamimura, A., Kanazawa, T., Kodaira, S., et al. (2002). Lower crustal seismic velocity-anomalies; magmatic underplating or serpentinized peridotite? Evidence from the Vøring Margin, NE Atlantic. *Marine Geophysical Researches*, *23*(2), 169–183. https://doi.org/10.1023/A:1022480304527

Mohn, G., Manatschal, G., Beltrando, M., Masini, E., & Kusznir, N. (2012). Necking of continental crust in magma-poor rifted margins: Evidence from the fossil Alpine Tethys margins. *Tectonics*, *31*(1). https://doi.org/10.1029/2011TC002961

Morley, C. K. (2016). Major unconformities/termination of extension events and associated surfaces in the South China Seas: Review and implications for tectonic development. *Journal of Asian Earth Sciences*, *120*, 62–86. https://doi.org/10.1016/j.jseaes.2016.01.013

Mortimer, E. J., Gouiza, M., Paton, D. A., Stanca, R., Rodriguez, K., Hodgson, N., & Hussein, A. A. (2020). Architecture of a magma poor passive margin – Insights from the Somali margin. *Marine Geology*, *428*, 106269. https://doi.org/10.1016/j.margeo.2020.106269

Müntener, O., & Manatschal, G. (2006). High degrees of melt extraction recorded by spinel harzburgite of the Newfoundland margin: The role of inheritance and consequences for the evolution of the southern North Atlantic. *Earth and Planetary Science Letters*, *252*(3), 437–452. https://doi.org/10.1016/j.epsl.2006.10.009

Müntener, O., Manatschal, G., Desmurs, L., & Pettke, T. (2010). Plagioclase Peridotites in Ocean–Continent Transitions: Refertilized Mantle Domains Generated by Melt Stagnation in the Shallow Mantle Lithosphere. *Journal of Petrology*, *51*(1–2), 255–294. https://doi.org/10.1093/petrology/egp087

Mutter, J. C., & Zehnder, C. M. (1988). Deep crustal structure and magmatic processes: the inception of seafloor spreading in the Norwegian-Greenland Sea. *Geological Society, London, Special Publications*, *39*(1), 35–48. https://doi.org/10.1144/GSL.SP.1988.039.01.05

Mutter, John C. (1993). Margins declassified. *Nature*, *364*(6436), 393–394. https://doi.org/10.1038/364393a0

Neuharth, D., Brune, S., Glerum, A., Heine, C., & Welford, J. K. (2021). Formation of Continental Microplates Through Rift Linkage: Numerical Modeling and Its Application to the Flemish Cap and Sao Paulo Plateau. *Geochemistry, Geophysics, Geosystems*, *22*(4). https://doi.org/10.1029/2020GC009615

Nirrengarten, M., Manatschal, G., Tugend, J., Kusznir, N., & Sauter, D. (2018). Kinematic Evolution of the Southern North Atlantic: Implications for the Formation of Hyperextended Rift Systems. *Tectonics*, *37*(1), 89–118. https://doi.org/10.1002/2017TC004495

Nirrengarten, M., Mohn, G., Kusznir, N. J., Sapin, F., Despinois, F., Pubellier, M., et al. (2020). Extension modes and breakup processes of the southeast China-Northwest Palawan conjugate rifted margins. *Marine and Petroleum Geology*, *113*, 104123. https://doi.org/10.1016/j.marpetgeo.2019.104123

Nonn, C., Leroy, S., Khanbari, K., & Ahmed, A. (2017). Tectono-sedimentary evolution of the eastern Gulf of Aden conjugate passive margins: Narrowness and asymmetry in oblique rifting context. *Tectonophysics*, *721*, 322–348. https://doi.org/10.1016/j.tecto.2017.09.024

Norcliffe, J. R., Paton, D. A., Mortimer, E. J., McCaig, A. M., Nicholls, H., Rodriguez, K., et al. (2018). Laterally Confined Volcanic Successions (LCVS); recording rift-jumps during the formation of magma-rich margins. *Earth and Planetary Science Letters*, *504*, 53–63. https://doi.org/10.1016/j.epsl.2018.09.033

Olyphant, J. R., Johnson, R. A., & Hughes, A. N. (2017). Evolution of the Southern Guinea Plateau: Implications on Guinea-Demerara Plateau formation using insights from seismic, subsidence, and gravity data. *Tectonophysics*, *717*, 358–371. https://doi.org/10.1016/j.tecto.2017.08.036

Parsiegla, N., Stankiewicz, J., Gohl, K., Ryberg, T., & Uenzelmann-Neben, G. (2009). Southern African continental margin: Dynamic processes of a transform margin. *Geochemistry, Geophysics, Geosystems*, *10*(3). https://doi.org/10.1029/2008GC002196

Paton, D. A., Pindell, J., McDermott, K., Bellingham, P., & Horn, B. (2017). Evolution of seaward-dipping reflectors at the onset of oceanic crust formation at volcanic passive margins: Insights from the South Atlantic. *Geology*, *45*(5), 439–442. https://doi.org/10.1130/G38706.1

Pérez-Gussinyé, M., & Reston, T. J. (2001). Rheological evolution during extension at nonvolcanic rifted margins: Onset of serpentinization and development of detachments leading to continental breakup. *Journal of Geophysical Research: Solid Earth*, *106*(B3). https://doi.org/10.1029/2000jb900325

Pérez-Gussinyé, M., Morgan, J. P., Reston, T. J., & Ranero, C. R. (2006). The rift to drift transition at non-volcanic margins: Insights from numerical modelling. *Earth and Planetary Science Letters*, *244*(1), 458–473. https://doi.org/10.1016/j.epsl.2006.01.059

Pérez-Gussinyé, M., Andrés-Martínez, M., Araújo, M., Xin, Y., Armitage, J., & Morgan, J. P. (2020). Lithospheric strength and rift migration controls on synrift stratigraphy and breakup unconformities at rifted margins: Examples from numerical models, the Atlantic and South China Sea mar-gins. *Tectonics*, *39*(12), e2020TC006255.

Péron-Pinvidic, G., & Manatschal, G. (2009). The final rifting evolution at deep magma-poor passive margins from Iberia-Newfoundland: a new point of view. *International Journal of Earth Sciences*, *98*(7), 1581–1597. https://doi.org/10.1007/s00531-008-0337-9

Peron-Pinvidic, G., & Osmundsen, P. T. (2016). Architecture of the distal and outer domains of the Mid-Norwegian rifted margin: Insights from the Rån-Gjallar ridges system. *Marine and Petroleum Geology*, *77*, 280–299. https://doi.org/10.1016/j.marpetgeo.2016.06.014

Péron-Pinvidic, G., Manatschal, G., Minshull, T. A., & Sawyer, D. S. (2007). Tectonosedimentary evolution of the deep Iberia-Newfoundland margins: Evidence for a complex breakup history. *Tectonics*, *26*(2). https://doi.org/10.1029/2006TC001970

Peron-Pinvidic, G., Manatschal, G., & Osmundsen, P. T. (2013). Structural comparison of archetypal Atlantic rifted margins: A review of observations and concepts. *Marine and Petroleum Geology*, *43*, 21–47. https://doi.org/10.1016/j.marpetgeo.2013.02.002

Peron-Pinvidic, G., Manatschal, G., & the "IMAGinING RIFTING" Workshop Participants. (2019). Rifted Margins: State of the Art and Future Challenges. *Frontiers in Earth Science*, *7*, 218. https://doi.org/10.3389/feart.2019.00218

Petri, B., Mohn, G., Štípská, P., Schulmann, K., & Manatschal, G. (2016). The Sondalo gabbro contact aureole (Campo unit, Eastern Alps): implications for mid-crustal mafic magma emplacement. *Contributions to Mineralogy and Petrology*, *171*(5), 52. https://doi.org/10.1007/s00410-016-1263-7

Picazo, S., Müntener, O., Manatschal, G., Bauville, A., Karner, G., & Johnson, C. (2016). Mapping the nature of mantle domains in Western and Central Europe based on clinopyroxene and spinel chemistry: Evidence for mantle modification during an extensional cycle. *Lithos*, *266–267*, 233–263. https://doi.org/10.1016/j.lithos.2016.08.029

Pichon, X. L., & Sibuet, J.-C. (1981). Passive margins: A model of formation. *Journal of Geophysical Research: Solid Earth*, *86*(B5), 3708–3720. https://doi.org/10.1029/JB086iB05p03708

Pinto, V. H. G., Manatschal, G., Karpoff, A. M., Ulrich, M., & Viana, A. R. (2017). Seawater storage and element transfer associated with mantle serpentinization in magma-poor rifted margins: A quantitative approach. *Earth and Planetary Science Letters*, *459*, 227–237. https://doi.org/10.1016/j.epsl.2016.11.023

Program, O. D. (1994). *Proceedings of the Ocean Drilling Program: Initial report. Part A*. The Program.

Qiu, X., Ye, S., Wu, S., Shi, X., Zhou, D., Xia, K., & Flueh, E. R. (2001). Crustal structure across the Xisha Trough, northwestern South China Sea. *Tectonophysics*, *341*(1), 179–193. https://doi.org/10.1016/S0040-1951(01)00222-0

Quirk, D. G., Shakerley, A., & Howe, M. J. (2014). A mechanism for construction of volcanic rifted margins during continental breakup. *Geology*, *42*(12), 1079–1082. https://doi.org/10.1130/G35974.1

Ranero, C. R., & Pérez-Gussinyé, M. (2010). Sequential faulting explains the asymmetry and extension discrepancy of conjugate margins. *Nature*, *468*(7321), 294–299. https://doi.org/10.1038/nature09520

Reid, I. (1989). Effects of lithospheric flow on the formation and evolution of a transform margin. *Earth and Planetary Science Letters*, *95*(1), 38–52. https://doi.org/10.1016/0012-821X(89)90166-0

Reston, T. J. (2007). The formation of non-volcanic rifted margins by the progressive extension of the lithosphere: the example of the West Iberian margin. *Geological Society, London, Special Publications*, *282*(1), 77–110. https://doi.org/10.1144/SP282.5

Reston, Tim J. (2009). The extension discrepancy and syn-rift subsidence deficit at rifted margins. *Petroleum Geoscience*, *15*(3), 217–237. https://doi.org/10.1144/1354-079309-845

Rey, P., Vanderhaeghe, O., & Teyssier, C. (2001). Gravitational collapse of the continental crust: definition, regimes and modes. *Tectonophysics*, *342*(3), 435–449. https://doi.org/10.1016/S0040-1951(01)00174-3

Rey, Patrice. (1993). Seismic and tectono-metamorphic characters of the lower continental crust in Phanerozoic areas: A consequence of post-thickening extension. *Tectonics*, *12*(2), 580–590. https://doi.org/10.1029/92TC01568

Ribes, C., Manatschal, G., Ghienne, J.-F., Karner, G. D., Johnson, C. A., Figueredo, P. H., et al. (2019). The syn-rift stratigraphic record across a fossil hyper-extended rifted margin: the example of the northwestern Adriatic margin exposed in the Central Alps. *International Journal of Earth Sciences*, *108*(6), 2071–2095. https://doi.org/10.1007/s00531-019-01750-6

Ros, E., Pérez-Gussinyé, M., Araújo, M., Romeiro, M. T., Andrés-Martínez, M., & Morgan, J. P. (2017). Lower Crustal Strength Controls on Melting and Serpentinization at Magma-Poor Margins: Potential Implications for the South Atlantic. *Geochemistry, Geophysics, Geosystems*, *18*(12), 4538–4557. https://doi.org/10.1002/2017GC007212

Rowan, M. G. (2014). Passive-margin salt basins: hyperextension, evaporite deposition, and salt tectonics. *Basin Research*, *26*(1), 154–182. https://doi.org/10.1111/bre.12043

Ru, K., & Pigott, J. D. (1986). Episodic Rifting and Subsidence in the South China Sea1. *AAPG Bulletin*, *70*(9), 1136–1155. https://doi.org/10.1306/94886A8D-1704-11D7-8645000102C1865D

Sapin, F., Ringenbach, J.-C., & Clerc, C. (2021). Rifted margins classification and forcing parameters. *Scientific Reports*, *11*(1), 8199. https://doi.org/10.1038/s41598-021-87648-3

Saunders, A. D., Norry, M. J., & Tarney, J. (1988). Origin of MORB and Chemically-Depleted Mantle Reservoirs: Trace Element Constraints. *Journal of Petrology*, *Special_Volume*(1), 415–445. https://doi.org/10.1093/petrology/Special_Volume.1.415

Saunders, A. D., Jones, S. M., Morgan, L. A., Pierce, K. L., Widdowson, M., & Xu, Y. G. (2007). Regional uplift associated with continental large igneous provinces: The roles of mantle plumes and the lithosphere. *Chemical Geology*, *241*(3), 282–318. https://doi.org/10.1016/j.chemgeo.2007.01.017

Savva, D., Meresse, F., Pubellier, M., Chamot-Rooke, N., Lavier, L., Po, K. W., et al. (2013). Seismic evidence of hyper-stretched crust and mantle exhumation offshore Vietnam. *Tectonophysics*, *608*, 72–83. https://doi.org/10.1016/j.tecto.2013.07.010

Savva, D., Pubellier, M., Franke, D., Chamot-Rooke, N., Meresse, F., Steuer, S., & Auxietre, J. L. (2014). Different expressions of rifting on the South China Sea margins. *Marine and Petroleum Geology*, *58*, 579–598. https://doi.org/10.1016/j.marpetgeo.2014.05.023

Sawyer, E. W. (1994). Melt segregation in the continental crust. *Geology*, *22*(11), 1019–1022. https://doi.org/10.1130/0091-7613(1994)022<1019:MSITCC>2.3.CO;2

Schimschal, C. M., & Jokat, W. (2018). The crustal structure of the continental margin east of the Falkland Islands. *Tectonophysics*, *724–725*, 234–253. https://doi.org/10.1016/j.tecto.2017.11.034

Schimschal, C. M., & Jokat, W. (2019). The Falkland Plateau in the context of Gondwana breakup. *Gondwana Research*, *68*, 108–115. https://doi.org/10.1016/j.gr.2018.11.011

Scrutton, R. A. (1979). On Sheared Passive Continental Margins. In C. E. Keen (Ed.), *Developments in Geotectonics* (Vol. 15, pp. 293–305). Elsevier. https://doi.org/10.1016/B978-0-444-41851-7.50020-0

Searle, M. P. (2010). Low-angle normal faults in the compressional Himalayan orogen; Evidence from the Annapurna–Dhaulagiri Himalaya, Nepal. *Geosphere*, *6*(4), 296–315. https://doi.org/10.1130/GES00549.1

Şengör, A. M. C. (1991). Plate tectonics and orogenic research after 25 years: Synopsis of a Tethyan perspective. *Tectonophysics*, *187*(1), 315–344. https://doi.org/10.1016/0040-1951(91)90427-T

Shi, X., Zhou, D., Qiu, X., & Zhang, Y. (2002). Thermal and rheological structures of the Xisha Trough, South China Sea. *Tectonophysics*, *351*(4), 285–300. https://doi.org/10.1016/S0040-1951(02)00162-2

Smallwood, J. R., & White, R. S. (2002). Ridge-plume interaction in the North Atlantic and its influence on continental breakup and seafloor spreading. *Geological Society, London, Special Publications*, *197*(1), 15–37. https://doi.org/10.1144/GSL.SP.2002.197.01.02

Sun, W. (2016). Initiation and evolution of the South China Sea: an overview. *Acta Geochimica*, *35*(3), 215–225. https://doi.org/10.1007/s11631-016-0110-x

Sun, Z., Lin, J., Qiu, N., Jian, Z., Wang, P., Pang, X., et al. (2019). The role of magmatism in the thinning and breakup of the South China Sea continental marginSpecial Topic: The

South China Sea Ocean Drilling. *National Science Review*, *6*(5), 871–876. https://doi.org/10.1093/nsr/nwz116

Sutra, E., Manatschal, G., Mohn, G., & Unternehr, P. (2013). Quantification and restoration of extensional deformation along the Western Iberia and Newfoundland rifted margins: Strain Distribution Along Rifted Margins. *Geochemistry, Geophysics, Geosystems*, *14*(8), 2575–2597. https://doi.org/10.1002/ggge.20135

Svensen, H., Planke, S., Malthe-Sørenssen, A., Jamtveit, B., Myklebust, R., Rasmussen Eidem, T., & Rey, S. S. (2004). Release of methane from a volcanic basin as a mechanism for initial Eocene global warming. *Nature*, *429*(6991), 542–545. https://doi.org/10.1038/nature02566

Taylor, B., & Hayes, D. E. (1980). The Tectonic Evolution of the South China Basin. In *The Tectonic and Geologic Evolution of Southeast Asian Seas and Islands* (pp. 89–104). American Geophysical Union (AGU). https://doi.org/10.1029/GM023p0089

Taylor, B., & Hayes, D. E. (1983). Origin and History of the South China Sea Basin. In *The Tectonic and Geologic Evolution of Southeast Asian Seas and Islands: Part 2* (pp. 23–56). American Geophysical Union (AGU). https://doi.org/10.1029/GM027p0023

Taylor, B., Goodliffe, A., & Martinez, F. (2009a). Initiation of transform faults at rifted continental margins. *Comptes Rendus Geoscience*, *341*(5), 428–438. https://doi.org/10.1016/j.crte.2008.08.010

Taylor, B., Goodliffe, A., & Martinez, F. (2009b). Initiation of transform faults at rifted continental margins. *Comptes Rendus Geoscience*, *341*(5), 428–438. https://doi.org/10.1016/j.crte.2008.08.010

Thybo, H., & Artemieva, I. M. (2013). Moho and magmatic underplating in continental lithosphere. *Tectonophysics*, *609*, 605–619. https://doi.org/10.1016/j.tecto.2013.05.032

Tomasi, S. (2017). *Interaction Magmatisme-déformation au sein des marges passives, une double approche qualitative : l'exemple du canal du Mozambique* (These en préparation). Strasbourg. Retrieved from http://www.theses.fr/s174395

Tomasi, S., Kusznir, N., Manatschal, G., & Despinois, F. (2021). The challenge in restoring magma-rich rifted margins: The example of the Mozambique-Antarctica conjugate margins. *Gondwana Research*, *95*, 29–44. https://doi.org/10.1016/j.gr.2021.03.009

Tucholke, B. E., Sawyer, D. S., & Sibuet, J.-C. (2007). Breakup of the Newfoundland–Iberia rift. *Geological Society, London, Special Publications*, *282*(1), 9–46. https://doi.org/10.1144/SP282.2

Tugend, J., Manatschal, G., Kusznir, N. J., & Masini, E. (2015). Characterizing and identifying structural domains at rifted continental margins: application to the Bay of Biscay margins and its Western Pyrenean fossil remnants. *Geological Society, London, Special Publications*, *413*(1), 171–203. https://doi.org/10.1144/SP413.3

Tugend, Julie, Gillard, M., Manatschal, G., Nirrengarten, M., Harkin, C., Epin, M.-E., et al. (2018). Reappraisal of the magma-rich versus magma-poor rifted margin archetypes. *Geological Society, London, Special Publications*, SP476.9. https://doi.org/10.1144/SP476.9

Tugend, Julie, Gillard, M., Manatschal, G., Nirrengarten, M., Harkin, C., Epin, M.-E., et al. (2020). Reappraisal of the magma-rich versus magma-poor rifted margin archetypes. *Geological Society, London, Special Publications*, *476*(1), 23–47. https://doi.org/10.1144/SP476.9

Van, J. W., Der, R. M. van, & Cloetingh, S. a. P. L. (2004). Crustal thickening in an extensial regime: application to the mid-Norwegian Voring margin. *Tectonophysics*, *387*, 217–228. https://doi.org/10.1016/j.tecto.2004.07.049

Vanderhaeghe, O. (2009). Migmatites, granites and orogeny: Flow modes of partially-molten rocks and magmas associated with melt/solid segregation in orogenic belts. *Tectonophysics*, *477*(3), 119–134. https://doi.org/10.1016/j.tecto.2009.06.021

Vanderhaeghe, O., Teyssier, C., & Wysoczanski, R. (1999). Structural and geochronological constraints on the role of partial melting during the formation of the Shuswap metamorphic core complex at the latitude of the Thor-Odin dome, British Columbia. *Canadian Journal of Earth Sciences*, *36*(6), 917–943. https://doi.org/10.1139/e99-023

Vink, G. E. (1982). Continental rifting and the implications for plate tectonic reconstructions. *Journal of Geophysical Research: Solid Earth*, *87*(B13), 10677–10688. https://doi.org/10.1029/JB087iB13p10677

Wang, P. (2019). New insights into marine basin opening. *National Science Review*, *6*(5), 870–870. https://doi.org/10.1093/nsr/nwz099

Wang, P., Li, Q., & Li, C.-F. (2014). *Geology of the China Seas*. Amsterdam: Elsevier.

Wang, Q., Zhao, M., Zhang, H., Zhang, J., He, E., Yuan, Y., & Qiu, X. (2020). Crustal velocity structure of the Northwest Sub-basin of the South China Sea based on seismic data reprocessing. *Science China Earth Sciences*. https://doi.org/10.1007/s11430-020-9654-4

Watts, A. B., & Schubert, G. (2009). *Treatise on Geophysics, Volume 6: Crust and Lithosphere Dynamics*. Elsevier.

Wernicke, B. (1981). Low-angle normal faults in the Basin and Range Province: nappe tectonics in an extending orogen. *Nature*, *291*(5817), 645–648. https://doi.org/10.1038/291645a0

Wernicke, B. (1985). Uniform-sense normal simple shear of the continental lithosphere. *Canadian Journal of Earth Sciences*, *22*(1), 108–125. https://doi.org/10.1139/e85-009

White, R., & McKenzie, D. (1989). Magmatism at rift zones: The generation of volcanic continental margins and flood basalts. *Journal of Geophysical Research: Solid Earth*, *94*(B6), 7685–7729. https://doi.org/10.1029/JB094iB06p07685

Whitmarsh, R. B., Manatschal, G., & Minshull, T. A. (2001). Evolution of magma-poor continental margins from rifting to seafloor spreading. *Nature*, *413*(6852), 150–154. https://doi.org/10.1038/35093085

Wilson, J. T. (1966). Did the Atlantic Close and then Re-Open? *Nature*, *211*(5050), 676–681. https://doi.org/10.1038/211676a0

Wu, Z., Li, J., Ruan, A., Lou, H., Ding, W., Niu, X., & Li, X. (2012). Crustal structure of the northwestern sub-basin, South China Sea: Results from a wide-angle seismic experiment. *Science China Earth Sciences*, *55*(1), 159–172. https://doi.org/10.1007/s11430-011-4324-9

Xie, X., Ren, J., Pang, X., Lei, C., & Chen, H. (2019). Stratigraphic architectures and associated unconformities of Pearl River Mouth basin during rifting and lithospheric breakup of the South China Sea. *Marine Geophysical Research*. https://doi.org/10.1007/s11001-019-09378-6

Yao, B., Zhang, L., Wei, Z., Yi, H., Lin, Z., Wan, L., et al. (2011). THE MESOZOIC TECTONIC CHARACTERISTICS AND SEDIMENTARY BASINS IN THE EASTERN MARGIN OF SOUTH CHINA: THE MESOZOIC TECTONIC CHARACTERISTICS AND SEDIMENTARY BASINS IN THE EASTERN MARGIN OF SOUTH CHINA. *Marine Geology & Quaternary Geology*, *31*(3), 47–60. https://doi.org/10.3724/SP.J.1140.2011.03047

Ye, Q., Mei, L., Shi, H., Camanni, G., Shu, Y., Wu, J., et al. (2018). The Late Cretaceous tectonic evolution of the South China Sea area: An overview, and new perspectives from 3D seismic reflection data. *Earth-Science Reviews*, *187*, 186–204. https://doi.org/10.1016/j.earscirev.2018.09.013

Zhang, C., Manatschal, G., Pang, X., Sun, Z., Zheng, J., Li, H., et al. (2020). Discovery of Mega-Sheath Folds Flooring the Liwan Subbasin (South China Sea): Implications for the Rheology of Hyperextended Crust. *Geochemistry, Geophysics, Geosystems*, *21*(7), e2020GC009023. https://doi.org/10.1029/2020GC009023

Zhang, Cuimei, Sun, Z., Manatschal, G., Pang, X., Li, S., Sauter, D., et al. (2021). Ocean-continent transition architecture and breakup mechanism at the mid-northern South

China Sea. *Earth-Science Reviews*, *217*, 103620. https://doi.org/10.1016/j.earscirev.2021.103620

Zhang, Cuimei, Sun, Z., Manatschal, G., Pang, X., Qiu, N., Su, M., et al. (2021). Syn-rift magmatic characteristics and evolution at a sediment-rich margin: Insights from high-resolution seismic data from the South China Sea. *Gondwana Research*, *91*, 81–96. https://doi.org/10.1016/j.gr.2020.11.012

Zhao, M., Sibuet, J.-C., & Wu, J. (2019). The South China Sea and Philippine Sea plate intermingled fates. *National Science Review*, nwz107. https://doi.org/10.1093/nsr/nwz107

CHAPTER II

The tectono-stratigraphic and magmatic evolution of conjugate rifted margins: insights from the NW South China Sea

Peng Chao[1*], Gianreto Manatschal[1*], Pauline Chenin[1], Jianye Ren[2], Cuimei Zhang[3], Xiong Pang[4], Jinyun Zheng[4], Linlong Yang[5] and Nick Kusznir[6]

[1]Université de Strasbourg, CNRS, ENGEES, ITES UMR 7063, Strasbourg F-67084, France

[2]College of Marine Science and Technology, China University of Geosciences, Wuhan, China

[3]Southern Marine Science and Engineering Guangdong Laboratory, Guangzhou, China

[4]CNOOC Ltd.-Shenzhen, Branch, Shenzhen , China

[5]Working Station for Postdoctoral Scientific Research, Shengli Oilfield, Dongying, China

[6]School of Environmental Sciences, Liverpool University, Liverpool, United Kingdom

[*]Corresponding authors:

Peng Chao (c.peng@unistra.fr) and Gianreto Manatschal (manat@unistra.fr)

Key Points:

- The tectono-stratigraphic architecture of a section across the NW South China Sea propagator is described and restored
- The stratigraphic and magmatic evolution of crustal thinning is documented in a Wheeler Diagram
- Distinction between stratigraphic and tectonic top basement has fundamental consequences for kinematic restorations

Abstract

This study is based on a careful analysis of high-quality, reflection seismic sections located at the tip of the NW South China Sea propagator. Based on the example of the CGN-1 section, one of the rare seismic lines imaging the complete tectono-sedimentary and magmatic architecture of a pair of conjugate rifted margins, we: 1) provide a detailed description of the crustal architecture, 2) define extensional domains, which we relate to specific deformation phases, and 3) determine the tectono-stratigraphic and magmatic evolution linked to rifting. Based on these, we propose a kinematic restoration relying on a systematic methodology that enables to quantify the amounts of extension and associated strain rates. We discuss the link between the kinematic evolution and the stratigraphic and magmatic record and illustrate it in a Wheeler Diagram. It is the first time such an approach is used to decipher the tectono-magmatic and sedimentary evolution of a complete syn-rift mega-sequence across a conjugate rifted margin. Based on the identification and characterization of distinct stratal patterns and crustal architectures, this study proposes qualitative and quantitative criteria to interpret two critical rifting events, which are necking and hyperextension. These two events are linked to the individualization and subsequent dismembering of a so-called keystone, here referred to as H-block. The results presented in this study challenge previous interpretations of correlative surfaces through introducing different types of top basement and distinguishing between syn-tectonic packages within the syn-rift record. This approach leads to new interpretations for the tectono-stratigraphic and magma evolution of the NW South China Sea and has the potential to be used as a new approach to analyze, quantify and correlate events recorded in seismic sections across rifted margins.

1. Introduction

In the last two decades, the understanding of rifted margins, in particular of their most distal parts has significantly evolved (Abdelmalak et al., 2015; Brune et al., 2014; Manatschal et al., 2015; Peron-Pinvidic et al., 2019; Peron-Pinvidic & Osmundsen,

2018). The access to high resolution, long-offset seismic and local drill hole data enabled the development of new concepts to explain crustal/lithospheric thinning, breakup and onset of seafloor spreading (Deng et al., 2020; Larsen et al., 2018; Osmundsen & Ebbing, 2008; Peron-Pinvidic et al., 2019; Reston, 2007; Sun et al., 2018; Sutra & Manatschal, 2012; Wang et al., 2018; Wang, 2019). However, at present, no detailed study has evaluated the spatial and temporal evolution of rifting at conjugate margins and documented it in a Wheeler Diagram (Qayyum et al., 2017; Wheeler, 1964). Such a documentation of the tectono-sedimentary and magmatic evolution requires the proper kinematic restoration of a complete transect across conjugate margins, and a first-order quantification of extension rates and creation of accommodation space during the necking and hyperextension stages.

At present, there are still many open questions related to when, how, and under what conditions major crustal thinning (necking) and crustal breakup occur and how these processes are recorded in the stratigraphic and magmatic “tape recorder”. Answering these questions will further improve the understanding of some of the most fundamental processes in Plate Tectonics, specifically how continents rift apart, rift basins form and seafloor spreading initiates. In order to answer to these questions, the access to the stratigraphic and magmatic tape recorder is fundamental. However, at present it is not only poorly understood but also barely documented, in particular in the most distal parts of rifted margins. In particular, the efficient record of syn-rift deformation in seismic data requires high sedimentation rates, which are, however, rare at distal margins. Moreover, most geophysical acquisitions and geological studies document only one margin, which makes it difficult to unravel the evolution of the entire conjugate rift system and associated breakup processes. Access to high quality seismic images of well-preserved pairs of conjugate margins displaying high sedimentation rates during rifting and breakup is rare and exists only in a handful of places such as the Red Sea (Ligi et al., 2018), the Gulf of Aden (Leroy et al., 2012), the Woodlark Basin (Taylor et al., 1999), the Gulf of California (Lizarralde et al., 2007) and the South China Sea (SCS).

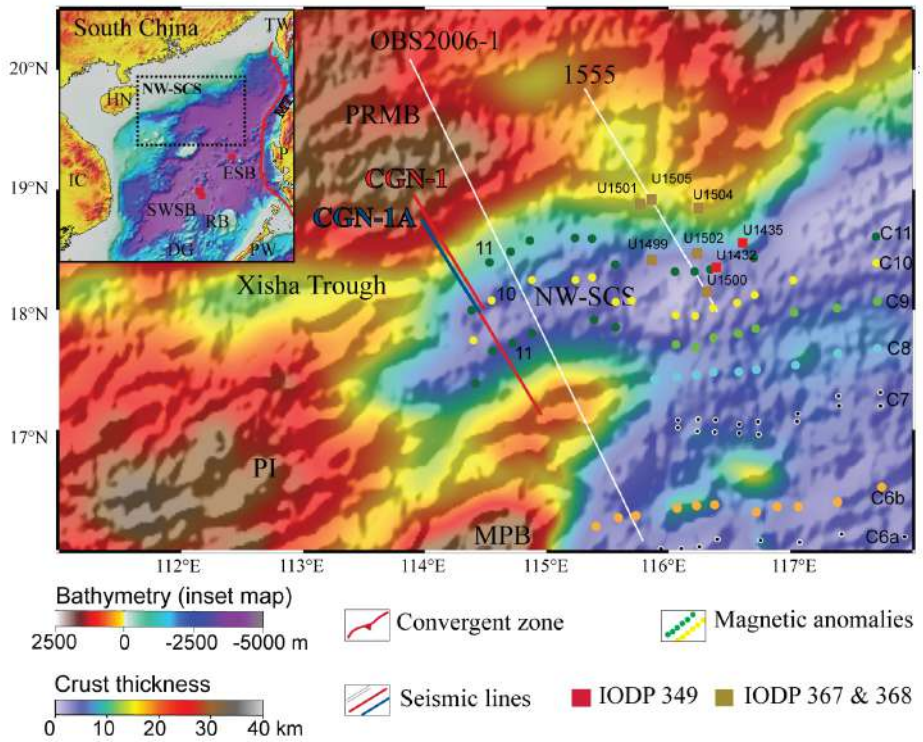

Figure II.1. *Crustal thickness map based on gravity inversion with superimposed shaded relief free-air gravity anomaly from Gozzard el al. (2019). Inset on the top left corner shows bathymetric map of the NW South China Sea (NW-SCS) with the location of the principal seismic reflection and refraction lines used in this paper and the IODP drill sites (Li et al., 2015; Sun et al., 2018). The location of the magnetic anomalies is based on Briais et al. (1993). Abbreviations used in the figure: DG, Dangerous Ground (Nansha); ESB, East Sub-Basin; HN, Hainan; IC, Indochina; MPB, Macclesfield-Paracel Bank; MT, Manila Trench; NW-SCS, North West South China Sea; North West Sub-Basin; PI, Paracel Islands (Xisha Islands); PRMB, Pearl River Mouth Basin; PW, Palawan; RB, Reed Bank (Liyue); SWSB, South West Sub-Basin; TW, Taiwan.*

In this study, we focus on the tip of the NW-SCS, where seafloor spreading propagated towards the Xisha Trough before it failed (Fig. II.1). In this region, numerous, high-resolution seismic reflection surveys provide a high quality imaging of the sediment-rich and magma-poor conjugate margins, providing an excellent and rare opportunity to explore and describe the complete rift evolution. Drill hole data of the International Ocean Discovery Program (IODP) Expeditions 367/368/368X drilled several sites at the Ocean–Continent Transition (OCT) approximately 200 km further east (Fig. II.1) (Larsen et al., 2018). More recent studies showed that rifting and breakup along the SCS are, in many regards, different from classical Atlantic-type magma-poor or magma-rich margins (Sun et al., 2018; Ding et al., 2019; Luo et al.,

2021). Neither evidence for exhumed mantle, nor Seaward Dipping Reflections (SDRs) have been found in the SCS. The occurrence of long-offset extensional detachment faults (Yang et al., 2018; Zhao et al., 2018; Deng et al., 2020; Zhang et al., 2020) and syn-rift magmatic systems (Ding et al., 2019; Zhang et al., 2021) show complex interactions between extensional and magmatic systems during rifting and breakup. These results require a more detailed analysis of the spatial and temporal tectono-magmatic and sedimentary evolution, which is the aim of this study.

This study is based on a careful analysis of a dense, high-resolution seismic reflection data set of exceptional quality that images the conjugate margins at the tip of the NW-SCS propagator. The overall margin architecture is best imaged in the CGN-1 reflection seismic section provided by CNOOC (Fig. II.2). The aim of this study is to: (1) provide a detailed description of the crustal architecture, define extensional domains as well as the margin architecture, and determine the tectono-sedimentary and magmatic evolution of this conjugate rift system; (2) understand the interplay between deformation, sedimentation and magmatic processes during rifting and breakup in 2D; (3) analyze the evolution of deformation through time and space by linking the tectono-stratigraphic evolution with the observed crustal thinning and synthesize it in a Wheeler diagram, and (4) quantify the amount of strain and strain-rate accommodated along these conjugate margins. The study proposes for the first time a Wheeler Diagram for a complete syn-rift mega-sequence that describes and quantifies the temporal and spatial evolution of a pair of conjugate rifted margins from crustal thinning (necking), to hyperextension, breakup and early seafloor spreading. Moreover, based on identifying and characterizing system tracts (a *system tract* or *tract* encompasses all the sediments deposited during a given period of time), distinctive stratal packages and crustal architectures, this study proposes qualitative and quantitative criteria that help to interpret the processes linked to two critical rift phases, which are the necking and hyperextension phases.

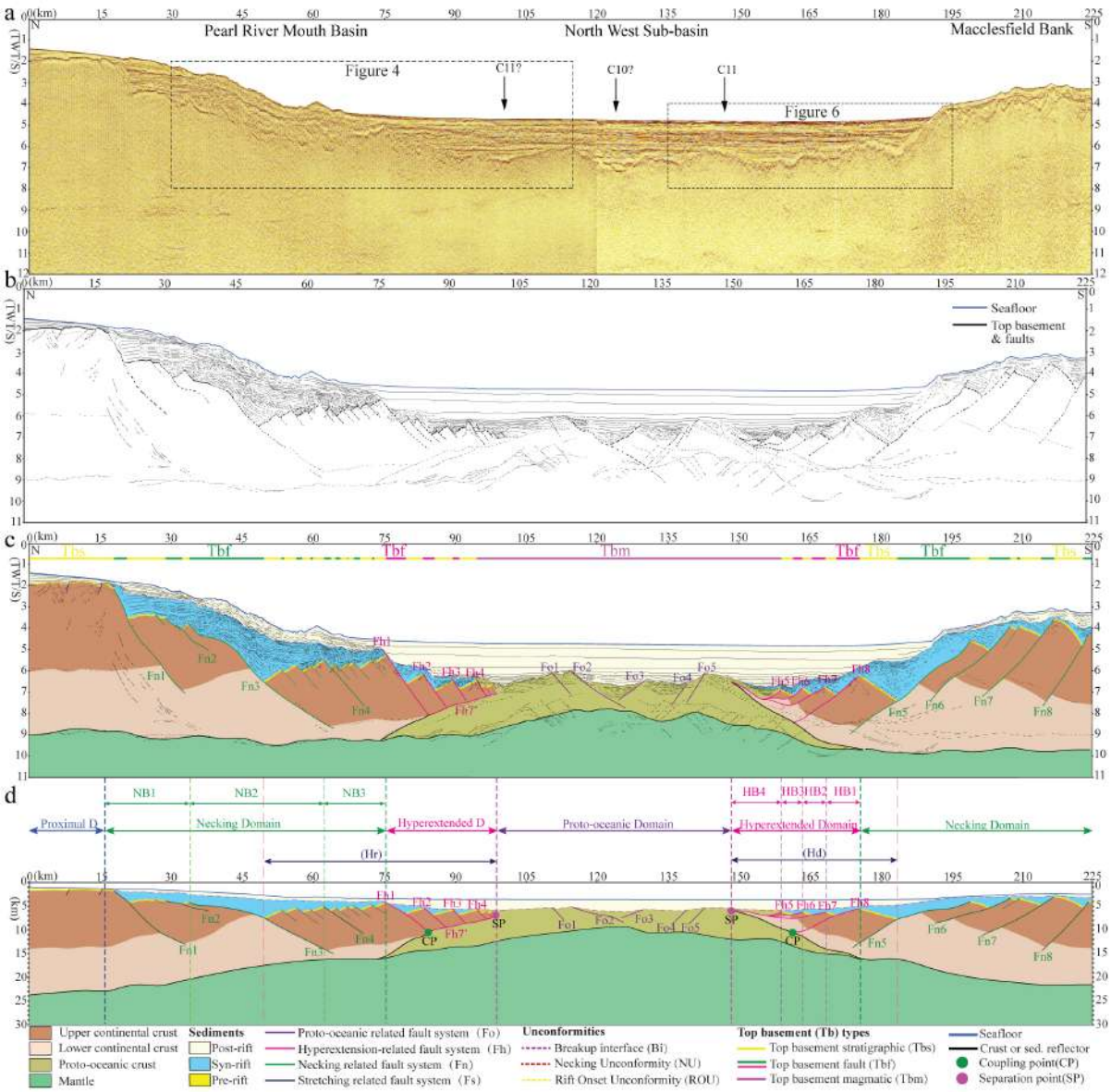

Figure II.2. *CGN-1 reflection seismic section across the NW-SCS. For location see Fig. II.1. (a) Time migrated reflection seismic section CGN-1. (b) Line drawing of the seismic section CGN-1. (c) Seismic interpretation of CGN-1. (d) Interpreted CGN-1 section with a time to depth conversion.*

2. Geological setting

2.1. Geological evolution of the SCS

The SCS is a rhomb-shaped marginal sea that is surrounded by three major tectonic plates, the Pacific, the Eurasian, and the Indian-Australian plates (Taylor & Hayes, 1983). The SCS is the largest marginal sea in the western Pacific region, which is comprised of three major sub-basins, the eastern, northwestern and southwestern sub-basins (Fig. II.1). To the east, the SCS subducts beneath the Luzon Arc along the

Manila Trench. To the west, the SCS is bounded by a strike-slip fault system. To the south it is bounded by the Dangerous Grounds and Reed Bank, corresponding to rifted blocks that collide with the Borneo Block further south. To the north, the SCS displays a more than 500 km-wide continental margin (Hall, 2012; Sibuet et al., 2016). The formation and evolution of the SCS are thus associated with both subduction and rift systems (Hall & Breitfeld, 2017; Lin et al., 2019). The pre-rift evolution of the SCS is complex and controlled by the Mesozoic Yanshanian Orogeny and the paleo-Pacific subduction (Li et al., 2018, 2020; Ye et al., 2018a and 2018b). Gravity and joint inversion methods show lateral variations of basement thicknesses across the conjugate margins (Gozzard et al., 2018; Nirrengarten et al., 2020). The thermal history and structural complexity observed along and across the SCS are partly controlled by the pre-rift evolution, pointing to the importance of orogenic/subduction inheritance in controlling subsequent rifting (Wang et al., 2018; Bai et al., 2019; Sun et al., 2019).

The age of onset of the SCS rifting is poorly constrained and usually referred to as 65 Ma, corresponding to the stratigraphic marker horizon “Tg” (Xie et al., 2019). Two phases of rifting have been defined: the first one is from early Paleocene to middle Eocene, the later one is from middle Eocene to early Oligocene. Breakup is widely accepted to propagate from east to west (Franke et al., 2011, 2014). At about 23 Ma, the active ridge stepped to the south, resulting in the opening of the southwestern sub-basin. Seafloor spreading stopped at about 16 Ma (Briais et al., 1993; Li et al., 2014, 2015)

2.2. Structure of the NW-SCS

The present study focuses on the NW-SCS, and more precisely on the termination of the V-shaped oceanic propagator, which separates the Western Pearl River Mouth Basin and the China continental shelf in the north from the Macclesfield-Paracel Block (Zhongsha-Xisha) in the south (Fig. II.1). Based on the presence of magnetic anomalies C11 and central C10, Briais et al. (1993) interpreted the opening of the NW-SCS to have occurred around 30 to 28 Ma (according to the geomagnetic time scale of Gee et al., 2007). In contrast, Cameselle et al. (2017) proposed a different magnetic anomaly interpretation, with two stages of opening: contemporaneous with the C9

magnetic anomaly in the south and somewhat younger in the north. Here we follow the interpretation of Briais et al., (1993). There is, however, a general consensus that the spreading center propagated westwards and died shortly before reaching the Xisha Trough. The crustal thickness of the study area is constrained by the refraction seismic line OBS2006-1 (for location see Fig. II.1) (Wu et al., 2012; Weiwei et al., 2012). Crustal thickness and thinning factors of the study area have been recently published by Gozzard et al. (2018). Seismic interpretations of the crustal structure have been discussed by Ding et al. (2011, 2019), Franke et al. (2014), Gao et al. (2016), Wang et al. (2020), Wu et al. (2012, 2019) and Cameselle et al. (2015, 2021). In this paper we focus on the tectono-stratigraphic and magmatic evolution during necking and breakup at the tip of NW-SCS propagator (Fig. II.1).

3. Data, methods and terminology

3.1. Data used and acquisition parameters

With permission of CNOOC, we had access to a dense, high-resolution seismic data set from which we chose two lines for publication, the CGN-1 and CGN-1A, the latter located 4 km west of the former (for location see Fig. II.1). Both lines are multichannel seismic (MCS) sections, which record down to 12 s Two-Way Travel Time (TWT). The seismic survey used an air gun array with a total volume of 3680 cubic inches and a towing depth of 6 m served as seismic source and cable line. Data were acquired with a 7.5 km long streamer with 600 channels and group intervals of 12.5 m. Record length was 12s TWT at a sampling interval of 2 ms and shot interval of 37.5 m (Lei & Ren, 2016). The CGN-1 line is one of the rare seismic reflection lines imaging the tectono-sedimentary and magmatic structure, intra-basement and Moho reflections, as well as the transition to first oceanic crust across a pair of conjugate rifted margins (Fig. II.2). The CGN-1 line images from the northern continental shelf to the Macclesfield-Paracel Bank. The line is 225 km long and consists of two parts. The northern part is 120 km, the southern is 105 km. The offset between the nearly parallel CGN-1 and CGN-1A lines is 4 km at the closest tip.

3.2. Method

In this study, we use seismic observations, geophysical methods and geological concepts to define and correlate stratigraphic horizons, and to describe crustal structures and the rift architecture. We define, based on reflection geometries and seismic facies, an acoustic basement and a sedimentary sequence that we subdivide into a syn- and a post-rift mega-sequence. Pre-rift sediments are likely to exist in the CGN-1 and CGN-1A lines but as they may be related to the complex Mesozoic evolution of the SCS, they are difficult to identify. Thus, we define them as part of the acoustic basement.

3.2.1. Seismic interpretation

The seismic interpretation presented in this study is subdivided in five successive steps. First (section 4.1), we identify first-order seismic interfaces (seafloor, top acoustic basement, Moho). Second (section 4.2), we define the crustal architecture and related rift domains based on the formerly identified first-order interfaces. Third (section 4.3), we describe the intra-sediment reflections, which enable us to define sedimentary mega-sequences, tracts, and syn- and post-tectonic packages (for terminology see below). Forth (section 4.4), we map intra-basement structures and faults, including fault offsets, sealing levels and decoupling levels. Finally (section 4.5), we identify magmatic additions. Since the description of a full magmatic system, including the complete plumbing system, is difficult if not impossible in seismic reflection data, this last step focuses only on magmatic additions that intrude into sediments and/or extrude during final rifting and early seafloor spreading. Note that the seismic interpretations presented in Fig. II.2, in particular the interpretation of the intra-sedimentary packages and the identification of intra-basement faults, are synthesized from dense set of high-resolution seismic sections, located both west and east of the CGN1 line.

The proposed approach builds on an interpretation, in which first-order and objective observations are first established (seafloor, Tb, Moho), providing the frame for subsequent, more subjective interpretations (intra-sediment and basement structures). It is important to state that, in the absence of drill hole data, there are multiple seismic interpretations for a given seismic section. Our aim here is to provide a

set of observations that enables us to produce a coherent description of the stratigraphic architecture of the conjugate margins based on observed seismic geometries, seismic facies and structures. Based on the seismic interpretation presented in section 4, we build a temporal and spatial framework (Wheeler Diagram) for the entire conjugate section, which links the stratigraphic tape recorder (magma and sediments) with structural/kinematic observations (faults).

3.2.1. Time to depth conversion of CGN-1 section

The CGN-1 section investigated in this study (Fig. II.2a) is in time. In order to propose a kinematic restoration of the section, we propose a time to depth conversion. The refraction line OBS 2006-1 (Wu et al., 2012) is located 35 km further west of the CGN-1 section (Fig. II.1). We therefore assume that the velocities defined in the refraction line can be used to convert our CGN-1 section from time to depth (Fig. II.2d). In the refraction line, two different sediment packages with different velocities have been defined, an upper part with 2.5 km/s, and a lower part with 3.5 km/s. Upper crustal velocities are defined with 6 km/s, the lower crust has average velocities of 6.5 km/s. The time-depth conversion included the follow steps: (1) interpretation of the seismic section CGN-1 in time: identification of seafloor, interface post- and syn-rift mega-sequence, top acoustic basement, interface between upper and lower crust (which can only be defined in the proximal margin), and Moho; (2) picking of the TWT depth of all five interfaces every ca. 3 km and at all singular points (i.e. in the presence of faults, the depth was determined on either side); (3) calculation of the depth of each of the five interfaces using the OBS 2006-1 velocity data referred above; (4) construction of an equivalent section in depth with the four depth interfaces; and (5) addition of the faults into the new depth section (the location of breakaways of faults in the depth converted section is same as in the time section).

3.3. Terminology

3.3.1. Definition of first order interfaces

Although first-order seismic interfaces such as top acoustic basement and Moho represent physical boundaries that can be objectively imaged and observed, their nature is subject to geological interpretation. Top acoustic Basement (Tb) is defined in

this study as a high-amplitude and well-imaged reflection that corresponds to the interface between compactable sediments and acoustic basement. In such a description, Tb represents an interface without any time or genetic connotation. In the discussion (section 6) we will distinguish between three types of Tb interfaces, which are: stratigraphic (Tb_s), tectonic/fault (Tb_f) and magmatic (Tb_m). Besides, we define the Moho as a reflector corresponding to a velocity contrast between crustal and mantle rocks. In time sections, Warner (1987) showed that Moho appears at a rather constant two-way travel time despite the highly variable structure of the crust above. The apparent flatness of the Moho on reflection seismic sections in time, also referred to as the "10 s rule", is an artefact produced when the crust is in local isostatic equilibrium. In the SCS, thermal equilibrium has not been achieved yet and the Moho is typically between 9 and 8 s TWT (Nirrengarten et al., 2020). Moho can correspond either to a contact between continental crust and mantle, between hydrated mantle (serpentinization front) and pristine mantle, or between new igneous material (oceanic crust) and mantle. Thus, Moho is either a petrological (compositional) or a geophysical (velocity) interface. Note that since different rocks can have similar velocities, the interpretation of Moho is non-unique when using geophysical data only.

3.3.2. Definition of rift domains

Rift domains have been defined based on: 1) total accommodation space, which we define as the space between sea level and Tb that is occupied by sediments or water; and 2) thickness and shape of the crust for the parts of the margins where magmatic additions are of subordinate importance (e.g., Sutra et al., 2013; Tugend et al., 2015; Haupert et al., 2016). From proximal to distal, these domains are the *stretching*, *necking*, *hyperextended* and *proto-oceanic* domains. These domains are thought to have formed sequentially as the result of different extension modes and due to changes in the bulk rheology of the extending lithosphere (Lavier and Manatschal 2006; Sutra et al. 2013; Ribes et al. 2019; Chenin et al., subm.). However, it is important to keep in mind that the rift domain concept has been developed for Atlantic-type magma-poor rifted margins and cannot be applied directly to the SCS. In this study we have adapted the rift domain concept to the study area.

3.3.3. Definition of sedimentary sequences, faults and magmatic additions

We define the sedimentary layer as that bounded by Tb and seafloor and made of compactable sediments. As stated above, sediments deposited prior to rifting (e.g., pre-rift sediments) are interpreted as part of the acoustic basement. The sedimentary layer is subdivided into a syn-rift mega-sequence and a post-rift mega-sequence. The limit between the two is defined as the breakup interface (Bi), which theoretically corresponds to an isochron but is in reality more complex. In seismic sections, it is marked by the onset of passive infill in the distal domain. The syn-rift mega-sequence is subdivided in 5 tracts. Each tract corresponds to a mappable time sequence. Each tract contains syn- and post-tectonic packages that are defined based on geometrical relationships between fault structures and reflections. Syn-tectonic packages are defined either by growth structures (thickening into faults) over upward concave faults or downlapping/wedging geometries over downward concave, long-offset faults (Fig. II.3). We stress that syn-tectonic packages are not limited to growth packages thickening into high-angle normal faults since syn-tectonic packages overlaying long-offset, exhumation faults can show wedging geometries as described from necking and hyperextended domains (Fig. II.3; see also Gillard et al., 2016). Note also that lateral transitions from high-angle to low-angle fault structures can result in a changes in the sediment architectures that also depend on the type of sediments involved and their transport diection (e.g., Fig. II.3; Peron-Pinvidic et al. (2007) and Masini et al., (2011)). Thus, syn-tectonic packages reflect local fault activity and the resulting sediment architecture depends on the fault architecture. In contrast, post-tectonic packages show passive infill (onlapping or draping sediments) and occur outside the locations of active deformation.

Faults are not directly imaged as such by seismic methods. However, high-angle faults can be deduced by the observation of offsets of Tb and/or other interfaces. In contrast, low-angle extensional detachment faults are more difficult to recognize since they can coincide with Tb. In this study, we identify the breakaways of faults and, wherever possible, the tract sealing a fault. This enables us to date the fault. We also define the level where faults sole out at depth. This location may coincide with a

rheological boundary (i.e., a brittle–ductile transition), which corresponds in the proximal margin to the interface separating brittle upper crust from ductile lower crust. In distal parts, distinguishing between brittle and ductile crusts is more difficult, in particular where the crust has been thinned to less than 10 km. The reason is that the rheology of the crust changes during rifting (e.g., embrittlement of the crust; Pérez-Gussinyé et al., 2003) and formerly ductile crust can evolve into the brittle field during exhumation along extensional detachment faults.

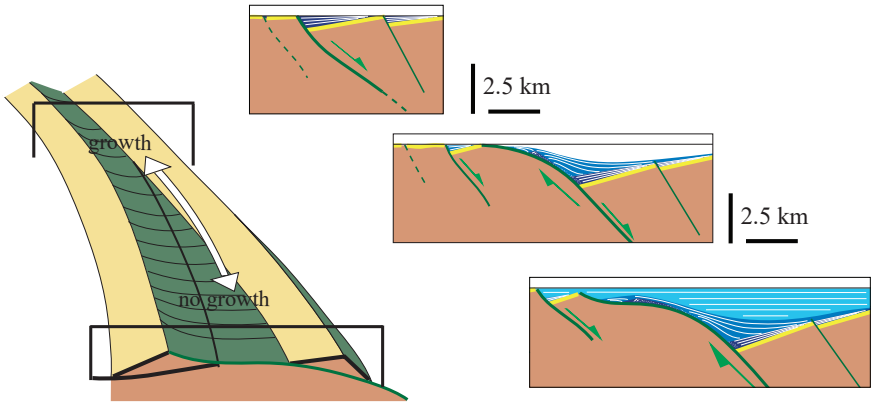

Figure II.3. *Along strike change of rift and sediment architecture from a high-angle normal fault to a down-ward convace long offset detachment fault (modified after Péron-Pinvidic et al. 2007).*

4. Seismic interpretation

4.1. Main interfaces

4.1.1. Seafloor

The seafloor is well imaged and corresponds to a high-amplitude, continuous reflection (Figs. II.2a and II.b). It is shallow dipping from km 0 to 20 and lies between 1.4 and 1.8 s TWT. From km 20 to 67, seafloor exhibits irregular undulations and is predominately dipping oceanward, while its depth drops from 1.8 to 4.4 s TWT. From km 67 to 190, seafloor is approximately horizontal, slightly higher at both ends, and lies between 4.4 and 4.7 s TWT. From km 190 to 225, seafloor rises gradually from 4.5 to 3.2 s TWT.

4.1.2. Top basement (Tb)

From km 0 to 18, Tb is a high-amplitude and well-imaged reflection laying between 2.2 and 1.8 s TWT, offset by small faults dipping continent-ward at km 8 and km 15. From km 15 to 22, Tb is offset by larger oceanward dipping faults and deepens from 2 to 3.5s TWT. From km 22 to 28, Tb is approximately horizontal and lies at ca. 3.5 s TWT. From km 28 to 50, Tb deepens from 3.5 to 6 s TWT. From km 50 to 75, Tb is offset by small faults. Although Tb is ill-defined at this location, we consider that it lies at the interface between two distinct types of seismic facies. Indeed, reflectivity is chaotic at deep levels (below 6.5 s TWT), while it is largely parallel and offset by small faults above 6 s TWT. Based on this assumption, we estimate that Tb rises from 6.5 to 5.3 s TWT between km 50 and 75. From km 75 to 100, Tb dips toward the north, is offset by small faults, and deepens from 5.3 to 6.8 s TWT. From km 100 to 115, Tb corresponds to a high-amplitude reflection that gradually rises from 6.8 to 6 s TWT. From km 115 to 130, Tb deepens from 6 to 7.3 s TWT, which is the deepest part of the basement across the section. Between km 130 and 185, Tb is tilted toward the south and dissected by faults. It lies between 6.8 and 6.2 s TWT and then rises from 7.2 to 6.2 s TWT. From km 185 to 225, Tb is tilted toward the south and offset by faults. It rises from 6.7 to 3.5 s TWT.

4.1.3. Moho

Moho is well imaged from km 0 to 75 at ca. 9 s TWT, where it corresponds to a high-amplitude and discontinuous reflection. In contrast, in the southern part, Moho is not clearly imaged. Moho reflection reappears from km 160 to 180, where it lies between 8 and 9.3 s TWT and is dipping southward. It is worth noting that between km 75 and 120 there are reflective layers underlying a strong and continuous reflector that rises dramatically between km 75 and 105 and reaches Tb at 7.5 s TWT at ca km 100.

4.2. First order crustal structure and rift domains

4.2.1. Proximal domain

In the CGN-1 line (Figs. II.2c and II.2d), the proximal domain is only observed in the northern margin and extends between km 0 and 20. Top basement and Moho are sub-parallel and the crustal thickness is approximately 7 s TWT (~ 22 km; see also

refraction seismic line OBS 2006-1 (Wu et al., 2012)). No rift basins are observed, and the total accommodation is ca. 2 s TWT in this domain. In the conjugate margin, a well-defined proximal domain does not exist, either because the line does not image far enough to the south, or because the southern margin was extended and thinned during the opening of the SW-SCS.

4.2.2. Necking domain

By definition the necking domain initiates where Tb and Moho start to converge, i.e., at the nickpoint between a horizontal and an oceanward-dipping trend of the Tb envelope. It terminates where the crust is thinned to less than 10 km. We define the continent-ward limit of the necking domain at km 20 in the north and km 225 in the south (Fig. II.2d). The oceanward limit lies at km 75 in the north and km 175 in the south. The northern necking zone is controlled by two large faults (F_{n1} and F_{n3}) offsetting Tb and bounding three terraces (Figs. II.2c and II.2d). The southern necking zone displays a wedge-shaped crust, and the size of related tilted blocks becomes smaller oceanward.

4.2.3. Hyperextended domain

The hyperextended domain is defined to start where the crust is thinned to 10 km and to terminate at the start of magmatic crust (Fig. II.2d). In line CGN-1, the edge of the continental crust, referred to as the *separation point* (SP) is interpreted to occur at km 100 in the northern margin and km 150 in the southern margin. An important observation is that the hyperextended domains at the two conjugate margins are asymmetric. At the northern margin, the hyperextended domain consists of blocks bounded by high-angle normal faults offsetting Tb, while at the southern margin fault structures are difficult to observe (for interpretation see section 6.1).

4.2.4. Proto-oceanic domain

The transition from hyperextended crust to oceanic crust is characterized by a a switch to strongly reflective basement, which displays a complex crustal structure (Fig. II.2b). Top basement is characterized by dipping, irregular reflection patterns reminiscent of magmatic additions that are onlapped by post-rift sediments. Tb is offset by normal faults that control tilted blocks. Moho is ill defined and disappears south of

km 155 (for further discussion see section 6.1). None of the diagnostic features characteristic of exhumed mantle, such as top basement deeper than 9 s TWT, a lack of Moho reflection or a stepping up of top basement onto first oceanic crust can be observed (Gillard et al., 2015, 2017, 2019). Therefore, we exclude the possibility that mantle was exhumed at this margin during crustal separation. Based on the complex crustal structure, the absence of the well-defined classical layered Penrose oceanic structure (Tb and Moho parallel and oceanic crust about 2 s TWT thick) we define this domain as proto-oceanic. However, future work will be necessary to futher characterize the nature of this crust.

4.3. Intra-sediment reflections and stratigraphic units

The description and identification of intra-sediment packages presented in the following relies on a dense set of high resolution seismic sections located both west and east of the CGN-1 line. These observations were synthesized in Fig. II.2 and more details are shown in Figs. II.4 and II.5 for the northern margin and Fig. II.6 for the southern margin. Fig. II.5 shows seismic section CGN-1A, a section located 4 km west of line CGN-1. It images the same structures and sedimentary units as those shown in Fig. II.4. Access to numerous lines similar to those shown in Fig. II.5 west and east of the CGN-1 line enabled to define seismic packages and faults and to project and correlate them into the CGN-1 line. This careful work enabled to subdivide the sedimentary sequence into a syn- and a post-rift mega-sequence limited by the Bi interface. Moreover, the syn-rift mega-sequence was further subdivided in 5 tracts and 4 magmatic units. A detailed description of the 3D sedimentary architecture of the NW-SCS is the theme of another paper in preparation. In this paper we describe the 2D evolution of the margin, at a crustal scale by focusing on the CGN-1 line. In order to separate observations from interpretations and being aware that the resolution and scale of published seismic sections always remains a problem, we present both linedrawings and their interpretation in terms of tracts and magmatic units in Figs. II.4, II.5 and II.6. Restorations of the sedimentary packages are provided in Figs. II.8 and II.9.

4.3.1. Syn- and post-rift mega-sequences

The sediment layer bounded by Tb and the seafloor can be subdivided in two mega-sequences separated by the breakup interface (B_i). B_i is a high-amplitude, continuous reflection (Figs. II.2c, II.4 and II.6). In the northern proximal domain and in the proto-oceanic domain, B_i coincides with Tb. Elsewhere, B_i is floored by tilted, unconformable reflections affected by faults that belong to the syn-rift mega-sequence. The reflections on top of B_i are sub-parallel to parallel, continuous and onlap onto B_i, in other words they belong to the post-rift mega-sequence. Only few faults offset B_i, none of which accommodate important fault offsets.

4.3.2. Syn-rift tracts

The syn-rift mega-sequence can be subdivided into 5 tracts as shown in Figs. II.4, II.5 and II.6. Each tract is defined by a top and basal interface that correspond to conformable or non-conformable contacts. In theory, the interfaces are considered to represent isochrons. Each tract contains syn- and/or post-tectonic packages (for definition see section 3.3.3.). While the tracts are well observed in the necking domain of the northern margin (Figs. II.4c and II.5), their definition in the hyperextended domain of both margins and in the necking domain of the southern margin is more difficult. One exception is tract 5 that is well imaged at both margins (Figs. II.4c and II.6c).

The lower boundary of basal tract 1 (T1) corresponds to Tb, while its upper boundary is marked by a moderate-amplitude, continuous reflector (orange in Fig. II.4c). T1 is characterized by low-amplitude, discontinuous or chaotic reflections. From km 35 to 45, T1 is cut by several normal faults, which sole into Fn3. Syn-tectonic packages showing thickening into the footwall of normal faults occur throughout T1.

T2 consists of semi-parallel, continuous, high-amplitude, high-frequency reflections defining oblique, progradational packages best developed at Necking Basin 2 (NB2 in Fig. II.4c). Reflections in T2 dip oceanward and downlap in the present section onto the top of T1. They diverge toward the center of NB2 and converge toward the northern end of NB2, where the T2 is almost a constant isopach. In NB 3 (Fig. II.4c), T2 is very thin and shows high-amplitudes, high-frequency continuous reflectors, cut by several

smaller south-dipping normal faults and filled by syn-tectonic packages. The main depocenter of T2 is located between km 45 and 50 in NB2.

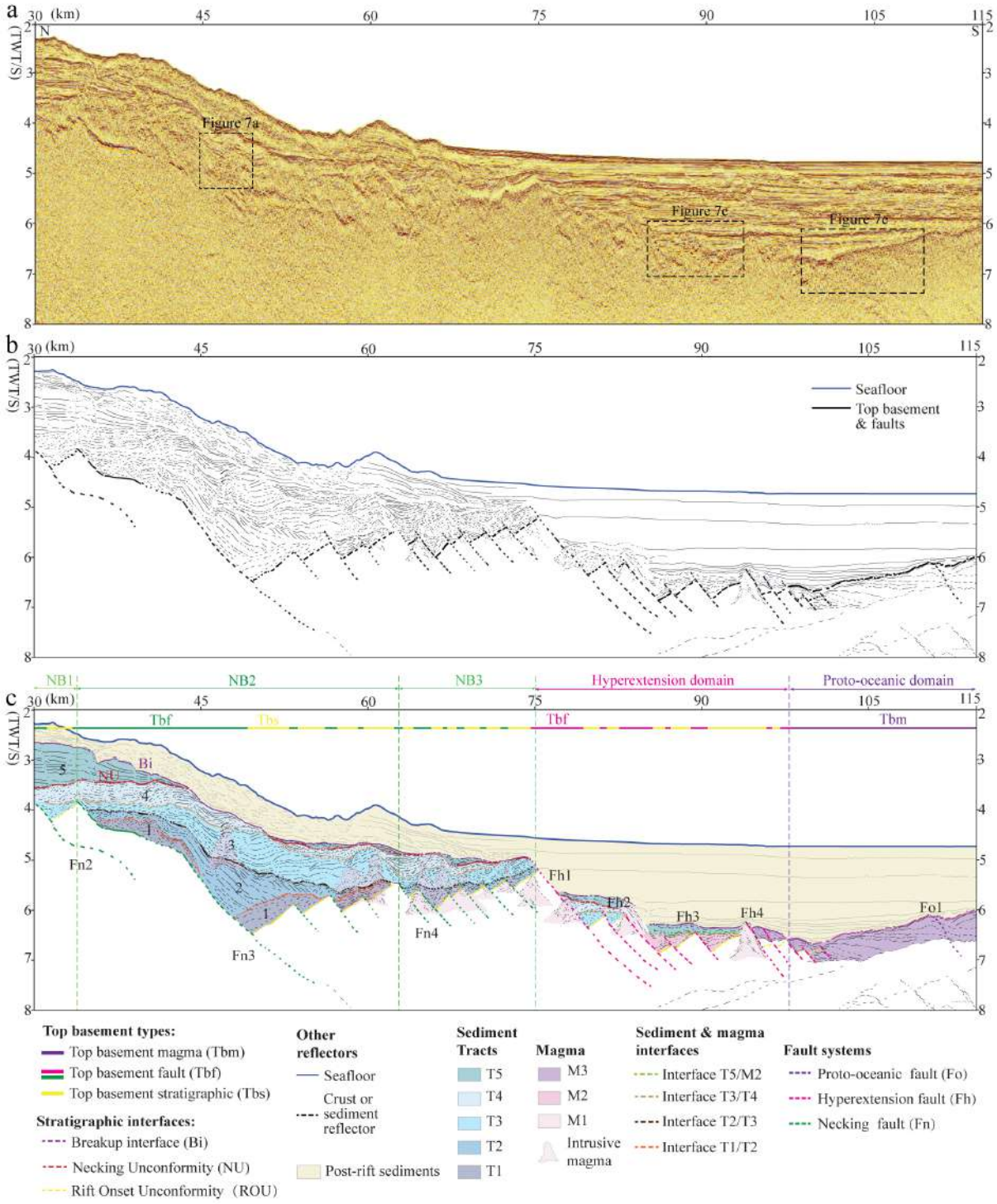

Figure II.4. *(a) Zoom on CGN-1 line showing the sedimentary architecture of the northern margin (for location see Fig. II.2a). (b) Line drawing of the section shown in (a). (c) Interpretation of seismic section shown in (a).*

The interface separating T2 and T3 (dark brown line in Fig. II.4c) is a strong reflection. T3 conformably overlies T2. T3 can be followed from NB2 to NB3 (Fig. II.4c) and the depocenter of T3 is located more oceanward compared to the one of T2. Syn-tectonic packages showing thickening into the footwall of faults and/or growth structures cannot be observed in T3.

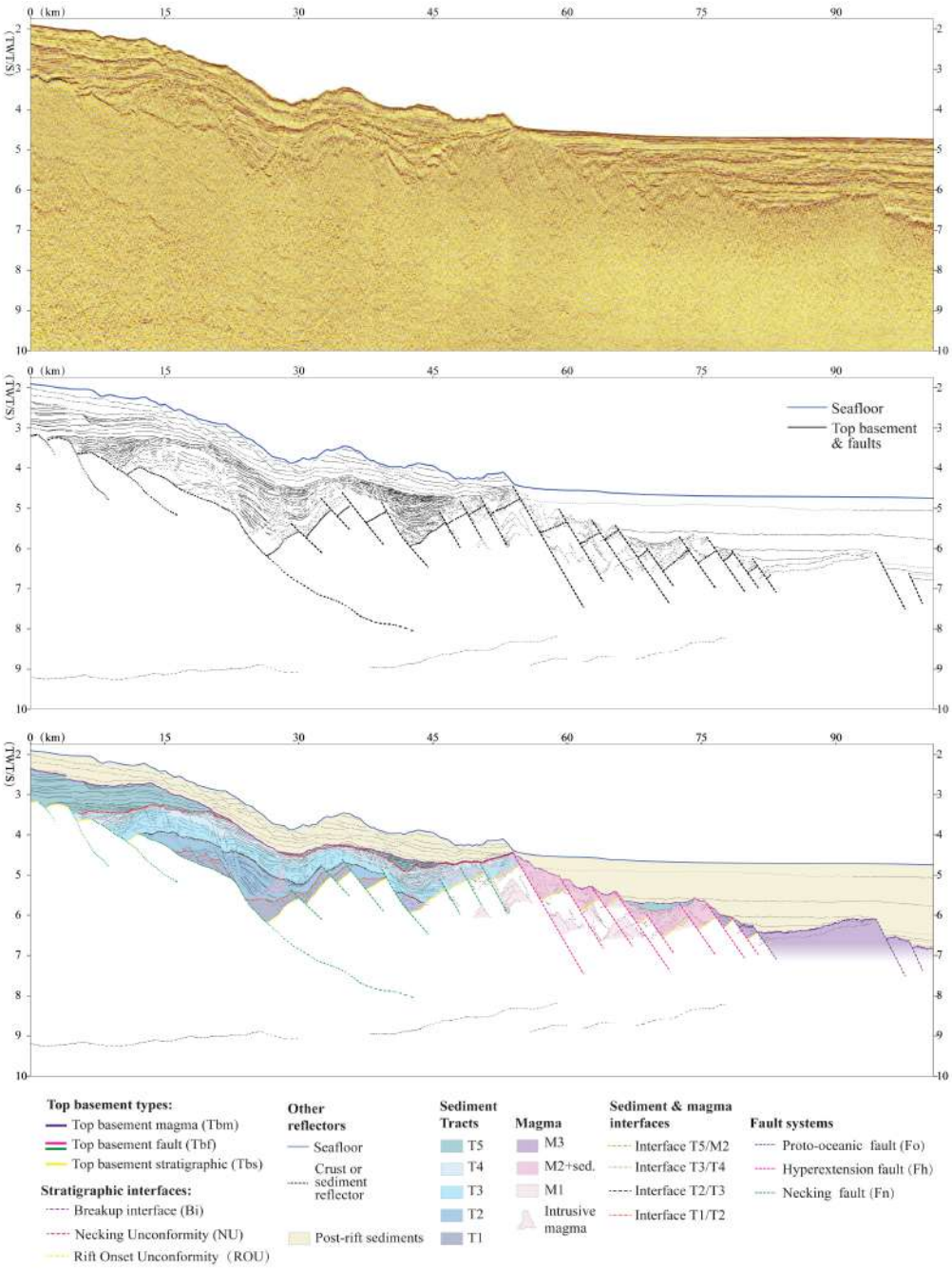

Figure II.5. *(a) Reflection seismic line CGN-1A located 4 km west of CGN-1 line (see Fig. II.1). (b) Line drawing of the section shown in (a) and interpretation of T1 to T5, Bi and Tb.*

The contact between T3 and T4 (light brown line in Fig. II.4c) is a high-amplitude, continuous, reflection. T4 is made of semi-parallel, continuous high-amplitude reflections. Two depocenters can be identified in T4, one at NB1–NB2 and the other at NB3 (Fig. II.4c). T4 represents, together with T3, the main infill of NB 3. Although the base of T4 is structured and divergent packages can be observed, the fact that the underlying tracts are continuous and not offset by faults suggests that T4 was controlled by detached, gravity driven systems rather than basement involved tectonics. Irregular, local, finger-like bodies that transect and overprint T3 and T4 with pull-up geometry in the core are interpreted as extrusive magmatic additions (light pink structures in Fig. II.4c; for more details see Figs. II.7a and II.7b and section 4.5).

T5 is made of downlapping reflectors in the north and parallel, continuous, high-amplitude, low-frequency reflections further south. T5 is thickest near the shoulder of the necking domain close to the proximal domain (NB 1 in Fig. II.4c) and thins out oceanward. T5 is sub-parallel and not fault-controlled in the necking domain. The upper and lower contacts of T5 are erosional boundaries in the necking domain but correspond to concordant or onlap boundaries in the hyperextended and proto-oceanic domain (Fig. II.4c).

Along the northern margin, all tracts (T1 to T5) contain syn-tectonic packages (growth and thickening structures), as well as post-tectonic packages (parallel/constant isopach). When looking at all tracts, we observe that the syn-tectonic part is migrating oceanward. This shows that the syn-tectonic sequence is diachronous and that extension migrated oceanward (see also discussion in sections 6.2 and 6.3). For example, T4 shows post-tectonic geometries in NB2 and syn-tectonic geometries in NB3 (Fig. II.4c). In contrast, T5 shows post-tectonic geometries in the entire necking basins (NB 1 to 3) but syn-tectonic geometries in the hyperextended domain (Fig. II.4c).

At the southern margin, the syn-rift mega-sequence is less well imaged and contains magmatic additions. Only T5 can be defined, while tracts T1 to T4 cannot be distinguished (Fig. II.6c). T5 shows the same characteristics like at the northern

margin. It displays post-tectonic packages and erosional contacts in the necking domain and syn-tectonic packages in the hyperextended domain (Fig. II.6c).

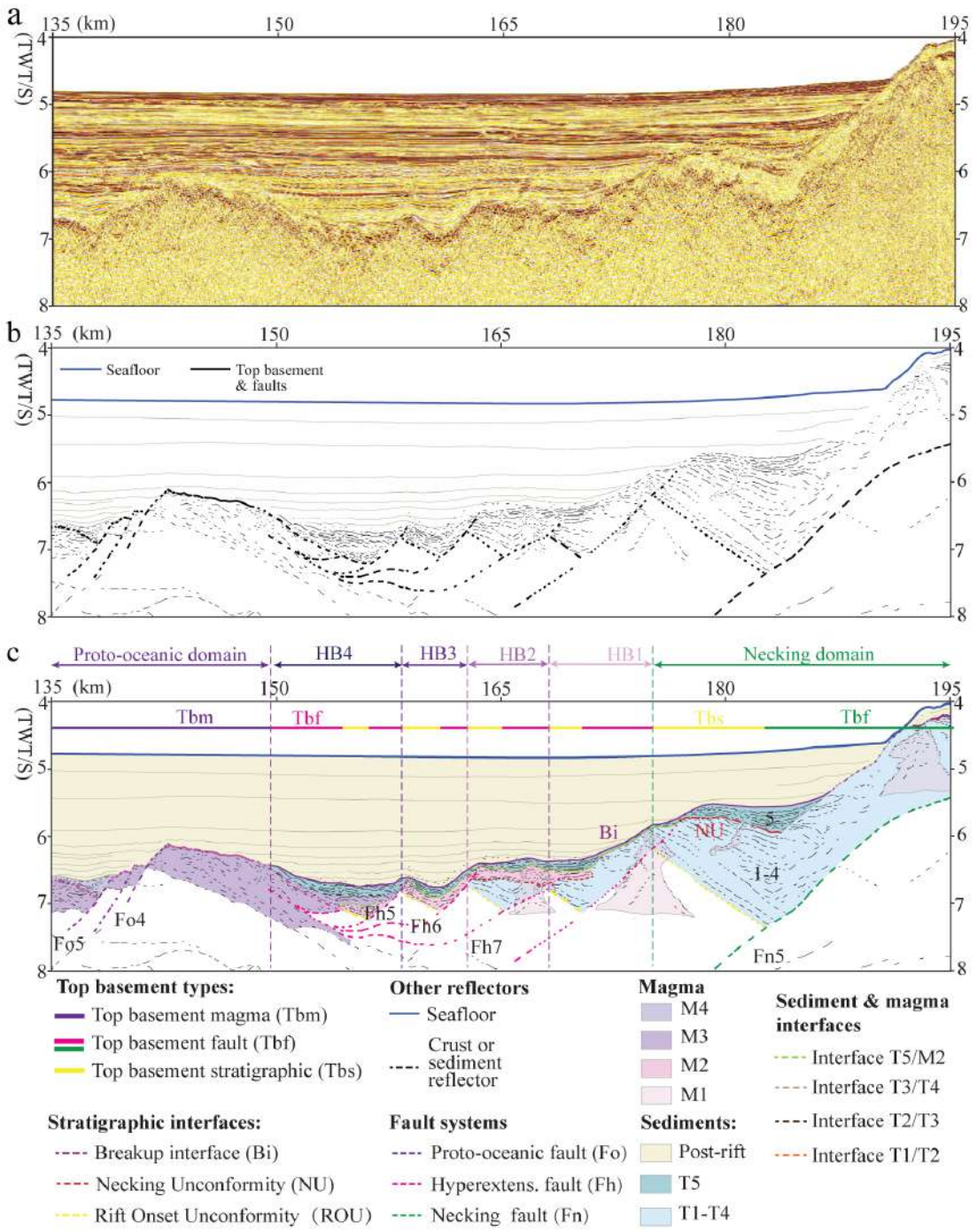

Figure II.6. *(a) Zoom on CGN-1 line showing the southern margin (for location see Fig. II.2a). (c). Line drawing of the section shown in (a). (c) Interpretation of seismic section shown in (a).*

4.3.3. Unconformities

Unconformities are often the expression of either eustatic sea level changes, dynamic/isostatic perturbations or are linked to significant tectonic events. On the CGN-1 section several sets unconformities can be observed. A first one, which is not well expressed everywhere, lies at the base of the syn-rift mega-sequence (e.g., km 45 to 75 in Fig. II.4c) and is referred to as Rift-Onset Unconformity (ROU). A second set of unconformities is observed within the syn-rift mega-sequence. It appears either in the necking domain between T3 that is tilted and eroded and T4 that onlaps onto the unconformity; and/or between T4 and T5 on both conjugate margins (in Fig. II.4c between km 30 and 45 and at km 60 and km 75 and in Fig. II.6c at km 180). The contact is an erosional unconformity, where either T5 or post-rift sediments down- or onlap directly onto the unconformity. We here encompass these unconformities under the term *Necking Unconformity* (NU) and relate them to the type of unconformities described by Chenin et al. (2019). A third set of unconformities is located at the top of the syn-rift mega-sequence and is referred to as Breakup interface (B_i). For the meaning and timing of these unconformities see discussion in section 6.2.

4.4. Intra-basement reflections and fault structures

Here we describe a set of structures, interpreted as faults, that either offset Tb or coincide with Tb. Some, but not all coincide with intra-basement reflections. In the following, we describe and label these structures according to their location in the margin. Indeed, each rift domain seems to be linked with specific fault types. We describe necking-related faults (F_n), hyperextension-related faults (F_h), and faults affecting the proto-oceanic domain (F_o) (Figs. II.2c, II.4c and II.6c). It is important to note that the numbering of the faults (1, 2, 3, …) is not a function of their age, but of their position in the margin. Numbering starts with 1 on the left (northern) side and continues southward.

4.4.1. Faults in the necking domain (F_n)

Faults in the necking domain include two different fault styles, namely high-angle faults offsetting Tb and exhumation faults that coincide with Tb. In the north a major high-angle fault can be identified, referred to as F_{n1} located at km 18 (Fig. II.2c). It

separates the proximal domain from the necking domain. The breakaway of F_{n1} is at 2 s TWT and soles out at ca. 7 s TWT that may correspond, as previously mentioned, to the brittle ductile transition. The fault throw is 1.5 s TWT and crustal thinning across the fault is approximately 1.5 s TWT. In the conjugate margin a series of high-angle faults are observed in the necking domain (e.g., F_{n6} to F_{n8} in Fig. II.2c). These faults show smaller throws compared with F_{n1} (less than 1 s TWT in the upper crust). These faults sole out at about 7 s TWT, at a depth that is interpreted as the brittle-ductile transition. Two exhumation faults related to necking can be observed, one in the north at km 33 (F_{n3}) and the other in the south at km 200 (F_{n5}). Both faults dip oceanward. They have large offsets, crustal thickness changes across the faults is significant and they are interpreted to exhume lower crustal rocks at the seafloor in their footwall. The fault throw of F_{n3} is 2.7 s TWT and that of F_{n5} is 3 s TWT.

4.4.2. Faults in the hyperextended domain (F_h)

At km 75 (Fig. II.4c) , a major normal fault (F_{h1}) offsets Tb. F_{h1} has a throw of 2 s TWT and juxtaposes a crust of about 4 s TWT against a set of small northward tilted blocks whose crustal thickness is less than 2 s TWT. In the southern margin faults F_{h5} to F_{h7} dip northward (for interpretation of these faults see section 6.1).

4.4.3. Faults in the proto-oceanic domain (F_o)

Between km 100 and 150, top basement is titled toward the north in the northern margin and toward the south in the southern margin. The observed normal faults cannot explain the tilt and higher elevation of top basement in the most distal part compared to the most continentward part of the proto-oceanic domain. From the intra-basement reflection geometry and the topography of basement, several faults can be defined in the proto-oceanic domain (e.g., F_{o1} to F_{o5}; Fig. II.2c).

4.5. Magmatic additions

Reflections and reflectivity patterns reminiscent of magmatic additions can be observed from the necking domain to the proto-oceanic domain (Figs. II.4, II.5 and II.6). Here we interpret magmatic additions and their relationship with the previously defined syn-rift tracts with the aim to link the timing of magma emplacement with that of the

deposition of syn-rift tracts. We define the geometry, seismic architecture and structure of 4 different magmatic units.

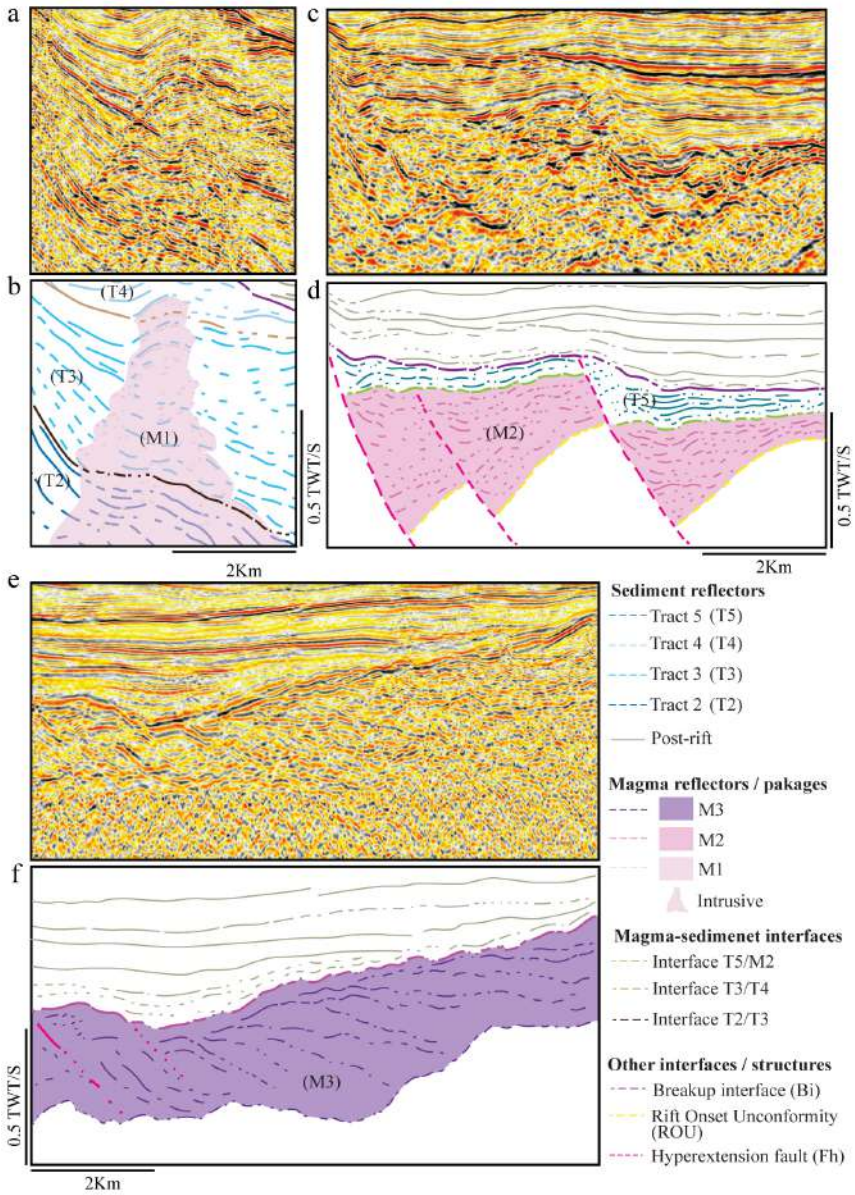

Figure II.7. *Zooms showing magmatic additions (for location see Fig. II.4a). (a) Seismic detail of magmatic unit 1 in the necking zone and (b) line drawing. (c) Seismic detail of magmatic unit 2 in the hyperextended unit and (d) line drawing. (e) Top magmatic basement in the proto-oceanic domain with oceanward dipping reflections onlapped by sediments of tract 5 and (f) line drawing.*

In the necking domain, between km 45 and 75 (Figs. II.4c, II.7a and II.7b), sub-vertical structures cored by chaotic reflectors affect and uplift the surrounding sediments. The geometrical relationships with encompassing sediments are chaotic,

which makes it difficult to define the exact timing and nature (extrusive or intrusive) and structure of the magmatic additions. Therefore, in the seismic sections we cannot define the detailed structures, but only the approximate location of magmatic additions. These magmatic additions form the first magma that can be observed in the necking basin NB2 (Fig. II.4c and II.6c). They intrude T2 to T4, while T5 covers the magmatic structures without being affected by it. Thus, we interpret that the first magma (unit 1) intruded simultaneously with the deposition of T4 (Fig. II.4c and II.6c).

In the hyperextended domain, lots of magmatic additions, probably interlayered with sediments and often linked to faults can be observed (Figs. II.4c and II.6c). Since these intrusive- and probably also extrusive bodies are truncated by normal faults and both intrude into and are sealed by T5, we interpret this magma, referred to as unit 2, as being emplaced during the deposition of T5.

The proto-oceanic domain (Fig. II.4c) between km 100 and 115 is characterized by oceanward dipping reflections, reminiscent of magmatic flows (Figs. II.7e and II.7f). Top and base of this dipping sequence, referred to as unit 3, are sub-parallel, the sequence is ca. 0.5 s TWT thick and tilted continentward at both margins. The underlying crust is made of a complex, reflective crust interpreted to be of igneous origin.

The magmatic additions of unit 3 predate a last magma emplacement observed between km 115 to 140, referred to as unit 4, which consists of sub-horizontal magmatic additions (Fig. II.2d). Since unit 4 floors post-rift sediments, we interpret it as the time-equivalent of the youngest sediments in T5. In the CGN-1 section, a few magmatic additions can be observed in the post-rift mega-sequence, however, we will not discuss them further here.

5. Kinematic restoration of section CGN-1: methodological approach

Here we present and discuss a kinematic restoration approach that enabled us to restore the interpreted depth-converted section CGN-1 from the present-day situation (Fig. II.8f) back to an initial stage (Fig. II.8a). Our restoration method includes:

- conservation of the area (volume) of the whole crustal section using the program ImageJ (freely available on the Internet: http://rsbweb.nih,gov/ij/)
- a restoration of fault heaves (Fig. II.2d) and magmatic accretion back to the initial Tb length

Assuming area conservation, i.e., neither addition nor loss of crust, and taken for granted that the kinematic extension was parallel to the kinematically restored section, the following set of simple equations can be formulated and used to test the coherence of our kinematic restoration

Equation 1: $\mathbf{A}c_{initial} = \mathbf{A}c_{final}$

where $\mathbf{A}c_{initial}$ is the area at the initial stage and $\mathbf{A}c_{final}$ is the area of the crust at the end of extension.

Equations 2 & 3: $\mathbf{T}b_{initial} \approx \mathbf{T}b_s$ and $\mathbf{T}b_{final} = \sum\mathbf{T}b_s + \sum\mathbf{T}b_f + \sum\mathbf{T}b_m = 225$ km

where $\mathbf{T}b_{initial}$ is the length of the top basement at the restored initial stage, Tb_s is the length of top pre-rift basement, $\mathbf{T}b_f$ is the length of top basement that is made of new exhumed fault planes, and Tm is the length of newly created top basement due to magmatic accretion. For the distribution of Tb_s, $\mathbf{T}b_f$ and $\mathbf{T}b_m$, which is based on seismic interpretation, see Fig. II.2c and Figs. II.4c and II.6c. It is important to note that both $\mathbf{T}b_f$ and $\mathbf{T}b_m$ represent *new real estate*.

Equation 4: $\mathbf{Z}_{initial} \times Tb_s = \mathbf{A}c_{initial} = \mathbf{A}c_{final}$ ($\mathbf{T}b_s = \mathbf{A}c_{final} / \mathbf{Z}_{initial}$)

where $\mathbf{Z}_{initial}$ is the initial thickness of the crust (i.e., the crustal thickness before necking), for which we use crustal thickness at km 0 as a proxy. At the northern margin $\mathbf{Z}_{initial}$ has been reckoned to 22 km by Wu et al. (2012) based on the velocity results obtained from the refraction seismic section OBS2006-1 (for location of refraction seismic section see Fig. II.1).

Table 1 summarizes the values of $\mathbf{A}c_{final}$, $\mathbf{T}b_{final}$, $\sum \mathbf{T}b_s$, $\sum \mathbf{T}b_f$, $\sum \mathbf{T}b_m$ determined for the final (present) section, as well as the β value obtained for each restoration step shown in Fig. II.8.

The assumptions made for the restoration of section CGN-1 are that: 1) the section is parallel to transport direction and no material is added and/or removed from the crust, apart from magmatic additions that are new real estate and thus do not need to be restored; and 2) Moho and Tb are accurately and correctly interpreted (in particular **T**b_s, **T**b_f and **T**b_m (see Fig. II.2c and Figs. II.4c, II.6c and II.8f), and the time to depth conversion is correct. Since equations 1 and 2 and 3 are independent from each other, the result of the restoration can be tested with equation 4, where $\mathbf{Z}_{initial}$ (crustal thickness before onset of necking) corresponds to the present-day crustal thickness in the proximal domain (22 km; see time to depth conversion). For the results of the restoration see Table 1.

Table 1.*Values obtained from the kinematic reconstruction of seismic section CGN-1 presented in Fig. II.8. For details see section 4. 2.*

	Ac	Tb	Tbs	Tbf	Tbm	Extension	β
	km^2	km					
figure5.f	2068.8	225	93.1	96.8	34.2	131	2.4
figure5.e	2086.2	175	93.1	82.3	0	82.3	1.9
figure5.d	2110.4	160	93.4	67.3	0	67.3	1.7
figure5.c	2020.3	124	93.3	31.3	0	31.3	1.3
figure5.b	2020.1	100	92.4	7.3	0	7.3	1.1
figure5.a	2031.2	92.7	92.7	0	0	0	1

The restored length of the crustal section, i.e., the initial Tb is 92.7 km. The restored length of the section at crustal separation is 175 km. This gives a total amount of crustal extension of 82.3 km, which corresponds to a bulk β value of 175 km/92.7 km = 1.86. The length of **T**b_s calculated using equation 4 is 94.025 km. Thus, there is a small deviation of less than 1.325 km between the restored length of the section **T**$b_{initial}$ and the calculated length of Tb_s. This shows that our interpretation of the nature of Tb as **T**b_s, **T**b_f and **T**b_m on the CGN-1 line (Fig. II.2c and Figs. II.4c and II.6c) is coherent with the restoration we present in Fig. II.8.

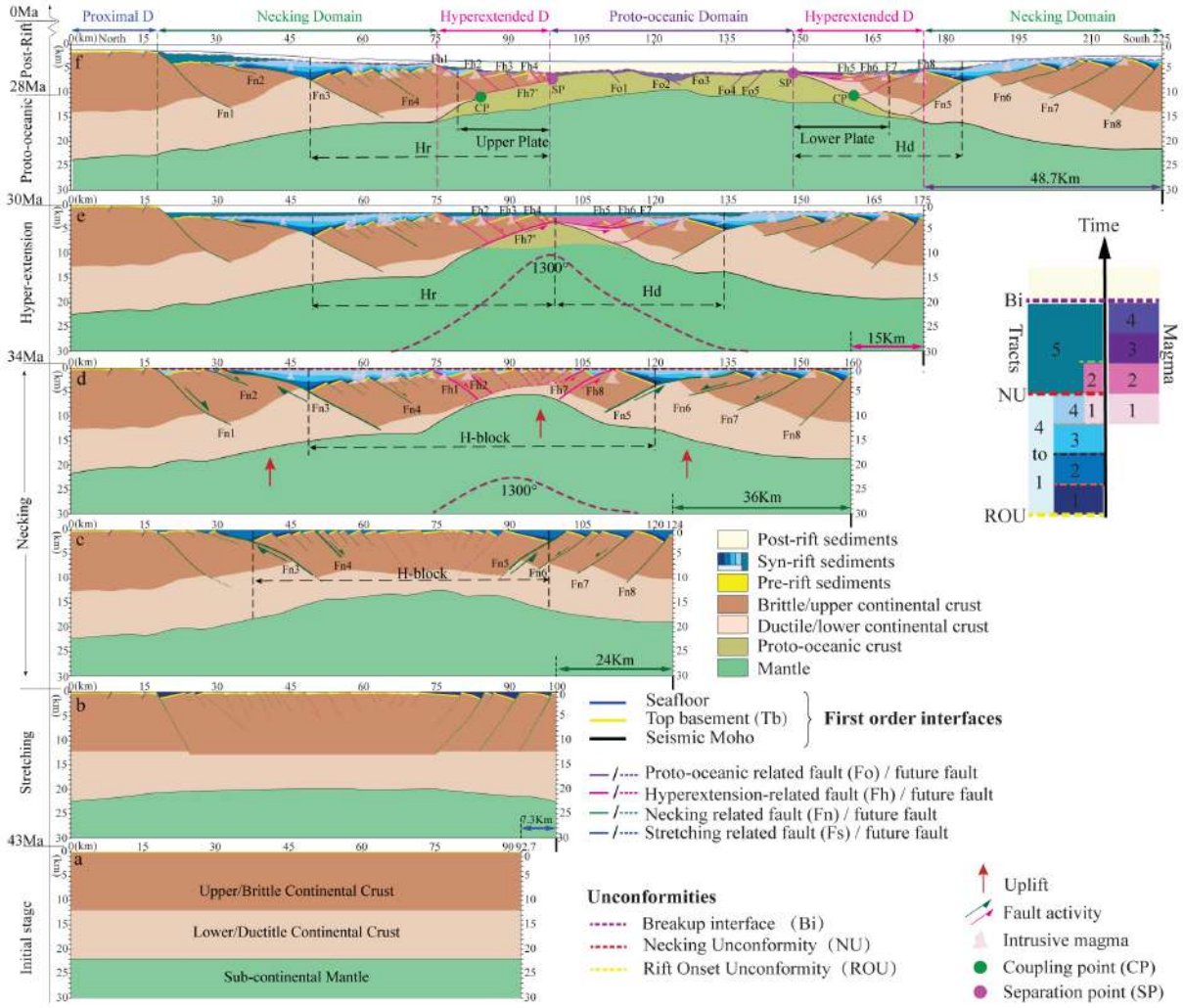

Figure II.8. *Restoration of the depth converted CGN-1 section. (a) Initial stage. (b) Stretching stage. (c) Early necking stage. (d) Transition from necking to hyperextension stage. (e) Hyperextension stage. (f) Present stage. Amount of horizontal extension is based on the restoration of fault heaves and of the pre-rift (Tb_s) back to a continuous horizontal line. Crustal restoration is based on the conceptual model published in Mohn et al 2012, which describe the distribution of brittle and ductile deformation during thinning and extension. Conservation of the area was achieved using the program ImageJ (freely available on the Internet: http://rsbweb.nih,gov/ij/).*

The assumption to keep the area of the pre-rift brittle and ductile crusts constant (see subsets of equation 1) enables us to trace the initial types of crusts (brittle and ductile) during rifting. In reality, however, ductile material moves during crustal thinning and exhumation into the brittle field (e.g., embrittlement concept due to rifting of Pérez-Gussinyé et al. (2003)). Using simple assumptions, brittle crust can be reconstructed by restoring fault heaves only. In contrast, the ductile crust is allowed to change shape (crustal flow) as long as it preserves its initial area/volume. These

assumptions may be realistic for proximal and necking domains, but not for hyperextended domains, where the whole crust, including the former ductile levels are deforming in the brittle domain. However, since the crustal surface of the hyperextended domain is minor compared to the total extended crustal surface within the restored section, the resulting error is small and does not significantly change the results of our restoration. This assumption leads to an overestimation of brittle crust in the final section.

6. Discussion

6.1. Rift architecture, H block and upper- vs. lower plate

In the CGN-1 section (Fig. II.8f), we recognize a residual H block (H_r) at the northern hyperextended domain and a delaminated H block (H_d) *sensu* Péron-Pinvidic & Manatschal (2010) at the southern hyperextended domain. H_r and H_d result from the dismembering of a former H-block or keystone (see concept of H-Block in Lavier & Manatschal, 2006; and Haupert et al., 2016). Their evolution is described in Fig. II.8c–II.8f and section 6.2. The H_r and H_d are bounded on their proximal side by a main necking fault, which is F_{n3} in the northern margin and F_{n5} in the southern margin (Fig. II.8c–II.8f). The oceanward terminations of H_r and H_d are masked by magma. At the northern margin the H_r is truncated by high-angle faults ($F_{h1\ to\ h4}$). These faults are in turn truncated at their base by a continentward dipping reflection interpreted as an exhumation fault ($F_{h7'}$). At the southern margin the H_d is bounded by low-angle, oceanward facing faults ($F_{h5\ to\ h8}$). We interpret these faults to break away in the south and to have their continuation in the north (i.e., F_h7'; Figs. II.8e and II.8f). Based on this interpretation we recognize the northern margin as the hanging wall (upper plate) and the southern margin as the footwall (lower plate) of the main detachment system ($F_{h5\ to}$ $F_{n7+h7'}$).

The definition of the hyperextension-related faults ($F_{h1\ to\ h8}$) also enables us to determine the location of the *coupling points* (CP; see Figs. II.2d and II.8f). This point corresponds to the location where the first fault crossed the whole crust and penetrated into mantle, which is F_{h1} in the north and F_{h8} in the south (Figs. II.2d and II.8f). Another

important point is the *separation point* (SP) that corresponds to the oceanward termination of the continental crust.

The asymmetry of the conjugate margins has implications for the sedimentary architecture. While the upper-plate (northern margin) was little affected by hyperextension faults (F_h) and preserves the early syn-rift stratigraphy (T1 to T4), the distal part of the lower-plate is dominated by exhumed basement and extensional allochthons, and thus early syn-rift sediments (T1 to T4) are rare, and when present are likely to be deformed. This may explain why the sedimentary section in the southern margin below T5 is less well resolved in the seismic image. It also implies that the nature of Tb is different at the two conjugate distal margins: while the upper plate is predominantly floored by upper crust with a stratigraphic contact to first sediments (i.e., Tb_s, km 50 to 75 in Fig. II.4c), the lower plate is mainly floored by exhumed basement/faults (Tb_f, i.e., km 150 to 175 in Fig. II.6c). In contrast Tb in the proto-oceanic domain is formed by magma (Tb_m, i.e., km 100 to 115 in Fig. II.7e and II.7f). Distinguishing between different types of Tb is fundamental not only for the kinematic reconstruction (see next section), but also for the evaluation of the tectono-sedimentary evolution discussed in sections 6.5 and 6.6.

Interpretation of seismic data from the NW-SCS has been presented in the past bay several authors among which more recently by Ding et al., (2011), Franke et al., (2014); Cameselle et al. (2017, 2021) and Wu et al., (2019). While Ding et al. (2011) and Wu et al. (2019) focused more to the crustal structure and the late syn-rift evolution, Franke et al (2014) and Cameselle et al. (2017, 2021) described the rift architecture of the margin and the rift domains, but did not focus in the detailed syn-rift stratigraphic architecture and the fault geometries related to crutal thinking, which is the major aim of this work. Apart from the proposed mantle exhumation (Franke et al. (2014) and the oceanward dipping faults proposed by Cameselle et al. (2021), this study does not show major disagreements concerning the time frame and crustal structure proposed by these previous studies.

6.2. Kinematic restoration of section CGN-1: tectono-structural evolution

In the restoration shown in Fig. II.8, three main stages can be defined: the initial/stretching stage; the necking stage during which the H-block is individualized; and the final dismembering of the H-block during hyperextension and breakup of the margin.

6.2.1. Initial stage

At the initial restored stage, the crust is already thinned to 22 km (Figs. II.2d and II.5a). In this study, we cannot determine whether this thickness corresponds to a regional standard un-thinned crust (our preferred interpretation), or if some extension has been accommodated prior to the initial stage shown in our reconstruction. The crustal architecture and crustal thickness at onset of rifting remain ill-defined, not only in our section, but throughout the SCS (Zhu et al., 2018; Ye et al., 2018). From drill hole data throughout the northern margin of the SCS, it is well documented that the depositional environment during early rifting remained sub-aerial with little residual topography (Lei & Ren, 2016; Ye et al., 2020). However, in order to explain the subaerial conditions prevailing over a 22 km thick crust, a thermal support is required. Such a thermal support may be inherited from the previous tectonic event (magmatic arc setting) or be linked to dynamic topography. Such a thermal support would also suggest elevated thermal gradients during early rifting, compatible with a ductile crustal rheology during early rifting followed by an elevated thermal subsidence. The observation that the first faults observed in the section ($F_{n1\ to\ n8}$; Figs. II.4c and II.8c) initiated with cut-off angles of approximately 45 to 60°, show vertical offsets ranging from hundreds to thousands of meters, and sole out at about 12 km suggest that the upper brittle crust was strong at onset of necking. This contrasts with the observation of very weak crust found further east in the Liwan basin (Zhang et al., 2020), where the crust is supposed to consist of forearc-derived meta-sediments.

The hypothesis of a strong pre-rift crust in the CGN-1 section is in line with an arc-derived basement consisting of quartz-dominated lithologies. In such a quartz bearing crust, the brittle–ductile transition would be expected to lie at about 300°C (Stipp et al., 2002), which would suggest a quite normal thermal gradient at onset of the necking

stage in the upper crust. Although this may appear to contradict the important thermal support that is necessary to keep a 22 km thick crust at sub-areal conditions, it is important to keep in mind that it is unlikely to expect a thermally equilibrated curst at the onset of rifting in the study area.

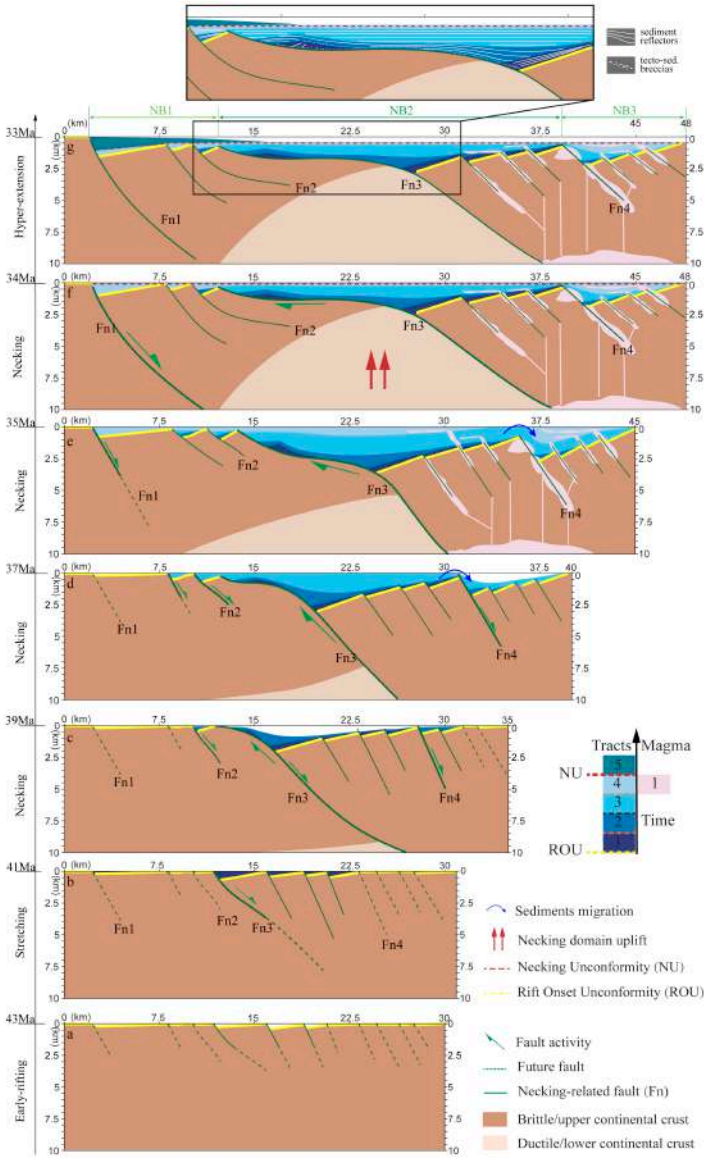

Figure II.9. *Restoration of the deformation observed in the brittle upper crust in the northern margin during the stretching, necking and hyperextension stage and link to deposition of tracts and magma. (a) Stretching stage. (b) Onset of localization along F_{n3} (main future necking fault) during T1. (c) Roll over of F_{n3} during deposition of T2. (d) Delocalization and formation/reactivation of F_{n2} and F_{n4} during deposition of T3. (e) Formation of F_{n1} and emplacement of magma unit 1 during deposition of T4. (f) Uplift and erosion (Necking Unconformity) at the end of deposition of T4. (g) Reactivation of Fn_1 during migration of the deformation to the distal margin (see Fig. II.8e) during deposition of T5.*

6.2.2. Necking stage and individualization of the H-block

Crustal thinning is first distributed and accommodated by a set of high-angle faults ($F_{n1\ to\ n8}$, see Fig. II.5c) before deformation localizes along two master faults (F_{n3} and F_{n5}). These two faults are responsible for the exhumation of mid-crustal rocks at the seafloor and frame the keystone referred to as H-block. Thus, necking is accompanied by the formation of exhumation faults that exhume new real estate basement (Tb_f) to the seafloor (Fig. II.9). The creation of new real estate along fault F_{n3} occurs during the deposition of tracts T2 and T3. In detail, deformation is first distributed (Fig. II.9a) before it localizes along one master fault (F_{n3}; Figs. II.9b and II.9c). In later stage, deformation becomes distributed again (Fig. II.9d and II.9e) along faults that occur on both sides of the master fault F_{n3} (e.g., F_{n1} and F_{n4} and syn-tectonic packages in T4). Deformation in the necking zone stops at the end of T4, simultaneous with emplacement of first magma and the uplift and erosion of compartments within the necking domain, leading to erosional unconformities referred to as Necking Unconformity (NU). Thus, two types of “unconformities” can be observed in the necking zone: 1) exhumation surfaces creating new real estate along master faults (Tb_f); and 2) erosional unconformities related to uplift and erosion (Fig. II.4c). Both types of unconformities can be observed at both margins, which suggests that the rift architecture was symmetrical during the necking phase. This overall evolution can be compared with model W5 presented in Chenin et al. (2020).

6.2.3. Dismembering of the H-block during hyperextension and breakup

The dismembering of the H-block and formation of the H_r and H_d (for description see section 6.1) is shown in Fig. II.8d to II.8f. These figures show the evolution from a late necking phase to the hyperextension phase during which a new set of faults (F_{h1} to F_{h8}) form. F_{h1} to F_{h8} are responsible for the dismembering of the H-block and to the creation of an upper plate (H_r) and a lower plate (H_d) margin. This new generation of faults formed when the crust was thinned to less than 10 km and started to embrittle (onset of hyperextension: no ductile material was left). As a consequence, deformation between the crust and the mantle became mechanically coupled (i.e., faults crosscut the thinned crust and penetrate into mantle; e.g., faults $F_{h1\ to\ h8}$ at the transition from Fig.

II.8d to II.8e). This evolution is linked to a change from symmetric to asymmetric rifting and two prominent unconformities form at the main breakaway faults F_{h1} and F_{h8} at km 75 and km 180 at both conjugate margins (Figs. II.4c, II.6c and II.8d). These unconformities, referred to as NU, are defined by the uplift and erosion of T4 and are sealed by T5 (Figs. II.4c and II.6c), suggesting that, at the onset of hyperextension (end of deposition of T4; Fig. II.8d), the future distal margin was still at sea level. This is consistent with observations reported by Zhang et al., (2019) from the Liwan subbasin located about 200 km further to the east.

In the later stages of hyperextension, deformation started to become dominated by downward concave faults that formed breakaways at the southern margin and dip northward (see $F_{h7\ to\ h5}$ in Fig. II.8e). The prolongation of these faults in the northern margin are interpreted to dip beneath the continental crust that would correspond the strong continentward dipping reflections shown in Fig. II.2c and ($F_{h7'}$ in Fig. II.8e). It is unclear whether the footwall of this exhumation fault is made of hydrated mantle, underplated magma or a combination of the two.

During hyperextension, deformation migrated sequentially from F_{h7} to F_{h6} to F_{h5} and finally resulted in the separation of the crust and the formation of the two conjugate margins (Fig. II.8e). At this stage the dismembering of the H-block was over and the upper plate (H_r) and lower plate (H_d) architecture was established. The dismembering of the H-block occurred during deposition of T5 and simultaneous emplacement of magmatic units 2 to 3. At this stage, no extension occurred at the necking or proximal domain. This is well demonstrated by the post-tectonic nature of T5 in both the proximal and necking domains. These observations show that the transition from a symmetric to asymmetric margin was limited to a short time and occurred during the deposition of T5. This transition was associated with detachment faulting and magma production in the distal margin and occurred simultaneously with subsidence of the entire margin. Extension and magma emplacement followed crustal separation, resulting in the formation of a proto-oceanic domain (Fig. II.7e and II.7f). During this stage, magmatic accretion became the dominant process, but fault activity persisted (see F_{o1} to F_{o5} in Fig. II.2c).

6.3. Time frame for rifting and related syn-rift tracts and magmatic units

Based on the studies of Zhou et al., (2018), Larsen et al., (2018), Xie et al., (2019) and Nirrengarten et al., (2020), we propose a stratigraphic framework, which enables us to put the different tectonic events, syn-rift tracts (T1 to T5) and the magmatic units (1 to 4) in a time frame (Fig. II.10). As the onset of rifting is ill-constrained, in this study, we are not able to define when rifting initiated. Following Xie et al., (2019), we interpret the onset of strain localization, which coincides with the evolution of stretching to necking (e.g., Figs. II.9a to II.9c) to initiate at 43 Ma, which also corresponds to the deposition of T1 and T2. Emplacement of T3 to T4 and magmatic unit 1 occurred simultaneous to the activity along necking faults (F_n), prior to the deposition of T5.

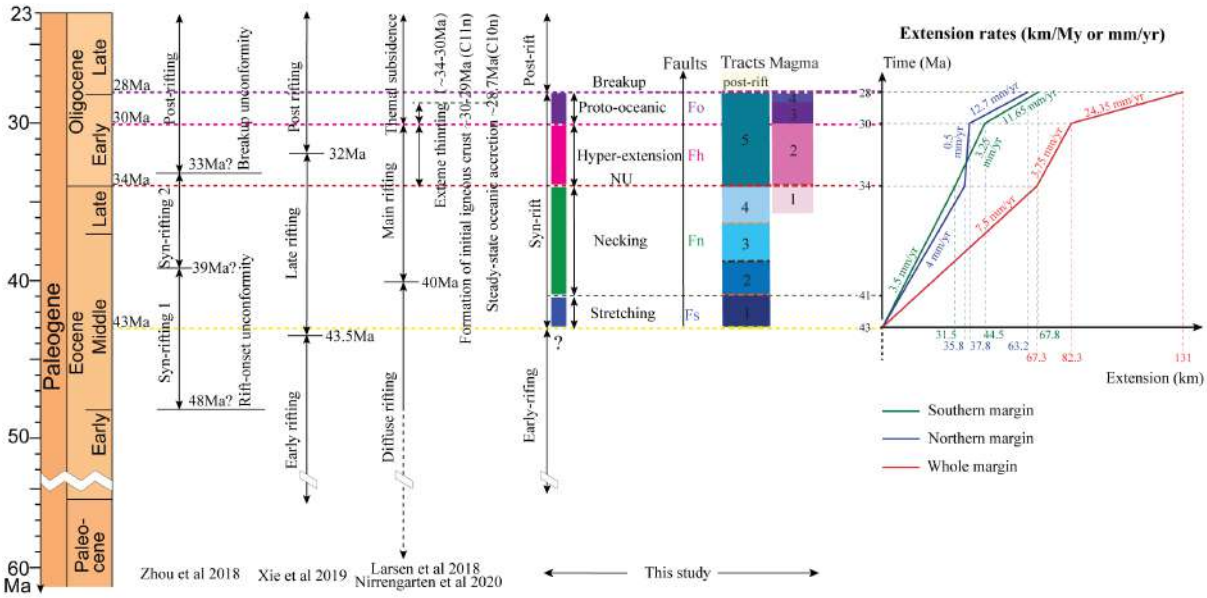

Figure II.10. *Time frame for the evolution of rifting in the NW-SCS linking regional studies with the tracts, magmatic units, faults and extension rates based on the results of quantification of the restoration shown in Fig. II.8.*

Onset of hyperextension, which is linked to the deposition of T5, magmatic unit 2 and localization of deformation along exhumation faults (F_h) in the future distal margin is interpreted to occur at 34 Ma. This is in line with the onset of extreme thinning observed in the northern Central SCS margin (Nirrengarten et al., 2020), which is based on IODP drilling results. It may also correspond to the event referred to as

“breakup” in the studies of Zhou et al. (2018) and Xie et al. (2019), which is assumed to occur slightly later.

Crustal separation and formation of first proto-oceanic crust occurred during deposition of T5, the emplacement of magmatic units 3 and 4 and the activity of faults $F_{o1\ to\ 5}$. All these events may have occurred at 30 Ma according to the results of IODP drilling (Nirrengarten et al., 2020) approximately 200 km further to the east. The formation of first steady-state Penrose-type oceanic curst may have occurred at 28 Ma considering that C10 is the first well-identified magnetic anomaly just east of the study area. Proposing a more precise timing for the different tracts and magmatic units is not possible in the absence of drill hole data.

6.4. Strain rates

Based on the detailed kinematic restoration shown in Fig. II.8 (for results see Table 1) and the time constraints presented in Fig. II.10, we define extension rates for the rift evolution recorded in the CGN-1 line. In Fig. II.10 we plot the timing of the events constrained and discussed in section 6.3 against the extension values obtained from the kinematic restoration (Fig. II.8). Extension rates obtained for the whole margin evolution are shown with the red line in Fig. II.10. The green line shows the strain rates for the southern margin, the blue line for the northern conjugate margin.

The results show that extension rates at the stage of early seafloor spreading are larger than that at initial rifting. Note that timing and therefore extension rates during initial rifting are difficult to define, but they are very likely lower than those calculated here for the necking phase. The average extension rates obtained here for the necking phase are 7.5 mm/yr. During hyperextension extension rates are lower (3.75 mm/yr). If one compares the rates calculated for the upper plate (blue line in Fig. II.10) with those calculated for the lower plate (green line in Fig. II.10), a net difference can be observed. Rates for the upper plate (0.5 mm/yr) are much lower than those for the lower plate (3.25 mm/yr), which is compatible with the strain accommodation along long offset north dipping detachment faults resulting in asymmetric exhumation during hyperextension. Rates of 24.35 mm/yr are obtained for the proto-oceanic domain. Our

values also compare well with those of Nirrengarten et al., (2020) who estimated, based on IODP drill hole data and magnetic anomalies, values of 27.1 to 37.6 mm/yr for the early seafloor spreading in the northern Central SCS. Although the values obtained from our restoration are compatible with the plate acceleration during continental rifting and early seafloor spreading proposed by Brune et al., (2016), their values are a factor 5 to 8 higher than those obtained in our study. An increase in extension rates at the transition between early rifting to seafloor spreading was also shown by Sutra et al. (2013) for the Iberia margin. However, at present only few strain rate data exist for rift systems and more data are necessary to see if the observed acceleration at the transition from rifting to seafloor spreading can be considered as a general rule.

6.5. The stratigraphic tape recorder of rifting: the Wheeler approach

In this study we subdivide the syn-rift mega-sequence into 5 tracts and 4 magmatic units. Each tract is made of syn- and post-tectonic packages, the former linked to fault structures, the later sealing faults. This approach enabled us to link the kinematic restoration of faults (Fig. II.8) with the stratigraphic tape recorder, allowing us to build a Wheeler diagram for the CGN-1 line (Fig. II.11). One first prerequisite for the construction of a Wheeler diagram is a time frame for the different rift events, faults, tracts and magmatic additions, that was established in Fig. II.10. The other prerequisite is a detailed kinematic restoration in which timing and offset along faults and creation and filling of accommodation space by sediments and magmatic additions are described (see Figs. II.8 and II.9).

In the Wheeler diagram shown in Fig. II.11b we represent the location of each tract, fault and magmatic unit interpreted in the seismic CGN-1 line and restored in Fig. II.8, and display its evolution through time. The duration of tracts and magmatic units are shown in Fig. II.10. Due to the lack of precise data for the necking stage, we assume that all the tracts deposited between 43 and 34 Ma (T1 to T4) have the same duration, which would correspond to 2.25 My per tract. We are aware that, in the absence of drill hole data, this is a strong simplification; however, it does not modify the

main conclusions of this work. The duration of T5, deposited during hyperextension and breakup between 34 and 28 Ma, is 6 Myr.

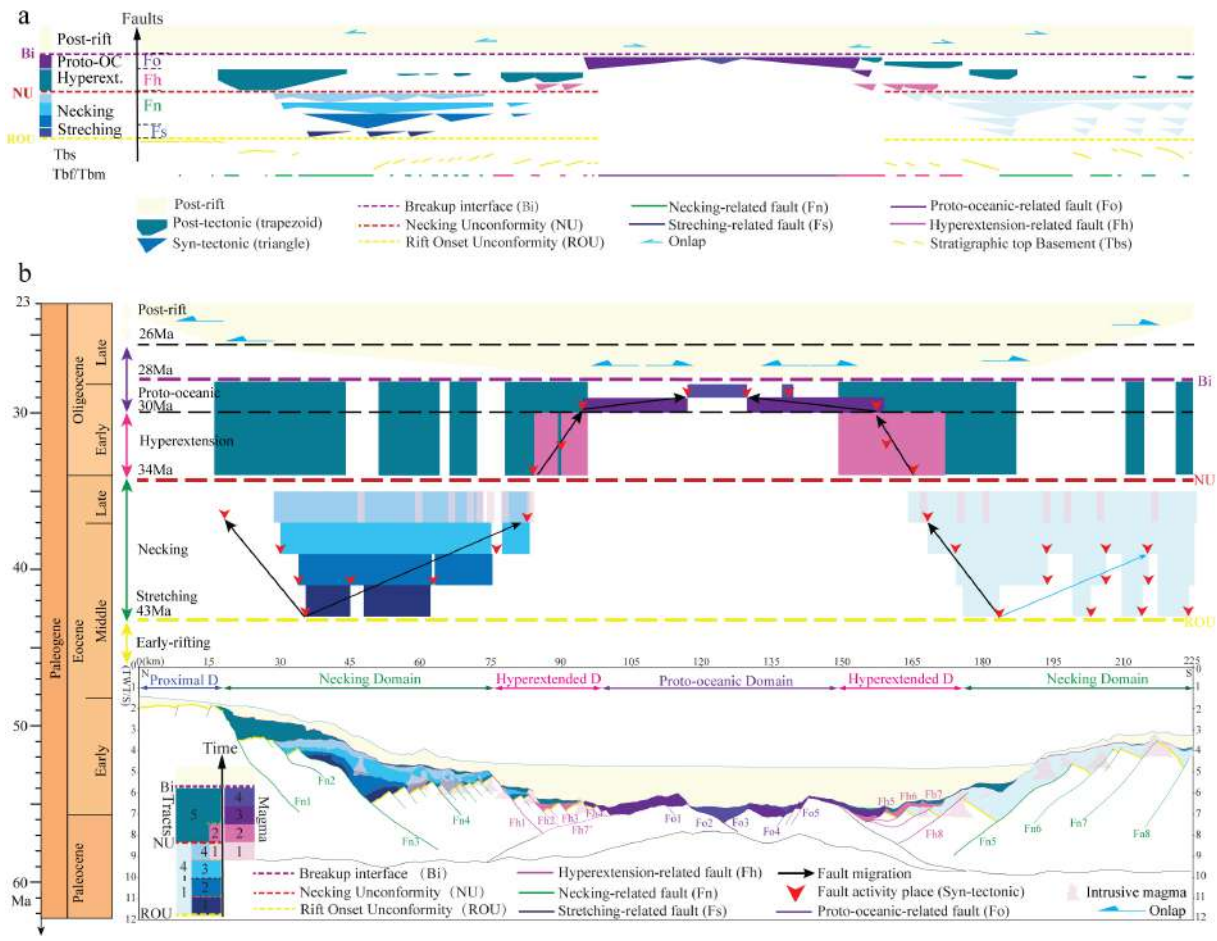

Figure II.11. *Time-space evolution of the tectonic (faults), sedimentary and magmatic system recorded in the section CGN-1 represented in a Wheeler diagram. (a) Evolution of different fault generations (F_n, F_h, F_o) and related depocenters during the formation of the conjugate rifted margins. (b) Evolution of tracts (T1 to T5) and magma (units 1 to 4) during evolution of the conjugate margins.*

Red arrows show the occurrence of syn-tectonic packages in the tracts (see also syn-tectonic triangle in Fig. II.11a). During the necking stage, deformation remains distributed at both margins, although some few faults (F_{n3} and F_{n5}) accommodate most of the deformation (for evolution at the northern margin during necking see Fig. II.9). The transition from necking to hyperextension at 34 Ma is marked by the formation of unconformities (NU), the first appearance of magma (unit 1), and by the subsequent creation of accommodation space across the whole margin (see also Fig. II.11a). This

is shown by deposition of sediments all across the margin, and the migration of deformation towards the future ocean during hyperextension (for details see Fig. II.8c to II.8f). This evolution is associated with the emplacement of magmatic units 2 to 4. Lithospheric breakup occurs at 28 Ma and is linked to the transition to passive infill in the distal margin, resulting in a well-defined unconformity above the breakup interface (Bi).

6.6. Strain localization during rifting and individualisation and dismembering of the H-block

The Wheeler diagram constructed for the CGN-1 section shown in Fig. II.11 provides an unpreceeded description of how extension, sedimentation and magmatism evolve through time and space during rifting and breakup at conjugate margins. Two main processes guide the evolution of rifting: 1) localization of deformation and focusing of magma, and 2) development of new rift domains that goes along with the creation of new real estate during rifting, leading to different types of Tb, which are Tb_s, Tb_f and Tb_m. Figs. II.12 and 13 show the evolution of strain localization and formation of rift domains across the transect with time. These representations highlight the early individualization and later dismembering of the H-block during rifting.

Figs. II.12 and II.13 build on the restoration shown in Fig. II.8. The localization of deformation, formation of rift domains and distribution of syn- and post tectonic packages during rifting are shown in time steps of 0.5 My, providing a top view of the restored evolution of rifting presented in Fig. II.8. Each bar represents a snapshot of the surface during the rift evolution. It distinguishes between type of sediments (no deposition or erosion; syn- or post-tectonic packages in the syn-rift mega-sequence and post-rift sediments, magma, and active or inactive faults. Fig. II.13a shows the formation of rift domains during rifting, Fig. II.13b the distribution of active and inactive faults and Fig. II.13c the distribution of syn- and post-tectonic packages belonging to the syn-rift mega-sequence as a function of the rift evolution.

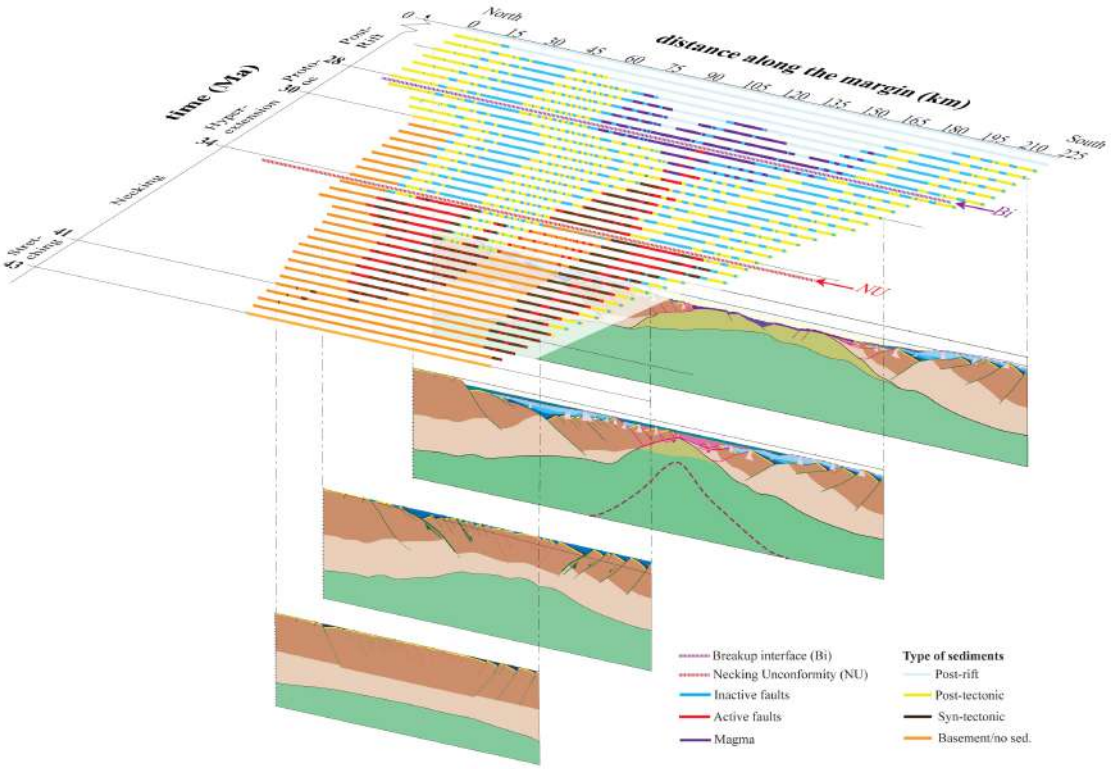

Figure II.12. *Temporal and spatial evolution of rifting shown in a section and map view based on the kinematic restoration shown in Fig. II.8. For section see Fig. II.8. The map view shows, in time steps of 0.5 Myr, a top view of the restored evolution of rifting presented in Fig. II.8. Each bar represents a snapshot of the surface during the rift evolution, representing type of sediments (no deposition or erosion; syn- or post-tectonic packages in the syn-rift mega-sequence, magma, and active or inactive faults.*

Figs. II.12 and II.13 highlight two main processes occurring during the rift evolution, which are: 1) strain localization and magma focusing, and 2) formation of rift domains and the individualization of an H-block during necking and its subsequent dismembering during hyperextension and the creation of new real estate that goes along with increasing extension. Strain localization evolves through three main steps. During the first stage, necking faults (F_n) localize around a keystone, and result in the individualization of an H-block. At this stage deformation is still distributed at the scale of the margin. During a second stage, deformation localizes inside the previously formed H-block (e.g., hyperextension faults F_h) and results in the dismembering of this block (see also Fig. II.8). During this stage, extension starts with distributed high-angle faults before it localizes along long-offset downward concave detachment faults. This process is accompanied by magmatic activity. During a last stage, deformation remains

active and evolves into a flip-flop stage (Epin & Manatschal, 2018; Epin et al., 2019; Gillard et al., 2016; Sauter et al., 2013) before final localized magmatic accretion. Strain localization goes along with the formation of new real estate (new Tb), which is key to the understanding of necking and hyperextended domains. New real estate can be formed either by exhumation faults (Tb_f), which occur in the necking domain (e.g., F_{n3} and F_{n5}) and in the hyperextended domain (e.g., $F_{h7\ to\ 7'}$), or by magmatic accretion (Tb_m), which becomes the dominant process at breakup (Figs. II.8, II.12 and II.13).

Several key observations can be deduced from Figs. II.12 and II.13.

The nature of top basement (Tb) changes during rifting, from a predominantly pre-rift stratigraphic top basement (Tb_s) to new real estate formed by either exhumed faults (Tb_f) in the necking and hyperextended domains to a magmatic top basement (Tb_m) in the proto-oceanic domain.

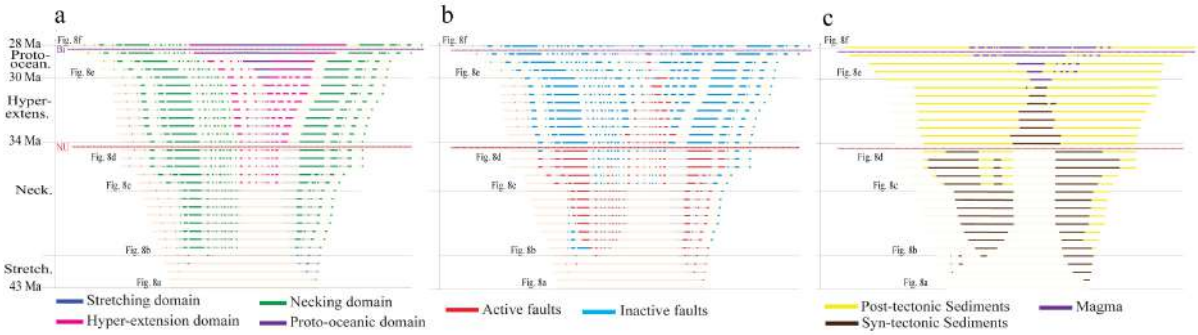

Figure II.13. *Strain localization and individualization and dismembering of the H-block and formation of new real estate (new Tb) by exhumation of basement along faults (Tb_f) or magmatic crust (Tb_m) as a function of rift evolution shown in a map view. (a) Formation of rift domains during rifting. (b) Distribution of active and inactive faults during rifting. (c) Distribution of syn- and post-tectonic packages and magmatic additions belonging to the syn-rift mega-sequence.*

The distribution of syn-tectonic and post-tectonic packages shows three distinct stages (Fig. II.13c). During early rifting, all deposits are syn-tectonic. However, most of the stretching domain and parts of the necking domain do not preserve sediments, either because sediments were not deposited (no accommodation space) or sediments have been deposited and then eroded during uplift related to necking. Thus, the base of the syn-rift mega-sequence is at most places an unconformity (e.g., Rift Onset

Unconformity). During necking, most of the deposition is syn-tectonic and accommodation space is created by faults. During hyperextension syn-tectonic sedimentation is localized into the domain of future breakup and occurs mostly over new real estate, while the rest of the margin is filled with post-tectonic sediments that are deposited over either inactive faults or allochthonous blocks. Accommodation space is created mainly by thermal subsidence. The key lesson is that, in regions where top basement is made of new real estate, pre-rift and/or early syn-rift sediments do not occur except over extensional allochthons. This has major implications for the correlation of stratigraphic packages from the proximal to the distal domain. Indeed, sediments downlapping onto new real estate (Tb_f or Tb_m) result in an apparent discordance between "basement" and overlying sediments (see Fig. II.11). This observation results in two potential interpretations: 1) either sediments are interpreted to onlap over an existing dynamic/subsiding topography, or 2) sedimentation occurred in a domain of active basement exhumation and/or magmatic accretion. The second interpretation is generally favored for oceanic and hyperextended domains. In contrast, such an interpretation remains disputed in the necking domain.

Although the isostatic evolution of rifting is difficult to determine, Fig. II.12 shows that the main event/change in the evolution of the rift system occurs at the transition between necking and hyperextension. Indeed, the occurrence of uplift during and/or at the end of necking is not limited to individual faults but results in widespread erosional unconformities, suggesting that vertical movements are linked to the rise of the asthenosphere and/or the yield of strong layers in the lithosphere or crust as suggested by Chenin et al. (2019, 2020). The synchronous occurrence of first magmatic additions with uplift and erosion further supports such an interpretation. This event is followed by a re-organization of the faults (from distributed to localized; see Fig. II.13b) and coincides with the onset of rapid subsidence and the deepening of the future distal margin.

7. Conclusion

The aim of this study was to find answers to when, how, and under what conditions major crustal thinning (necking) and hyperextension occur and how these processes are recorded in the stratigraphic and magmatic “tape recorder”. In order to answer to these questions, we had access to a world-class dense and high-resolution seismic data set. In order to describe the rift evolution we focused to the reflection seismic section CGN-1 that is one of the rare lines imaging the complete stratigraphic and magmatic architecture of a syn-rift mega-sequence across a conjugate pair of rifted margins. At present, no detailed study has evaluated in detail the complete spatial and temporal evolution of necking and hyperextension at the conjugate margins of the NW-SCS using in a Wheeler diagram approach. Such a documentation of the tectono-sedimentary and magmatic evolution requires a detailed kinematic restoration of the whole conjugate margin system and a first-order quantification of extension values and rates and description of the depositional systems during the necking and breakup stages. The main conclusions of this study can be summarized as follows:

(1) On the basis of identifying and characterizing total accommodation space, the thickness and shape of the crust, four rift domains were identified: proximal domain, necking domain, hyperextended domain, proto-oceanic domain. The sediments have been subdivided into a syn-rifting mega-sequence and a post-rift mega-sequence. The syn-rift mega-sequence was subdivided in 5 tracts and 4 magma units. The use of simple correlative surfaces within the syn-rift mega-sequence is hampered by the fact that rifting is polyphase, rift activity migrates and is diachronous and the mode of rifting changes through time. Therefore, the syn-rift mega-sequence has been subdivided in 5 tracts and in each tract syn- and post-tectonic packages have been defined. This approach enabled to decipher the sedimentary evolution associated with the deformation phases during the syn-rift time interval.

(2) A Wheeler approach has been used to build a time/space frame to describe the different tectonic events. On the basis of identifying and characterizing seismic data it was possible to identify two critical rifting events. A first one is the

necking stage that occurred from 43 to 34 Ma and was responsible for the thinning of crust to less than 10 km during deposition of tracts 1 to 4. A second event was the breakup that occurred from 34 to 28 Ma and was linked to hyperextension and onset of seafloor spreading during deposition of tract 5.

(3) Based on a detailed kinematic restoration we quantify extension values and rates for the different rift events. The results show that extension rates increase from rifting to seafloor spreading, with lower values during hyperextension.

(4) The restoration of the CGN-1 line enables to distinguish between three stages: During the first stage, necking faults localize around the keystone resulting into the individualization of an H-block. During the second stage deformation localizes inside the H-block and results in the dismembering of the block during hyperextension. During the final stage magmatic accretion becomes dominant but is still associated with extensional faults.

The new high-quality seismic data enabled us to propose a coherent 2D structural and tectonic model for the evolution of the NW-SCS margins. Future work will aim to investigate the study area in 3D. We believe that the results presented here will help to better understand crustal thinning (necking) and lithosphere breakup and the way these processes are recorded in the stratigraphic and magmatic tape recorder not only for the NW-SCS, but for rifted margins general.

Acknowledgments

This manuscript benefited from reviews of Anne Briais and Brian Taylor. We thank Duncan Erratt, Jean François Ghienne, Emmanuel Masini and Laetitia LePourhiet for helpful discussions. This research was financed and supported by National Natural Science Foundation of China (No.41830537;NO.41772109), China Scholarship Council (No.201706410090) and supported by the M5 consortium. The authors acknowledge CNOOC for the permission to publish the CGN-1 and CGN-1A seismic reflection lines. All the data used in this study will be archived in Figshare repository(https://doi.org/xxxxxxx) after acceptance.

References

Abdelmalak, M. M., Andersen, T. B., Planke, S., Faleide, J. I., Corfu, F., Tegner, C., et al. (2015). The ocean-continent transition in the mid-Norwegian margin: Insight from seismic data and an onshore Caledonian field analogue. *Geology*, *43*(11), 1011–1014. https://doi.org/10.1130/G37086.1

Bai, Y., Dong, D., Brune, S., Wu, S., & Wang, Z. (2019). Crustal stretching style variations in the northern margin of the South China Sea. *Tectonophysics*, *751*, 1–12. https://doi.org/10.1016/j.tecto.2018.12.012

Briais, A., Patriat, P., & Tapponnier, P. (1993). Updated interpretation of magnetic anomalies and seafloor spreading stages in the south China Sea: Implications for the Tertiary tectonics of Southeast Asia. *Journal of Geophysical Research: Solid Earth*, *98*(B4), 6299–6328. https://doi.org/10.1029/92JB02280

Brune, S., Heine, C., Pérez-Gussinyé, M., & Sobolev, S. V. (2014). Rift migration explains continental margin asymmetry and crustal hyper-extension. *Nature Communications*, *5*(1), 4014. https://doi.org/10.1038/ncomms5014

Brune, S., Williams, S. E., Butterworth, N. P., & Müller, R. D. (2016). Abrupt plate accelerations shape rifted continental margins. *Nature*, *536*(7615), 201–204. https://doi.org/10.1038/nature18319

Cameselle, A. L., Ranero, C. R., Franke, D., & Barckhausen, U. (2017). The continent-ocean transition on the northwestern South China Sea. *Basin Research*, *29*, 73–95. https://doi.org/10.1111/bre.12137

Cameselle, A. L., Ranero, C. R., & Barckhausen, U. (2020). Understanding the 3D Formation of a Wide Rift: The Central South China Sea Rift System. Tectonics, 39(12), e2019TC006040.

Chenin, P., Schmalholz, S. M., Manatschal, G., & Karner, G. D. (2018). Necking of the Lithosphere: A Reappraisal of Basic Concepts With Thermo-Mechanical Numerical Modeling. *Journal of Geophysical Research: Solid Earth*, *123*(6), 5279–5299. https://doi.org/10.1029/2017JB014155

Chenin, P., Manatschal, G., Decarlis, A., Schmalholz, S. M., Duretz, T., & Beltrando, M. (2019). Emersion of Distal Domains in Advanced Stages of Continental Rifting Explained by Asynchronous Crust and Mantle Necking. *Geochemistry, Geophysics, Geosystems*, *20*(8), 3821–3840. https://doi.org/10.1029/2019GC008357

Deng, H., Ren, J., Pang, X., Rey, P. F., McClay, K. R., Watkinson, I. M., et al. (2020). South China Sea documents the transition from wide continental rift to continental break up. *Nature Communications*, *11*(1), 4583. https://doi.org/10.1038/s41467-020-18448-y

Ding, W., Li, M., Zhao, L., Ruan, A., & Wu, Z. (2011). Cenozoic tectono-sedimentary characteristics and extension model of the Northwest Sub-basin, South China Sea. *Geoscience Frontiers*, *2*(4), 509–517. https://doi.org/10.1016/j.gsf.2011.05.010

Ding, W., Sun, Z., Mohn, G., Nirrengarten, M., Tugend, J., Manatschal, G., & Li, J. (2020). Lateral evolution of the rift-to-drift transition in the South China Sea: Evidence from multi-channel seismic data and IODP Expeditions 367&368 drilling results. *Earth and Planetary Science Letters*, *531*, 115932. https://doi.org/10.1016/j.epsl.2019.115932

Epin, M. -E., & Manatschal, G. (2018). Three-Dimensional Architecture, Structural Evolution, and Role of Inheritance Controlling Detachment Faulting at a Hyperextended Distal Margin: The Example of the Err Detachment System (SE Switzerland). *Tectonics*, 2018TC005125. https://doi.org/10.1029/2018TC005125

Epin, M.-E., Manatschal, G., Amman, M., Ribes, C., Clausse, A., Guffon, T., & Lescanne, M. (2019). Polyphase tectono-magmatic evolution during mantle exhumation in an ultra-distal, magma-poor rift domain: example of the fossil Platta ophiolite, SE Switzerland. *International Journal of Earth Sciences*. https://doi.org/10.1007/s00531-019-01772-0

Franke, D., Barckhausen, U., Baristeas, N., Engels, M., Ladage, S., Lutz, R., et al. (2011). The continent-ocean transition at the southeastern margin of the South China Sea. *Marine and Petroleum Geology*, *28*(6), 1187–1204. https://doi.org/10.1016/j.marpetgeo.2011.01.004

Franke, Dieter, Savva, D., Pubellier, M., Steuer, S., Mouly, B., Auxietre, J.-L., et al. (2014). The final rifting evolution in the South China Sea. *Marine and Petroleum Geology*, *58*, 704–720. https://doi.org/10.1016/j.marpetgeo.2013.11.020

Gao, J., Wu, S., McIntosh, K., Mi, L., Liu, Z., & Spence, G. (2016). Crustal structure and extension mode in the northwestern margin of the South China Sea: CRUSTAL EXTENSION OF THE SOUTH CHINA SEA. *Geochemistry, Geophysics, Geosystems*, *17*(6), 2143–2167. https://doi.org/10.1002/2016GC006247

Gee, J. S., & Kent, D. V. (2007). Source of oceanic magnetic anomalies and the geomagnetic polarity time scale, 455–507. https://doi.org/10.7916/D8DV1V8P

Gillard, M., Autin, J., Manatschal, G., Sauter, D., Munschy, M., & Schaming, M. (2015). Tectonomagmatic evolution of the final stages of rifting along the deep conjugate Australian-Antarctic magma-poor rifted margins: Constraints from seismic observations: Australian-Antarctic margins evolution. *Tectonics*, *34*(4), 753–783. https://doi.org/10.1002/2015TC003850

Gillard, M., Sauter, D., Tugend, J., Tomasi, S., Epin, M.-E., & Manatschal, G. (2017). Birth of an oceanic spreading center at a magma-poor rift system. *Scientific Reports*, *7*(1). https://doi.org/10.1038/s41598-017-15522-2

Gillard, M., Tugend, J., Müntener, O., Manatschal, G., Karner, G. D., Autin, J., et al. (2019). The role of serpentinization and magmatism in the formation of decoupling interfaces at magma-poor rifted margins. *Earth-Science Reviews*, *196*, 102882. https://doi.org/10.1016/j.earscirev.2019.102882

Gozzard, S., Kusznir, N., Franke, D., Cullen, A., Reemst, P., & Henstra, G. (2019). South China Sea crustal thickness and oceanic lithosphere distribution from satellite gravity inversion. *Petroleum Geoscience*, *25*(1), 112–128. https://doi.org/10.1144/petgeo2016-162

Hall, R. (2012). Late Jurassic–Cenozoic reconstructions of the Indonesian region and the Indian Ocean. *Tectonophysics*, *570–571*, 1–41. https://doi.org/10.1016/j.tecto.2012.04.021

Hall, R., & Breitfeld, H. T. (2017). Nature and demise of the Proto-South China Sea, *63*, 16.

Haupert, I., Manatschal, G., Decarlis, A., & Unternehr, P. (2016). Upper-plate magma-poor rifted margins: Stratigraphic architecture and structural evolution. *Marine and Petroleum Geology*, *69*, 241–261. https://doi.org/10.1016/j.marpetgeo.2015.10.020

Larsen, H. C., Sun, Z., Stock, J. M., Jian, Z., Alvarez Zarikian, C. A., Klaus, A., et al. (2018). Expedition 367/368 summary. *Sun, Z., Jian, Z., Stock, JM, Larsen, HC, Klaus, A., Alvarez Zarikian, CA, and the Expedition*, *367*, 368.

Larsen, H. C., Mohn, G., Nirrengarten, M., Sun, Z., Stock, J., Jian, Z., et al. (2018). Rapid transition from continental breakup to igneous oceanic crust in the South China Sea. *Nature Geoscience*, *11*(10), 782–789. https://doi.org/10.1038/s41561-018-0198-1

Lavier, L. L., & Manatschal, G. (2006). A mechanism to thin the continental lithosphere at magma-poor margins. *Nature*, *440*(7082), 324–328. https://doi.org/10.1038/nature04608

Lei, C., & Ren, J. (2016). Hyper-extended rift systems in the Xisha Trough, northwestern South China Sea: Implications for extreme crustal thinning ahead of a propagating ocean. *Marine and Petroleum Geology*, *77*, 846–864. https://doi.org/10.1016/j.marpetgeo.2016.07.022

Leroy, S., Razin, P., Autin, J., Bache, F., d'Acremont, E., Watremez, L., et al. (2012). From rifting to oceanic spreading in the Gulf of Aden: a synthesis. *Arabian Journal of Geosciences*, *5*(5), 859–901. https://doi.org/10.1007/s12517-011-0475-4

Li, C. F., Lin, J., Kulhanek, D. K., & Expedition 349 Scientists (Eds.). (2015). *South China Sea Tectonics* (Vol. 349). International Ocean Discovery Program. https://doi.org/10.14379/iodp.proc.349.2015

Li, C.-F., Xu, X., Lin, J., Sun, Z., Zhu, J., Yao, Y., et al. (2014). Ages and magnetic structures of the South China Sea constrained by deep tow magnetic surveys and IODP Expedition 349. *Geochemistry, Geophysics, Geosystems*, *15*(12), 4958–4983. https://doi.org/10.1002/2014GC005567

Li, F., Sun, Z., & Yang, H. (2018). Possible Spatial Distribution of the Mesozoic Volcanic Arc in the Present-Day South China Sea Continental Margin and Its Tectonic Implications. *Journal of Geophysical Research: Solid Earth*. https://doi.org/10.1029/2017JB014861

Li, F., Sun, Z., Yang, H., Lin, J., Stock, J. M., Zhao, Z., et al. (2020). Continental interior and edge breakup at convergent margins induced by subduction direction reversal: A numerical modeling study applied to the South China Sea margin. *Tectonics*. https://doi.org/10.1029/2020TC006409

Ligi, M., Bonatti, E., Bosworth, W., Cai, Y., Cipriani, A., Palmiotto, C., et al. (2018). Birth of an ocean in the Red Sea: Oceanic-type basaltic melt intrusions precede continental rupture. *Gondwana Research*, *54*, 150–160. https://doi.org/10.1016/j.gr.2017.11.002

Lin, J., Xu, Y., Sun, Z., & Zhou, Z. (2019). Mantle upwelling beneath the South China Sea and links to surrounding subduction systems. *National Science Review*, nwz123. https://doi.org/10.1093/nsr/nwz123

Lizarralde, D., Axen, G. J., Brown, H. E., Fletcher, J. M., González-Fernández, A., Harding, A. J., et al. (2007). Variation in styles of rifting in the Gulf of California. *Nature*, *448*(7152), 466–469. https://doi.org/10.1038/nature06035

Luo, P., Manatschal, G., Ren, J., Zhao, Z., Wang, H., & Tong, D. (2021). Tectono-magmatic and stratigraphic evolution of final rifting and breakup: evidence from the tip of the southwestern propagator in the South China Sea. Marine and Petroleum Geology, 105079.

Manatschal, G., Lavier, L., & Chenin, P. (2015). The role of inheritance in structuring hyperextended rift systems: Some considerations based on observations and numerical modeling. *Gondwana Research*, *27*(1), 140–164. https://doi.org/10.1016/j.gr.2014.08.006

Masini, E., Manatschal, G., & Mohn, G. (2013). The Alpine Tethys rifted margins: Reconciling old and new ideas to understand the stratigraphic architecture of magma-poor rifted margins. *Sedimentology*, *60*(1), 174–196. https://doi.org/10.1111/sed.12017

Masini, E., Manatschal, G., Tugend, J., Mohn, G., & Flament, J.-M. (2014). The tectono-sedimentary evolution of a hyper-extended rift basin: the example of the Arzacq–Mauléon rift system (Western Pyrenees, SW France). *International Journal of Earth Sciences*, *103*(6), 1569–1596. https://doi.org/10.1007/s00531-014-1023-8

Mohn, G., Manatschal, G., Beltrando, M., Masini, E., & Kusznir, N. (2012). Necking of continental crust in magma-poor rifted margins: Evidence from the fossil Alpine Tethys margins. *Tectonics*, *31*(1). https://doi.org/10.1029/2011TC002961

Nirrengarten, M., Mohn, G., Kusznir, N. J., Sapin, F., Despinois, F., Pubellier, M., et al. (2020). Extension modes and breakup processes of the southeast China-Northwest Palawan conjugate rifted margins. *Marine and Petroleum Geology*, *113*, 104123. https://doi.org/10.1016/j.marpetgeo.2019.104123

Osmundsen, P. T., & Ebbing, J. (2008). Styles of extension offshore mid-Norway and implications for mechanisms of crustal thinning at passive margins. *Tectonics*, *27*(6). https://doi.org/10.1029/2007TC002242

Pérez-Gussinyé, M., Ranero, C. R., Reston, T. J., & Sawyer, D. (2003). Mechanisms of extension at nonvolcanic margins: Evidence from the Galicia interior basin, west of Iberia. *Journal of Geophysical Research: Solid Earth*, *108*(B5). https://doi.org/10.1029/2001JB000901

Péron-Pinvidic, G., & Manatschal, G. (2009). The final rifting evolution at deep magma-poor passive margins from Iberia-Newfoundland: a new point of view. *International Journal of Earth Sciences*, *98*(7), 1581–1597. https://doi.org/10.1007/s00531-008-0337-9

Peron-Pinvidic, G., & Osmundsen, P. T. (2018). The Mid Norwegian - NE Greenland conjugate margins: Rifting evolution, margin segmentation, and breakup. *Marine and Petroleum Geology*, *98*, 162–184. https://doi.org/10.1016/j.marpetgeo.2018.08.011

Peron-Pinvidic, G., Manatschal, G., & the "IMAGinING RIFTING" Workshop Participants. (2019). Rifted Margins: State of the Art and Future Challenges. *Frontiers in Earth Science*, *7*, 218. https://doi.org/10.3389/feart.2019.00218

Qayyum, F., Betzler, C., & Catuneanu, O. (2017). The Wheeler diagram, flattening theory, and time. *Marine and Petroleum Geology*, *86*, 1417–1430. https://doi.org/10.1016/j.marpetgeo.2017.07.034

Reston, T. J. (2007). The formation of non-volcanic rifted margins by the progressive extension of the lithosphere: the example of the West Iberian margin. *Geological Society, London, Special Publications*, *282*(1), 77–110. https://doi.org/10.1144/SP282.5

Ribes, C., Ghienne, J.-F., Manatschal, G., Decarlis, A., Karner, G. D., Figueredo, P. H., & Johnson, C. A. (2019). Long-lived mega fault-scarps and related breccias at distal rifted margins: insights from present-day and fossil analogues. *Journal of the Geological Society*, jgs2018-181. https://doi.org/10.1144/jgs2018-181

Ribes, C., Manatschal, G., Ghienne, J.-F., Karner, G. D., Johnson, C. A., Figueredo, P. H., et al. (2019). The syn-rift stratigraphic record across a fossil hyper-extended rifted margin: the example of the northwestern Adriatic margin exposed in the Central Alps. *International Journal of Earth Sciences*, *108*(6), 2071–2095. https://doi.org/10.1007/s00531-019-01750-6

Ribes, C., Petri, B., Ghienne, J.-F., Manatschal, G., Galster, F., Karner, G. D., et al. (2020). Tectono-sedimentary evolution of a fossil ocean-continent transition: Tasna nappe, central Alps (SE Switzerland). *GSA Bulletin*, *132*(7–8), 1427–1446. https://doi.org/10.1130/B35310.1

Sauter, D., Cannat, M., Rouméjon, S., Andreani, M., Birot, D., Bronner, A., et al. (2013). Continuous exhumation of mantle-derived rocks at the Southwest Indian Ridge for 11 million years. *Nature Geoscience*, *6*(4), 314–320. https://doi.org/10.1038/ngeo1771

Sibuet, J.-C., Yeh, Y.-C., & Lee, C.-S. (2016). Geodynamics of the South China Sea. *Tectonophysics*, *692*, 98–119. https://doi.org/10.1016/j.tecto.2016.02.022

Stipp, M., Stünitz, H., Heilbronner, R., & Schmid, S. M. (2002). The eastern Tonale fault zone: a 'natural laboratory' for crystal plastic deformation of quartz over a temperature range from 250 to 700°C. *Journal of Structural Geology*, *24*(12), 1861–1884. https://doi.org/10.1016/S0191-8141(02)00035-4

Sun, Z., Jian, Z., Stock, J. M., Larsen, H. C., Klaus, A., Alvarez Zarikian, C. A., & Expedition 367/368 Scientists (Eds.). (2018). *Volume 367/368: South China Sea Rifted Margin* (Vol. 367/378). International Ocean Discovery Program. https://doi.org/10.14379/iodp.proc.367368.2018

Sun, Zhen, Lin, J., Qiu, N., Jian, Z., Wang, P., Pang, X., et al. (2019). The role of magmatism in the thinning and breakup of the South China Sea continental marginSpecial Topic: The South China Sea Ocean Drilling. *National Science Review*, *6*(5), 871–876. https://doi.org/10.1093/nsr/nwz116

Sutra, E., & Manatschal, G. (2012). How does the continental crust thin in a hyperextended rifted margin? Insights from the Iberia margin. *Geology*, *40*(2), 139–142. https://doi.org/10.1130/G32786.1

Sutra, E., Manatschal, G., Mohn, G., & Unternehr, P. (2013). Quantification and restoration of extensional deformation along the Western Iberia and Newfoundland rifted margins: Strain Distribution Along Rifted Margins. *Geochemistry, Geophysics, Geosystems*, *14*(8), 2575–2597. https://doi.org/10.1002/ggge.20135

Taylor, B., & Hayes, D. E. (1983). Origin and history of the South China Sea basin. In D. E. Hayes (Ed.), *Geophysical Monograph Series* (Vol. 27, pp. 23–56). Washington, D. C.: American Geophysical Union. https://doi.org/10.1029/GM027p0023

Taylor, B., Goodliffe, A. M., & Martinez, F. (1999). How continents break up: Insights from Papua New Guinea. *Journal of Geophysical Research: Solid Earth*, *104*(B4), 7497–7512. https://doi.org/10.1029/1998JB900115

Tugend, J., Manatschal, G., & Kusznir, N. J. (2015). Spatial and temporal evolution of hyperextended rift systems: Implication for the nature, kinematics, and timing of the Iberian-European plate boundary. *Geology*, *43*(1), 15–18. https://doi.org/10.1130/G36072.1

Tugend, Julie, Gillard, M., Manatschal, G., Nirrengarten, M., Harkin, C., Epin, M.-E., et al. (2018). Reappraisal of the magma-rich versus magma-poor rifted margin archetypes. *Geological Society, London, Special Publications*, SP476.9. https://doi.org/10.1144/SP476.9

Wang, J., Pang, X., Liu, B., Zheng, J., & Wang, H. (2018). The Baiyun and Liwan Sags: Two supradetachment basins on the passive continental margin of the northern South China Sea. *Marine and Petroleum Geology*, *95*, 206–218. https://doi.org/10.1016/j.marpetgeo.2018.05.001

Wang, P. (2019). New insights into marine basin opening. *National Science Review*, *6*(5), 870–870. https://doi.org/10.1093/nsr/nwz099

Wang, Q., Zhao, M., Zhang, H., Zhang, J., He, E., Yuan, Y., & Qiu, X. (2020). Crustal velocity structure of the Northwest Sub-basin of the South China Sea based on seismic data reprocessing. *Science China Earth Sciences*. https://doi.org/10.1007/s11430-020-9654-4

Warner, M. R. (1987). Seismic reflections from the Moho -- the effect of isostasy. *Geophysical Journal International*, *88*(2), 425–435. https://doi.org/10.1111/j.1365-246X.1987.tb06651.x

Weiwei, D., Schnabel, M., Franke, D., Aiguo, R., & Zhenli, W. (2012). Crustal Structure across the Northwestern Margin of South China Sea: Evidence for Magma-poor Rifting from a Wide-angle Seismic Profile. *Acta Geologica Sinica - English Edition*, *86*(4), 854–866. https://doi.org/10.1111/j.1755-6724.2012.00711.x

Wheeler, H. E. (1964). Baselevel, Lithosphere Surface, and Time-Stratigraphy. *Geological Society of America Bulletin*, *75*(7), 599. https://doi.org/10.1130/0016-7606(1964)75[599:BLSAT]2.0.CO;2

Wu, Y., Ding, W., Clift, P. D., Li, J., Yin, S., Fang, Y., & Ding, H. (2019). Sedimentary budget of the Northwest Sub-basin, South China Sea: controlling factors and geological implications. *International Geology Review*, *0*(0), 1–18. https://doi.org/10.1080/00206814.2019.1597392

Wu, Z., Li, J., Ruan, A., Lou, H., Ding, W., Niu, X., & Li, X. (2012). Crustal structure of the northwestern sub-basin, South China Sea: Results from a wide-angle seismic experiment. *Science China Earth Sciences*, *55*(1), 159–172. https://doi.org/10.1007/s11430-011-4324-9

Xie, X., Ren, J., Pang, X., Lei, C., & Chen, H. (2019). Stratigraphic architectures and associated unconformities of Pearl River Mouth basin during rifting and lithospheric breakup of the South China Sea. *Marine Geophysical Research*. https://doi.org/10.1007/s11001-019-09378-6

Yang, L., Ren, J., McIntosh, K., Pang, X., Lei, C., & Zhao, Y. (2018). The structure and evolution of deepwater basins in the distal margin of the northern South China Sea and their implications for the formation of the continental margin. *Marine and Petroleum Geology*, *92*, 234–254. https://doi.org/10.1016/j.marpetgeo.2018.02.032

Ye, Q., Mei, L., Shi, H., Shu, Y., Camanni, G., & Wu, J. (2018). A low-angle normal fault and basement structures within the Enping Sag, Pearl River Mouth Basin: Insights into late

Mesozoic to early Cenozoic tectonic evolution of the South China Sea area. *Tectonophysics*, *731–732*, 1–16. https://doi.org/10.1016/j.tecto.2018.03.003

Ye, Q., Mei, L., Shi, H., Camanni, G., Shu, Y., Wu, J., et al. (2018). The Late Cretaceous tectonic evolution of the South China Sea area: An overview, and new perspectives from 3D seismic reflection data. *Earth-Science Reviews*, *187*, 186–204. https://doi.org/10.1016/j.earscirev.2018.09.013

Ye, Q., Mei, L., Shi, H., Du, J., Deng, P., Shu, Y., & Camanni, G. (2020). The influence of pre-existing basement faults on the Cenozoic structure and evolution of the proximal domain, northern South China Sea rifted margin. *Tectonics*. https://doi.org/10.1029/2019TC005845

Zhang, C., Su, M., Pang, X., Zheng, J., Liu, B., Sun, Z., & Manatschal, G. (2019). Tectono-sedimentary analysis of the hyper-extended Liwan sag basin (mid-northern margin of the South China Sea). *Tectonics*. https://doi.org/10.1029/2018TC005063

Zhang, Cuimei, Sun, Z., Manatschal, G., Pang, X., Qiu, N., Su, M., et al. (2020). Syn-rift magmatic characteristics and evolution at a sediment-rich margin: Insights from high-resolution seismic data from the South China Sea. *Gondwana Research*. https://doi.org/10.1016/j.gr.2020.11.012

Zhang, C., Sun, Z., Manatschal, G., Pang, X., Qiu, N., Su, M., ... & Zhao, Y. (2021). Syn-rift magmatic characteristics and evolution at a sediment-rich margin: Insights from high-resolution seismic data from the South China Sea. Gondwana Research, 91, 81-96.

Zhao, Y., Ren, J., Pang, X., Yang, L., & Zheng, J. (2018). Structural style, formation of low angle normal fault and its controls on the evolution of Baiyun Rift, northern margin of the South China Sea. *Marine and Petroleum Geology*, *89*, 687–700. https://doi.org/10.1016/j.marpetgeo.2017.11.001

Zhou, Z., Mei, L., Liu, J., Zheng, J., Chen, L., & Hao, S. (2018). Continentward-dipping detachment fault system and asymmetric rift structure of the Baiyun Sag, northern South China Sea. *Tectonophysics*, *726*, 121–136. https://doi.org/10.1016/j.tecto.2018.02.002

Zhu, J., Xu, H., Qiu, X., Ye, C., & Li, S. (2018). Crustal structure and rifting of the northern South China Sea margin: Evidence from shoreline-crossing seismic investigations. *Geological Journal*, *53*(5), 2065–2083. https://doi.org/10.1002/gj.3034

CHAPTER III

The transition from continental to lithospheric breakup recorded in proto-oceanic crust: Insights from the NW South China Sea

Peng Chao[1], Gianreto Manatschal[1], Cuimei Zhang[2], Pauline Chenin[1], Jianye Ren[3], Xiong Pang[4], Jingyun Zheng[4]

[1]Université de Strasbourg, CNRS, ENGEES, ITES UMR 7063, Strasbourg 67084, France

[2] Southern Marine Science and Engineering Guangdong Laboratory, Guangzhou, China

[3]College of Marine Science and Technology, China University of Geosciences, Wuhan, China

[4]CNOOC Ltd.-Shenzhen, Branch, Shenzhen, China

Key Points:

- Breakup in NW-South China Sea is a lasting event that starts with continental breakup and ends with lithospheric breakup
- The ocean-continent transition records a shift from faulting-dominated to magmatic accretion-dominated accommodation of extension
- High sedimentation rates and significant magmatic activity provide an efficient tape recorder of the tectono-magmatic evolution

Continental breakup, lithospheric breakup, proto-oceanic crust, NW-South China Sea, syn-tectonic magmatism

Abstract

The formation of a new plate boundary and creation of first oceanic crust, two of the most important processes of Plate Tectonics, remain yet little understood. While older studies used to assume a sharp *Ocean Continent Boundary (OCB)* between continent and ocean, recent studies suggest a progressive *Ocean Continent Transition (OCT)* between unequivocal continental and oceanic crust. In the latter view, *breakup* is not instantaneous but a lasting *breakup phase*, which raises questions on: (1) the nature of the *OCT* basement; and (2) the nature of the processes operating between continental and lithospheric breakup. Based on detailed observations of high quality and yet unpublished reflection seismic data, we describe and interpret the characteristic structures of the NW-South China Sea OCT and their relationship with overlying syn-*breakup phase* sediments. The result shows that the OCT displays a transition from fault-dominated rifting to magma-dominated seafloor spreading. On its continent-ward side, the OCT is made of *hybrid crust* where extensional thinning of continental crust is compensated by syn-extensional magmatic addition. Oceanward, this *hybrid crust* evolves into a fully magmatic but fault-dominated *proto-oceanic crust*, and finally turns into a mature *Penrose-type oceanic crust*. Relying on the growth structures of the syn-breakup sedimentary sequences and magmatic additions, we propose a kinematic restoration of the breakup phase where out-of-sequence flip-flop detachment faulting show a progressive decrease in fault heaves and is finally replaced by fully magmatic accretion. This restoration can account for the observed switch from asymmetric fault-dominated- to symmetric and fully magmatic seafloor accretion.

1. Introduction

Regardless of recent progress in describing and understanding both continental rifting and Mid-Ocean Ridges (MOR), the spatial and temporal transition between the two, as well as the processes involved in this transition remain little understood. This is not only

due to the complexity of the interactions between tectonic and magmatic processes and the resultant hybrid crusts (i.e., composite crust made of both continental crust and magmatic additions), but also to the lack of data and observations. At magma-rich margins the transition from the emblematic Seaward Dipping Reflection (SDR) to mature oceanic crust is well imaged, little is known about the nature of the underlying lower crust (Geoffroy et al., 2015, Paton et al., 2017, McDermott et al., 2018, Norcliffe et al., 2018). In contrast, at magma-poor margins such as the Galicia margin (Dean et al. 2015 and Davy et al., 2016), the Gulf of Guinea (Gillard et al., 2017), the E-India margin (Harkin et al., 2019), the Somalia margin (Mortimer et al. 2020) and the Labrador Sea (Gouiza and Paton, 2019), and at so-called young margins such as the Red Sea (Ligi et al. 2018), Gulf of Aden (Nonn et al., 2017), or Gulf of California (Lizarralde et al. 2007), the transition to mature oceanic crust has been intensely explored. However, no high-quality seismic data of the OCT comparable to those from the SCS (e.g., Zhang et al., 2021) have been published at any of these margins. In this study, we had access to an exceptional set of seismic reflection lines that image the whole crust down to 12 seconds Two Way Travel time (TWT) across the tip of a NW-SCS propagator (Fig. III.1a). Apart from the high-quality data set, the high sedimentation rates during breakup and the well imaged sedimentary architectures provide an efficient tape recorder to document the breakup process. This is rare and has so far only been observed at a few rifted margins, such as the Antarctica - South Australian conjugate margins (Gillard et al., 2015) and at the Gabon OCT (Epin et al., 2021). These studies suggested that the sequential evolution of detachment systems resulted in a complex sedimentary architecture, very similar to the observations described in this study.

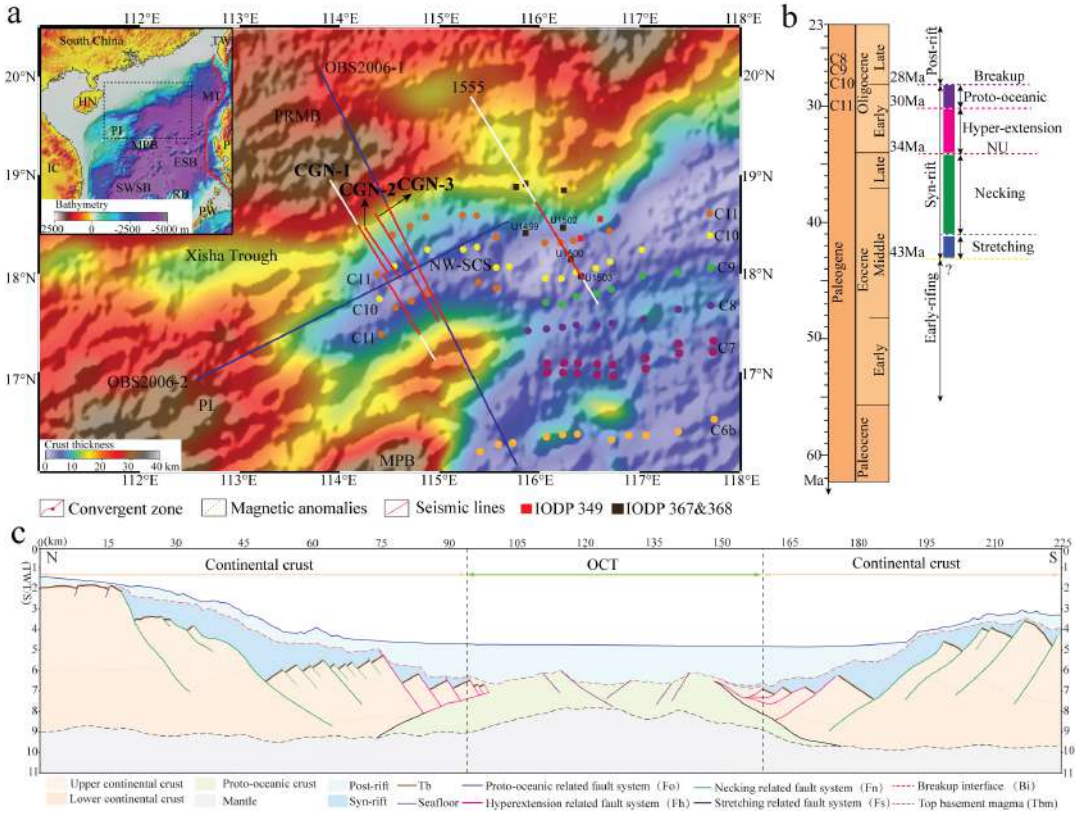

Figure 1. *Location of the study area in the NW South China Sea (SCS) and the used datasets. (a) Crustal thickness map based on gravity inversion with superimposed shaded relief free-air gravity anomaly from Gozzard el al. (2019). Inset on the top left corner shows bathymetric map of the NW-SCS with the location of the principal seismic reflection lines (red lines) and refraction lines (blue lines) presented in this paper and the IODP drill sites (Li et al., 2015; Sun et al., 2018). The location of the magnetic anomalies is based on Briais et al. (1993). White lines show the reflection seismic lines CGN-1 from Chao et al. (subm.) and the 1555 (white line) from Zhang el al. (2019). (b) Time frame for the evolution of rifting in the NW-SCS modified from Chao et al. (subm.). (c) Seismic interpretation of CGN-1 seismic reflection line modified from Chao et al. (subm.) showing the first order seismic architecture of the two conjugate margins across the NW SCS (for details see Chao et al. (subm). Abbreviations used in the figure: DG, Dangerous Ground (Nansha); ESB, East Sub-Basin; HN, Hainan; IC, Indochina; MPB, Macclesfield-Paracel Bank; MT, Manila Trench; NW-SCS, North West South China Sea; NU, Necking unconformity; PI, Paracel Islands (Xisha Islands); PRMB, Pearl River Mouth Basin; P, Palawan; RB, Reed Bank (Liyue); SW-SB, South West Sub-Basin; TW, Taiwan.*

Previous studies in the northern SCS described a narrow, 15 to 25 km wide OCT (Zhang et al., 2019). Larsen et al. (2018) and Ding et al. (2019) proposed that a short and focused magmatic event at the end of rifting triggered continental breakup and initiated seafloor spreading. In contrast, Zhang et al. (2020) and Chao et al. (subm.) proposed that the first magma formed during crustal necking and that the magmatic budget steadily increased with time and progressively focused at the location of final lithospheric breakup. Implicit in this interpretation is that magma and extension interacted already during rifting. Thus, the classical binary view that margins are either magma-rich or magma-poor is challenged by observations, which show that tectonic and magmatic activity interact during rifting (e.g., Zhang et al., 2020; Tugend et al., 2020). Recent studies in the SCS showed that neither mantle exhumation nor SDR can be found, which suggests that the SCS rifted margins are *intermediate margins* between the *magma-rich* and *magma-poor* endmembers (Larsen et al. 2018; Ding et al. 2019). Zhang et al. (2021) provided a detailed description of the OCT in the central northern SCS margin and proposed that breakup was achieved via the interplay between detachment faulting and simultaneous magma-production. Quirk et al. (2014) investigated the link between extension and magmatic processes in the OCT of the East Greenland margin in the N-Atlantic. They proposed a tectono-magmatic model with magmatic growth structures to explain continental breakup at this magma-rich rifted margin. Péron-Pinvidic and Naliboff (2020) described where, when and how detachment faults originate in an exhumation system during rifting. Gillard et al. (2019) proposed a model to explain how the *breakup phase* is recorded at magma-poor rifted margins. They highlighted a transition from an exhumed mantle stage dominated by flip-flop detachment faulting and hydration processes to a magmatic stage during which (proto-)oceanic crust is formed. Based on field observations, Epin et al. (2019) and Coltat et al. (2020) proposed conceptual models for the tectono-magmatic evolution of final rifting showing that detachment systems are active simultaneous to emplacement of extrusive magmatic additions. Sauter et al. (2021) described sub-axial deformation in the oceanic lower crust based on seismic and outcrop observations. These authors argued for local and short-term deformation within the axial zone of oceanic

spreading systems. However, none of these studies focused on the nature of the proto-oceanic crust and its syn-breakup sedimentary record.

Falvey (1974) stated that breakup is recorded by a so-called *« breakup unconformity »*, a concept that has been widely used and abused in the literature. Braun and Beaumont (1989) modeled an isostatic adjustment following the mechanical breakup of the lithosphere. However, their modeled isostatic respond may not correspond to the onset of seafloor spreading but may correspond to a necking-related mechanical collapse (e.g., Chenin et al. 2019, 2020). This is in line with the study of Pérez-Gussinyé et al. (2020), who showed that lithospheric breakup, is not associated with a significant stress drop. Whether breakup results in a margin-wide, carriable unconformity remains until present highly debated (Tucholke and Sibuet, 2007; Peron-Pinvidic et al., 2007; Ribes et al., 2019; Pérez-Gussinyé et al., 2020).

The aim of this study is to document and describe the crustal structure and related sedimentary architecture of the OCT domain located between unequivocal continental and oceanic crust. In other words, we aim to investigate the process at play between continental and lithospheric breakup. Practically, we describe the seismic characteristics and geometrical and spatial relationships between syn-tectonic magmatic additions and sediments in the OCT of the NW South China Sea (SCS) propagator. The observations enable us to address the following questions: 1) are detachment faults active during breakup? 2) if yes, how do they interact with magma? and 3) what is the role of magma during breakup. Answering to these questions enable to understand the spatial and temporal tectonic and magmatic evolution during the breakup phase and to discuss the processes leading to the formation of a mature oceanic spreading centre. This study takes advantage of an exceptional, high-quality reflection seismic data set that images one of the few examples worldwide of the tip of an oceanic propagator where sedimentation rates are sufficiently high to record the syn-breakup tectono-magmatic evolution in the OCT.

2. Geological setting

The SCS, the largest marginal sea in the western Pacific region, is surrounded by three major tectonic plates, the Pacific, the Eurasian, and the Indian-Australian plates (Fig. III.1a). It includes two V-shaped propagators, an older one in the NW and a younger in the SW. In this study we focus on the termination of the NW V-shaped oceanic propagator that separates the Western Pearl River Mouth Basin (PRMB) in the north from the Macclesfield-Paracel Block (Zhongsha-Xisha) in the south (Fig. III.1a). Cameselle et al. (2017) suggested that the spreading centre propagated westwards and died shortly before reaching the Xisha Trough in late Early Oligocene. Chao et al. (subm) established the timing of rifting based on the detailed analysis of the stratigraphic record imaged in Line CGN-1 (Fig. III.1a) and a review of regional studies (Fig. III.1b). Crustal thickness in the study area is constrained by refraction seismic lines (see OBS2006-1 and OBS 2006-2 in Fig. III.1a; Wu et al., 2012；Ding et al., 2012；Wang et al., 2020). Crustal thickness and thinning factors of the area have been published by Gozzard et al. (2018). Seismic interpretations of the crustal structure and their link to refraction seismic data and potential field data have been discussed by Ding et al. (2012); Wu et al. (2012); Franke et al. (2014); Gao et al. (2016); Cameselle et al. (2017, 2021); Wang et al. (2020); and Chao et al. (subm). Our study focuses on the OCT at the tip of NW-SCS propagator (Fig. III.1a).

The age of onset of rifting in the SCS is poorly constrained and usually assumed to occur at 65 Ma in the PRMB, which corresponds to the stratigraphic marker horizon Tg (Xie et al., 2019). Based on the occurrence of magnetic anomalies C11 and C10 defined by Briais et al. (1993), the lithospheric breakup occurred around 32 Ma (Early Oligocene). Here we will focus on the short time frame between crustal separation and onset of seafloor spreading, i.e., between continental and lithospheric breakup. The intervening OCT domain is 30 ± 10 km wide, which may correspond, using the spreading rates determined by Chao et al. (subm), to a formation period of ca. 2 My. However, since breakup is widely accepted to propagate from east to west and to be diachronous, the age

of breakup is expected to change along strike. Thus, here we prefer to use the timeline constrained by sedimentary units rather than precise ages for breakup.

3. Data, methods, and terminology

3.1 Data used and acquisition parameters

With permission of the China National Offshore Oil Corporation (CNOOC), we had access to a large, high resolution seismic data set, from which we selected three seismic lines referred to as CGN-1, CGN-2, CGN-3. These multichannel seismic (MCS) sections, which record down to 12 s Two-Way Travel time (TWT) belong to a large survey that imaged about 5000 km of multichannel 2D sections covering the NW-SCS subbasin (about 35,000 km²). All seismic profiles are oriented NNW-SSE with a spacing of 20 km and ENE-WSW with a spacing of about 15 km. The seismic signal was generated using a Bolt Longlife Airgun (3850 cubic inches) by means of compressed air (2000 psi). The record length and sampling rate were set at 11996 ms TWT and 2 ms, respectively. The acquired signals were recorded within 396 channels using a fold of 99, and lie in the frequency range of 40-60 Hz, allowing a vertical resolution up to 40 m. The data were processed through Omega V1.8.1 software, applying a bandpass filter (ranging from 6 Hz of low-cut frequency and 12 dB/s of low-cut slope to 136 Hz of high-cut frequency and 276 dB/s of high-cut slope), a denoising and amplitude compensation and a post-stack time Kirchhoff migration (for more details see Hui Chen, 2021).

To compare our results from the NW-SCS with those from the central N-SCS, where International Ocean Discovery Program (IODP) Expeditions 367/368/368X (Larsen et al., 2018) drilled several sites in the OCT, we added line 1555. This line is located approximately 170 km further east of the study area and has been penetrated by an IODP drill site (Fig. III.1a). The section has been interpreted and published by Zhang et al. (2021). Adding this line enables us to compare the calibrated sedimentary sequences and the nature of the crust at line 1555 with the lines CGN-1 to 3 we interpret in this study. We are, however, aware that a precise correlation with the IODP drill holes in the central N-

SCS is not possible if one assumes that the breakup propagated westwards. However, we consider that the time difference is minor, which is supported by the observation that magnetic anomalies can be correlated in between the two sites (Fig. III.1a).

3.2 Methods

In the analysis of seismic reflection data, there is a thin line between an objective description and a subjective interpretation, and thus it is important to keep in mind that seismic interpretations are non-unique. Our aim here is to provide a coherent description of geometrical relationships imaged in reflection seismic lines. To do so, we first undertake a careful line drawing of the high-resolution seismic sections. Then we perform an interpretation in four successive steps, namely: 1) identification of first-order seismic interfaces (seafloor, top acoustic basement, Moho) and rift domain boundaries; 2) definition of sedimentary sequences based on geometrical relationships between sediment reflections and top acoustic basement; 3) characterization of the nature of basement in the OCT, including a comparison with refraction seismic data of OBS lines 2006-1 and 2006-2 published by Wu et al. (2012); Ding et al. (2012) and Wang et al. (2020) (for location see Fig. III.1a) and IODP drill holes; and 4) mapping and description of faults, including fault offsets, sealing levels, fault terminations and decoupling levels. This approach enables us to build a coherent interpretation, in which first-order and objective observations are first established, building the frame for subsequent, more subjective interpretations. Using observations made in the sedimentary section, we build a relative temporal and spatial framework that we link with structural observations and magmatic processes in the basement.

3.3 Terminology

Definition of first order interfaces

Although first-order seismic interfaces such as top acoustic basement and Moho represent physical boundaries that can be objectively imaged and observed, their nature is subject to geological interpretation. Top acoustic Basement (Tb) is defined in this study as

a high-amplitude and well-imaged reflection that corresponds to the interface between compactable sediments and acoustic basement. In such a description, Tb represents an interface without any time or genetic connotation. In time sections, Warner (1987) showed that Moho appears at a relatively constant two-way travel time despite the highly variable structure of the overlying crust. The apparent flatness of seismic Moho on reflection seismic sections in time, also referred to as the “10 s rule”, is an artefact produced when the crust is in local isostatic equilibrium. In the NW-SCS, where breakup occurred between 30 and 28 Ma (Briais et al., 1993) and thermal equilibrium has not been achieved yet, seismic Moho is typically between 9 to 8 s TWT (Chao et al., subm). However, Moho as a geological interface is difficult to interpret in an OCT since it can correspond either to an initial contact between continental and mantle rocks, between hydrated and non-hydrated mantle (serpentinization front), or between new igneous material and mantle (Zhang et al., 2021). Thus, when interpreting Moho, it is important to distinguish between petrological Moho (compositional) and seismic Moho (velocity). In OCTs the definition of the first-order interfaces such as Tb and/or Moho is particularly challenging since their nature can change from pre-rift inherited, to tectonic or magmatic contacts.

Definition of rift domains

Rift domains in the OCT of magma-poor margins have been defined by Gillard et al. (2019) and Tugend et al. (2020). However, rifted margins in the SCS show many differences to the classical magma-rich or magma-poor margins defined in the N-Atlantic. This study will mainly focus to the most distal margins and its transition to oceanic crust. Ding et al. (2020) and Zhang et al. (2021) defined OCTs in the SCS as the domain between unequivocal continental and oceanic crusts, an approach that we follow. Here we define *unequivocal continental crust* as a wedging crust with only minor magmatic additions and where thinning is essentially related to faulting. Where magmatic additions become dominant and cover and underplate thinned continental crust, we considered it as a *hybrid crust*. *Proto-oceanic crust* is defined as fully magmatic crust, with magmatic and faulting processes that are not localized yet, and where rocks comprising a vertical section

do not result from 1D accretion. Instead, crustal sections in proto-oceanic domains result from the tectonic juxtaposition of magmatic rocks formed at different time and crustal levels. We define *unequivocal oceanic crust* as a box-shaped crust, where Tb is sub-horizontal and parallel to seismic Moho (when observed) and the overlying sediments show passive infill and the spreading process is steady state. The OCT lying between unequivocal continental and oceanic crusts therefore consists of hybrid and proto-oceanic crusts in our definition. The term OCT does not presuppose the nature of the underlying crust, which may be either hybrid or fully magmatic. While the term OCT is descriptive, the definitions of hybrid and proto-oceanic crusts are interpretative, and we only use them in the discussion where we examine the processes related to the formation of the breakup phase.

Definition of sedimentary sequences, faults and magmatic additions

In this study, we define the sediment layer as the layer made of compactable sediments bounded by Tb and the seafloor. We focus on sediments deposited during final rifting and early seafloor spreading, i.e. only the deepest sediments deposited over Tb and occurring in the OCT, which we define as the *syn-breakup sedimentary sequence*. These sediments show geometrical relationships to faults and magmatic additions that help to deduce the evolution of the OCT. The base of the syn-breakup sedimentary sequence coincides with Tb. Its top coincides with the breakup interface (Bi), which corresponds to the timeline synchronous to the formation of first unequivocal oceanic crust (for details see section 4.2). All sediments above Bi show passive infill and do not display evidence for an important tectonic overprint. In our seismic interpretation, we distinguish between three different sedimentary sequences (S1 to S3). We consider Sx to be *synchronous across one given seismic line*. Laterally (i.e., along the propagator), Sx are *diachronous* but we consider them to be deposited at a *similar timing relative to the breakup process*.

Faults are not directly imaged by seismic methods, however their existence can be deduced from offsets in Tb and/or other interfaces/reflections. In this study, we identify the breakaways of high-angle normal faults and, wherever possible, syn-tectonic sedimentary-

and/or magmatic sequences, as well as post-tectonic sequences which seal faults. Such observations enable us to determine relative fault ages. We also define the levels where faults sole out at depth. These levels may correspond to brittle-ductile transitions (Sutra et al., 2012) or, alternatively, the top of underplated material (Zhang et al., 2021). In OCTs magma emplacement, hydration and the occurrence of extensional detachment systems result in a complexity that cannot be deduced from seismic observations alone. Although interpretations of faults and magmatic additions are non-unique, their explanation should be coherent and fit with the geophysical and geological observations.

4. Seismic interpretation of the OCT

4.1. Seismic observations and location of the OCT

CGN-1 line

The CGN-1 line (Fig. III.2a) is a conjugate, long offset high-quality reflection seismic line that has been described, interpreted and restored in Chao et al. (subm) (for location see Fig. III.1a, and for complete section see Fig. III.1c). Here we focus on the OCT only. In CGN-1 seafloor is sub-horizontal and lies at about 4.5 s TWT. Top basement (Tb) can be traced across the whole line, where it corresponds to a strong reflection (Fig. III.1b). It separates sub-parallel and tilted reflections interpreted as compactable sediments from a reflective basement where single reflections are difficult to define. Tb deepens abruptly from 5–6 s TWT to ca. 7 s TWT on the first 5 km at both ends of the line and remains at a relatively constant depth of 6 to 7 s TWT between km 5 and 110. However, between km 25 and 40 and km 70 and 85 Tb dips slightly continent-wards. Tb is offset by normal faults in numerous places along the entire section. Moho reflections are difficult to define but may correspond to a set of reflections that occur at about 9 s TWT.

Based on the description of Tb, but also of the sedimentary architecture and intra-basement reflections (for details see next sections), we define a boundary separating an unequivocal continental crust from the OCT at about km 10 in the north and km 100 in the south. North of km 10 Tb is ill defined but presumably staircase-shaped (i.e., truncated and

offset by narrowly spaced south-dipping normal faults) and overlain by chaotic reflections. The southern boundary at km 10 occurs where the general trend of Tb changes from south- to first flat and then slightly north dipping. South of km 100, Tb is offset by major north dipping faults more widely spaced than on the conjugate northern margin and overlain by transparent packages. The southern boundary at km 100 corresponds also to a change of the general dip of Tb from sub-horizontal to south dipping. Unequivocal oceanic crust is not observed in this section.

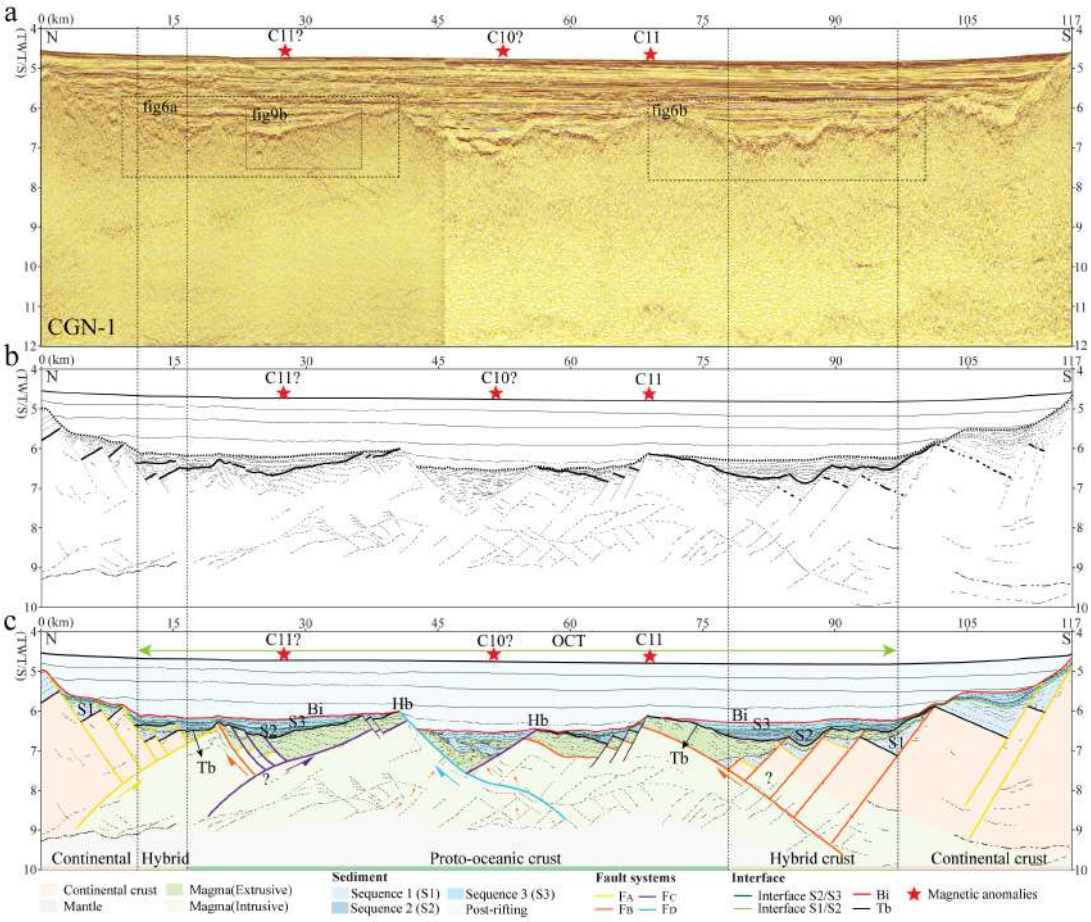

Figure III.2. *CGN-1 reflection seismic section across the NW-SCS with location of magnetic anomalies. For location see Fig. III.1a. (a) Time migrated reflection seismic section CGN-1 with location of magnetic anomalies (red stars). (b) Line drawing of the seismic section CGN-1, the bold lines are Tb and Bi. (c) Seismic interpretation of CGN-1 with first-order interfaces, stratigraphic horizons and the tectonic structures. Three sedimentary sequences (S1-S3) and four fault systems (FA, FB, FC, FD) were defined (for explanation see discussion section). Abbreviations used in the figure: Bi, Breakup interface; Tb, Top acoustic Basement; Hb, basement high.*

CGN-3 line

The CGN-3 line (Fig. III.3a) is parallel to the CGN-1 line and located ca. 25 km further east (Fig. III.1a). In CGN-3 (Fig. III.3b) seafloor is sub-horizontal and lies at about 5 s TWT. Tb corresponds to a characteristic, strong reflection between 6 and 7s TWT across the whole line. Note that it dips continent-wards between km 20 and 40 and km 90 and 110. It is offset by minor, widely spaced faults between km 15 and 40 and between km 70 and 115. Between km 15 and 115, Tb is more difficult to observe and its interpretation, as well as that of faults, are more subjective. Between km 40 and 70, Tb is sub-horizontal and not faulted. Between km 15 and 115, Tb and its relation to the overlying sediments are well imaged. Moho reflections are difficult to define but may correspond to a set of reflectors that occurs at ca. 9 s TWT across the entire section. The interrelationship between Tb and Moho varies from convergent to parallel.

Based on the description of Tb, the sedimentary architecture and intra-basement reflectivity (for details see below), we place the boundary between unequivocal continental crust and the OCT domain at km 15 in the north and km 115 in the south. Continent-ward of these two boundaries, the continental domain is complex with an ill-defined Tb affected by low-angle oceanward dipping faults and overlain by chaotic reflective packages. Oceanward of these boundaries, the OCT domain displays a well-defined Tb offset by faults that dip at higher angle towards the center of the section. In the OCT domain, Tb is underlain by reflective, about 0.5 s thick reflective material and faint dipping reflections. In the overlaying sediments, tilted and wedging sequences can be observed. At km 40 in the north and km 70 in the south, we define a boundary between the OCT and unequivocal oceanic crust. The oceanic domain is characterized by flat, continuous, and non-faulted top basement overlain by passive infill sediment.

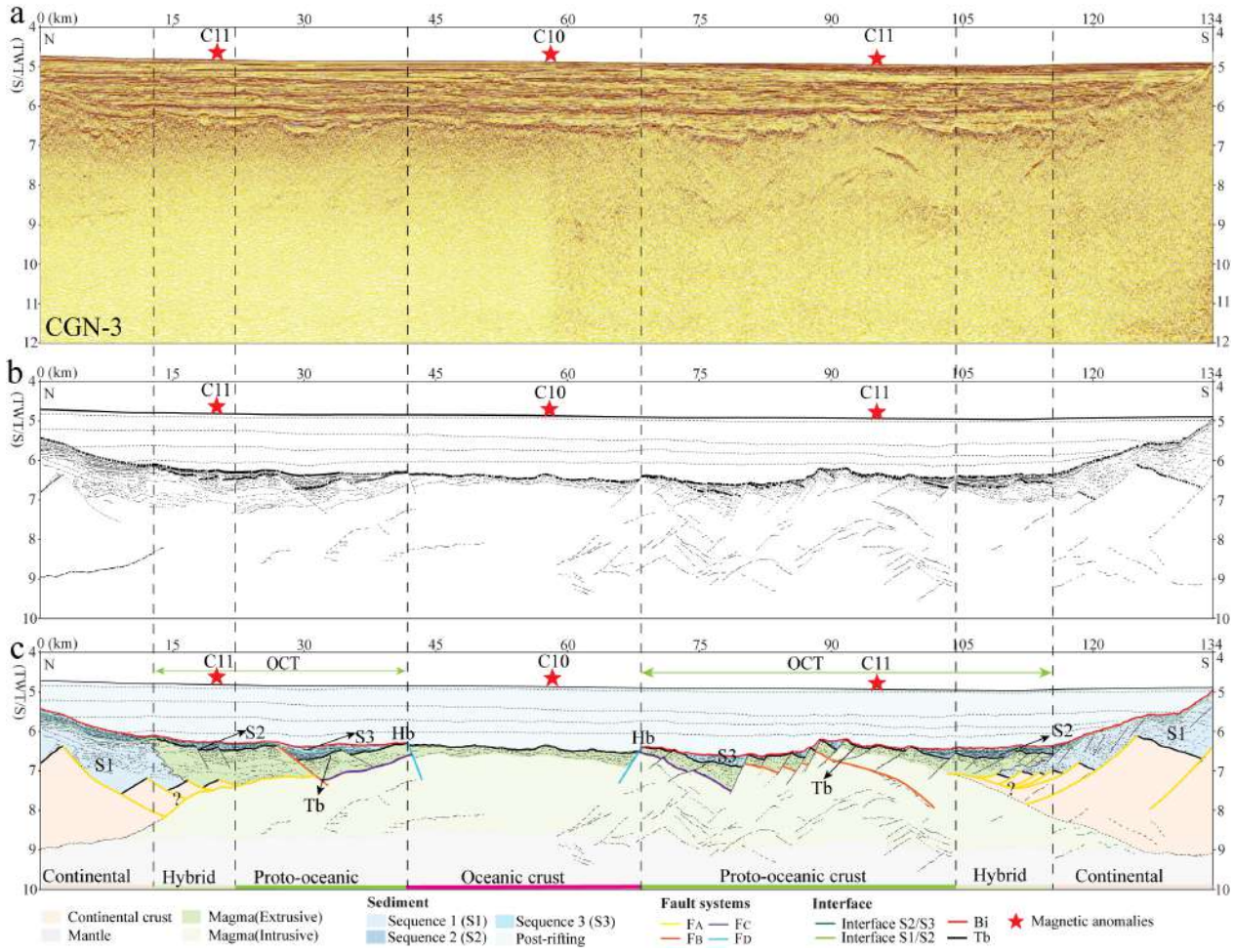

Figure III.3. *CGN-3 reflection seismic section across the NW-SCS with location of magnetic anomalies (red stars). For location see Fig. III.1a. (a) Time migrated reflection seismic section CGN-3. (b) Line drawing of the seismic section CGN-3, the bold lines are Tb and Bi. (c) Seismic interpretation of CGN-3 with first-order interfaces, stratigraphic horizons and the tectonic structures (for explanation see discussion section). Three sedimentary sequences (S1-S3) and four faults systems (Fa, Fb, Fc, Fd) were defined. Abbreviations used in the figure: Bi, Breakup interface; Tb, Top acoustic Basement; Hb, basement high.*

CGN-2 line

The CGN-2 line (Fig. III.4a) is located between the CGN-1 and CGN-3 lines and images the transition from continental to oceanic crust at the northern margin of the NW-SCS propagator (Fig. III.1a). The seafloor is slightly south-dipping to sub-horizontal and lies at ca. 4.5 s TWT (Fig. III.4b). Tb corresponds to a characteristic, strong reflection that

lies between 6 and 7 s TWT south of km 15. Between about km 15 and 45, Tb dips northwards. North of km 15, Tb deepens from 5 to 7 s and is offset by south-dipping normal faults and overlain by chaotic reflective material. We define at about km 15 the northern boundary of the OCT. In the OCT, Tb is well imaged and offset and tilted northward along south dipping faults, which show small offsets. The underlying basement shows some faint reflectivity. In the overlying sediments, tilted and wedging sequences can be recognized. Moho reflections are well imaged in the north at ca. 9 to10 s TWT, while to the south Moho may correspond to a set of reflectors at ca. 9 s TWT as in other sections. Based on the description of Tb, the link between sediment architecture and underlying intra-basement reflections, and in analogy with section CGN-3, we propose a domain boundary at about km 45 separating the OCT from unequivocal oceanic crust. The oceanic domain is characterized by a flat and reflective Tb at 6.5 s TWT overlain by sub-horizontal sediments showing passive infill. No reflectivity can be observed in the underlying basement. Moho is located at 8.5 s TWT and the crust is about 2 s TWT thick with a parallel Tb and Moho.

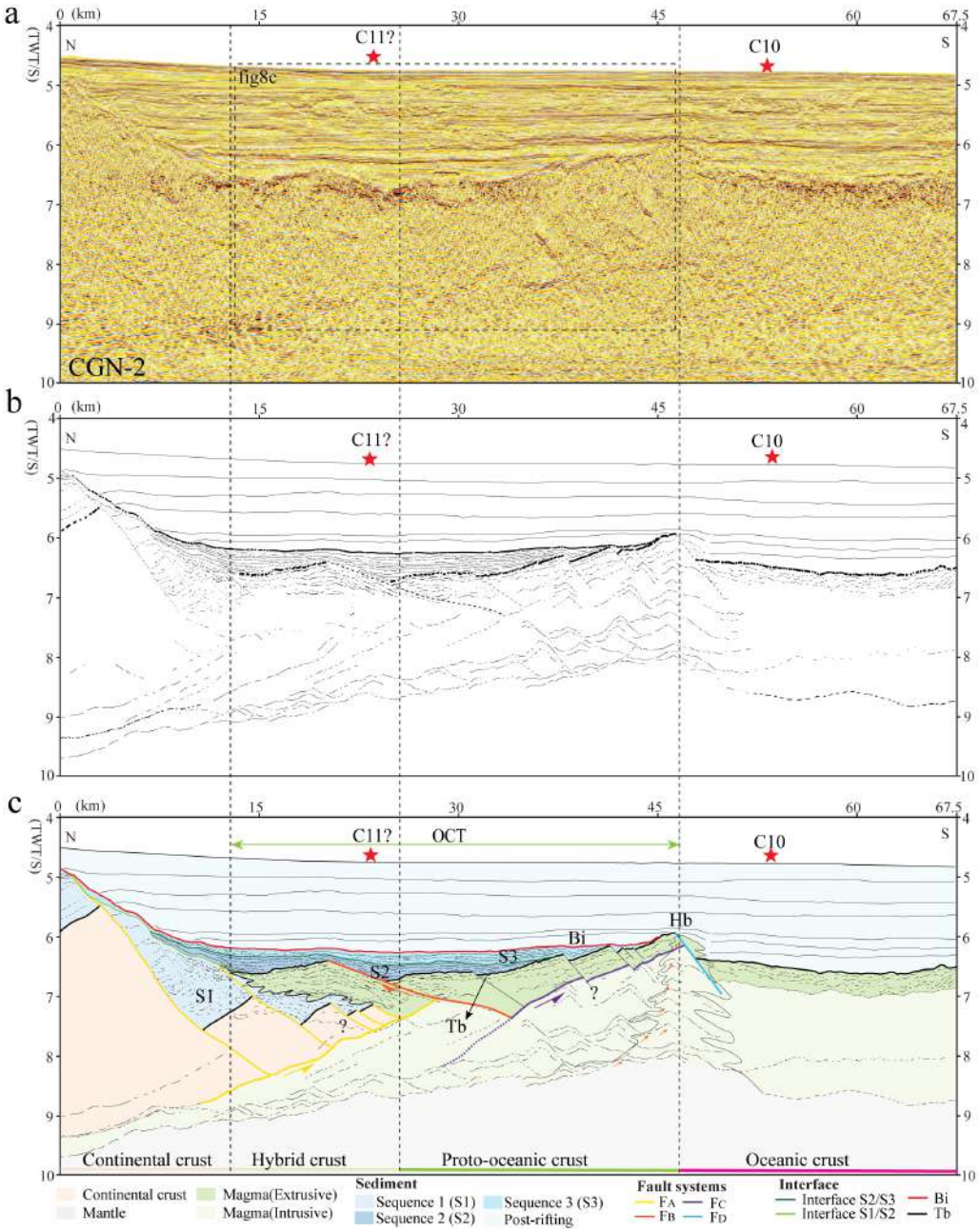

Figure III.4. *CGN-2 reflection seismic section with location of magnetic anomalies (red star). For location see Fig. III.1a. (a) Time migrated reflection seismic section CGN-2. (b) Line drawing of the seismic section CGN-2, the bold lines are Tb and Bi. (c) Seismic interpretation of CGN-2 with first-order interfaces, stratigraphic horizons and the tectonic structures. Three sedimentary sequences (S1-S3) and four fault systems (Fa, Fb, Fc, Fd) were defined (for explanation see discussion section). Abbreviations used in the figure: Bi, Breakup interface; Tb, Top acoustic Basement; Hb, basement high.*

Line 1555

Line 1555 (Fig. III.5a) is located about 200 km east of CGN-3 and images the transition from continental to oceanic crust (Fig. III.1a) where IODP drilled the OCT (see position of IODP Sites U1499, U1500, U1502 and U1503 in Fig. III.1a and Fig. III.5b). An interpretation of the line has been published by Zhang et al. (2021). Adding this line enables us to compare the nature of the crust and sediments calibrated by IODP drill holes with the previously presented sections for which we do not have drill hole calibration. Here we base our interpretation on that published by Zhang et al. (2021)

The seafloor in line 1555 is slightly south-dipping to sub-horizontal and lies at about 5 s TWT (Fig. III.5b). Tb corresponds to a characteristic, strong reflection between 6 and 7 s TWT. North of km 20, Tb is difficult to interpret but relying on the interpretation of Zhang et al. (2021) and the IODP results, the underlying basement is interpreted as continental. Based on the trend of Tb, the link between sediment architecture and underlying intra-basement reflections, and following the IODP results, we locate the domain boundary between OCT and unequivocal oceanic crust at km 35. In the OCT Tb is offset and tilted northwards along south dipping faults with small offsets. The underlying basement shows some faint reflectivity. The overlaying sediments show tilted and wedging sequences. Moho reflections are difficult to recognize. The oceanic domain is characterized by a flat and reflective Tb between 6.5 and 7 s TWT offset by minor, south-dipping faults overlain by a transparent package that in turn is overlain by sub-horizontal reflective material. A sub-horizontal set of reflectivity parallel to Tb can be observed in the underlying basement between 8 and 9 s TWT. The thickness of the crust is ca. 2 s TWT.

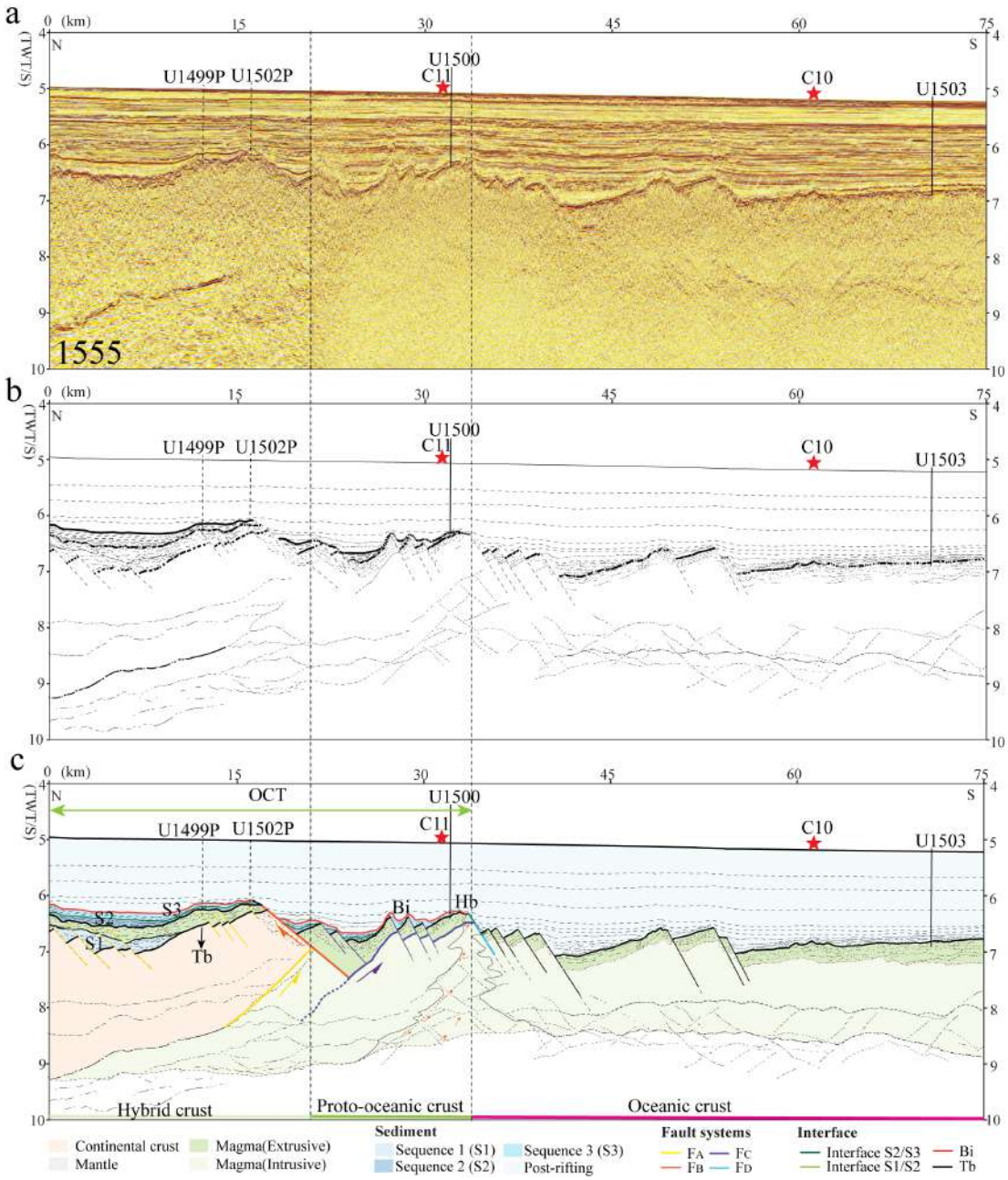

Figure III.5. *1555 reflection seismic section with location of magnetic anomalies (red stars) and IODP drill holes (projected). For location see Fig. III.1a. (a) Time migrated reflection seismic section 1555. (b) Line drawing of the seismic section 1555, the bold lines are Tb and Bi. (c) Seismic interpretation of 1555 with first-order interfaces, stratigraphic horizons and the tectonic structures. Three sedimentary sequences (S1-S3) and four fault systems (FA, FB, FC, FD) were defined. Abbreviations used in the figure: Bi, Breakup interface; Tb, Top acoustic Basement; Hb, basement high.*

4.2. Sediment architecture in the OCT

A key difference between the OCT as defined in Figs. III.2b to III.5b and the adjacent continental and oceanic domains is the overlying sedimentary architecture. In the continental domain the sedimentary architecture is complex. It includes syn-rift sediments that display either a syn- or post-tectonic architectures (for a detailed description see Chao et al. subm). In the oceanic domain the sedimentary architecture is much simpler since it only includes passive infill. Here we focus on the syn-breakup sedimentary sequences in the OCT domain. Fig. III.6 shows zooms on the OCT sedimentary sequence on either side of line CGN-1 (see Fig. III.2a for location of the zooms within the section). Three sedimentary sequences can be defined, referred to as S1, S2 and S3. These sequences display both syn- and post-tectonic architectures. Similar sequences can be defined in the OCT of all sections shown in Figs. III.2b to III.5b (see Fig. III.7 where a zoom on the sedimentary sequence is shown for each section). To better highlight the sediment architecture, we use a strong vertical exaggeration in Fig. III.7 and focus on the sedimentary packages.

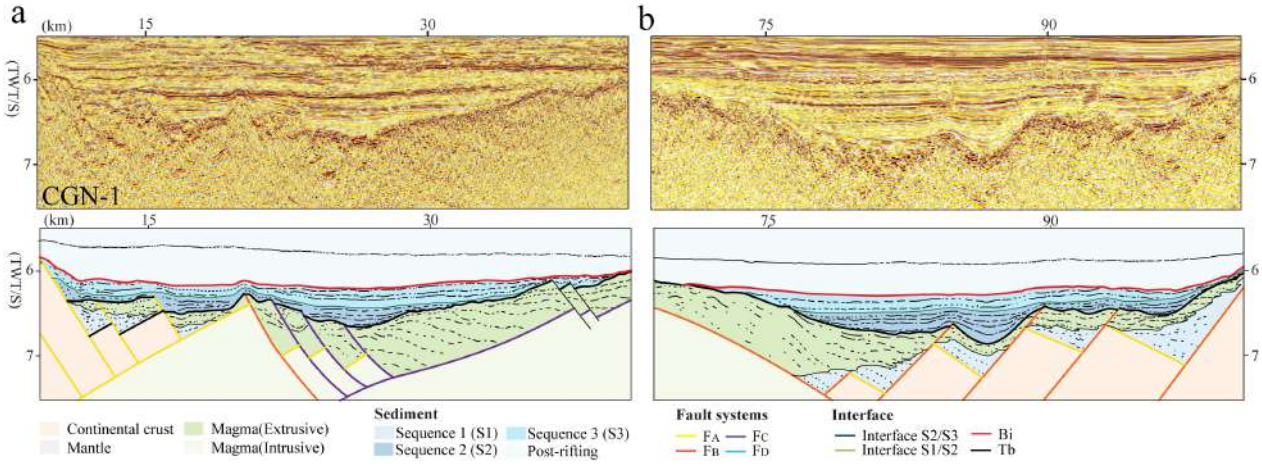

Figure III.6. *(a) Zoom on CGN-1 line showing the sedimentary architecture of the northern margin. Section below shows line drawing and interpretation of seismic section. (b) Zoom on CGN-1 line showing the sedimentary architecture of the southern margin and line drawing and interpretation in underlying section. For location of zooms see Fig. III.2a.*

Sequence 1 (S1): The architecture of S1 is best imaged in lines CGN-1 and 1555 (Figs. III.7a and III.7d). S1 shows thickening into faults in the continental domain indicating a syn-tectonic nature. Oceanward, this sequence interfingers with magmatic additions. That S1 shows syn-tectonic relationships with faults offsetting continental basement. Since they interfingers with magmatic additions, i.e., are time equivalent, its deposition had to occurred during final rifting simultaneous to crustal thinning and magma emplacement. While S1 is overlain by S2 in the continent-ward part of the OCT domain, S1 is either overlain by and/or interfingers with massive packages further oceanward. These packages lack well defined continuous reflections and are interpreted as extrusive magmatic additions (see next section).

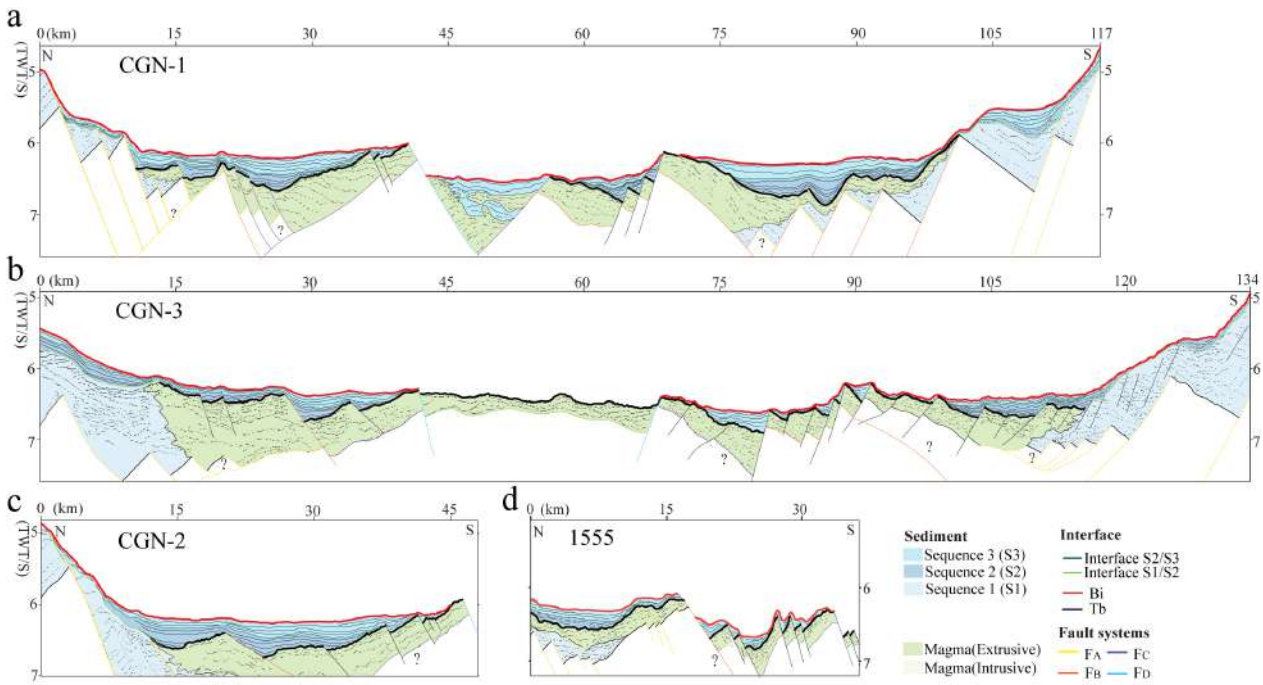

Figure III.7. *Zoom on the sedimentary sequence shown for the CGN-1(a), the CGN-3(b), the CGN-2(c) and the 1555(d) sections. To better highlight the sediment architecture, we use a strong vertical exaggeration and focus on the sedimentary packages only. Bold black line below is Tb (top basement) and bold red line is Bi (breakup interface).*

Sequences 2 & 3 (S2 & S3): Both sequences are well imaged in all sections and the following characteristics can be observed: 1) S2 seals faults over the continental domain and is conformably overlain by S3; 2) S2 and S3 show thickening into oceanward dipping faults and oceanward wedging sequences; and 3) S2 is back tilted and onlapped by S3 oceanward. These geometrical relationships can be observed in all sections in Fig. III.7. In contrast, in the oceanic domain no syn-tectonic sedimentary architectures can be observed, and all sediments show passive infill. A comparison of the S2 and S3 in the OCT of the conjugate margins imaged in CGN-1 and CGN-3 shows an increasing symmetry toward the section centre and an oceanward migration of deformation.

The ages of sequences S1 to S3 range within the timing of the *breakup phase* and may be similar in sections CGN-1, CGN-2 and CGN-3 due to the relative proximity of the lines (about 15 km distance apart). In contrast, an age correlation with line 1555 is more difficult considering that breakup propagated westwards (Cameselle et al., 2015). However, it is interesting to note that the three sequences identified in line 1555 show the same geometrical relationships relative to breakup as those recognized in CGN1–3, which are: 1) an oceanward migration of the syn-tectonic sequence with time, 2) an oceanward wedging of sedimentary sequences, and 3) a tilting and onlapping of successive sedimentary sequences oceanward. The interpretation of the sedimentary sequences and their importance for the understanding of the breakup process is discussed in Section 5.2.

4.3. Nature of basement in the OCT

Geophysical characteristics

The nature and architecture of basement in OCTs are complex and cannot be deduced from reflection seismic observations alone. The OBS2006-1 refraction seismic section (Fig. III.8a; ref. Ding et al. 2012) located east of the CGN-3 line (Fig. III.1a) shows the velocity structure across the conjugate margins, including the OCT and oceanic domains. Velocity sections through the continental-, OCT- and oceanic domains are shown in Fig. III.8d. Refraction seismic data display the characteristic wedging of mid-crustal velocities ranging between 6 and 7 km/s and depict an asymmetry between the two

conjugate margins (Fig. III.8a), confirming observations previously reported from the nearby reflection seismic section CGN-3 (Fig. III.3). The basement in the OCT shows a change in the velocity gradient and crustal thickness from the continent towards the ocean, with a gradual increase of lower crustal velocity and the establishment of a classical three-layered crust oceanward (see read and blue lines in Fig. III.8a). Note, however, that the velocity structure in the OCT is similar to that of oceanic crust, which suggests that basement composition may be comparable in these two domains.

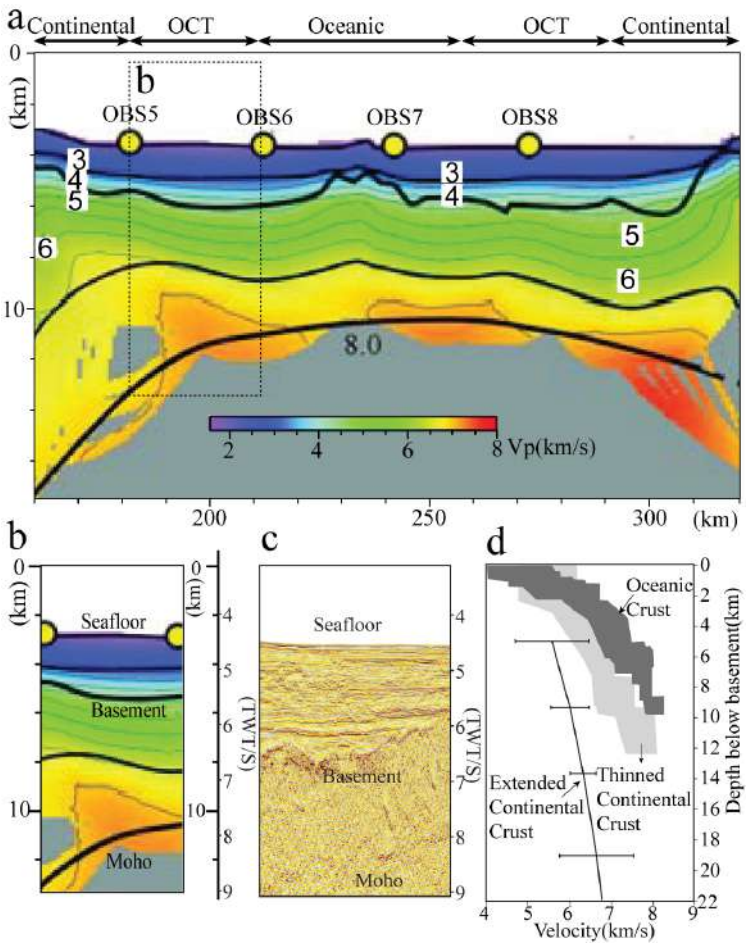

Figure III.8. *(a) The OBS2006-1 refraction seismic section from Ding et al. (2012). The OBS2006-1 section is located east of the CGN-3 line (for location see Fig. III.1a) and shows the velocity structure across the conjugate margins. (b) refraction image from OCT (for location see Fig. III.8a). (c) reflection image from OCT (for location see Fig.4a). (d) Velocity sections through the continental-, OCT- and oceanic domains.*

Fig. III.8b and Fig. III.8c shows a reflection and refraction image from the OCT. Since the refraction line is in depth while the reflection line is in time a direct comparison between the two is not possible. However, the two main interfaces that are Tb and Moho are expected to correspond to sharp velocity contrasts providing good reflections. While this is true for Tb, Moho appears to be linked to a more complex velocity structure in the OCT, which may be linked to the nature of the lower crust and the possible occurrence of high velocity cumulates (for discussion see below). Overall, the comparison between the refraction- and reflection sections supports the classical three-layer subdivision commonly found in Penrose-type oceanic crust. The top layer is characterized by very reflective seismic facies (for an example see Fig. III.9b) and shows velocities ranging from 5 to 6 km/sec (Figs. III.8a and III.8c). Such a layer can be best interpreted as extrusive magmatic additions. This is also supported by IODP Site U1500 in line 1555 (see Fig. III.5a for location of the drill hole) that penetrated basalts with a MOR signature. The reminder of the crust shows velocities of 7 km/s and higher, which suggests that this domain is made of mafic igneous material.

Extrusive magmatic additions *(dark green layer in Figs. III.2c–III.5c)*

Extrusive magmatic additions have been interpreted in all seismic lines (Figs. III.2c to III.5c) and have also been drilled at line 1555 (Fig. III.5c). In reflection seismic lines, magmatic additions are difficult to define, which adds some ambiguity to the seismic interpretation. In all sections, (Figs. III.2c to III.5c) the top ~ 0.5 s of the basement in the OCT is made of more reflective material. The best-imaged example is shown in Fig. III.9b, which displays a zoom of the top basement of line CGN-1 (Fig. III.2a). It shows oceanward dipping/stacking reflections that are comprised within a 0.5 s wide strip whose base is sub-parallel to Tb. These reflections bear some similarities with the classical Seaward Dipping Reflections (SDR) at magma-rich margins, however they are much smaller/shorter. While the top of this strip is relatively smooth, the base is more structured. The resolution of the image does, however, not allow us to make more precise observations of the nature of contact to the underlying basement. We interpret these structures as basalt flows that

formed during accretion of the OCT. Oceanward dipping faults affect these structures but cannot account for the oceanward tilting of the reflections.

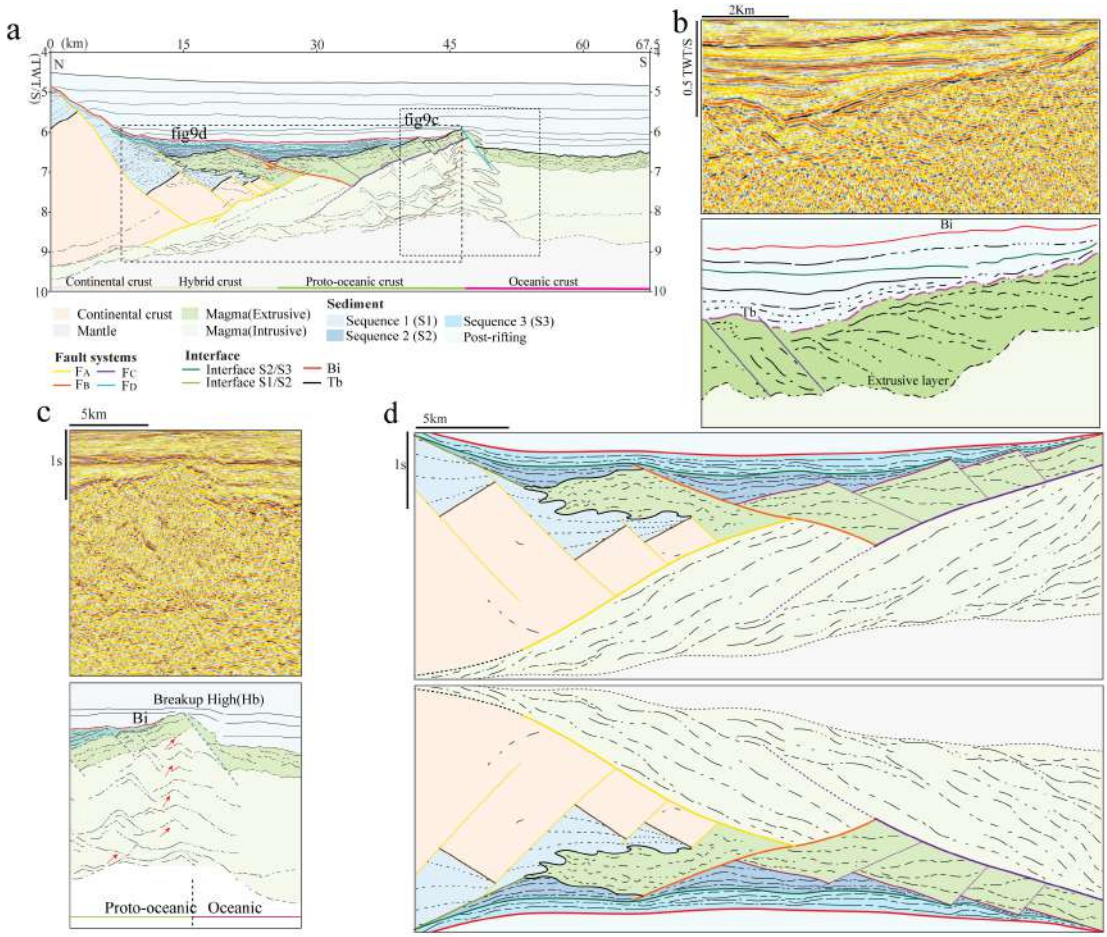

Figure III.9. *(a) CGN-2 reflection seismic section. (b) Extrusive magmatic addition at the top of the basement of line CGN-1(for location see Fig. III.2a). The oceanward dipping reflections are comprised within a 0.5s wide strip with a base that is sub-parallel to Tb. (c) The oceanward end of of the OCT formed by a basement high referred to as Breakup High (Hb) (for location see Fig.9a). (d) The upper panel line shows a line drawing of the crustal structure (for location see Fig. III.9a and for details see line CGN-2 shown in Fig. III.4. The lower section is a mirrored image of the interpretation. Note that the reflections dipping continent ward in the upright section show similarities to Sea Dipping Reflection Sequences (SDR) described from volcanic margins.*

In all sections (Figs. III.2c to III.5c), the oceanward end of the OCT coincides with the termination of the continent-ward dipping Tb, i.e., with a basement high (H_b). At a crustal scale, H_b appears to coincide with a series of oceanward dipping normal faults. However, a zoom on this structure (Fig. III.9c) shows that it corresponds to a constructive, positive structure onlapped on both sides by sub-horizontal reflections. On the oceanward side, strong and high frequency reflections are interfingered with the sub-horizontal continuous reflections (Fig. III.9c). These structures are reminiscent of a volcano, with a basal part showing intrusive contacts to the adjacent sediments.

Complex structures are also observed in the continent-ward part of all OCTs, where interfingering between sediment-looking reflections and more massive, partly more reflective and often heterogeneous material can be observed (interfingering between blue (S1) and dark green (extrusive magma) material in Fig. III.7). The resolution of the seismic imaging makes it difficult to interpret these structures in detail, however they are not critical to the results of this study.

Intrusive magmatic additions *(light green layer in Figs. III.2c–III.5c)*

The intrusive magmatic additions are shown with light green layers in Figs. III.2c to III.5c. The black lines correspond to reflections that can be seen on the high-resolution seismic data but may, unfortunately, not be well seen on the lower resolution crustal-scale seismic sections presented in Figs. III.2a to III.5a. Fig. III.9d shows in the upper panel a line drawing of line CGN-2 (Fig. III.2b). Intra basement reflectivity in the light green domain can be best characterized as bundles of reflections that are tilted continent-ward and diverge oceanward. The reflections are limited at their top by faults. These faults can be observed to cross the extrusive (dark green) layer, to offset and tilt Tb and to occur during deposition of S2 and S3 (e.g., relationships described in Fig. III.7). Thus, tilting of reflections in the proto-oceanic curst (light green layer) occurred along faults that also tilted Tb continent-ward and were sealed by the syn-breakup sediments. The wedging of the reflections into these faults in the light green layer resembles magmatic growth structures

with a focal point located approximately at the tilt axis of Tb. In the lower panel Fig. III.9d, a mirrored image of the line drawing in shown. In this picture, which is upside down, intra-basement reflections in the light green layer show some similarity to SDRs packages, suggesting a syn-tectonic control of emplacement of these units as underplates. Besides, we suggest that these magmatic units are sequentially emplaced oceanward during an active crustal growth that is accommodated by in-sequence oceanward dipping faults contemporaneous to the deposition of S2 and S3 (for details see section 5.3). Oceanward, below the basement high $H_{b,}$ divergent reflection bundles stop and are not observed anymore within the adjacent oceanic domain. This is best observed on line 1555 (Fig. III.5c). Fig. III.9c shows a detailed line drawing of the transition from the OCT to the oceanic domain that we discuss below. It is important to note that the switch from OCT to first oceanic crust occurs where Tb changes from continent-ward dipping to sub-horizontal. Since the sediments overlying Bi and oceanic crust are sub-horizontal, the tilt of the underlying layers had to be acquired during the breakup phase.

4.4. Faults in the OCT

Faults can be interpreted in the OCT of all sections (Figs. III.2c to III.5c) and can be linked with growth packages in sediments (S2 and S3; Fig. III.7). The link between faults and overlying sediments shows that they played during the formation of the OCT. Based on the relationship between faults and overlying sedimentary sequences S2 and S3 (see Fig. III.7), we conclude that faults in the OCT become younger oceanward. These faults offsetting Tb have either small heaves i.e., are post-magmatic, or alternatively they play contemporaneously with magmatism and continue playing after magma-emplacement. In such a case, the fault heave would be much larger and difficult to define. In the following discussion we will try to demonstrate that the latter interpretation is the more likely one and that most faults occurring in the OCT are syn-magmatic. As a matter of fact, such low-angle, syn-magmatic faults are difficult to image and therefore to observe and describe, which does, however, not mean that they do not exist. We therefore discuss these faults,

interpreted as red, orange and purple faults in the following discussion part, since the clearly result from the interpretation and restoration of the section.

5. Discussion

While many studies concentrated either on rifting or on seafloor spreading, here we focus on how rifting evolves into seafloor spreading. A requirement to discuss this evolution is to better define terms such as breakup and to link the magmatic and sedimentary processes occurring in the OCT. In this discussion, we first define the nature of crust and the evolution recorded in the overlying syn-breakup sedimentary section; then we propose a kinematic restoration model of the transition between continental- and lithospheric breakup; finally we discuss the processes intervening during this transition.

5.1. Major characteristics of OCT and definition of proto-oceanic crust

In Fig. III.10 we show a section summarizing the main observations reported in the previous section and illustrated in Figs. III.2, III.5, III.7 and III.9 with the aim to unravel the nature and characteristic structures of the crust in the OCT. The continent-ward boundary of the OCT is complex and difficult to define since it can include hybrid crust, i.e., a crust in which the continental wedge is under- and overlain by magmatic additions (e.g., sandwich architecture of Gillard et al., 2017). The overlap, both in space and time, between crustal extension and magma emplacement is best documented in the sedimentary sequence (S1). The observation that S1 is both syn-tectonic relative to faults thinning the continental crust and syn-magmatic as indicated by its interfingering with magmatic additions indicates that both processes occur simultaneously. We expect basalts emplaced over this domain to show trace element signatures linked to inheritance (alkaline or T-MORB signatures) while those further ocean-wards may show a N-MORB signature (e.g., Amann et al. 2020). Thus, a decrease of crustal/lithospheric inheritance is expected to occur from inboard to outboard in the OCT.

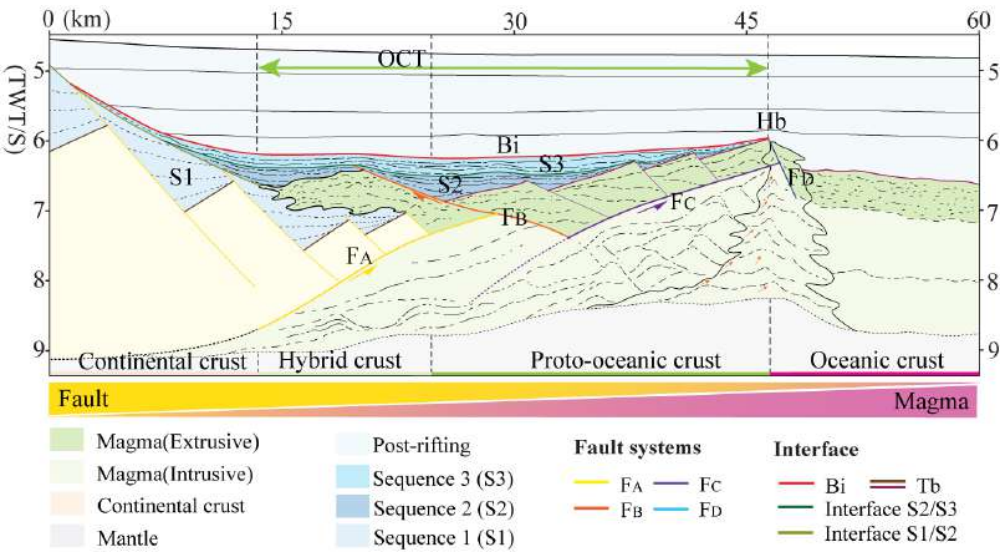

Figure III.10. *Cartoon showing a schematic representation of the nature and characteristic structures of the crust in the OCT and their link to the sedimentary sequences and magmatic additions. The section summarizes the main observations described from sections CGN-1, 2, 3 and 1555.*

The oceanward part of the OCT consists of proto-oceanic crust, here defined as fully magmatic crust that results from a transition from faulting-dominated rifting to magma-dominated accretion. Its crustal structure and evolution are complex and differ from those of adjacent continental and oceanic crusts. In contrast to continental crust that wedges out oceanward, and oceanic crust that is defined by a “constant-thickness”, ca. 2 s TWT thick crust with parallel Tb and Moho, the proto-oceanic crust thickens oceanward and its extent along dip is ca. 30 ± 10 km wide at all margins observed in this study. We define the continent-ward boundary of proto-oceanic crust as the location where continental crust terminates (oceanward end of the *hybrid crust*), i.e., where continental breakup occurs. The limit is difficult to interpret in seismic sections since it does not coincide with the first arrival of magma. Moreover, the basement may be strongly modified by the magmatic additions. The oceanward limit of proto-oceanic crust displays a more abrupt limit with conjugate and symmetric syn-magmatic normal faults that occur at the outer basement high (Hb). In the oceanic domain, the crust is defined as a 2 s TWT thick crust with parallel Tb and Moho. This limit between the proto-oceanic and oceanic crust represents the

location where lithospheric breakup occurs, i.e., where steady state seafloor spreading initiates.

5.2. The syn-breakup sedimentary record

The relationship between Tb and the three sedimentary sequences S1, S2 and S3 described in Fig. III.7 changes across the OCT. S1 is deposited during crustal thinning and simultaneously with magma-emplacement, i.e., over hybrid crust. Oceanward, S2 and S3 are deposited onto proto-oceanic crust. The observation that S2 wedges out oceanward and that S3 becomes the first sediment overlying Tb suggests that S2 and S3 form simultaneous to the accretion of the underlying proto-oceanic crust. The successive sealing of faults by S2 and then S3 oceanward suggests that faults become also younger oceanward. This migration and localization of deformation can be observed at both conjugate margins in Figs. III.7a and III.7b. The back-tilting of Tb and older sediments and their sealing by onlapping younger sediments oceanward suggests that the formation of the proto-oceanic crust is linked to an oceanward migration and relative uplift of the outer part of the proto-oceanic crust. This evolution can be seen at both conjugate OCTs (Figs. III.2c, III.3c and III.7).

The oceanward limit of the proto-oceanic crust coincides with a basement high, referred to as the “breakup high” (H_b). H_b can be seen in all lines, separating proto-oceanic and mature oceanic crusts (see Figs. III.3c to III.5c and III.7). A sediment interface marking the onset of mature seafloor spreading, referred to as the *breakup interface (Bi)* can be defined at the top of S3. Bi corresponds to a continuous reflection in the sedimentary sequence in the OCT that onlaps oceanward onto H_b. In the mature oceanic domain, Bi does not exist since this crust post-dates lithospheric breakup. Continent-ward, Bi lies within post-tectonic sediments and onlap onto S1. These observations show that the concept of a unique “breakup unconformity”, proposed by Falvey (1974), is difficult to apply in the SCS. The original idea of this popular concept used to date lithospheric breakup assumed that breakup was recorded by an unconformity that was interpreted as the result of an isostatic adjustment following the mechanical rupture of the lithosphere

(Braun and Beaumont, 1989). More recent studies questioned the existence of such an unconformity, for instance Tucholke and Sibuet (2007) and Peron-Pinvidic et al. (2007) and Pérez-Gussinyé et al., (2020) who showed evidence for the existence of complex structures and unconformities in OCTs. Gillard et al. (2015) showed for the Antarctic-Australian conjugate margins that a sequential evolution of detachment systems can result in complex sedimentary architectures, very similar to those described in this study. Bronner et al. (2011) suggested, based on drilling results from ODP Sites 1276 and 1277 from the Newfoundland OCT that breakup was linked to an upwarping of exhumed mantle due to underplating (see Fig. III.2 in Bronner et al., 2011). In their example, syn-breakup Aptian sediments (analogues to S2 and S3 in this study), have been first tilted, together with Tb continent-wards along oceanward dipping normal faults and then onlapped and sealed by the post-breakup Albian sediments. Thus, the Aptian/Albian interface drilled off Newfoundland at ODP Site 1276 would correspond to the Bi described herein. Bronner et al. (2011) proposed that the upwarping of Tb is the result of syn-breakup magmatic underplating, an interpretation that is similar to ours. It is interesting to note that the first magnetic anomaly, corresponding to the J anomaly off Newfoundland, overlies the basement high drilled at ODP Site 1277. Bronner et al. (2011) suggested that the J anomaly did not form during seafloor spreading but was linked to a pulse of magmatism that triggered lithospheric breakup. In this context it is worth mentioning that along the northern SCS, the outer basement high (Hb), which can be an analogue of the basement high drilled at ODP Site 1277, often coincides with the location of the first magnetic anomaly. Future studies are needed to further investigate the nature and origin of the first magnetic anomaly along the northern SCS.

These observations allow us to conclude that uplift and continent-ward tilting of Tb in the OCT domain is accommodated along normal faults. Growth, onlapping and sealing of these structures by S2 and S3 enable to link sedimentation to the tectono-magmatic and uplift history in the proto-oceanic domain. Our observations suggest that during the formation of proto-oceanic crust, accretion was controlled by faulting and magmatic activity

that were about to migrate and localize into the area of final breakup. Normal faulting may continue during steady-state seafloor spreading, as shown in Fig. III.5, but it is less important as during creation of the proto-oceanic crust.

5.3. From continental to lithospheric breakup: the link between faults, sediments and magma

As described in section 4 and discussed in sections 5.1 and 5.2, proto-oceanic crust forms through a complex tectono-magmatic evolution that is intimately linked to the activity of faults and documented in the syn-breakup sedimentary sequences (S1 to S3). In Fig. III.11 we present a restoration of the final stage shown in Fig. III.11a (based on Figs. III.2b and 3b), back to the initial hyperextension stage shown in Fig. III.11f. This step-by-step restoration enables us to describe the evolution from continental to lithospheric breakup and to identify and discuss the related processes. The restoration enables us to link the sedimentary sequences (S1 to S3) to a sequence of faults (Fa to Fd) and to the emplacement of magmatic bodies (see table 1). It can be summarized in four different steps illustrated in Fig. III.11a to III.11f.

Step 1: continental breakup linked to fault system F_A

Fig. III.11f illustrates the continental breakup stage, which coincides with the moment when the two margins are separated via the play of a main northward-dipping detachment fault system (F_A) (for details see also Chao et al. subm). The asymmetric crustal architecture shows a wider margin controlled by extensional detachment faults in the south and a sharper margin controlled by high-angle normal faults in the north. These observations are reminiscent of a lower plate margin in the south and an upper plate margin in the north (for more details see Chao et al. subm). S1 is emplaced contemporaneously with the play of both Fa (syn-Fa) and related high-angle faults in the upper plate margin. S1 is also deposited simultaneously to magma-production. The footwall of detachment fault Fa can be mantle and/or magmatic underplates. Structures related to this initial stage can be found in Figs. III.2c to III.4c at the transition from the continental domain to the OCT. Details of the sediment architecture are shown in Fig. III.7

(see S1 sequence). It is important to note that at this stage the main structures are asymmetric and controlled by a northward dipping detachment system.

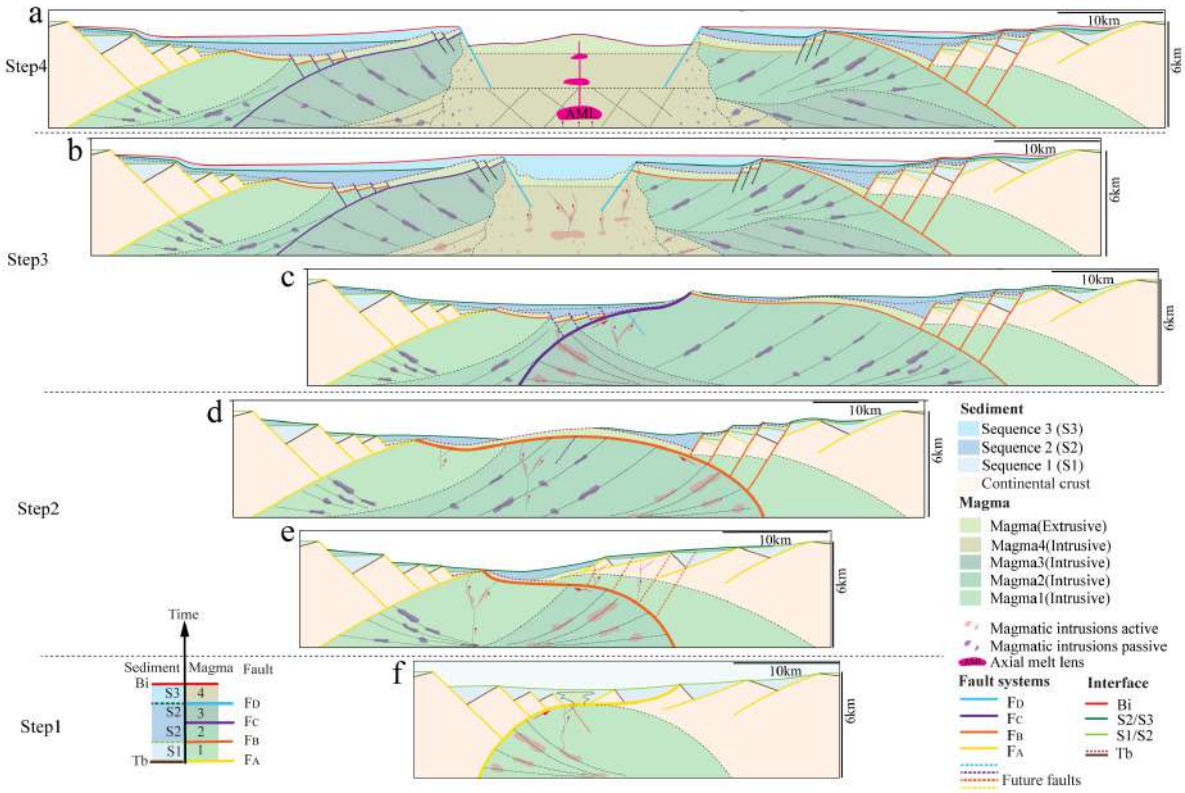

Figure III.11. *Kinematic restoration of the OCT crustal structure and sedimentary architecture from the moment of lithospheric breakup back to the moment of crustal separation (breakup). (a) Steady-state seafloor spreading stage: section is based on the observed sections CGN-1 and CGN-3). (b) Lithospheric breakup stage: lithospheric breakup is triggered at a pair of syn-magmatic conjugate normal faults FD, which break away at the outer high (Breakup High, Hb). (c) OCT stage: F_C is a northward-dipping detachment fault truncating the older F_B. Both faults are syn-magmatic and form during deposition of the sedimentary sequences S2 and S3). (d) OCT stage: FB act as a long offset detachment fault creating new real estate simultaneous to the emplacement of extrusive and intrusive magma and deposition of S2. (e) OCT stage: Onset of formation of FB offsetting FA and S1 and dipping southward. (f) Continental breakup stage: FA is a northwad-dipping detachment fault separating the two margins and controlling the S1 deposition and related magmatic additions.*

Step 2: tectono-magmatic accretion linked to fault system F_B

A new fault system (F_B) is interpreted to truncate F_A (Fig. III.11e) and to dip southwards, opposite to F_A. It offsets and therefore post-dates both F_A and S1. F_B is

interpreted to accommodate large amounts of extension, to create new real estate and to juxtapose deep crustal levels (lower crustal magmatic or mantle rocks) against extrusive magmatic rocks and/or sediments. F_B is sealed in the north by S2 and thus must be older, however further south, S2 may be deposited during exhumation along Fb (Fig. III.11d). As shown in Fig. III.11d, we propose that the concave downward extensional detachment fault F_B is associated with a conjugated set of high-angle normal faults (red high-angle faults in Fig. III.11d) that occur in the hanging wall and sole out onto the detachment surface of F_B. Note also that these faults offset F_A, which makes it difficult to recognise. We interpret, the bundle of reflections that thicken towards this fault as the result of syn-F_B magmatic growth (for a description see Fig. III.9d). Syn-tectonic sedimentary sequences and extrusive packages can also be seen in the small fault blocks in the hanging wall.

Step 3: tectono-magmatic accretion linked to fault system F_C

A new fault (F_C), with a northward dip nucleates and truncates F_B (Fig. III.11c). F_C shows similar structures like F_B, i.e, growth structures in the footwall, and brittle high-angle faults in the hanging wall offsetting Tb and filled syn-tectonically by S2 and S3 (Fig. III.11c). Magmatic packages can also downlap onto the active detachment surface on the exhumed footwall (for an example see Fig. III.9b). The main difficulty in interpreting such structures in seismic images is that the main detachment surface is covered by magmatic additions, similar to what has been described from field examples (Coltat et al., 2020). Moreover, the sequential overprint of alternating dipping faults makes that the final basement structure is complex and difficult to observe in seismic sections. However, dipping and converging bundles of weak reflections in the proto-oceanic crust may represent fingerprints pointing to the existence of detachment systems.

Step 4: lithospheric breakup

Fig. III.11b documents the stage of lithospheric breakup that coincides with the onset of steady-state seafloor spreading shown in Fig. III.11a. Lithospheric breakup occurs at a pair of conjugate normal faults F_D that break away at the outer high (H_b). These faults are syn-magmatic (for details see Fig. III.9c) and juxtapose crusts of different thickness and

structure, i.e., complex proto-oceanic crust against a mature oceanic crust. As shown in Fig. III.11b, these faults are interpreted to form during lithospheric breakup, when the asthenosphere is rising to its shallowest level and magmatic accretion starts to trigger seafloor spreading. One of the striking observations is that the uplift and continent-ward tilting if the proto-oceanic crust appears to abruptly stop and the transition to normal, sub-horizontal layered oceanic crust occurs simultaneous to activity along F_D. Gillard et al. (2016b) made comparable observations, highlighting a localization of faulting and magmatic activity towards the area of future breakup. They linked the localization and simultaneous uplift with the rise of the asthenosphere, an interpretation that can also explain the evolution observed in this study. However, the observed uplift documented in the sedimentary sequences S2 and S3 is unlikely linked to a rise of the asthenosphere only. In such a case the uplift would be thermally controlled and therefore it would be transient, which is, however, not the case in our example. A flexural origin is unlikely for several reasons: 1) the width of the uplift, which is about 20 km, is far too large for the observed throw (< 1 s TWT); 2) the uplift is not instantaneous and appears to occur and migrate oceanward simultaneous with the deposition of S2 and S3; and 3) the crustal thickness changes across the fault by about 1 s TWT. This leads to question the nature of the structure and the processes that are at the origin of the observed uplift and breakup shown in Fig. III.11b. Since F_D can be observed at conjugate pairs bounding Hb (Figs. III.2 and III.3) and is syn-magmatic (Fig. III.9c) we interpret these structures to correspond to the magmatic rupture of the crust, similar to structures described by Quirk et al. (2014) from magmatic margins. The abrupt change from tectonic-dominated extension to magma-controlled accretion is best observed in line 1555 (Fig. III.5) and is also manifested in the sediments. Indeed, sediments overlying Bi, which is syn-F_D, are sub-horizontal and show a passive infill. This is compatible with the onset of steady-state, localized seafloor spreading that does not include major, crustal-scale faulting and associated rotations. Although we consider that the final breakup is abrupt and may occur along a pair of conjugate faults (Figs. III.2c and III.3c), elsewhere (Fig. III.5c) it may be linked to several high-angle faults.

6. Conclusion

The aim of this study was to discuss the evolution and processes linked to breakup and formation of a new plate boundary. Our results show that breakup is neither an event nor does it produce a sharp boundary. Instead, we suggest that it is a phase that starts with crustal separation, referred to as *continental breakup*, and ends with the onset of steady-state seafloor spreading, referred to as *lithospheric breakup*. Thus, breakup and formation of a new plate boundary is documented in Ocean Continent Transition (OCT). The tectono-magmatic evolution during the breakup phase is well documented in the high-quality seismic data from the NW propagator of the SCS. The following main conclusions can be drawn from its interpretation:

The crustal structure of the OCT is best described on its continent-ward side by a hybrid crust where extensional thinning of the crust is compensated by syn-extensional magmatic addition leading to a sandwich type crust and at its oceanward side by a fully magmatic, but not yet mature proto-oceanic crust, dominated by fault-controlled magmatic additions and a complex, non- layered crustal structure.

Relying on seismic interpretations and restoration of sections we propose that the breakup phase includes out-of-sequence, flip-flop detachment faults showing a progressive decrease in fault heaves and a transition to magmatic accretion. This evolution is likely to be controlled by the rise of the asthenosphere that may not only control the focusing of the syn-tectonic magma into the spreading rift center, but also the localization of deformation as nicely documented in the syn-breakup sedimentary sequences S1 to S3.

A striking observation is the uplift and continent-ward tilting of the proto-oceanic crust during breakup, which results in the formation of a diagnostic outer basement high (Hb) that bounds mature oceanic crust. This evolution is documented in the syn-breakup sedimentary sequence overlying the proto-oceanic

crust by the oceanward migration of the syn-tectonic sedimentary sequence that occurs simultaneous to uplift and continent-ward tilting of the proto-oceanic domain. Tilting is controlled by syn-magmatic faults as documented by the converging reflection bundles in the crust, which are interpreted as magmatic growth structures associated with magmatic underplating.

Our kinematic restoration from continental to lithospheric breakup shows an evolution from asymmetric detachment-controlled extension to out-of-sequence, asymmetric flip-flop detachment faulting to syn-magmatic normal faulting. In other words, breakup in the NW propagator in the SCS corresponds to an evolution from fault- to magma-dominated extension. This evolution is similar to that previously described for the conjugate Australia–Antarctica OCTs.

References

Braun, J., & Beaumont, C. (1989). A physical explanation of the relation between flank uplifts and the breakup unconformity at rifted continental margins. *Geology*, *17*(8), 760–764. https://doi.org/10.1130/0091-7613(1989)017<0760:APEOTR>2.3.CO;2

Briais, A., Patriat, P., & Tapponnier, P. (1993). Updated interpretation of magnetic anomalies and seafloor spreading stages in the south China Sea: Implications for the Tertiary tectonics of Southeast Asia. *Journal of Geophysical Research: Solid Earth*, *98*(B4), 6299–6328. https://doi.org/10.1029/92JB02280

Bronner, A., Sauter, D., Manatschal, G., Péron-Pinvidic, G., & Munschy, M. (2011). Magmatic breakup as an explanation for magnetic anomalies at magma-poor rifted margins. *Nature Geoscience*, *4*(8), 549.

Cameselle, A. L., Ranero, C. R., Franke, D., & Barckhausen, U. (2017). The continent-ocean transition on the northwestern South China Sea. *Basin Research*, *29*, 73–95. https://doi.org/10.1111/bre.12137

Cameselle, A. L., Ranero, C. R., & Barckhausen, U. (2020). Understanding the 3D Formation of a Wide Rift: The Central South China Sea Rift System. *Tectonics*, *39*(12). https://doi.org/10.1029/2019TC006040

Chen, H., Stow, D. A. V., Xie, X., Ren, J., Mao, K., Gao, Y., et al. (2021). Depositional architecture and evolution of basin-floor fan systems since the Late Miocene in the Northwest Sub-Basin, South China Sea. *Marine and Petroleum Geology*, *126*, 104803. https://doi.org/10.1016/j.marpetgeo.2020.104803

Chenin, P., Manatschal, G., Decarlis, A., Schmalholz, S. M., Duretz, T., & Beltrando, M. (2019). Emersion of Distal Domains in Advanced Stages of Continental Rifting Explained by Asynchronous Crust and Mantle Necking. *Geochemistry, Geophysics, Geosystems*, *20*(8), 3821–3840. https://doi.org/10.1029/2019GC008357

Chenin, P., Jammes, S., Lavier, L. L., Manatschal, G., Picazo, S., Müntener, O., et al. (2019). Impact of Mafic Underplating and Mantle Depletion on Subsequent Rifting: A Numerical Modeling Study. *Tectonics*, *38*(7), 2185–2207. https://doi.org/10.1029/2018TC005318

Coltat, R., Branquet, Y., Gautier, P., Boulvais, P., & Manatschal, G. (2020). The nature of the interface between basalts and serpentinized mantle in oceanic domains: Insights from a geological section in the Alps. *Tectonophysics*, *797*, 228646. https://doi.org/10.1016/j.tecto.2020.228646

Davy, R. G., Minshull, T. A., Bayrakci, G., Bull, J. M., Klaeschen, D., Papenberg, C., et al. (2016). Continental hyperextension, mantle exhumation, and thin oceanic crust at the continent-ocean transition, West Iberia: New insights from wide-angle seismic. *Journal of Geophysical Research: Solid Earth*, *121*(5), 3177–3199. https://doi.org/10.1002/2016JB012825

Dean, S. L., Sawyer, D. S., & Morgan, J. K. (2015). Galicia Bank ocean–continent transition zone: New seismic reflection constraints. *Earth and Planetary Science Letters*, *413*, 197–207. https://doi.org/10.1016/j.epsl.2014.12.045

Ding, W., Schnabel, M., Franke, D., Aiguo, R., & Zhenli, W. (2012). Crustal Structure across the Northwestern Margin of South China Sea: Evidence for Magma-poor Rifting from a Wide-angle Seismic Profile. *Acta Geologica Sinica - English Edition*, *86*(4), 854–866. https://doi.org/10.1111/j.1755-6724.2012.00711.x

Ding, W., Sun, Z., Mohn, G., Nirrengarten, M., Tugend, J., Manatschal, G., & Li, J. (2020). Lateral evolution of the rift-to-drift transition in the South China Sea: Evidence from multi-channel

seismic data and IODP Expeditions 367&368 drilling results. *Earth and Planetary Science Letters*, *531*, 115932. https://doi.org/10.1016/j.epsl.2019.115932

Epin, Marie-Eva, Manatschal, G., Sapin, F., & Rowan, M. G. (2021). The tectono-magmatic and subsidence evolution during lithospheric breakup in a salt-rich rifted margin: insights from a 3D seismic survey from southern Gabon. *Marine and Petroleum Geology*, 105005. https://doi.org/10.1016/j.marpetgeo.2021.105005

Epin, M.-E., Manatschal, G., Amman, M., Ribes, C., Clausse, A., Guffon, T., & Lescanne, M. (2019). Polyphase tectono-magmatic evolution during mantle exhumation in an ultra-distal, magma-poor rift domain: example of the fossil Platta ophiolite, SE Switzerland. *International Journal of Earth Sciences*. https://doi.org/10.1007/s00531-019-01772-0

Falvey, D. A. (1974). THE DEVELOPMENT OF CONTINENTAL MARGINS IN PLATE TECTONIC THEORY. *The APPEA Journal*, *14*(1), 95–106. https://doi.org/10.1071/aj73012

Franke, D., Savva, D., Pubellier, M., Steuer, S., Mouly, B., Auxietre, J.-L., et al. (2014). The final rifting evolution in the South China Sea. *Marine and Petroleum Geology*, *58*, 704–720. https://doi.org/10.1016/j.marpetgeo.2013.11.020

Gao, J., Wu, S., McIntosh, K., Mi, L., Liu, Z., & Spence, G. (2016). Crustal structure and extension mode in the northwestern margin of the South China Sea: CRUSTAL EXTENSION OF THE SOUTH CHINA SEA. *Geochemistry, Geophysics, Geosystems*, *17*(6), 2143–2167. https://doi.org/10.1002/2016GC006247

Geoffroy, L., Burov, E. B., & Werner, P. (2015). Volcanic passive margins: another way to break up continents. *Scientific Reports*, *5*, 14828. https://doi.org/10.1038/srep14828

Gillard, M., Autin, J., Manatschal, G., Sauter, D., Munschy, M., & Schaming, M. (2015). Tectonomagmatic evolution of the final stages of rifting along the deep conjugate Australian-Antarctic magma-poor rifted margins: Constraints from seismic observations: Australian-Antarctic margins evolution. *Tectonics*, *34*(4), 753–783. https://doi.org/10.1002/2015TC003850

Gillard, M., Autin, J., & Manatschal, G. (2016). Fault systems at hyper-extended rifted margins and embryonic oceanic crust: Structural style, evolution and relation to magma. *Marine and Petroleum Geology*, *76*, 51–67. https://doi.org/10.1016/j.marpetgeo.2016.05.013

Gillard, M., Sauter, D., Tugend, J., Tomasi, S., Epin, M.-E., & Manatschal, G. (2017). Birth of an oceanic spreading center at a magma-poor rift system. *Scientific Reports*, *7*(1). https://doi.org/10.1038/s41598-017-15522-2

Gillard, M., Tugend, J., Müntener, O., Manatschal, G., Karner, G. D., Autin, J., et al. (2019). The role of serpentinization and magmatism in the formation of decoupling interfaces at magma-poor rifted margins. *Earth-Science Reviews*, *196*, 102882. https://doi.org/10.1016/j.earscirev.2019.102882

Gozzard, S., Kusznir, N., Franke, D., Cullen, A., Reemst, P., & Henstra, G. (2019). South China Sea crustal thickness and oceanic lithosphere distribution from satellite gravity inversion. *Petroleum Geoscience*, *25*(1), 112–128. https://doi.org/10.1144/petgeo2016-162

Harkin, C., Kusznir, N., Tugend, J., Manatschal, G., & McDermott, K. (2019). Evaluating magmatic additions at a magma-poor rifted margin: An East Indian case study. *Geophysical Journal International*. https://doi.org/10.1093/gji/ggz007

Larsen, H. C., Mohn, G., Nirrengarten, M., Sun, Z., Stock, J., Jian, Z., et al. (2018). Rapid transition from continental breakup to igneous oceanic crust in the South China Sea. *Nature Geoscience*, *11*(10), 782–789. https://doi.org/10.1038/s41561-018-0198-1

Li, C.-F., Lin, J., Kulhanek, D. K., Williams, T., Bao, R., Briais, A., et al. (2015). Expedition 349 summary. In *Li, C.-F.; Lin, J.; Kulhanek, D.K.; Williams, T.; Bao, R.; Briais, A.; Brown, E.A.; Chen, Y.; Clift, P.D.; Colwell, F.S.; Dadd, K.A.; Ding, W.-W.; Hernandez Almeida, Ivan; Huang, X.-L.; Hyun, S.; Jiang, T.; Koppers, A.A.P.; Li, Q.; Liu, C.; Liu, Q.; ... (2015).*

Expedition 349 summary. In: South China Sea Tectonics. Proceedings of the International Ocean Discovery Program: Vol. 349 (pp. 1-43). International Ocean Discovery Program 10.14379/iodp.proc.349.101.2015 <http://dx.doi.org/10.14379/iodp.proc.349.101.2015> (Vol. 349, pp. 1–43). International Ocean Discovery Program. Retrieved from https://boris.unibe.ch/68255/

Ligi, M., Bonatti, E., Bosworth, W., Cai, Y., Cipriani, A., Palmiotto, C., et al. (2018). Birth of an ocean in the Red Sea: Oceanic-type basaltic melt intrusions precede continental rupture. *Gondwana Research*, *54*, 150–160. https://doi.org/10.1016/j.gr.2017.11.002

Lizarralde, D., Axen, G. J., Brown, H. E., Fletcher, J. M., González-Fernández, A., Harding, A. J., et al. (2007). Variation in styles of rifting in the Gulf of California. *Nature*, *448*(7152), 466–469. https://doi.org/10.1038/nature06035

McDermott, C., Lonergan, L., Collier, J. S., McDermott, K. G., & Bellingham, P. (2018). Characterization of Seaward-Dipping Reflectors Along the South American Atlantic Margin and Implications for Continental Breakup. *Tectonics*, *37*(9), 3303–3327. https://doi.org/10.1029/2017TC004923

Mortimer, E. J., Gouiza, M., Paton, D. A., Stanca, R., Rodriguez, K., Hodgson, N., & Hussein, A. A. (2020). Architecture of a magma poor passive margin – Insights from the Somali margin. *Marine Geology*, *428*, 106269. https://doi.org/10.1016/j.margeo.2020.106269

Nonn, C., Leroy, S., Khanbari, K., & Ahmed, A. (2017). Tectono-sedimentary evolution of the eastern Gulf of Aden conjugate passive margins: Narrowness and asymmetry in oblique rifting context. *Tectonophysics*, *721*, 322–348. https://doi.org/10.1016/j.tecto.2017.09.024

Norcliffe, J. R., Paton, D. A., Mortimer, E. J., McCaig, A. M., Nicholls, H., Rodriguez, K., et al. (2018). Laterally Confined Volcanic Successions (LCVS); recording rift-jumps during the formation of magma-rich margins. *Earth and Planetary Science Letters*, *504*, 53–63. https://doi.org/10.1016/j.epsl.2018.09.033

Paton, D. A., Pindell, J., McDermott, K., Bellingham, P., & Horn, B. (2017). Evolution of seaward-dipping reflectors at the onset of oceanic crust formation at volcanic passive margins: Insights from the South Atlantic. *Geology*, *45*(5), 439–442. https://doi.org/10.1130/G38706.1

Pérez-Gussinyé, M., Andrés-Martínez, M., Araújo, M., Xin, Y., Armitage, J., & Morgan, J. P. (2020). Lithospheric strength and rift migration controls on synrift stratigraphy and breakup unconformities at rifted margins: Examples from numerical models, the Atlantic and South China Sea mar-gins. *Tectonics*, *39*(12), e2020TC006255.

Peron-Pinvidic, G., & Naliboff, J. (2020). The exhumation detachment factory. *Geology*. https://doi.org/10.1130/G47174.1

Péron-Pinvidic, G., Manatschal, G., Minshull, T. A., & Sawyer, D. S. (2007). Tectonosedimentary evolution of the deep Iberia-Newfoundland margins: Evidence for a complex breakup history. *Tectonics*, *26*(2), TC2011.

Quirk, D. G., Shakerley, A., & Howe, M. J. (2014). A mechanism for construction of volcanic rifted margins during continental breakup. *Geology*, *42*(12), 1079–1082. https://doi.org/10.1130/G35974.1

Ribes, C., Manatschal, G., Ghienne, J.-F., Karner, G. D., Johnson, C. A., Figueredo, P. H., et al. (2019). The syn-rift stratigraphic record across a fossil hyper-extended rifted margin: the example of the northwestern Adriatic margin exposed in the Central Alps. *International Journal of Earth Sciences*, *108*(6), 2071–2095. https://doi.org/10.1007/s00531-019-01750-6

Sauter, D., Werner, P., Ceuleneer, G., Manatschal, G., Rospabé, M., Tugend, J., et al. (2021). Sub-axial deformation in oceanic lower crust: Insights from seismic reflection profiles in the Enderby Basin and comparison with the Oman ophiolite. *Earth and Planetary Science Letters*, *554*, 116698. https://doi.org/10.1016/j.epsl.2020.116698

Sun, Z., Jian, Z., Stock, J. M., Larsen, H. C., Klaus, A., Alvarez Zarikian, C. A., & Expedition 367/368 Scientists (Eds.). (2018). *Volume 367/368: South China Sea Rifted Margin* (Vol. 367/378). International Ocean Discovery Program. https://doi.org/10.14379/iodp.proc.367368.2018

Sutra, E., & Manatschal, G. (2012). How does the continental crust thin in a hyperextended rifted margin? Insights from the Iberia margin. *Geology*, *40*(2), 139–142. https://doi.org/10.1130/G32786.1

Tucholke, B. E., Sawyer, D. S., & Sibuet, J.-C. (2007). Breakup of the Newfoundland–Iberia rift. *Geological Society, London, Special Publications*, *282*(1), 9–46. https://doi.org/10.1144/SP282.2

Tugend, J., Gillard, M., Manatschal, G., Nirrengarten, M., Harkin, C., Epin, M.-E., et al. (2020). Reappraisal of the magma-rich versus magma-poor rifted margin archetypes. *Geological Society, London, Special Publications*, *476*(1), 23–47. https://doi.org/10.1144/SP476.9

Wang, Q., Zhao, M., Zhang, H., Zhang, J., He, E., Yuan, Y., & Qiu, X. (2020). Crustal velocity structure of the Northwest Sub-basin of the South China Sea based on seismic data reprocessing. *Science China Earth Sciences*. https://doi.org/10.1007/s11430-020-9654-4

Warner, M. R. (1987). Seismic reflections from the Moho -- the effect of isostasy. *Geophysical Journal International*, *88*(2), 425–435. https://doi.org/10.1111/j.1365-246X.1987.tb06651.x

Wu, Z., Li, J., Ruan, A., Lou, H., Ding, W., Niu, X., & Li, X. (2012). Crustal structure of the northwestern sub-basin, South China Sea: Results from a wide-angle seismic experiment. *Science China Earth Sciences*, *55*(1), 159–172. https://doi.org/10.1007/s11430-011-4324-9

Xie, X., Ren, J., Pang, X., Lei, C., & Chen, H. (2019). Stratigraphic architectures and associated unconformities of Pearl River Mouth basin during rifting and lithospheric breakup of the South China Sea. *Marine Geophysical Research*. https://doi.org/10.1007/s11001-019-09378-6

Zhang, C., Su, M., Pang, X., Zheng, J., Liu, B., Sun, Z., & Manatschal, G. (2019). Tectono-sedimentary analysis of the hyper-extended Liwan sag basin (mid-northern margin of the South China Sea). *Tectonics*. https://doi.org/10.1029/2018TC005063

Zhang, Cuimei, Sun, Z., Manatschal, G., Pang, X., Li, S., Sauter, D., et al. (2021). Ocean-continent transition architecture and breakup mechanism at the mid-northern South China Sea. *Earth-Science Reviews*, *217*, 103620. https://doi.org/10.1016/j.earscirev.2021.103620

Zhang, Cuimei, Sun, Z., Manatschal, G., Pang, X., Qiu, N., Su, M., et al. (2021). Syn-rift magmatic characteristics and evolution at a sediment-rich margin: Insights from high-resolution seismic data from the South China Sea. *Gondwana Research*, *91*, 81–96. https://doi.org/10.1016/j.gr.2020.11.012

CHAPTER IV

A 3D snapshot of crustal breakup deduced from seismic analysis of the tip of the NW South China Sea

Peng Chao[1], Gianreto Manatschal[1], Pauline Chenin[1], Cuimei Zhang[2], Jianye Ren[3], Xiong Pang[4], Jingyun Zheng[4]

[1] Université de Strasbourg, CNRS, ENGEES, ITES UMR 7063, Strasbourg F-67084, France

[2] Southern Marine Science and Engineering Guangdong Laboratory, Guangzhou, China

[3]College of Marine Science and Technology, China University of Geosciences, Wuhan, China

[4]CNOOC Ltd.-Shenzhen, Branch, Shenzhen, China

Key Points:

First time show 3D structure and sediment architecture at tip of NW SCS propagator

Key Words:

Lithospheric breakup, NW South China Sea, rift propagator, syn-tectonic magmatism, oceanic crust,

Abstract

In this study we describe and map, based on a high-resolution reflection seismic dataset, rift domains at the tip of the NW-SCS. We compare our rift domain map with refraction seismic, magnetic and gravity field data and previously mapped Continent-Ocean Boundaries (COB). We also analyze and define syn-breakup sedimentary sequences and map them across the study area. This work enables us to describe the 3D architecture and nature of the crust at the tip of the NW SCS and allows us to discuss the along strike structural and crustal variability, to investigate the extensional and magmatic processes interacting during breakup and to propose a kinematic evolution for how rifting evolves, breakup occurs and finally stalls in the NW SCS. The results of this study provide a well-documented example of the spatial and temporal evolution of a rift system during breakup. It enables us to discuss how breakup evolves at the tip of a so-called propagator, which may actually correspond to a “retrogador” documenting the reorganization of a failing rift system.

1. Introduction

The breaking up of continents and formation of new oceanic crust is a crucial phase of plate tectonics. Unlike seafloor spreading or subduction, both of which are steady-state processes, breakup is a transient event and is therefore rare and difficult to observe. There are only a handful of examples, among which the Woodlark basin (Taylor et al. 2009), the Gulf of California (Lizzaralde et al., 2007), the northern tip of the Red Sea (Ligi et al., 2018), and the Afar/western Gulf of Aden (Nonn et al., 2019) where the breakup stage is documented. However, the magmatic budget, potential driving mechanisms and kinematic settings are different among these examples and at present no universal model exist to explain how lithospheric breakup propagates. Different models for rifting propagation were proposed by Vink (1982) and Taylor et al. (2009), among others. Both models concluded that the tip of the propagator is not an Eulerian pole, which is in line with numerical

simulations proposed by Le Pourhiet et al. (2018) for the SCS. Nirrengarten et al. (2018) proposed a more complex model for rift propagation for the southern North Atlantic, where extension was simultaneously partitioned between different basins that formed ahead of a propagating lithospheric breakup. This model is similar to the one Luo et al. (2021) proposed for the SW SCS (see their Fig. 12c). This model is also supported by Neuharth et al. (2021) who showed, based on numerical modelling, that the linkage of rift segments can result in the formation of continental micro-blocks. While these models explain how rift propagators may develop, only the model of Le Pourhiet et al. (2018) tries to resolve why rift propagators in the SCS were not able to break through the continent and why they finally stalled. These authors suggested that the far-field compression due to the west-to-east topographic gradient across the Indochinese Peninsula prevented continental breakup propagation. Two alternative explanations are: (1) the inherited magmatic arc-crust trending NE-SW ahead of the NW-SCS propagator was too strong and inhibited a successful breakup; and (2) slab-pull related to the subduction systems bounding the SCS to the south and to the east that may have controlled the extensional kinematic setting in the SCS. One of the aims of this study is to discuss why and when did rift propagation fail in NW-SCS and how strain was distributed during this failure.

The advantage of investigating the tip of the NW-SCS propagator is that it enables to look at a snapshot of a propagating breakup system. Other advantages are the excellent dataset available, the limited volume of magmatic additions and the lack of salt, both of which can mask the crustal structure, high sedimentation rates during breakup, which provide an efficient tape recorder for the tectono-stratigraphic evolution, and the proximity of IODP drill hole data.

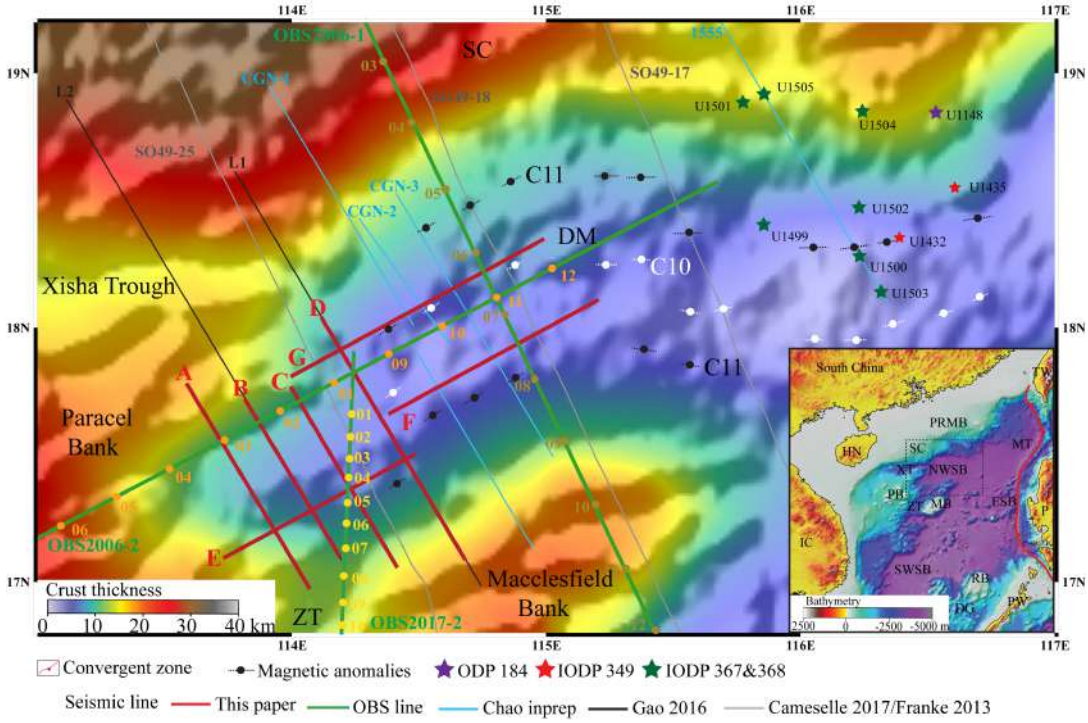

Figure IV.1. *Location of the study area in the NW South China Sea (SCS) and the used datasets. Crustal thickness map based on gravity inversion with superimposed shaded relief free-air gravity anomaly from Gozzard el al. (2019). Inset on the right lower corner shows bathymetric map of the SCS. Location of the principal seismic reflection lines (red lines) and refraction lines (green lines) presented in this paper. The location of the IODP drill sites based on Li et al. (2015) and Sun et al. (2018). The location of the magnetic anomalies is based on Briais et al. (1993). Blue lines show the reflection seismic lines CGN-1, CGN-2, CGN-3 from Chao et al. (in prep.), the 1555 (blue line) from Zhang et al. (2019), the black lines L1 and L2 from Gao et al.(2016), the grey line SO49-25, SO49-18, SO49-17 from Cameselle et al (2017) and Franke et al (2013).The OBS2006-1from WU et al. (2012) and Ding et al. (2012), the OBS2006-2 from Wang et al. (2020), the OBS2017-2 from Li et al. (2021). Abbreviations used in the figure: DG, Dangerous Ground (Nansha); DM Double-peak Seamount, ESB, East Sub-Basin; HN, Hainan; IC, Indochina; MB, Macclesfield-Paracel Bank; MT, Manila Trench; NW-SCS, North West South China Sea; PB, Paracel Bank (Xisha Islands); PRMB, Pearl River Mouth Basin; P, Palawan; RB, Reed Bank (Liyue); SC, South China continental Margin; SW-SB, South West Sub-Basin; TW, Taiwan; ZT, Zhongsha Trough.*

Of major importance is the recent study by Li et al. (2021) who investigated the crustal structure below the Zhongsha Block (Macclesfield Block) and adjacent abyssal basins, complementing earlier work by Ding et al. (2012) and Wu et al. (2012). Based on refraction seismic studies, these authors proposed a crustal model for the NW-SCS that forms the foundation of this study. Cameselle et al. (2017, 2020) and Franke et al. (2014) proposed seismic interpretations (for locations of their lines see Fig. IV.1) that partially conflicts with the interpretations by Ding et al. (2020), in particular concerning the structure of the ocean continent transition (OCT). A detailed description of the OCT from the central N-SCS was proposed by Zhang et al. (2021) based on IODP drill hole data and reflection seismic lines located more than 250 km west of the area investigated in the present study. The results of this work compare well with our results for the OCT structure, and in the present study we go further by proposing a model and discussing how breakup propagates in a V-shaped rift system.

The aim of the present study is twofold. In a first part we describe the 3D crustal architecture of the OCT and its along-strike variability at the tip of the NW-SCS, we analyze the syn-rift sedimentary sequence and map the distribution of rift domains. The results of this first part enables us to propose a 3D crustal model showing a snapshot of the propagator in 3D and to discuss how extensional and magmatic processes interact and are recorded in the syn-rift sedimentary sequence. In a second part we correlate the syn-rift sedimentary sequences along strike, discuss how breakup evolved at tip of the NW-SCS propagator and investigate the processes controlling whether a rift system goes to breakup, reorganizes, or stalls.

2. Geological setting

The SCS, the largest marginal sea in the western Pacific region, includes two V-shaped propagators, an older one in the NW and a younger in the SW. In this study we focus on the termination of the NW propagator, which separates the Western Pearl River Mouth Basin and the China continental margin in the north from the Macclesfield-Paracel

Block (Zhongsha-Xisha) in the south (Fig. IV.1). Cameselle et al. (2017, 2020) suggested that the spreading centre propagated westwards and died shortly before reaching the Xisha Trough in the late Early Oligocence. On a first order, this interpretation is in line with those of Ding et al. (2012); Wu et al. (2012, 2012); Franke et al. (2014); Gao et al. (2016); Cameselle et al. (2017, 2021); Wang et al. (2020); and Chao et al. (subm). However, differences exist on the interpretation of the magmatic budget at breakup time, the distribution of the Continent Ocean Boundary (COB) or the limits of the Ocean Continent Transition (OCT), and the details of the breakup process. These aspects will be discussed in section 6.2 of this study. Here we focus on the structure of the OCT located at the tip of NW-SCS propagator and compare our results with those of previous studies.

The age of rifting onset in the NW SCS is poorly constrained and usually referred to as 65 Ma, which corresponds to the stratigraphic marker horizon Tg (Xie et al., 2019). Based on the occurrence of magnetic anomalies C11 and C10, Briais et al. (1993) and Gee et al. (2007) suggested that breakup occurred at ca. 30-28 Ma (late Early Oligocene). A key to understand the characteristics of breakup is to evaluate the tectono-magmatic evolution and its link to the OCT architecture. While Franke et al. (2014) proposed that the NW-SCS is a magma-poor rifted margin with possible exhumed mantle domains, Ding et al. (2020) showed that there is neither evidence for Sea Dipping Reflections (SDR) nor for mantle exhumation and classified the NW SCS margins as intermediate margins. This interpretation is in line with refraction data showing a high velocity lower crust in the OCT (more than 7 km/s), which suggest that breakup was controlled by magma. Further details on the breakup process were provided by Zhang et al. (2021) from the central N-SCS. These authors demonstrated, based on reflection seismic data and access to IODP 367/368 drill hole data, that the OCT includes hybrid crust (i.e., crust that is comprised of both extended pre-rift continental crust and newly formed magmatic crust), and that breakup was linked to the interaction between detachment faulting and magmatic processes. These authors also constrained the age of breakup to occur at anomaly C11 (about 30 Ma), in line with Nirrengarten et al. (2020). However, these studies are located

more than 250 km east of the present study area. Since breakup is considered to propagate westwards, the age of breakup might be younger than 30 Ma in the present study area. Without drill hole calibration it is not possible to precisely determine the age of breakup, and thus in this study we base our ages on the occurrence of anomaly C10n, dated 28 Ma by Briais et al. (1993).

3. Data, methods and terminology

3.1 Data used and acquisition parameters

With permission of the China National Offshore Oil Corporation (CNOOC), we had access and interpreted a large, high-resolution seismic dataset, from which we selected seven seismic lines referred to as lines A to G (Fig. IV.1). These multichannel seismic (MCS) sections, which record down to 12 s Two-Way Travel Time (TWT), belong to a large survey that imaged ca. 5000 km of multichannel 2D sections covering the entire NW-SCS sub-basin (about 35,000 km²). NNW-SSE-oriented seismic lines have a spacing of 20 km and those oriented ENE-WSW a spacing of ca. 15 km. The seismic signal was generated using a Bolt Longlife Airgun (3850 cubic inches) by means of compressed air (2000 psi). Record length and sampling rate were set at 11996 ms TWT and 2 ms, respectively. The acquired signals were recorded within 396 channels using a fold of 99 and lie in the frequency range of 40-60 Hz, allowing a vertical resolution up to 40 m. Data were processed through Omega V1.8.1 software, applying a bandpass filter (ranging from 6 Hz of low-cut frequency and 12 dB/s of low-cut slope to 136 Hz of high-cut frequency and 276 dB/s of high-cut slope), a denoising and amplitude compensation and a post-stack time Kirchhoff migration (for more details see Hui Chen (2021)).

In order to compare our interpretation of reflection seismic data and to obtain further constraints on the nature of the crust in the study area, we include 3 refraction seismic lines (OBS2006-1 and OBS2006-2 published and described by Wu et al. (2012), and OBS2017-2 line published and described by Li et al. (2021); see Fig. IV.1 for location).

The nearest drill holes penetrating the OCT are those from the International Ocean Discovery Program (IODP) Expeditions 367/368/368X (Larsen et al., 2018; see Fig. IV.1 for location). These drill sites, located approximately 300 km east of the study area, have been described by Zhang et al., (2021). We are aware that a precise stratigraphic correlation between our seismic sections and the IODP drill hole data is not possible due to the distance between the two sites. However, we consider that the time difference between the breakup event at the two sites is minor, which is supported by the fact that they contain magnetic anomalies of same age (for more details see Chao et al. in prep).

3.2 Methods

The present study is based on a careful analysis of high-resolution reflection seismic data from the tip of the NW SCS, with the aim to describe the structures, magmatic additions and sediment deposits formed during the breakup phase and to deduce where, when and how breakup occurred. The aim of our reflection seismic interpretation is to provide a coherent description of the geometrical relationships observed in the lines. For the seven seismic lines presented in this paper, we show the seismic raw section, add a line drawing and an interpretation in terms of sedimentary sequences. This enables the reader to comprehend and verify our observations and to compare them with our interpretations. Our interpretation workflow is based on four successive steps, namely: 1) identification of first-order seismic interfaces (seafloor, top acoustic basement, Moho) and of rift domain boundaries; 2) definition of sedimentary sequences based on geometrical relationships between sediment reflections and top acoustic basement; 3) characterization of the nature of basement in the OCT, including a comparison with refraction seismic data; and 4) mapping and description of faults, including fault offsets, sealing levels and terminations of reflectors. This approach enables us to build a coherent interpretation, in which first-order and objective observations are established first, building the frame for subsequent, more subjective interpretations. The definition of sedimentary sequences enables us to build a relative temporal and spatial framework for the formation of the OCT at the tip of the NW-SCS.

3.3 Terminology and definitions used in this study

Definition of first-order interfaces

In this study we define the top of acoustic basement (Tb) as a high-amplitude and well-imaged reflection corresponding to the interface between compactable sediments and acoustic basement. Since acoustic basement is partially made of highly metamorphosed pre-rift sediments emplaced during previous tectonic events, in our interpretation Tb represents an interface without any time or genetic connotation. Following Warner (1987), Moho is interpreted to occur in time sections at a constant two-way travel time, despite the highly variable structure of the overlying crust. The apparent flatness of seismic Moho, also referred to as the "10 s rule", is an artefact produced when the crust is in local isostatic equilibrium. Because breakup in the NW-SCS occurred at ca. 28 Ma (Briais et al., 1993; see also previous section) thermal equilibrium has not been achieved yet, and thus seismic Moho is typically between 9 to 8 s TWT (Chao et al., subm).

Although both Tb and Moho represent physical interfaces that can be objectively imaged and observed, their nature is subject to geological interpretation, in particular in the OCT. In this domain, Tb corresponds either to an initial, inherited contact between pre-rift sediments and continental crust, also referred to as Tg, which is the classical interpretation of Tb; or Tb can represent an exhumed fault or the top of a newly created magmatic crust. Similarly, the Moho can either represent an interface separating continental and mantle rocks (classical interpretation), or correspond to a fault contact, or represent an alteration front (e.g., serpentinization front beneath hyperextended crust or at exhumed mantle domains), or else represent a contact with newly formed igneous rocks (underplated, or oceanic domains). Note that in the line drawings we consider Tb and Moho without any genetic connotation, while in the interpreted sections we provide a geological interpretation of the nature of both Tb and Moho.

Definition of rift domains and domain boundaries

In this contribution, we consider three main rift domains that are *continental*, *OCT* and *oceanic*. The definition of these domains relies principally on crustal shapes (i.e., the

outline formed by Tb and Moho), total accommodation space and top basement topology (Tugend et al., 2014), altogether observable in reflection seismic sections. The *continental domain* is characterized by a wedging crustal shape, a total accommodation space that is moderate compared to the domains considered, and a structured/faulted Tb. The *oceanic domain* is characterized by a box-shaped crust with a smooth Tb, sub-horizontal and parallel to seismic Moho (when observed), where accommodation space is large and where sediments show only passive infill geometries. The domain in-between corresponds to the OCT domain. It is characterized by a structured Tb dominated by magmatic additions, and thus may display uneven topography. Its continent-ward limit is marked by a break in the slope or a lowering in dip of Tb compared to the adjacent continental domain. The oceanward boundary of the OCT often corresponds to a basement high and is marked by a break in the slope of Tb, from continent-ward dipping to sub-horizontal in the adjacent oceanic domain.

Each of these domains is associated with a specific type of crust. On the one hand, the basement of the continental domain is entirely made of unequivocal continental crust. When the continental crust is less than 3 s TWT-thick, we refer to it as *hyperextended crust*. On the other hand, the basement of the oceanic domain is made of unequivocal, Penrose-type oceanic crust. The basement of the OCT domain between them is more complex: while its continent-ward part may be comprised of hybrid crust, its oceanward part is made of highly structured but fully magmatic proto-oceanic crust (see Chao et al. in prep for a detailed discussion).

Definition of sedimentary mega-sequences, faults and magmatic additions

In this study, we define the sediment layer as the layer made of compactable sediments bounded by Tb and the seafloor. We distinguish between two mega-sequences, a syn-rift one and a post-rift one. We define the base of the syn-rift sedimentary mega-sequence as Tb that is capping seismic basement. Its top is defined as the *breakup interface* (*Bi*), a surface that represents the breakup time and that is approximated as an isochron in the limited-extent area of our study. Therefore, in our definition, the syn-rift

mega-sequence includes the sediments deposited during the formation of the OCT domain, in other words during the *breakup phase* (cf. paragraph *Definition of Breakup* below). All sediments above Bi show passive infill and do not display evidence for significant tectonic overprint and belong to the post-rift mega-sequence.

Faults are not directly imaged by seismic methods; however their existence can be deduced from offsets in Tb and/or in other interfaces/reflections. In this study, we identify the breakaways of high-angle normal faults and, wherever possible, syn-tectonic sedimentary- and/or magmatic sequences, as well as post-tectonic sequences that seal faults. Such observations enable us to determine relative fault ages. We also define, where possible, the levels where faults sole out at depth. These levels may correspond to brittle-ductile transitions (Sutra et al., 2012) or, alternatively, to the top of underplated material. In OCTs, magma emplacement, hydration and the occurrence of extensional detachment systems result in a complexity that cannot be deduced from seismic observations alone. Although interpretations of faults and magmatic additions are non-unique, their explanation should be coherent and fit with both geophysical and geological observations.

Definition of breakup

The term *breakup* is here used to describe the transition from crustal separation, referred to as crustal breakup, to steady-state seafloor spreading, referred to as lithospheric breakup. Defining the two is essential since breakup is a lasting event that is expressed by a transition zone (the OCT) rather than an instantaneous event that would correspond to a well-defined and mappable boundary.

4. Reflection seismic lines: from observations to seismic interpretations

4.1. First-order seismic interfaces and rift domain boundaries

In the present section we define the main interfaces, i.e., seafloor, top basement (Tb) and Moho and distinguish between a continental domain that includes thinned continental crust and hyperextended crust (i.e., where crust is ≤ 3 s TWT), an OCT domain and an oceanic domain (for definitions see section 3.3). In the following section we first only refer to the line drawings of Figs. IV.2b to IV.8b and will refer and discuss the interpretations shown in Figs. IV.2c to IV.8c in later parts of this paper, when integrating second-order and more subjective observations and interpretations.

Line A

Line A (Fig. IV.2a) is the westernmost section that images across the tip of the propagator (for location see Fig. IV.1). Seafloor is slightly structured and lies at ca. 2.5 s TWT from km 0 to 17, and then deepens down to 4.5 s TWT. From km 30 to 80, seafloor is flat, before it steps up and remains at ca. 3.5 s TWT. Seafloor steps down again at km 100 to 4 s TWT.

Tb is largely sub-horizontal and offset by only small normal faults from km 0 to 17 (Fig. IV.2b). A major fault with an offset of ca. 4 s TWT separates the sub-horizontal Tb from a continent-ward tilted block that is offset by minor oceanward dipping normal faults. Between km 55 and 65 Tb deepens abruptly down to 8 s TWT. In the south, Tb is affected by minor high-angle faults but remains sub-horizontal at ca. 4 s TWT between km 80 and 100. Between km 60 and 75, a crustal wedge offset by north-dipping faults pinches out at km 65 and at 8s TWT, which represents the location with the thinnest crust. Moho reflections are difficult to define but may correspond to a set of reflectivity that occurs at ca. 9 s TWT.

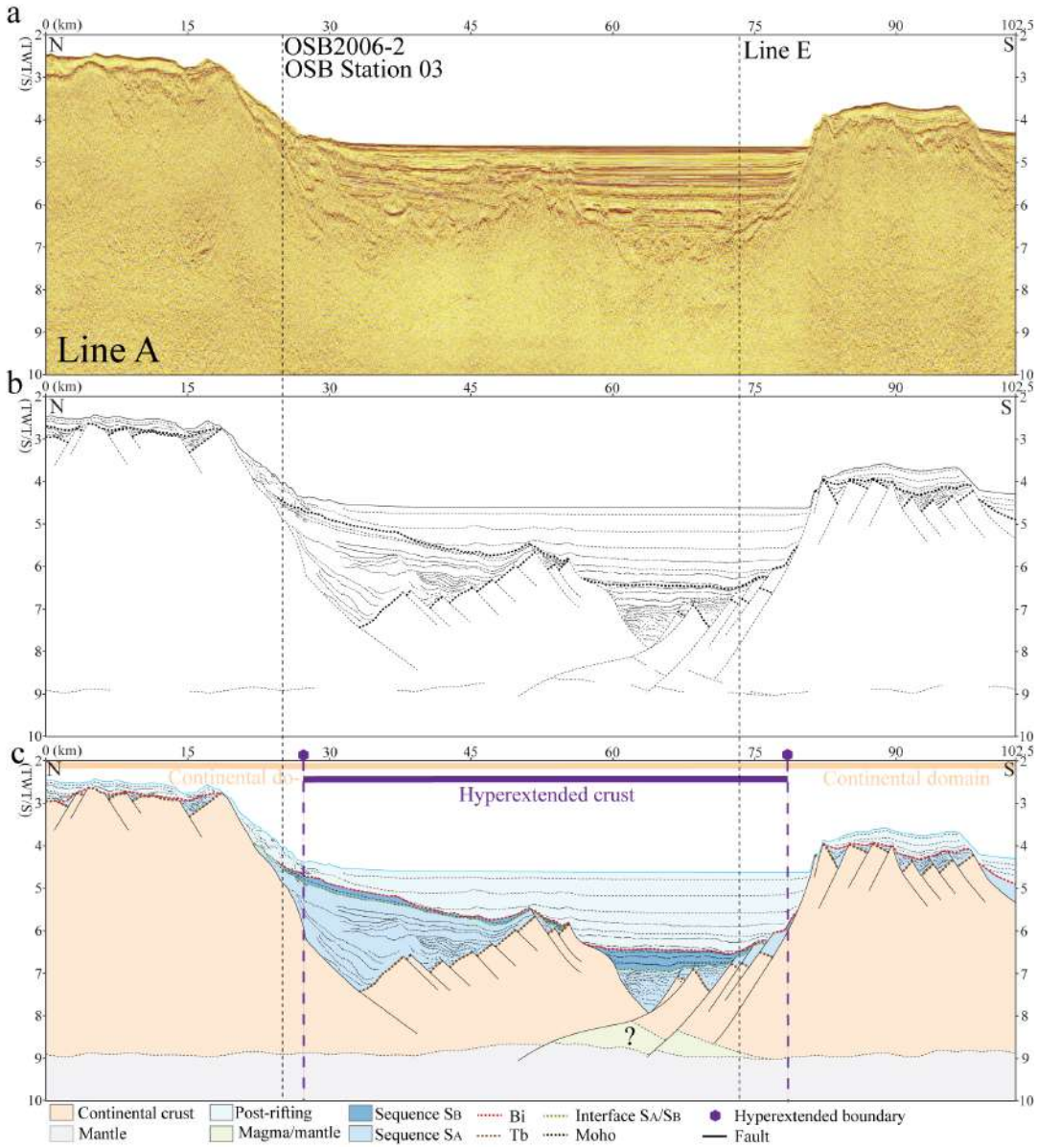

Figure IV.2. *Reflection seismic section Line A across the tip of the propagator, for location see Fig. IV.1. (a) Time migrated reflection seismic section Line A with location of cross lines (dashed lines). (b) Line drawing of the seismic section Line A, the bold lines are Tb and Bi. (c) Seismic interpretation of Line A with first-order interfaces, stratigraphic horizons and the tectonic structures. Three sedimentary sequences (S_A, S_B and post-rifting) were defined (for explanation see discussion section). Abbreviations used in the figure: Bi, Breakup interface; Tb, Top acoustic Basement.*

Based on our definition (see section 3.3) we interpret the whole line as belonging to the continental domain. This is based on the observation of a Tb offset by high-angle faults, crustal thicknesses that are between 6 and 4 s TWT in the north and south. The crust is strongly structured and tilted between km 30 and 55, and shows wedging shapes between km 80 and 65. Unequivocal magmatic crust is not observed in this section. We identify hyperextended crust between km 25 and 80.

Line B

Line B (Fig. IV.3a) is parallel to Line A and about 22 km further east (for location see Fig. IV.1). Seafloor is sub-horizontal between km 10 and 75 and at 4.5 s TWT (Fig. IV.3b). Further south and north it is structured and rises up. Tb is offset and steps down across south-dipping faults from km 0 to 25. From km 25 to 40 Tb is offset by south-dipping faults, but the overall trend of Tb remains sub-horizontal. At km 45 a change from south- to north-dipping faults occurs and crustal wedging, offset by north-dipping faults occurs from km 45 (tip of the wedge with a Tb that is at 8 s TWT) to a crust that is 3 to 4 s TWT-thick at km 70. Although at a crustal scale the northern margin shows a wedging/thinning of the crust, there is no tip to this wedge.

Based on our definition (see section 3.3) we define the whole section as belonging to the crustal domain. This is based on the topology of Tb, which is offset across the whole line by high-angle faults. The overall shape of the crust is wedging towards km 45, although a more complex crustal block with a rather constant crustal thickness and made of tilted bocks can be observed between km 25 and 40, which we consider to belong to the continental domain. We identify hyperextended crust between km 10 and 70. Possible magmatic additions are only observed at the center of the basin between km 45 and 55 (for description see below). Moho is essentially not observed due to the imaging depth that is limited to 8 s TWT in this line.

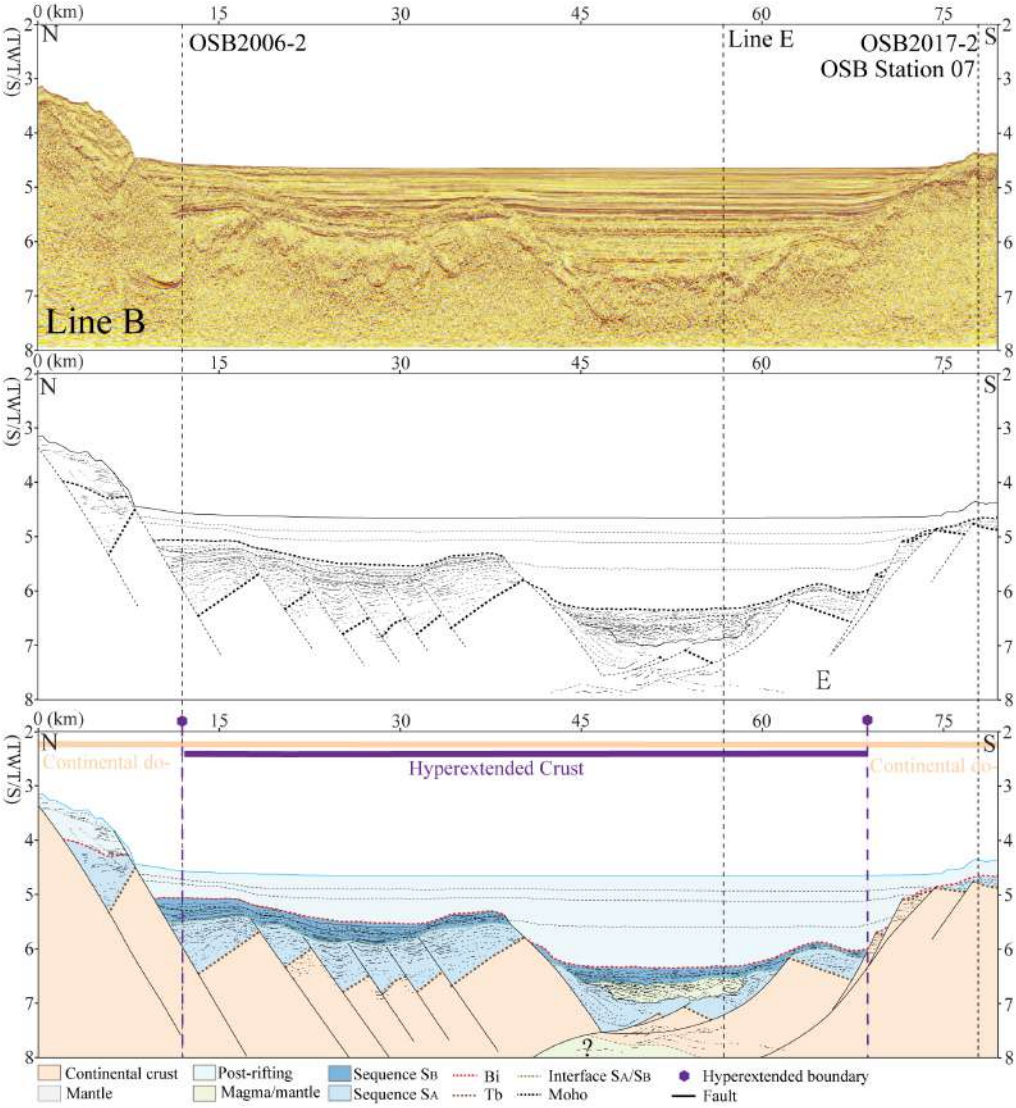

Figure IV.3. *Reflection seismic section Line B across the tip of the propagator, for location see Fig. IV.1. (a) Time migrated reflection seismic section Line B with location of cross lines (dashed lines). (b) Line drawing of the seismic section Line B, the bold lines are Tb and Bi. (c) Seismic interpretation of Line B with first-order interfaces, stratigraphic horizons, and the tectonic structures. Three sedimentary sequences (S_A, S_B and post-rifting) were defined (for explanation see discussion section). Abbreviations used in the figure: Bi, Breakup interface; Tb, Top acoustic Basement. Line B is the same line with seismic section L2, which has been published in Gao et al. (2016).*

Line C

Line C (Fig. IV.4a) is parallel to Line B and ca. 18 km further east (for location see Fig. IV.1). Seafloor is sub-horizontal between km 3 and 80 and at 4.5 s TWT (Fig. IV.4b). Further south and north it is structured and rises up. Tb is offset and steps down across south-dipping faults in the north from km 0 to 20, and in the south from km 90 to 75 across north-dipping faults. Between km 20 and 75, Tb is defined by a strong reflection and affected by normal faults with minor offset. Between km 20 and 35 Tb is tilted northward and from km 35 to 40 it steps down across south-dipping normal faults. Further south, Tb is made of 3 highs at km 50, 55 and 65 that we interpret as late volcanoes. To the south Tb rises from 6.5 s to 5.5 s TWT between km 75 and 55, across northward dipping normal faults. Moho reflections are difficult to identify in this section.

Based on our definition (see section 3.3) we define the continental domains between km 0 and 20 and km 75 and 90. This is based on the wedging shape of the crust and the oceanward stepping Tb offset by normal faults. We identify hyperextended crust between km 10 and 20 and between km 75 and 80. We define an OCT domain separating the two continental domains between km 20 and 75. The limit occurs where a break in the slope and a change in dip of Tb occur. This change is accompanied by a change of the topology of Tb, from fault-structured, bookshelf like in the continent to rougher but still fault-structured in the OCT. Fault offsets are however much smaller, and magmatic additions can be defined. No unequivocal oceanic crust can be observed in this section.

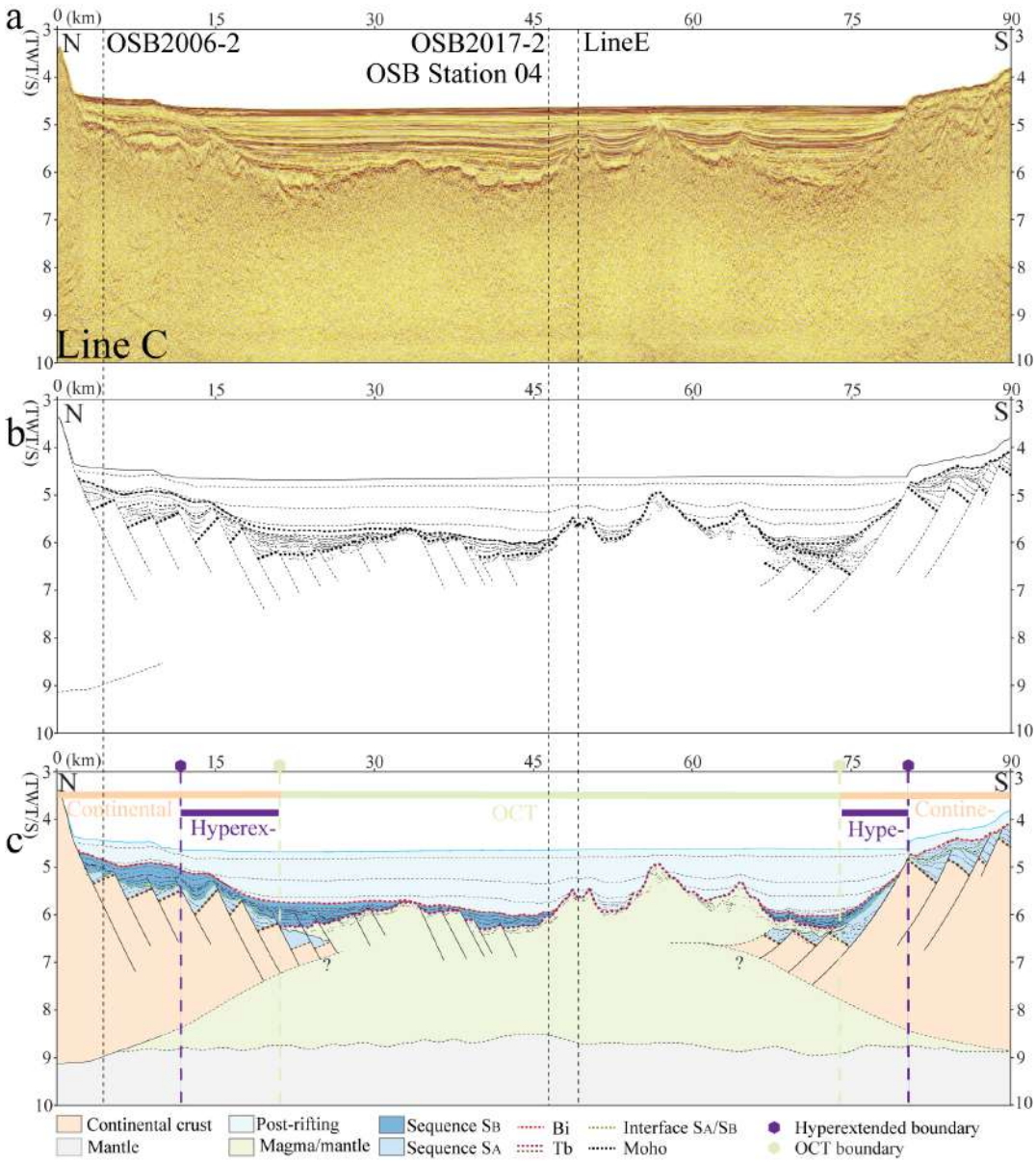

Figure IV.4. *Reflection seismic section Line C across the tip of the propagator, for location see Fig. IV.1. (a) Time migrated reflection seismic section Line B with location of cross lines (dashed lines). (b) Line drawing of the seismic section Line C, the bold lines are Tb and Bi. (c) Seismic interpretation of Line C with first-order interfaces, stratigraphic horizons, and the tectonic structures. Three sedimentary sequences (S_A, S_B and post-rifting) were defined (for explanation see discussion section). Abbreviations used in the figure: Bi, Breakup interface; Tb, Top acoustic Basement.*

Line D

Line D (Fig. IV.5a) is parallel to Line C and ca. 27 km further east (for location see Fig. IV.1). Seafloor is sub-horizontal between km 5 and 65 and lies at 4.5 s TWT (Fig. IV.5b). Further south and north it is structured and rises up. Tb is more complex to the north, displaying a graben-type structure bounded by north- and south-dipping faults between km 0 and 35. This structure is limited southward by a basement high, between km 30 and 45. From km 45 to the south, Tb is offset by south-dipping faults and remains sub-horizontal between km 50 and 90. There, Tb is defined by a strong reflector offset by normal faults with minor displacement. South of km 90, Tb is offset by first minor northward-dipping faults with small offset, then major northward-dipping faults with large offsets. Moho reflections are difficult to define but may correspond to a set of reflectivity that occurs at ca. 9 s TWT.

Based on our definition (see section 3.3) we define the continental domain between km 0 and 50 and south of km 90. This interpretation is based on the wedging of the crust in the north and the south and the structured Tb offset by oceanward-dipping normal faults. We define the block between km 30 and 45 as belonging to the continental domain, although Tb may coincide with minor magmatic additions. In-between this block and further south, wedging and fault-structured hyperextended crust is identified between km 10 and 30, between km 45 and 50 and between km 90 and 100. We interpret the domain from km 50 to 90 as an OCT with a crust that is made primary of igneous material. The crust displays an irregular Tb but not a wedging shape.

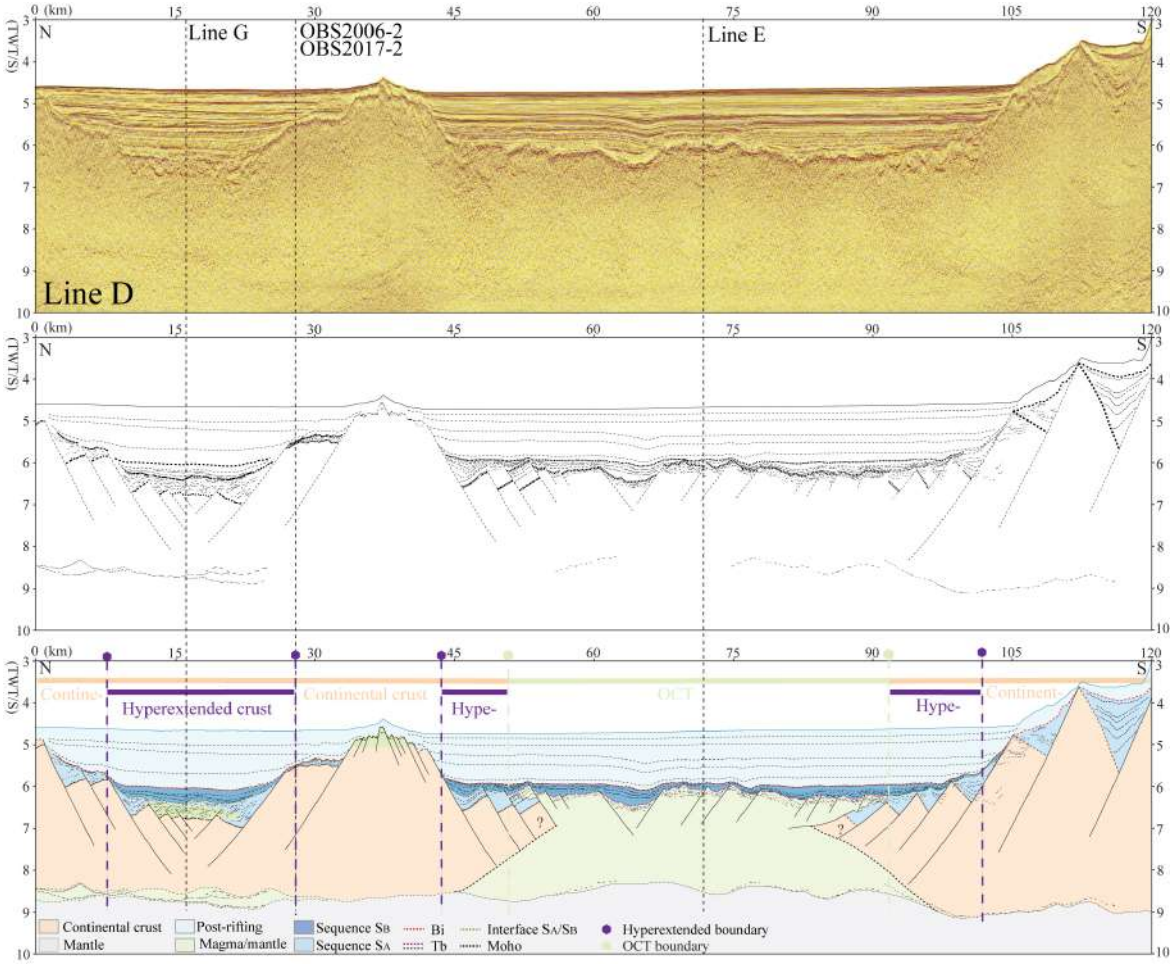

Figure IV.5. *Reflection seismic section Line D across the tip of the propagator, for location see Fig. IV.1. (a) Time migrated reflection seismic section Line D with location of cross lined (dashed lines). (b) Line drawing of the seismic section Line D, the bold lines are Tb and Bi. (c) Seismic interpretation of Line D with first-order interfaces, stratigraphic horizons, and the tectonic structures. Three sedimentary sequences (S_A, S_B and post-rifting) were defined (for explanation see discussion section). Abbreviations used in the figure: Bi, Breakup interface; Tb, Top acoustic Basement. Line D is the same line with seismic section L1, which has been published in Gao et al. (2016).*

Line E

Line E (Fig. IV.6a) is a strike line and perpendicular to lines A to D (for location see Fig. IV.1). Seafloor is sub-horizontal and lies at ca. 5 s TWT with exception of km 0 to 15 where Tb strongly rises up (Fig. IV.6b). Tb is well imaged and can be observed across the whole line. From km 5 to 30, Tb dips toward the east from 4 s to 7.5 s TWT. From km 30 to 70 Tb rises to 5 s and then drops down to 7 s TWT over a structure that is quite symmetric. Note that at the intersection with line C, the seismic nature of the crust corresponds to magmatic additions with a general thickening of the crust to the east (see intersection with line C in Fig. IV.4b), suggesting the existence of a magmatic ridge. Moho reflections are difficult to define but may correspond to a set of reflectivity that occurs at ca. 9 s TWT between km 15 and 50.

Based on our definition (see section 3.3) we define the continental domain to occur between km 0 and 35 and we recognize the rest of the section as belonging to the OCT domain and as made of first hybrid and then fully magmatic crust. The interpretation of the continental domain is based on the wedging shape of the crust with a Tb offset by normal faults. Its eastern termination corresponds to hyperextended crust between km 20 and 35. The rest of the section shows a Tb that is smooth to slightly uneven and dipping continent-wards.

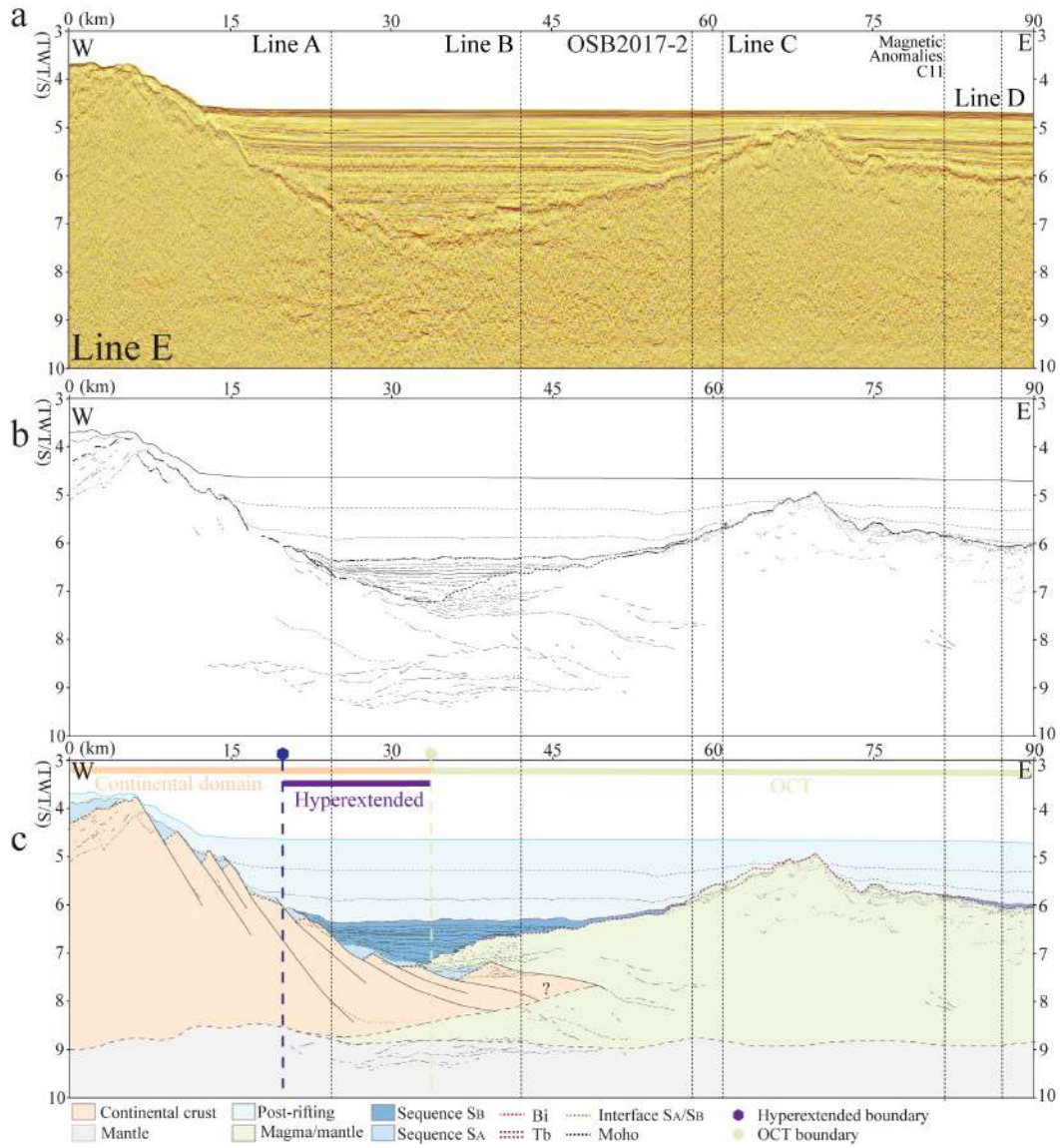

Figure IV.6. *Reflection seismic section Line E is strike line and perpendicular to line A to D, for location see Fig. IV.1. (a) Time migrated reflection seismic section Line B with location of cross line and magnetic anomalies C11 (dash line). (b) Line drawing of the seismic section Line E, the bold lines are Tb and Bi. (c) Seismic interpretation of Line E with first-order interfaces, stratigraphic horizons and the tectonic structures. Three sedimentary sequences (S_A, S_B and post-rifting) were defined (for explanation see discussion section). Abbreviations used in the figure: Bi, Breakup interface; Tb, Top acoustic Basement.*

Line F

Line F (Fig. IV.7a) is a strike line parallel to line E, located ca. 21 km further north. This line images the eastward continuation of the center of the propagator (for location see Fig. IV.1). Seafloor is sub-horizontal and lies at ca. 5 s TWT. Tb is well imaged and can be observed across the whole line as a more complex and uneven surface from km 0 to about 45 and as a strong reflection from km 45 to 100, except for a volcano-shaped body at km 70. Moho reflections are well imaged and at 9 s TWT from 55 to 100, while further west the Moho cannot be observed.

Based on the box-shaped architecture of the crust, the smooth Tb and the passive infill of the overlying sediments, we define the oceanic domain as lying between km 55 and 100. We define the domain between km 0 and 55 as in the OCT domain since it does neither show a wedging of the crust nor a structured Tb offset by normal faults. It is worth noting that there is a change in the intra-basement reflectivity in the OCT from relatively transparent in the west to more reflective and displaying seaward dipping reflectors. Reflectivity in the oceanic domain is sub-horizontal and layered.

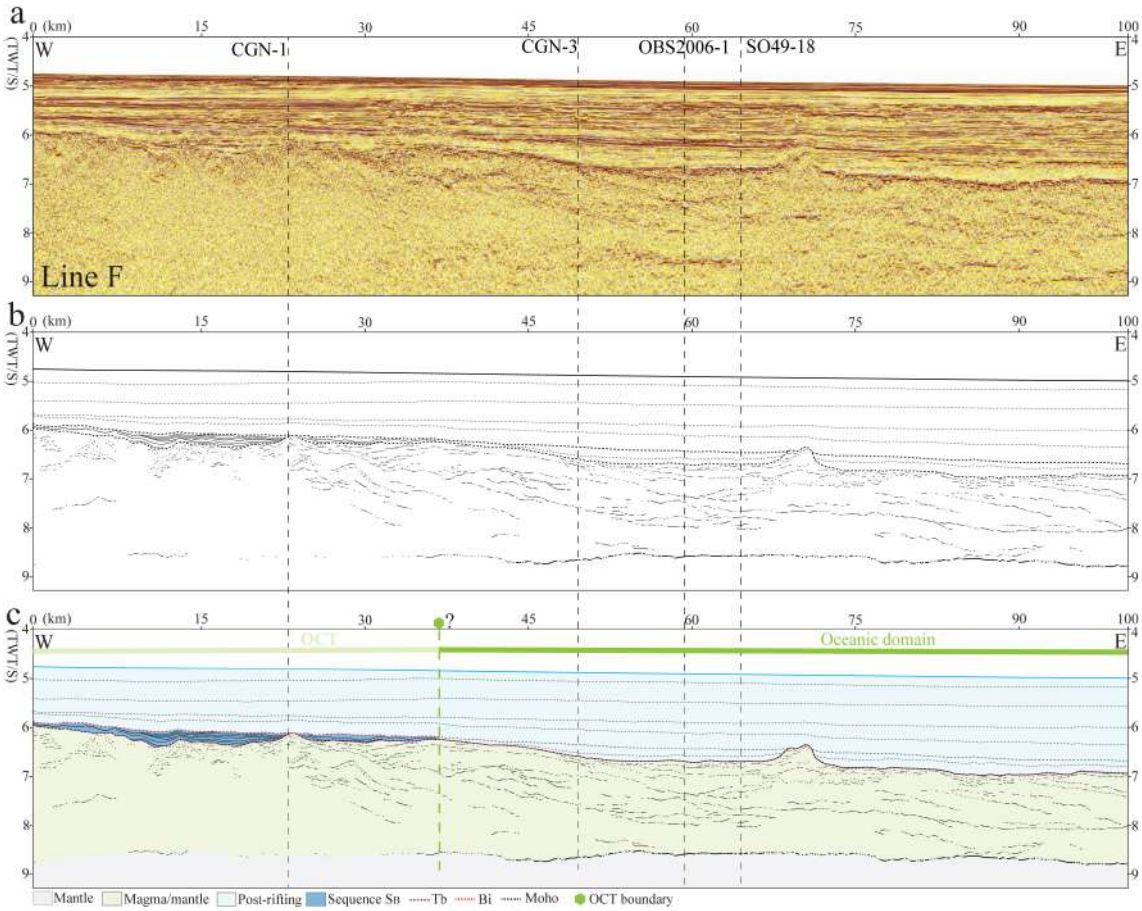

Figure IV.7. *Reflection seismic section Line F is strike line parallel to line E, located 21km further north, for location see Fig. IV.1. (a) Time migrated reflection seismic section Line E with location of cross line. (b) Line drawing of the seismic section Line F, the bold lines are Tb and Bi. (c) Seismic interpretation of Line F with first-order interfaces, stratigraphic horizons and the tectonic structures. Two sedimentary sequences (S_B and post-rifting) were defined (for explanation see discussion section). Abbreviations used in the figure: Bi, Breakup interface; Tb, Top acoustic Basement.*

Line G

Line G (Fig. IV.8a) is a strike line parallel to lines E and F and just north of the OBS2006_2 line that is shown, for comparison, on the same section (for location see Fig. IV.1). Seafloor is sub-horizontal and lies at ca. 5 s TWT except for its western termination (Fig. IV.8b). Tb is well imaged from km 20 to 120 and more difficult to define westwards of km 20. We interpret Tb to be offset by faults and to step down from ca. 4 s TWT to ca. 7 s

TWT, indicating a wedging of the crust that tips out at ca. km 35. Tb is defined as a strong reflection from km 20 to the end of the section in the east. From ca. km 20 to 60 it dips toward the east, i.e., towards the continent. Faint and discontinuous Moho reflections can be seen west of km 60 at about 9 s TWT while Moho reflections are difficult to observe further east.

Based on our definition (see section 3.3) we define the wedge-shaped crust with a fault-structured Tb west of km 20 as belonging to the continental domain. We identify hyperextended crust between km 15 and 25. We define an OCT domain between km 20 and 65, which displays a continent-ward dipping Tb that terminates eastward at a basement high at km 65. The crust east of this high shows a horizontal, smooth Tb (except for a volcano at km 95) and passive infill qualifying for an unequivocal oceanic domain.

Crustal structure and domains: main observations

The interpretation of seismic reflection lines located at the tip of the SW SCS propagator enables us to characterize the main interfaces, domains and domain boundaries. In the continental domain, Tb is offset by faults and tilted, and lies between 3 and 7s TWT. Moho lies globally at 9 s TWT. In the OCT domain Tb displays a rough morphology and ranges between depths of 7.5 and 6 s TWT and Moho lies between 9 and 8 s TWT. In the oceanic domain, Tb and Moho are parallel and the crust is 2 s TWT-thick. Tb is smooth and lies at 6.8 s TWT while Moho lies at 8.8 s TWT.

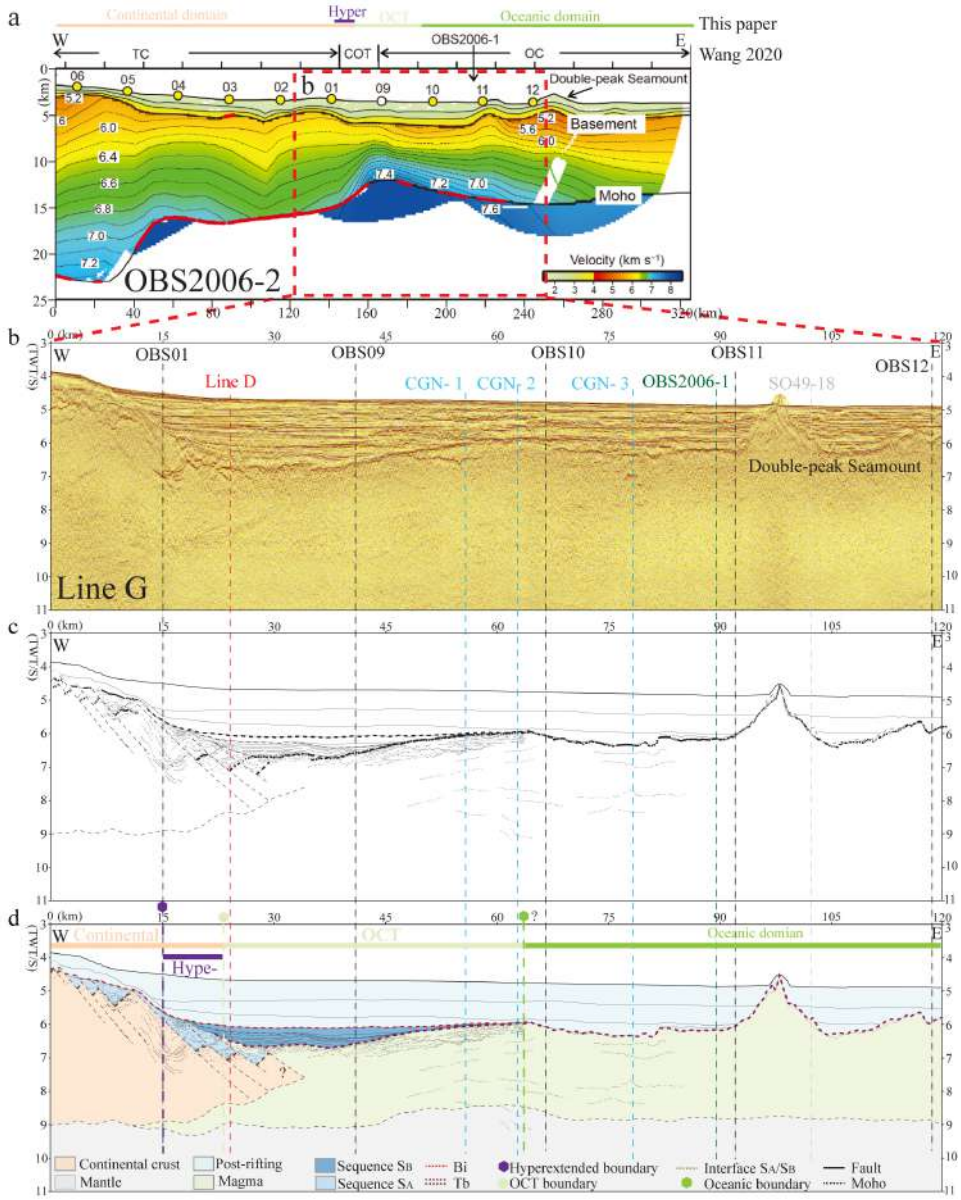

Figure IV.8. *Reflection seismic section Line G is strike line parallel to line E and F, Line G and OBS2006-2 only 8 km apart, for location see Fig. IV.1. (a) OBS2006-2 Velocity structure of the inverse model by using Tomo2D software, for more detail see Wang et al. (2020), red dotted box is same location with Line G. (b) Time migrated reflection seismic section Line G with location of cross line and OBS station points. (c) Line drawing of the seismic section Line G, the bold lines are Tb and Bi. (d) Seismic interpretation of Line G with first-order interfaces, stratigraphic horizons, and the tectonic structures. Three sedimentary sequences (S_A, S_B and post-rifting) were defined (for explanation see discussion section). Abbreviations used in the figure: Bi, Breakup interface; Tb, Top acoustic Basement; TC, Thinned Continental crust; OC, Oceanic crust.*

4.2. Sedimentary sequences

Compactable sediments in lines A to G shown in Figs. IV.2 to IV.8 are comprised between Tb and the seafloor. They can be subdivided into a syn-rift and a post-rift mega-sequence. The occurrence of pre-rift sediments over continental crust is likely, but their presence is difficult to confirm without drill hole data. We therefore include them in the acoustic basement capped by Tb. Distinguishing between the syn- and post-rift sequence is difficult in a polyphase rift system where the strain is supposed to localize with time and where the syn-tectonic sequence is diachronous across both dip and strike sections (Luo et al., 2021; Chenin et al., subm). Indeed, since sediments deposited during the time of rifting can be deposited outside the tectonically active zone, the syn-rift sequence can include both syn- and post-tectonic sediments, and the latter are difficult to distinguish from post-rift sediments. Chao et al. (in prep) defined three sequences (S1 to S3) east of the study area along lines CGN-1 to 3 (for location see Fig. IV.1). In this study we subdivide the syn-rift mega-sequence observed over the continental and OCT domains into two sequences, referred to as S_A and S_B respectively. S_A and S_B are correlated among seismic sections based on both their seismic facies and the geometric control resulting from the numerous intersections between the studied seismic sections (cf. Fig. IV.1 and the trace of crosscutting seismic sections displayed in Fig. IV.2-IV.8). This allows us a relatively reliable mapping. S_A does not occur over the OCT and may correspond to S1 of Chao et al. (in prep). S_B is the first sediment deposited over the OCT and may correspond to S2 and S3 of Chao et al. (in prep). The post-rift mega-sequence is the first sedimentary sequence deposited over the oceanic domain. A characteristic of the post-rift mega-sequence is that it does not show syn-tectonic architectures throughout the study area. The limit between the syn- and post-rift mega-sequences is defined as the breakup interface Bi, which can be mapped across the study area as explained below.

The first sequence (S_A) is best defined in Line B (Fig. IV.3c). It shows growth structures bounded by normal faults offsetting Tb in the continental domain. S_A is floored by either Tb or faults, and its sediments thicken into faults. The top of S_A is largely

continuous and it locally seals faults, suggesting relatively high sedimentation rates. In dip lines C and D and strike line E (Figs. IV.4c, IV.5c and IV.6c), regular and relatively continuous reflections characteristic of sedimentary deposits are interfingering with strong and discontinuous reflections associated with cluttered and more massive reflectivity that may represent magmatic additions. Thus, S_A either interfingers or is intruded by what we interpret as magmatic additions, but we can never see S_A neither downlapping nor onlapping onto magmatic Tb in the OCT. The use of dip and strike lines allows us to identify and correlate S_A across the whole tip of the NW SCS. It systematically occurs over structured and wedging crust like the S1 sequence mapped by Chao et al. (in prep) further east.

The second sequence (S_B) is best defined in line C (Fig. IV.4c). It onlaps continent-ward either onto S_A or directly onto basement and down- or onlaps outboard onto a reflective Tb, interpreted as the top of a magmatic curst belonging to the OCT. S_B wedges out oceanward over the OCT (lines C, D, E, G; Figs. IV.4c, IV.5c, IV.6c, and IV.8c), and shows growth structures linked to minor normal faults that offset Tb in the OCT. Similar observations can be made in the dip line D (Fig. IV.5c) or on the strike lines E and G (Figs. IV.6c and IV.8c). In line E, S_B is tilted continent-wards and onlapped by younger post-rift sediments (Fig. IV.6c). On lines A and B (Figs. IV.2c and IV.3c) S_B occurs over S_A and does only show minor thickness changes across faults. In these lines, S_B is clearly post-tectonic and shows passive infill geometries. The mapping of S_B in the western tip is based on correlations along strike of line E (Fig. IV.1). Oceanward, as shown in lines F and G (Figs. IV.7c and IV.8c), S_B wedges out and does not occur over oceanic crust.

The top of the S_B sequence, referred to as Bi, is best defined on lines C to G (Figs. IV.4c and IV.8c). In line C, Bi coincides with the base of passive infill. In line G, Bi terminates against the basement high that marks the end of the continent-ward tilting of the Tb in the OCT and forms the limit to first oceanic crust (for a similar situation see Fig. II.10 in Chapter II). This geometrical relationship defines the relative age of Bi corresponding to the time of lithospheric breakup and formation of first oceanic crust at the

tip of the NW SCS. Based on the correlation of Bi across the dip and strike lines shown in Fig. IV.1, we can trace Bi across the tip of the NW SCS. Oceanward, Bi either onlaps on the outer high located at the oceanward limit of the OCT (line G; Fig. IV.8c), or down-dips onto first oceanic crust (line F; Fig. IV.7c). Continent-ward, Bi lies within the post-tectonic sequence (line A; Fig. IV.2c). Thus, rift cessation at the tip of the NW SCS in the west predates onset of seafloor spreading further east.

The third sequence defined in our study is the post-rift mega-sequence. It overlies Bi, does not show any growth structures throughout the study area and it is the first sequence overlying mature oceanic crust. In the following, we will not further discuss the post-rift mega-sequence since the aim of this study is to discuss the tectono-stratigraphic history/signature of breakup and its propagation at the tip of the NW SCS.

5. Mapping rift domains at the tip of the NW SCS

5.1. Mapping rift domains based on reflection seismic data

In the previous section we defined rift domains based on reflection seismic interpretations from the tip of the NW SCS. The aim of this section is to build with these results a rift domain map. The methodology to create such maps has been first described by Tugend et al. (2014) and definitions of rift domains and domain boundaries are provided in section 3.3. A rift domain map does neither show structural details, nor does it consider the composition of the underlying crust, although the link between lithologies and rift domains is apparent for the oceanic and continental domains.

To construct the map shown in Fig. IV.9b, we used all lines presented in this manuscript as well as lines that are already published/in the public domain (for location see Figs. IV.9a and IV.9b). We applied the approach described above to all the lines of the survey that are shown in the inset in Fig. IV.9a. This enabled us to produce a rift domain map that is well constrained, in particular at the region of the tip of the propagator. Indeed, for each of the seismic lines shown in Fig. IV.9a and crossing the study area, we defined

the rift domain boundaries and linked them into a continuous domain boundary. In the continental domain we also used the refractions data (for description see next section). Comparing the crustal thickness map (Fig. IV.9a) with the rift domain map (Fig. IV.9b) shows that there is a first-order correspondence between crustal thickness defined by gravity inversion (Fig. IV.9a; ref) and the domain boundaries defined from reflection seismic data (Fig. IV.9b). This result is not surprising, since crustal thickness and thinning gradients (e.g. wedge vs. box shape) is a first-order characteristic of rift domains. However, since the two maps are independent from each other, the good fit supports the validity of our approach. A main observation is that the continent-ward limit of the hyperextended domain coincides with a change in the thinning gradient (Fig. IV.9a), while the boundary between hyperextended crust and the OCT domain and between the OCT and oceanic domains are difficult to define in a crustal thickness map. These domain boundaries involve different types of crust with different velocity structures and can therefore be imaged using refractions seismic data, however, as discussed later, they are better and more precisely defined using high-quality, long offset reflection seismic data.

Our rift domain map (Fig. IV.9b) shows a complex crustal structure at the tip of the propagator that includes three crustal blocks, continental China to the north, the Macclesfield Block to the south and the Parcel Block to the west. These domains of thicker continental crust are separated by hyperextended domains in the west. Eastward, an oceanic domain appears, and the related crustal structure is simpler. From the map, it is obvious that the tip is not a simple structure. The distribution of hyperextended domains is complex and does not show the commonly assumed idea of a wide and distributed rift in front of a propagating oceanic domain. It is surprising that the tip of the oceanic domain does not follow the trend of the hyperextended domains in its frontal part. This is even more surprising considering that in the east, the oceanic domain splits the hyperextended and OCT evenly on both sides.

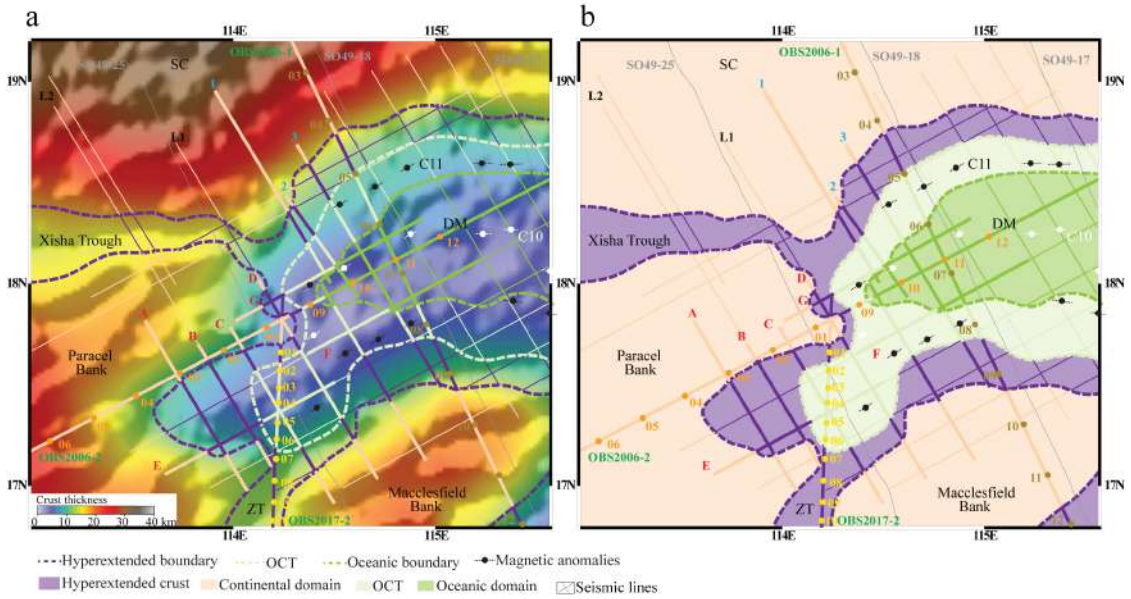

Figure IV.9. *Map showing rift domains in the study area in the NW-SCS. The domain boundaries are derived from seismic interpretations, by tracing the Hyperextended boundary, OCT, Oceanic boundary of each line shown in the figure.*

5.2. Nature of crust at the tip of the propagator: constraints from refraction seismic data

In absence of drill hole data it is impossible to determine unambiguously the lithologies forming the crust. In distal, sediment-rich margins it is anyway difficult to penetrate basement, and where it has been done, it was limited to basement highs (e.g. IODP Legs 1505 SCS; ODP Legs 103, 149, 173 and 210 Iberia-Newfoundland). Access to refraction seismic and potential field data can provide indirect constraints on the composition of the crust, however such methods are non-unique, since velocities, densities and magnetic properties cannot be assigned to one lithology only. Péron-Pinvidic et al. (2016) showed that significant mismatches may arise between structural interpretations based on reflection and refraction seismic data and/or on potential field methods for distal rifted margins. Here we discuss the results of three refraction seismic lines crossing the tip of the NW SCS propagator (Fig. IV.10; for location of lines see Fig. IV.1). Lines OBS2006-1 and OBS2006-2 have been published and described by Wu et al.

(2012), and line OBS2017-2 by Li et al. (2021). The aim to present these sections in our study is twofold, it allows: 1) to compare our seismic reflection interpretation with the refraction seismic data (see Fig. IV.8, and IV.2) to compare the refraction seismic data with our rift domain map (Fig. IV.9).

Refraction line OBS2006-2 and reflection line G shown in Figs. IV.8a and IV.8b are parallel lines only 8 km apart (for location see Fig. IV.1). Thus, comparing the two lines offer the possibility to link a velocity structure (OBS data) with a rift domain. As shown in Fig. IV.8, OBS01 samples the velocity structure of the hyperextended crust, OBS09 that of the OCT and OBS11 that of the oceanic domain. Already from the velocity structure shown in Fig. IV.8a it is clear that each of the domains is characterized by a different velocity structure, indicating different crustal compositions. A first main observation is that crustal thinning from about 10 km at OBS 01 to about 6 km at OBS 09 occurs in the hyperextended domain and is linked to a narrow rise of the Moho. A change in the crustal velocity structure across the hyperextended and OCT domains as shown by OBS01, OBS09 and OBS10 is compatible with the interpreted change from a hybrid to a fully magmatic crust in the OCT shown in Fig. IV.8d. The thickening of the crust oceanward in the OCT shown by OBS09 and OBS10 is in line with the observed uplift and continent-ward tilting of Tb, that has been interpreted by Chao et al. (in prep) to be linked to underplating. Unfortunately, the oceanward part of the section is perturbed by the emplacement of late volcanoes, well imaged in the reflection seismic section at km 95 and showing that late magmatic activity may result in local thickening of the oceanic crust.

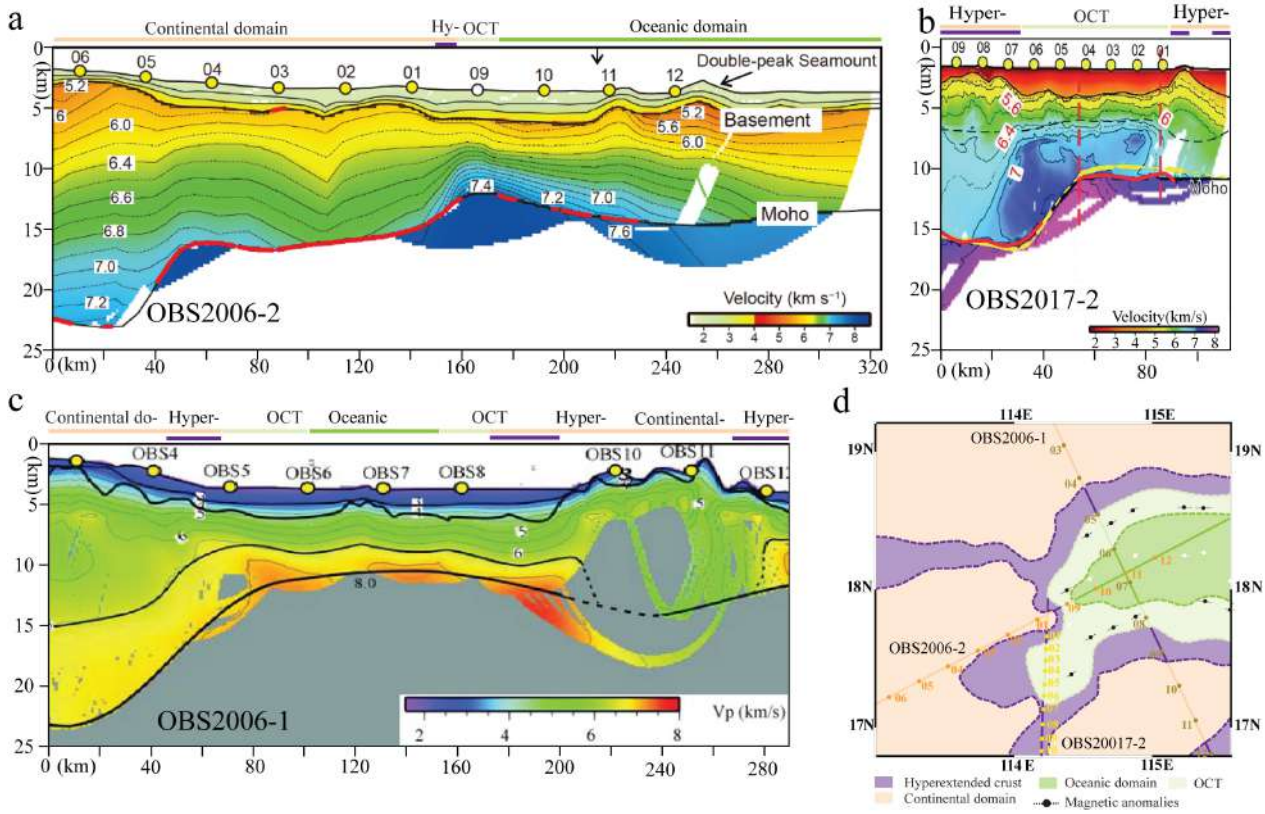

Figure IV.10. *Three refraction seismic lines crossing the tip of the NW SCS propagator. Compare our seismic reflection interpretation with the refraction seismic data and the rift domain map.*

In Fig. IV.10d, we plot the position of the three refraction seismic sections (Figs. IV.10a, IV.10b and IV.10c) in the rift-domain map and show, along each refraction line, the imaged domain (bar with the color of the domain above the line). This allows to define the range of velocities and thickness for each mapped domain. The crustal thickness does not significantly change across the distal margin: the hyperextended domain ranges from 10 to 6 km showing a wedging oceanwards; the OCT is thinnest on its continent-ward side (about 6 km) and slightly thickens oceanward to 7 or 8 km; the thickness of oceanic crust is difficult to determine due to the existence of late magmatic additions on OBS2006-2 but is in the order of 5 to 6 km in OBS2006-1. In contrast to the crustal thickness variations that may not allow to distinguish between these domains, the velocity structure is more characteristic and show important differences between the continental and oceanic domain

with a characteristic velocity structure for the OCT. The main difference between the continental and oceanic crusts is the high-velocity layer characterizing the lower crust in the oceanic domain. On all sections the limit between the hyperextended domain and the OCT coincides with an abrupt rise of the Moho and a significant thinning of the crust over a narrow region. In contrast, the transition to oceanic crust seems more gradual.

5.3. Comparison with existing OCB maps and potential field data

In Fig. IV.11a we compare our rift domain map with previously published locations of the COB, spreading centers and other structures. Zhang et al. (2012) defined the COB and abandoned spreading center using magnetic data. This interpretation is similar to that of Li et al. (2012). Their COB includes parts of the hyperextended crust, and OCT. It's also interesting to see that these authors proposed a transform fault separating two oceanic segments. Cameselle et al. (2017) used reflection seismic data and gravity data to define two spreading centers with very narrow COBs and interpreted the southern ridge as the older one and the northern as the younger one due to a ridge jump. These authors mapped most of what we consider as oceanic and OCT domains as thinned continental crust. More recently Li et al. (2021) defined the COB in the western part of the tip based on reflection and refraction seismic data and using gravity and magnetic data for the eastern parts. In their interpretation the COB correlates with our OCT.

The differences among the interpretations show that: 1) defining the location of breakup is complex and non-unique and depends on the used dataset, method and definition of the COB. 2) The different interpretations yet show similarities with our mapped boundaries, in that the COB of Zhang matches with the continent-ward part of our hyperextended domain; the COB of Li et al. (2021) corresponds to the continent-ward limit of our OCT; and the location of the northern spreading ridge and segmentation of Zhang et al. (2012) match with the location of our oceanic domain. In these cases, the methods and/or observations may provide similar results but the definition of domains/crusts is different. However, some interpretations are difficult to reconcile, for instance the COB's of Cameselle et al. (2017) is contradictory with our observations.

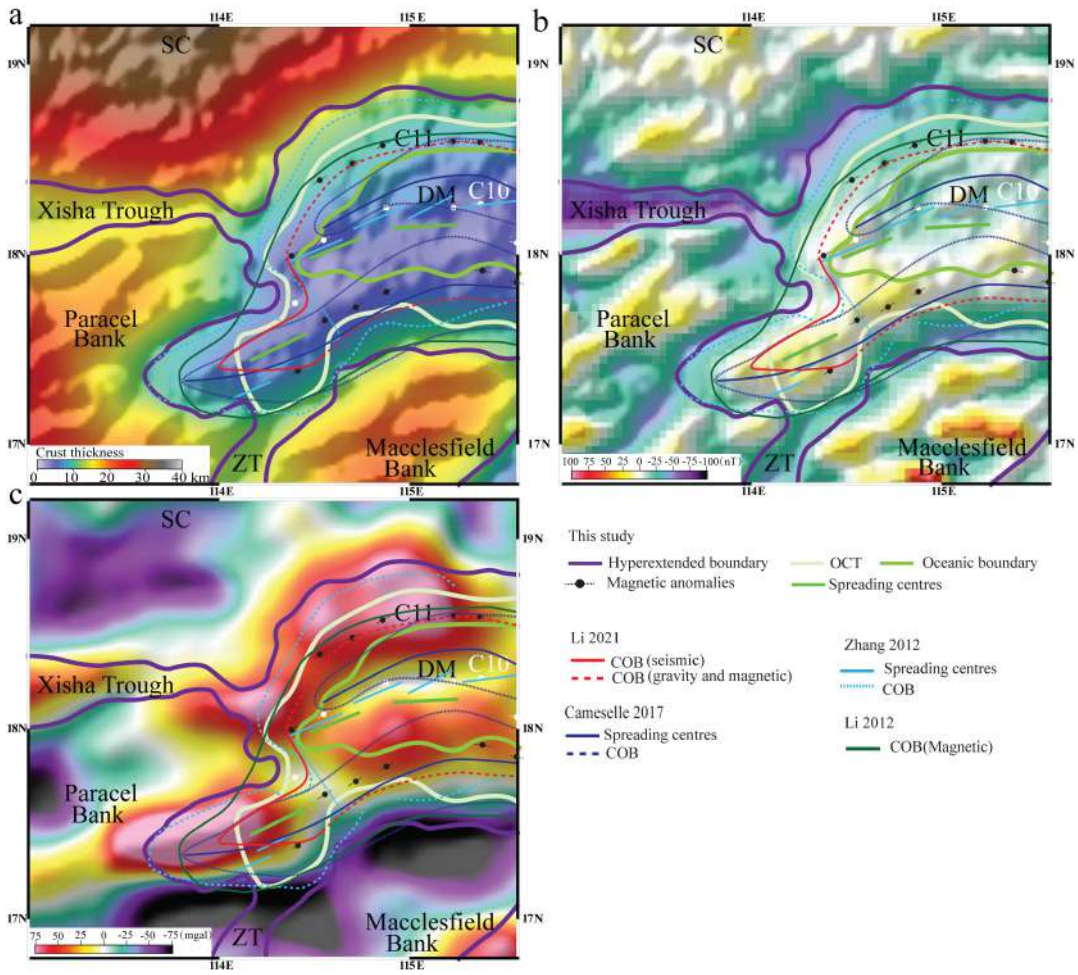

Figure IV.11. *Compare rift domain map with previously published locations of the COB, spreading centers and other structures. (a) The crust thickness map. (b) The free-air gravity anomaly map. (c) The magmatic anomaly map. Maps from Gozzard el al. (2019). The light blue solid line and the blue dashed line show the locations of spreading center and locations of COB in the NW-SCS interpreted by Zhang et al. (2012). The solid red line marks the location of COB where constraint by seismic results, while the dashed segments represent the COB deduced from gravity and magnetic data by Li et al. (2021). The heavy blue solid line and dashed line show the location of the spreading center and COB in the NW-SCS interpreted by Cameselle et al. (2017) based on MCS data. The green solid line represents the COB deduced from magnetic data by Li et al. (2012).*

A comparison between the rift domains mapped in different studies and free air gravity data from Gozzard et al. (2018) is shown in Fig. IV.11b. A good correlation exists between the hyperextended domain and a negative gravity anomaly, which is compatible with the observation of a strong crustal thinning. The anomaly is sharper and stronger on the

continent side than on its oceanward side, which is compatible with the observed crustal thickness variations observed from seismic data across the margin.

A comparison between the rift domains mapped in different studies and magnetic data is shown in Fig. IV.11c. Within the magnetic map, low values correlate well with thick continental blocks. An exception is the hyperextended domain imaged by line OBS2017-2 separating the Macclesfield from the Parcel Blocks. Within the more extended/oceanic domain three positive magnetic anomalies can be observed. One is overlying oceanic crust and parallel to oceanic magnetic anomalies. This anomaly correlates well with the oceanic domain we mapped. A second, major anomaly can be recognized further north. It is parallel to the hyperextended and OCT domains and shows an abrupt termination towards the west. Although this anomaly is parallel to magnetic anomaly C11 as well as to the limits between the hyperextended domain and OCT, it remains unclear what may be the origin of this anomaly. The most surprising is that nothing comparable can be found on the conjugate margin. Even in the refraction line OBS2006-1 crossing the anomaly, nothing particular can be found below OBS5 that is located right above the anomaly. Similarly, the anomaly overlying the tip of the propagator occurs over hyperextented crust where we interpret tilted blocks (see line B; Fig. IV.3a). Some evidence for magmatic additions can be seen and are shown in line B (Fig. IV.3c) but it is difficult to determine if this can explain the magnetic anomaly. The strong magnetic anomaly may explain why most interpretations (Zhang et al., 2012; Cameselle et al., 2017; Li et al., 2012, 2021) put the tip of the oceanic propagator at this location.

5.4. Distribution of sedimentary sequences at the tip of the NW SCS

We defined and discussed S_A and S_B as well as Tb and Bi in section 4.2. Maps showing the distribution of S_A, S_B and the post rift sequence are shown in Fig. IV.12. Since we were able to map these sequences through all lines (see Fig. IV.9a) and not only along the lines presented here, we are confident that S_A and S_B are of the same age across the small extent of our study area, which is not necessarily true for the whole NW SCS propagator. We also assume that Bi represents a timeline in the study area, and

corresponds to the timing of lithospheric breakup in the eastern part of the study area. Independently if we regard dip or strike lines, Bi and Tb are converge basinward/oceanward and, as expected for an interface defined as “breakup interface”, it on- or down-laps onto the location of lithospheric breakup, i.e., the outer limit of the OCT. This line defines the oceanward limit of the extent of S_B. Away from this limit, towards the north, south and west, the syn-rift mega-sequence bonded by Tb and Bi (i.e., S_A plus S_B) thickens, as observed in the sections shown in Figs. IV.2c to IV.8c. Moreover, we systematically observe that S_A wedges out first, while S_B continues further oceanward. However, in contrast to S_B, the wedging point/line of S_A is difficult to observe. In all sections where the OCT can be defined (lines C, D, E and G; Figs. IV.4c, IV.5c, IV.6c, IV.8c) S_A appears to either terminate into or to be overlain by magmatic additions. In our maps we put the oceanward termination of S_A at the limit between the hyperextended and OCT domains. However, we can not exclude that S_A continues underneath the magmatic additions that form the continent-ward edge of the OCT (Fig. IV.12). In our interpretations, we show a sandwich-like position of S_A between a continental Tb and the magmatic Tb of a new crust in the OCT. When mapping Bi across lines from the continent towards the tip of the propagator, we observe that this timeline post-dates active faulting in this segment but corresponds to lithospheric breakup in the neighboring eastern segment.

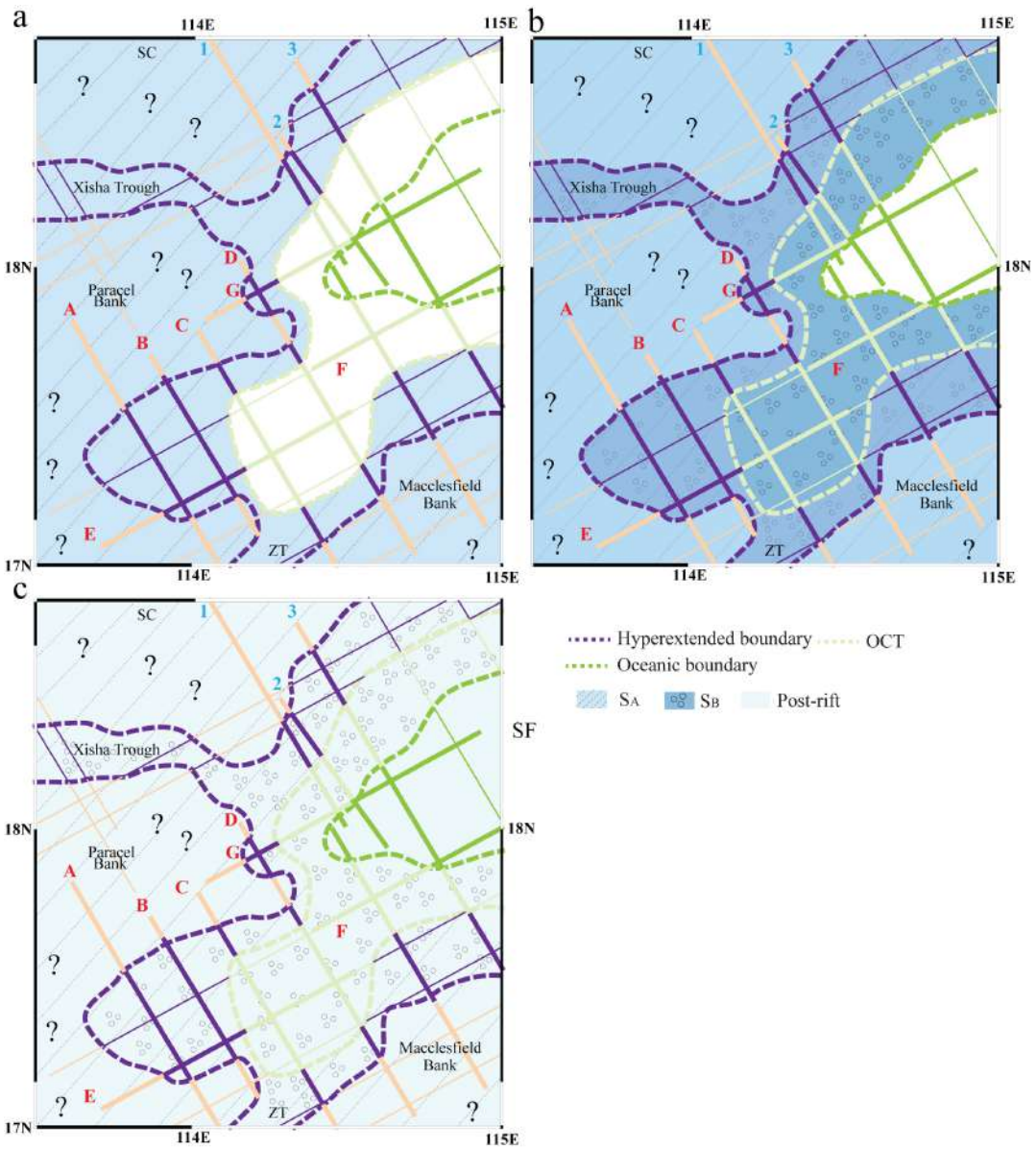

Figure IV.12. *Maps showing the distribution of S_A, S_B and the post rifting sequence. (a) The distribution of S_A. (b) The distribution of S_B. (c) The distribution of the post rifting sequence.*

6. Discussion

In this study, we described and mapped rift domains at the tip of the NW-SCS based on a high-resolution reflection seismic dataset. We produced a rift domain map and compared it with refraction seismic, magnetic and gravity field data as well as previously mapped COBs. We also analysed and defined syn-hyperextension and syn-breakup

sedimentary sequences (S_A and S_B, respectively) and mapped them across the study area. This work enables us to now discuss the 3D architecture of the crust at the tip of the NW SCS, its tectono-magmatic evolution related to breakup, and to examine how breakup evolves and finally stalls in the NW SCS.

6.1. 3D crustal architecture at the tip of the NW SCS

The 3D crustal architecture of the NW SCS corresponds, at a plate tectonic scale, to a V-shaped failed oceanic basin that pinches out westwards into rifted crust. At a regional scale the V-shaped basin can be subdivided into a rear, which corresponds to a classical rifted margin with two conjugate margins separated by oceanic crust, and a tip where the ocean pinches out into a severely thinned/hyperextended continental crust, as nicely illustrated in Fig. IV.13. Here, we investigate the tip and its relation to the rear and the rifted crust further to the west.

The 3D crustal block with the rift domain map at its top (Fig. IV.13a) shows the crustal architecture observed at the tip of the NW SCS. A sequential set of sections across the tip are shown in Fig. IV.13b, documenting the breakup process at the tip. Fig. IV.13c shows a synthetic strike line documenting the transition from the continental domain, including a hyperextended crust, to an OCT and an oceanic domain. The section documents also the observed relationships between deformation, magmatism and sedimentation. The sediments of S_A seal the faults responsible for hyperextension and interfinger oceanward with magmatic additions. The sediments of S_B onlap onto the Tb of the OCT. The top interface of S_B, referred to as the breakup interface (Bi), terminates at a basement high (Hb) that limits the OCT from first oceanic crust. These relationships, documented in the reflection seismic sections Figs. IV.2 to IV.8 and described in the previous sections, enable a precise temporal and spatial description of the crustal, magmatic and sedimentary evolution at the tip of the NW SCS during breakup.

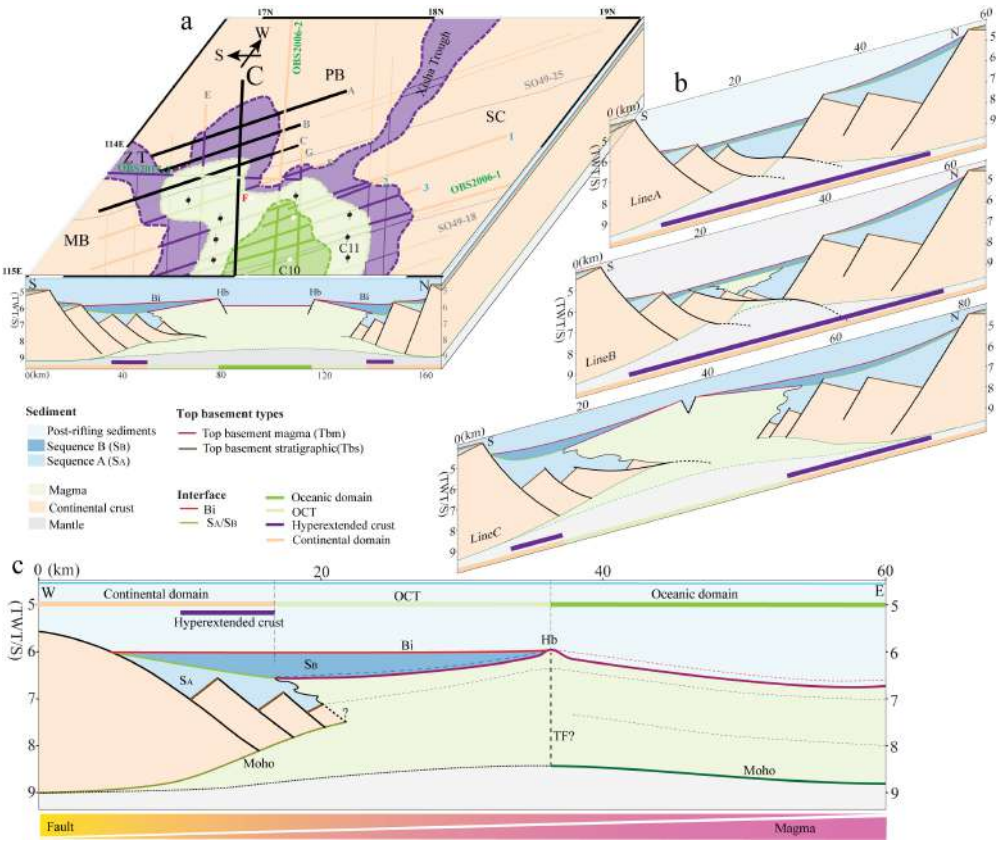

Figure IV.13. *(a) The 3D crustal block with the rift domain map. (b) A sequential set of sections across the tip, which is Line A, B and C. (C) A synthetic strike line documenting the transition from the continental domain, including a hyperextended crust, OCT and oceanic domain.*

The first-order description shown in Fig. IV.13 and its interpretation are, however, conflicting with previous interpretations. As shown in Fig. IV.11, C. Li and Song (2012); Y. Li et al. (2021); Zhang et al. (2012) and Cameselle et al. (2017) came to different conclusions and interpretations for the same area. These authors interpreted the tip, imaged by the sections shown in Fig. IV.13b, as the termination of oceanic crust. This interpretation was mainly based on the interpretation of magnetic data, showing a strong positive anomaly (Fig. IV.11c). However, when looking in detail the reflection seismic sections across the tip, fault-bounded basins with syn-tectonic stratigraphy can be recognized (Figs. IV.2, IV.3 and IV.4). Moreover, sediments belonging to S_A can be mapped throughout the tip, always overlying wedging continental crust, and showing syn-

tectonic growth structures. The basement underlying S_A shows indeed the structural characteristics of continental crust with diagnostic features such as a wedging crust and a Tb offset by faults. More recent and better documented studies tend, however, to put the COB further eastwards. This is nicely documented in Fig. IV.11a, where C. Li and Song (2012) and Zhang et al. (2012) mapped first the COB with the green line (C. Li & Song, 2012) and the light blue line (Zhang et al. 2012), suggesting that the domain shown in Fig. IV.13b with crustal blocks is floored by oceanic crust. Later, and based on refraction data, Y. Li et al., (2021) put the COB further eastwards (see red line in Fig. IV.11a). We analyzed the refraction data from Y. Li et al. (2021) (see OBS2017-2; Fig. IV.9b) and compared it with the refraction data from Wu et al. (2012) (OBS2006-1 and OBS2006-2; Figs. IV.9a and IV.9c). It appears that Y. Li et al. (2021) interpret our OCT as oceanic crust. Although the definition of OCT may be challenging and difficult to follow and apply, we don't think that the contact between unequivocal continental and oceanic crusts is sharp and can be mapped with a COB. Our observations show that these two types of crusts are separated by a transition zone, referred to as OCT. In the present study we can see that the OCT has some diagnostic features that can be used for mapping. First, the OCT is overlain by a syn-tectonic sequence (S_B) that is never observed over oceanic crust where sediments show passive infill. Another characteristic is the continent-ward tilting of Tb in the OCT domain and the occurrence of an outer high (see Hb in Fig. IV.13c) that can be observed all along the NW SCS (see Chao et al., in prep). Moreover, refraction seismic data show a transitional velocity structure in the domain we map as an OCT, different from that of both the adjacent continental and oceanic domains. Thus, we consider that mapping a transition, i.e., an OCT instead of a sharp COB between unequivocal continental and oceanic crusts is more correct, is important for the accuracy of maps, and also has major implications for the interpretations of the breakup process as discussed in Chao et al. (in prep).

6.2. Tectono-magmatic evolution during breakup at the tip of the SW SCS

Although the observed structures and distribution of magmatic additions and their link to the sedimentary sequence are reasonably well understood in 2D reflection seismic sections (e.g., Fig. IV.13c), it is difficult to understand their relationship in 3D. A key question is how the relatively classical rift structures observed in the rear of the tip terminate and can be linked to the complex rift structures located west of the tip (Fig. IV.13a). Unlike many propagating rift and oceanic systems showing well defined segments (for examples see Woodlark basin (Taylor et al. 2009), the Gulf of California (Lizzaralde et al., 2007), the northern tip of the Red Sea (Ligi et al., 2018), and the Afar/western Gulf of Aden (Nonn et al., 2019)), in the NW SCS a segmentation is difficult to observe. First-order structural features, such as the trend of magnetic anomalies, the fossil ridge, or the strike of the hyperextended Xisha Trough can be mapped showing, undoubtedly, a N-S directed extension. However, it is difficult to define, in detail, how these structures terminate, and/or to propose transfer zones/faults parallel to the presumed NNW-SSE extension direction. Thus, it remains unclear how the mature oceanic system in the east can be linked to the hyperextended systems in the west, both spatially and temporally. This also leads to the question if tectonic extension in the west occurred simultaneously with magmatic accretion in the east, in which case this interaction should be observed somewhere in between, spatially and temporally. Chao et al. (in prep) discussed the transition from tectonic extension to magmatic accretion for the area located in the rear of the tip and they concluded that it occurred during the formation of the OCT, documented in lines CGN-CGN-1 to 3 (see Fig. IV.1 for location). A similar evolution is not imaged in the study area in lines imaging the OCT (Figs. IV.4, IV.5, IV.6, IV.7 and IV.8). This may either be explained by the fact that it existed but has not been resolved and documented in the reflection seismic lines, or that breakup at the tip evolved differently from breakup at the rear.

An interesting observation, well illustrated in the crustal domain map (Fig. IV.13a), is that the tip corresponds to a sort of triple point, where two hyperextended domains join

and link with the tip of the NW SCS, separating three crustal blocks, i.e., the China continental margin in the north, the Macclesfield Bank to the south and the Paracel Bank to the west. Jourdon et al. (2020) were able to successfully reproduce such a structural complexity ahead of a propagator with a numerical model. In their model, the Xisha Trough is presumed to form ahead and simultaneous to the oceanic domain further east (see model in Fig. IV.14a). Our 3D snapshot (Fig. IV.13a), showing a comparable 3D distribution of crustal domains, does, however, not allow tell how this system was acquired and if the model of Jourdon et al. (2020) is applicable to our area, despite the fact that it looks very similar. To understand the evolution of the rift system and to evaluate how it propagated, it is important to have access to the sedimentary architecture, since it is the only recorder, apart from the magnetic anomalies, that can actually constraint the temporal evolution of a rift system.

In this study, we defined two sedimentary sequences S_A and S_B and we mapped them, as shown in Fig. IV.12 across the tip of the NW SCS. While S_A was deposited during the hyperextension phase, S_B was deposited during the OCT formation (for detailed discussion see sections 4.2 and 5.4). Due to the correlation across the tight network of lines and the relatively small area, we are confident that each one of these sequences is of same age across the study area. The implication of this observation is that the frontal part is not active while the ocean is forming in the rear. Thus, we can exclude a propagation mode in which an oceanic domain propagates while hyperextension occurs simultaneously further to the west. Our observations suggest, indeed, that the system is not propagating as commonly interpreted, but retrograding, i.e., when seafloor starts in the east, hyperextension in the western is not anymore active. Thus, the system does not stall but it reorganizes. In order to explain this evolution and discuss its consequences for the local and regional geological evolution of the NW SCS, we propose a conceptual model shown in Fig. IV.14.

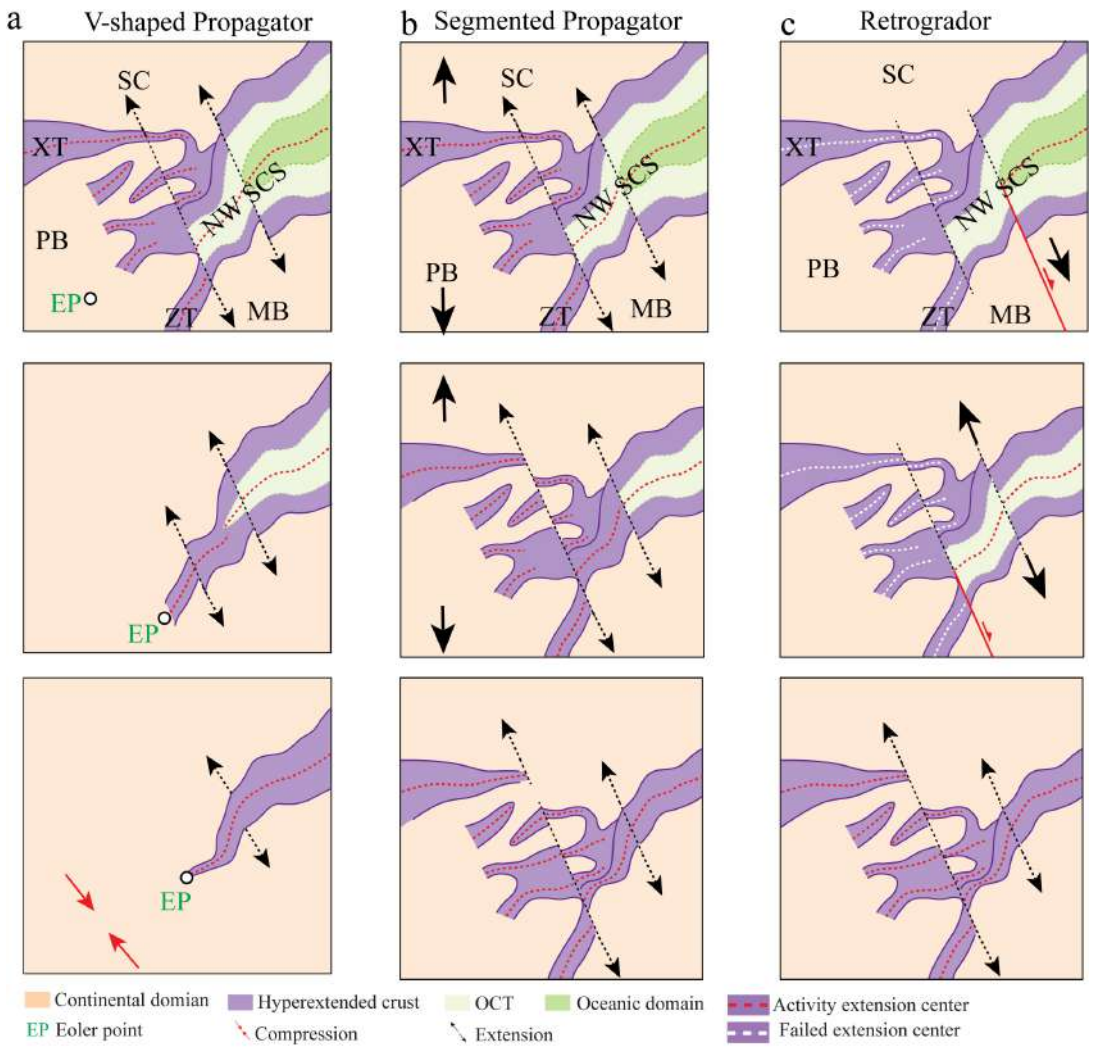

Figure IV.14. *Three kinematic models for the NW SCS. (a) A simple V-shaped propagation without extensional structures ahead of the tip, and compression ahead of the propagator. (b) Rift propagation model whith widespread hyperextension that occurs simultaneous to the propagation of the oceanic system. (c) The retrograder model in which the ocean is not propagating into an active rift system, but the whole active rift system is stepping back while breakup occurs.*

6.3. Propagating vs retrograding: a new kinematic model for the NW SCS

In Fig. IV.14 we show three kinematic models for the NW SCS. Note that the final stage is the same for all three models and represents the present-day situation as shown in our rift domain map (Fig. IV.9b). Models shown in Figs. IV.14a and IV.14b are both propagator models. The first one (Fig. IV.14a) is showing a simple V-shaped propagation

without extensional structures ahead of the tip. Such a model would assume that the domain in front of the propagator would be in compression (Martin, 1984). Le Pourhiet et al. (2018) and Luo et al. (2021) showed that such a model in not realistic for the SCS. In Fig. IV.14b, we show a model in which widespread hyperextension is occurring simultaneous to the propagation of the oceanic system. This model is similar to what has been initially proposed by Vink (1982) and proposed for the Woodlark Basin (Taylor et al., 1995) and the southern N-Atlantic (Nierrengarten et al., 2018). It is also in line with what Luo et al. (2021) proposed for the SW SCS and the model of Le Pourhiet et al. (2018) and Jourdon et al. (2020). This model is, however, not compatible with the observations we made in the study area. Therefore, we propose an alternative model that we refer to as *retrogrador*. In such a model the ocean is not prograding into an active rift system, but the whole active rift system is stepping back while breakup occurs. Thus, cessation of rifting and seafloor spreading in the NW SCS is not due to a stalling of the spreading system but due to its re-organization. This may be fundamentally different for the SW SCS that represents a stalling oceanic spreading system (e.g., Luo et al., 2021; Le Pourhiet et al. (2018).

The new model (Fig. IV.14c) has major implications for the interpretation of the whole NW SCS at a regional scale, since it not only requires reassessing the ages of rifting and the way the rift systems are stacking in time and space, but also to determine and compare the amount of accommodated extension across sections parallel to the extensional direction through time. It also leads to the question of how and where the back stepping of the rift and spreading system is accommodated, since it asks for transfer zones at the termination of an active segment. Such transfer zones are difficult to determine. One possibility is that the OCT at the tip of the NW SCS acted as decoupling zone between the hyperextended systems in the west (e.g., Xisha Trough) and the oceanic domain in the rear. More research needs to be done to test this hypothesis.

The new model has, however, also more fundamental implications on how plate boundaries are forming and ask to distinguish between stalling and reorganization of

spreading systems, which imply different geodynamic consequences. Last but not least, it leads to the question if plate boundary formation (i.e., breakup) is controlled by tectonic extension or by magmatic processes. In the example of the SCS the stalling of the breakup has been explained by gravitational forces (Le Pourhiet et al., 2018) or due to the occurrence of stronger arc related rocks (Li et al. 2018). In both cases failure of breakup would have a tectonic origin. However, both hypotheses are conflicting with the observation that the zone ahead of the oceanic crust was dissected by hyperextended basins, suggesting that the strengths/forces were not an obstacle for rifting. An alternative interpretation could be that when the spreading system entered into the former magmatic-arc region with a depleted mantle, magma production was not sufficient to keep seafloor spreading going. A similar interpretation has been proposed to explain magma-poor breakup in the southern N-Atlantic, where it appears that inherited arc settings are not favorable for breakup, leading to V-shaped basins (e.g., Rockall, Porcupine, Orphan; Chenin et al., 2018). This interpretation would also explain why the only rift basin in the SCS from where mantle exhumation has been proven, exemplifying magma-poor rifting, is the Phu Khanh Basin (Savva et al., 2014) that formed over a former arc domain.

7. Conclusion

Access to a high-resolution reflection seismic dataset from the tip of the NW SCS enabled us to define and map rift domains and, by comparing them with refraction seismic, magnetic and gravity field data, to define the crustal structure of the OCT. We also analyzed and defined two sedimentary sequences, a first one (S_A) deposited during hyperextension and a second one (S_B) during breakup. These two sequences, floored by Tb and topped by Bi, the latter defined as the breakup interface and dating lithospheric breakup, have been mapped across the tip of the NW SCS. The combination of the rift domain map with the time constraints obtained from the distribution of S_A and S_B enabled us to discuss the 3D structural and crustal variability, to investigate the extensional and magmatic processes interacting during breakup, and to propose a kinematic evolution for

the NW SCS. The results of this study provide a well-documented example of the spatial and temporal evolution of a rift system during breakup and shows that the V-shaped NW SCS may not be the result of a stalling oceanic propagator but be explained by the retrogradation and reorganization of a rift system. Whether the observed evolution can be linked to the inherited arc setting and related depleted mantle preventing magmatic breakup needs to be evaluated by future work.

References

Briais, A., Patriat, P., & Tapponnier, P. (1993). Updated interpretation of magnetic anomalies and seafloor spreading stages in the south China Sea: Implications for the Tertiary tectonics of Southeast Asia. *Journal of Geophysical Research: Solid Earth*, *98*(B4), 6299–6328. https://doi.org/10.1029/92JB02280

Cameselle, A. L., Ranero, C. R., Franke, D., & Barckhausen, U. (2017). The continent-ocean transition on the northwestern South China Sea. *Basin Research*, *29*, 73–95. https://doi.org/10.1111/bre.12137

Cameselle, A. L., Ranero, C. R., & Barckhausen, U. (2020). Understanding the 3D Formation of a Wide Rift: The Central South China Sea Rift System. *Tectonics*, *39*(12). https://doi.org/10.1029/2019TC006040

Chen, H., Stow, D. A. V., Xie, X., Ren, J., Mao, K., Gao, Y., et al. (2021). Depositional architecture and evolution of basin-floor fan systems since the Late Miocene in the Northwest Sub-Basin, South China Sea. *Marine and Petroleum Geology*, *126*, 104803. https://doi.org/10.1016/j.marpetgeo.2020.104803

Ding, W., Schnabel, M., Franke, D., Aiguo, R., & Zhenli, W. (2012). Crustal Structure across the Northwestern Margin of South China Sea: Evidence for Magma-poor Rifting from a Wide-angle Seismic Profile. *Acta Geologica Sinica - English Edition*, *86*(4), 854–866. https://doi.org/10.1111/j.1755-6724.2012.00711.x

Ding, W., Sun, Z., Mohn, G., Nirrengarten, M., Tugend, J., Manatschal, G., & Li, J. (2020). Lateral evolution of the rift-to-drift transition in the South China Sea: Evidence from multi-channel seismic data and IODP Expeditions 367&368 drilling results. *Earth and Planetary Science Letters*, *531*, 115932. https://doi.org/10.1016/j.epsl.2019.115932

Franke, D., Savva, D., Pubellier, M., Steuer, S., Mouly, B., Auxietre, J.-L., et al. (2014). The final rifting evolution in the South China Sea. *Marine and Petroleum Geology*, *58*, 704–720. https://doi.org/10.1016/j.marpetgeo.2013.11.020

Gao, J., Wu, S., McIntosh, K., Mi, L., Liu, Z., & Spence, G. (2016). Crustal structure and extension mode in the northwestern margin of the South China Sea: CRUSTAL EXTENSION OF THE SOUTH CHINA SEA. *Geochemistry, Geophysics, Geosystems*, *17*(6), 2143–2167. https://doi.org/10.1002/2016GC006247

Gee, J. S., & Kent, D. V. (2007). Source of oceanic magnetic anomalies and the geomagnetic polarity time scale, 455–507. https://doi.org/10.7916/D8DV1V8P

Gozzard, S., Kusznir, N., Franke, D., Cullen, A., Reemst, P., & Henstra, G. (2019). South China Sea crustal thickness and oceanic lithosphere distribution from satellite gravity inversion. *Petroleum Geoscience*, *25*(1), 112–128. https://doi.org/10.1144/petgeo2016-162

Jourdon, A., Le Pourhiet, L., Mouthereau, F., & May, D. (2020). Modes of Propagation of Continental Breakup and Associated Oblique Rift Structures. *Journal of Geophysical Research: Solid Earth*, *125*(9). https://doi.org/10.1029/2020JB019906

Larsen, H. C., Mohn, G., Nirrengarten, M., Sun, Z., Stock, J., Jian, Z., et al. (2018). Rapid transition from continental breakup to igneous oceanic crust in the South China Sea. *Nature Geoscience*, *11*(10), 782–789. https://doi.org/10.1038/s41561-018-0198-1

Le Pourhiet, L., Chamot-Rooke, N., Delescluse, M., May, D. A., Watremez, L., & Pubellier, M. (2018). Continental break-up of the South China Sea stalled by far-field compression. *Nature Geoscience*, *11*(8), 605–609. https://doi.org/10.1038/s41561-018-0178-5

Li, C., & Song, T. (2012). Magnetic recording of the Cenozoic oceanic crustal accretion and evolution of the South China Sea basin. *Chinese Science Bulletin*, *57*(24), 3165–3181. https://doi.org/10.1007/s11434-012-5063-9

Li et al. - 2021 - Crustal structure beneath the Zhongsha Block and t.pdf. (n.d.).

Li, Y., Huang, H., Grevemeyer, I., Qiu, X., Zhang, H., & Wang, Q. (2021). Crustal structure beneath the Zhongsha Block and the adjacent abyssal basins, South China Sea: New insights into rifting and initiation of seafloor spreading. *Gondwana Research*, S1342937X2100188X. https://doi.org/10.1016/j.gr.2021.06.015

Ligi, M., Bonatti, E., Bosworth, W., Cai, Y., Cipriani, A., Palmiotto, C., et al. (2018). Birth of an ocean in the Red Sea: Oceanic-type basaltic melt intrusions precede continental rupture. *Gondwana Research*, *54*, 150–160. https://doi.org/10.1016/j.gr.2017.11.002

Lizarralde, D., Axen, G. J., Brown, H. E., Fletcher, J. M., González-Fernández, A., Harding, A. J., et al. (2007). Variation in styles of rifting in the Gulf of California. *Nature*, *448*(7152), 466–469. https://doi.org/10.1038/nature06035

Luo, P., Manatschal, G., Ren, J., Zhao, Z., Wang, H., & Tong, D. (2021). Tectono - Magmatic and stratigraphic evolution of final rifting and breakup: Evidence from the tip of the southwestern propagator in the south China sea. *Marine and Petroleum Geology*, *129*, 105079. https://doi.org/10.1016/j.marpetgeo.2021.105079

Neuharth, D., Brune, S., Glerum, A., Heine, C., & Welford, J. K. (2021). Formation of Continental Microplates Through Rift Linkage: Numerical Modeling and Its Application to the Flemish Cap and Sao Paulo Plateau. *Geochemistry, Geophysics, Geosystems*, *22*(4). https://doi.org/10.1029/2020GC009615

Nirrengarten, M., Manatschal, G., Tugend, J., Kusznir, N., & Sauter, D. (2018). Kinematic Evolution of the Southern North Atlantic: Implications for the Formation of Hyperextended Rift Systems. *Tectonics*, *37*(1), 89–118. https://doi.org/10.1002/2017TC004495

Nirrengarten, M., Mohn, G., Kusznir, N. J., Sapin, F., Despinois, F., Pubellier, M., et al. (2020). Extension modes and breakup processes of the southeast China-Northwest Palawan conjugate rifted margins. *Marine and Petroleum Geology*, *113*, 104123. https://doi.org/10.1016/j.marpetgeo.2019.104123

Nonn, C., Leroy, S., Lescanne, M., & Castilla, R. (2019). Central Gulf of Aden conjugate margins (Yemen-Somalia): Tectono-sedimentary and magmatism evolution in hybrid-type margins. *Marine and Petroleum Geology*, *105*, 100–123. https://doi.org/10.1016/j.marpetgeo.2018.11.053

Peron-Pinvidic, G., & Osmundsen, P. T. (2016). Architecture of the distal and outer domains of the Mid-Norwegian rifted margin: Insights from the Rån-Gjallar ridges system. *Marine and Petroleum Geology*, *77*, 280–299. https://doi.org/10.1016/j.marpetgeo.2016.06.014

Savva, D., Pubellier, M., Franke, D., Chamot-Rooke, N., Meresse, F., Steuer, S., & Auxietre, J. L. (2014). Different expressions of rifting on the South China Sea margins. *Marine and Petroleum Geology*, *58*, 579–598. https://doi.org/10.1016/j.marpetgeo.2014.05.023

Sutra, E., & Manatschal, G. (2012). How does the continental crust thin in a hyperextended rifted margin? Insights from the Iberia margin. *Geology*, *40*(2), 139–142. https://doi.org/10.1130/G32786.1

Taylor, B., Goodliffe, A., & Martinez, F. (2009). Initiation of transform faults at rifted continental margins. *Comptes Rendus Geoscience*, *341*(5), 428–438. https://doi.org/10.1016/j.crte.2008.08.010

Tugend, J., Manatschal, G., Kusznir, N. J., Masini, E., Mohn, G., & Thinon, I. (2014). Formation and deformation of hyperextended rift systems: Insights from rift domain mapping in the Bay of Biscay-Pyrenees. *Tectonics*, *33*(7), 1239–1276. https://doi.org/10.1002/2014TC003529

Vink, G. E. (1982). Continental rifting and the implications for plate tectonic reconstructions. *Journal of Geophysical Research: Solid Earth*, *87*(B13), 10677–10688. https://doi.org/10.1029/JB087iB13p10677

Wang, Q., Zhao, M., Zhang, H., Zhang, J., He, E., Yuan, Y., & Qiu, X. (2020). Crustal velocity structure of the Northwest Sub-basin of the South China Sea based on seismic data reprocessing. *Science China Earth Sciences*. https://doi.org/10.1007/s11430-020-9654-4

Warner, M. R. (1987). Seismic reflections from the Moho -- the effect of isostasy. *Geophysical Journal International*, *88*(2), 425–435. https://doi.org/10.1111/j.1365-246X.1987.tb06651.x

Wu, Z., Li, J., Ruan, A., Lou, H., Ding, W., Niu, X., & Li, X. (2012). Crustal structure of the northwestern sub-basin, South China Sea: Results from a wide-angle seismic experiment. *Science China Earth Sciences*, *55*(1), 159–172. https://doi.org/10.1007/s11430-011-4324-9

Xie, X., Ren, J., Pang, X., Lei, C., & Chen, H. (2019). Stratigraphic architectures and associated unconformities of Pearl River Mouth basin during rifting and lithospheric breakup of the South China Sea. *Marine Geophysical Research*. https://doi.org/10.1007/s11001-019-09378-6

Zhang, C., Sun, Z., Manatschal, G., Pang, X., Li, S., Sauter, D., et al. (2021). Ocean-continent transition architecture and breakup mechanism at the mid-northern South China Sea. *Earth-Science Reviews*, *217*, 103620. https://doi.org/10.1016/j.earscirev.2021.103620

Zhang, T., Gao, J. Y., Li, J. B., Wu, Z. C., Wu, Z. L., Zhao, L. H., et al. (2012). The magnetic lineation identifications and segmentations of the northwestern sub-basin in the South China Sea[in Chinese with English abstract]. *Chinese J. Geophys.-Chinese. Ed*, 55(9), 3163-3172. https://doi.org/10.6038/j.issn.0001-5733.2012.09.034

CHAPTER V

Discussion

The main goal of my PhD project was to focus on the tectono-stratigraphic and magmatic architecture and evolution at the tip of the NW SCS propagator, with the aim to understand how continents rift and breakup, and how new oceanic crust forms. To understand the complete rift evolution, I explored how the tectono-magmatic evolution is recorded in the stratigraphic tape recorder, i.e., to learn to observe, describe and interpret reflection seismic sections. Since the subject was too broad, I had to focus my research to few overarching questions that finally guided my work and built the foundation of chapters II to IV that have been written as scientific papers. However, the short format of scientific papers allowed to present only a small fraction of the total seismic interpretation on which my work is built on. During my PhD, I analyzed a complete survey of 5000 km length covering an area of 35'000 km^2 (for additional examples of seismic interpretations see annexes). I subdivided my study in three steps. First, I investigated the tectono-stratigraphic record of the conjugate NW SCS margins, kinematically restored extensional structures to an initial (pre-rift) stage, and linked them to together by synthesizing them in a Wheeler diagram. Second, I focused on the description of the NW SCS OCT by analyzing seismic sections imaging the evolution from continental to lithospheric breakup. A main challenge was to describe the tectono-magmatic evolution during breakup and to link it to the syn-breakup stratigraphic record. Third and lastly, I focused on the 3D evolution of rifting and breakup propagation at the tip of the NW SCS oceanic propagator. In the following, I will discuss, based on the main questions defined in the introduction and the results presented in chapters II to IV, how my work complements to the existing work in the NW SCS. Then I will discuss possible new outcomes and implications of my work for

the understanding of rifting, breakup and early seafloor spreading in the NW SCS and how the new observations I made may change existing thinking on rifting/rifted margins in general and allow to formulate new questions for future research.

1. The syn-rift mega-sequence and its link to the tectono-magmatic evolution in a polyphase rift system: how to define, describe and interpret?

What was done before?

Seismic reflection and refraction data and interpretations from the NW-SCS have been published in numerous papers in the last few years. The studies of Ding et al., (2011), Franke et al., (2014) and more recently also Cameselle et al. (2017, 2021) and Wu et al., (2019) focused mainly on the crustal structure and/or structural evolution of the NW SCS. By describing the structure and evolution of the distal margin of the N SCS, they provided, together with the studies of Yang et al. (2018), Deng et al. (2019) and Zhang et al. (2020), a good template for the overall crustal structure of the N and NW SCS distal margin. These studies provided insights into the structural evolution during the NW SCS rifting and discussed the rheological and tectono-magmatic evolution, showing similarities and differences to the classical Atlantic-type rifted margins. The discovery of a dome structure (Deng et al., 2020) and related magmatic additions (Zhang et al., 2020) show, however, that the distal margins is complex and that new studies are necessary to understand how these complex structures and magmatic additions can be linked to the stratigraphic evolution. So far, only few studies concentrated on the analysis of the syn-rift stratigraphic architectures and their link to fault geometries and magmatic additions, while most recent studies in the NW SCS investigated essentially the post-rift sequence. For instance, Chen et al. (2021) focused on the depositional architecture and evolution of Late Miocene basin-floor fan systems. Liang et al. (2020) studied sediment dispersal patterns in the deep-water Central Canyon, and Wang et al. (2020) studied middle Miocene sedimentation rates based on the information from deep-see drilling cores and seismic

data. Studies on the syn-rift evolution have been published by Zhang et al., (2019; 2020) and Sun et al., (2019b). They defined the syn-rift stratigraphic and magmatic evolution of the central N-SCS margin based on IODP drilling results. Xie et al. (2019) used a modern approach to propose correlations between the proximal and distal margins in the N-SCS. Based on the description of the stratigraphic architecture and associated unconformities within the syn-rift sequence, they proposed correlations between proximal and distal parts of the margin. These authors also showed that the syn-rift sedimentary packages are polyphase and are dominated by high-angle normal faults in proximal margin, while in the necking and distal domains three types of stratigraphic architectures can be found; small half-graben, sub-basins floored by large-scale detachment and small sags. Luo et al. (2021) analyzed the syn-rift sedimentary sequence at the tip of the SW SCS propagator and showed that the syn-rift sequence is diachronous and can be subdivided into three system tracts, each one including syn- and post-tectonic packages. However, this study was only based on sparse seismic data with a data quality that is much lower than that available for the NW SCS.

Main results from this study

In my study I undertook a careful analysis of the syn-rift mega-sequence, taking advantage of the high-quality reflection seismic sections located at the tip of the NW SCS propagator. I chose the example of the CGN-1 section, one of the rare seismic lines imaging the complete tectono-stratigraphic and magmatic architecture of a pair of conjugate rifted margins, to illustrate the 2D syn-rift sedimentary evolution that I studied in 3D. In this line, I identified and described necking zones and related faults, defined a residual H block (H_r) at the northern margin and a delaminated H block (H_d) at the southern margin (see Haupert et al. 2016 for definition and characterization of the residual vs delaminated keystones), and defined the transition to first proto-oceanic crust (Fig. V.1e). I interpreted the faults responsible for crustal thinning (necking faults (F_n) bounding the H Block, and the faults responsible for its delamination and crustal separation (hyperextension faults (F_h)). I also determined the location of coupling point (CP: location

where complete embrittlement of the crust occurs) and that of the separation point (SP: oceanward termination of the continental crust). I defined a generic top basement (Tb), which I further characterized by distinguishing between a stratigraphic top basement (Tb_s) corresponding to the top pre-rift Tg stratigraphic level, a tectonic top basement (Tb_t) corresponding to exhumed fault surfaces, and a magmatic to basement (Tb_m) in the OCT and over the oceanic domain. This structural interpretation enabled me to perform a sequential kinematic restoration of the section, relying on a systematic methodology that allowed to quantify the amount of extension and associated strain rates (for details see chapter II). The restoration shown in Fig. V.1 combines an areal-conservative restoration of crustal surface with a length-conservative restoration of the initial (pre-rift) stratigraphic layer Tbs, both of which are independent. This restoration approach, which is new and has been developed in my PhD, enabled me to restore the section back in time with some confidence, which is a prerequisite to investigate the syn-rift mega-sequence across a conjugate rifted margin.

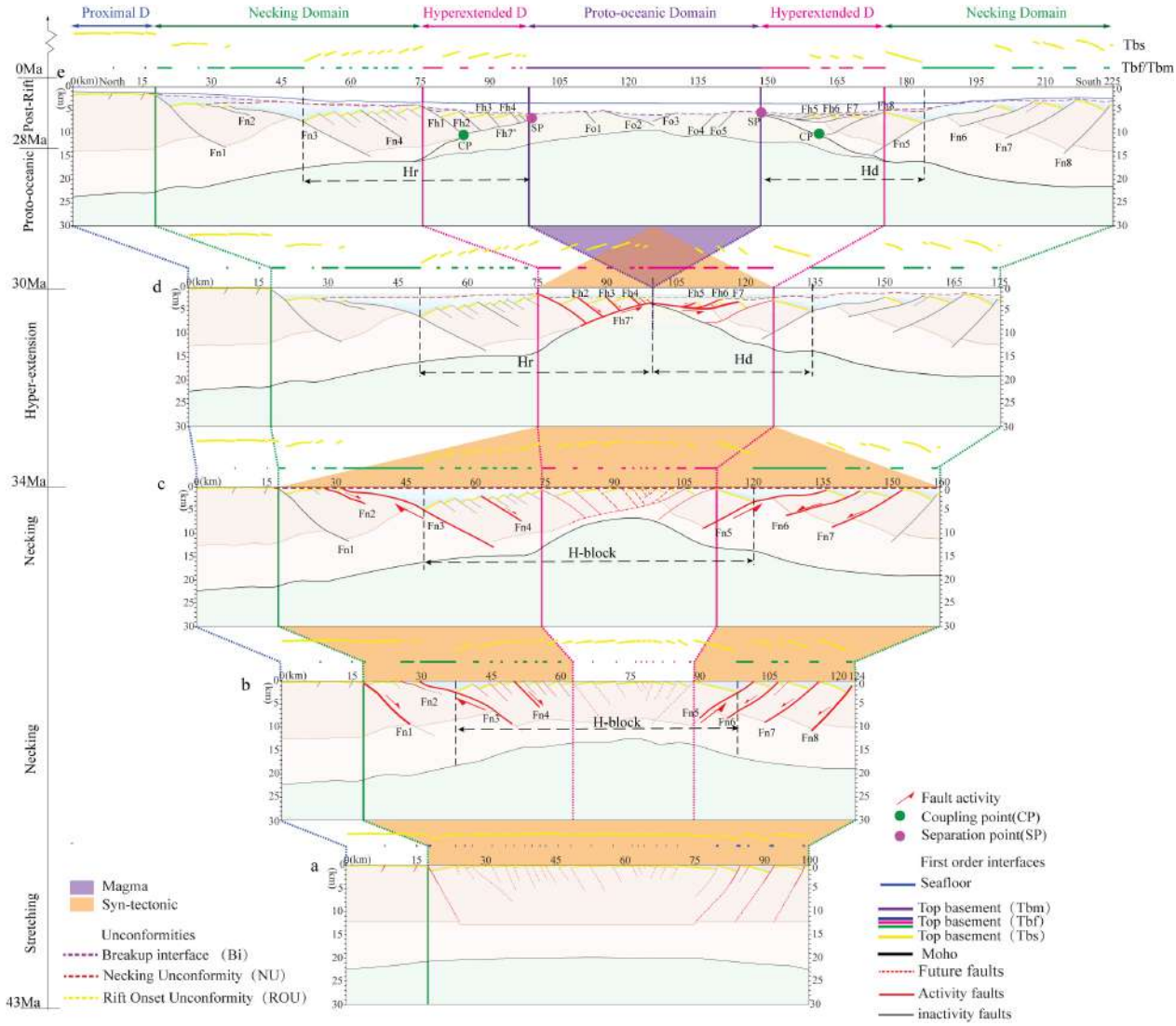

Figure V.1. *Strain localization and individualization and dismembering of the H-block and formation of new real estate (new Tb) by exhumation of basement along faults (Tbf) or magmatic crust (Tbm) as a function of rift evolution. (a) Initial stretching stage with distributed deformation and dominated by Tbs. (b) Onset of necking and individualization of an H-block. (c) Onset of dismembering of the H-block. (d) Hyperextension and creation of exhumation faults (Tbf). (e) Magmatic accretion (Tbm) and onset of seafloor spreading.*

In a second step, and in order to introduce time in the restoration, I defined two mega-sequences, a syn- and a post-rift mega-sequence sensu Hubbard (1988). I subdivided the syn-rift mega-sequence in five system tracts. A system tract, as used in my study, encompasses all the sediments deposited during a given period. In addition, I also defined 4 magmatic units. Based on the identification and characterization of the defined system

tracts, of distinctive stratal packages and of crustal architectures, I was able to propose a qualitative and quantitative description of the NW SCS rifting evolution, including the two critical rift phases, which are the necking phase (Figs. V.1b and V.1c) and the hyperextension phase (Fig. V.1d). The complete evolution of rifting observed in the CGN-1 section is described in a Wheeler Diagram (Fig. V.2) that illustrates the complete tectono-stratigraphic and magmatic evolution recorded in the syn-rift mega-sequence. I was also able to reproduce restored maps showing the distribution of type of top basement, syn- and post-rift sediments, active and inactive faults, and magma through time (Fig. V.3). These results enabled me to show the formation of a keystone during crustal necking (see H-Block in Fig. V.1). The H-Block is bounded on both sides by active faults (Fig. V.3c) that are overlain by syn-tectonic sediments (Fig. V.3d) deposited in the necking domain (Fig. V.3b). At the stage of crustal coupling (Fig. V.1d), active faults start to localize and separate the H-Block in a residual (Hr) and delaminated (Hd) block, forming asymmetric upper- and lower plate margins (Fig. V.1d). At this stage the syn-tectonic sequence starts to focus into the future area of breakup and the rest of the margin is affected by post-tectonic sedimentation (Fig. V.3d) and magma starts to form, resulting in continental separation (Fig. V.1e).

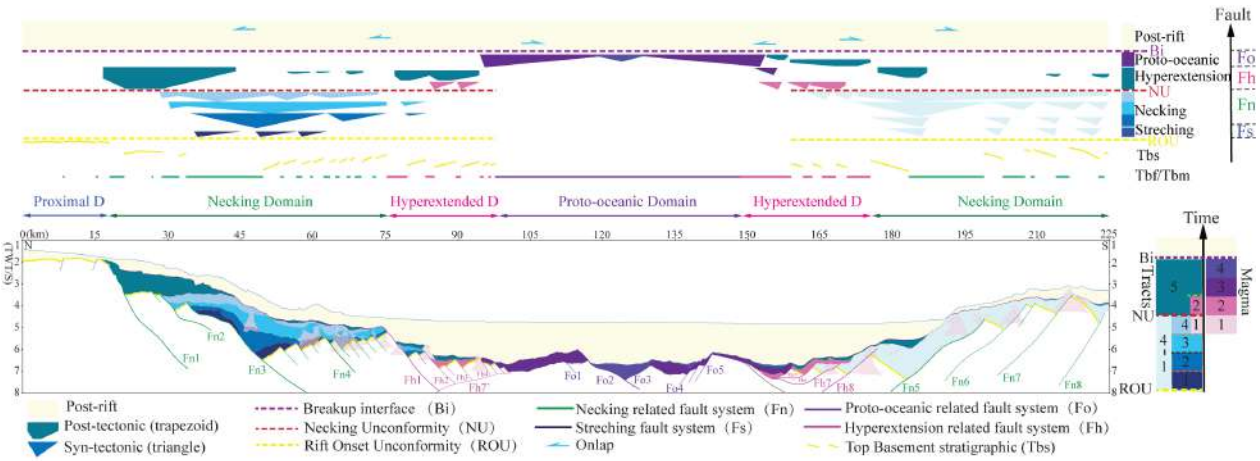

Figure V.2. *Final rift architecture showing the distribution of tracts (T1 to T5), magmatic units (1 to 4) and different fault generations (Fn, Fh, Fo) in a section and a simple Wheeler diagram showing the distribution of depocenters during the formation of the conjugate rifted margins.*

The results presented in this study and illustrated in Fig. V.2 challenge previous interpretations of the syn-rift mega sequence. Indeed in this study, I introduce correlative surfaces that bound system tracks, I distinguish between syn-rift and syn-tectonic and I include different types of top basement. This new approach leads to new interpretations for the tectono-stratigraphic and magmatic evolution of the NW SCS and has the potential to be used to analyse, quantify and correlate, both in time and space, events recorded in seismic sections. I provide a visual synthesis of these conclusions in the Wheeler diagram shown in Fig. V.2. More generally, this new approach enables to better understand when, where and how accommodation space is created and show that specific domains of rifted margins are associated with: (1) specific periods of tectonic activity; (2) a proper style of deformation associated with specific tectono-stratigraphic architectures; (3) particular ratios of horizontal vs vertical accommodation space creation; and (4) specific depositional environments.

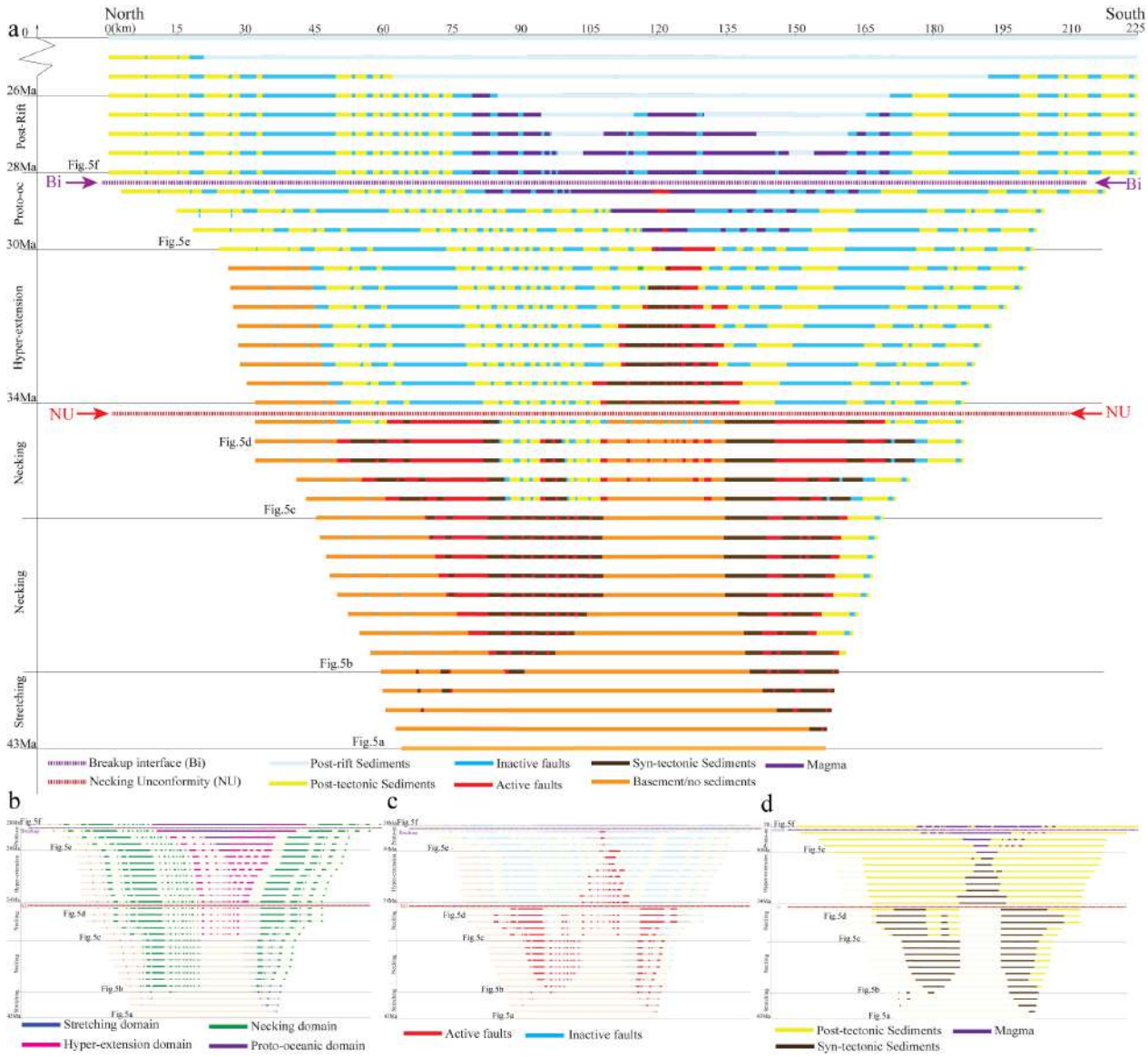

Figure V.3. *Temporal and spatial evolution of rifting shown in a map view. The figure shows, in time steps of 0.5 Myr, a top view of the restored evolution of rifting presented in Fig. V.5 (see also Fig. II.10 for evolution of faults and rift domains). Each bar represents a snapshot of the surface during the rift evolution. (a) Representation of type of sediments (no deposition or erosion; syn- or post-tectonic packages in the syn-rift mega-sequence, magma, and active or inactive faults. (b) Formation of rift domains during rifting. (c) Distribution of active and inactive faults during rifting. (d) Distribution of syn- and post-tectonic packages and magmatic additions belonging to the syn-rift mega-sequence.*

Remaining questions

Due to the lack of direct drill holes in the study area, the main next step is to validate the results by drilling. Undeniably, the NW SCS is among the best places to calibrate tectono-stratigraphic models of rifting and breakup and to validate and calibrate these models. Among the main questions that remain to be explored are the nature of unconformities, their correlatability and the processes that are at their origin. It remains, for instance unclear how to define the rift onset unconformity. In most sections I inspected in my work, the base of the *syn-rift section* is formed by an unconformity, however its age remains unknown. The basal contact is typically well defined and corresponds to either the top of tilted blocks, or to the base of wedge-shaped syn-rift sedimentary infill. Erosional truncations resulting in an angular unconformity occasionally occur beneath that horizon, indicating that it was formed by an erosional phase. Thin-layered successions between the top of the pre-rift unit and the seismically transparent basement can sporadically be observed, indicating pre-rift sedimentary strata. However, it remains difficult to define the age of these sequences and consequently, it remains unclear of how to interpret the early stages of rifting.

Another open question is how to define the unconformities within the syn-rift mega-sequence, how to use them to correlate sequences across the margin, and how to define the processes controlling their formation? Are they related to the necking event as suggested by Chenin et al. subm)? It the case, they would represent isochronous surfaces that could be used to make correlations across the whole margin.

A last, but not least important question related to unconformities is if breakup is recorded in the stratigraphic tape recorder, as suggested by Falvey (1974). He stated that breakup is recorded by a so-called *« breakup unconformity »*. Possible answers to this question can be found in the next section that addresses more specifically the problems related to the record of breakup.

It is also interesting to note that unconformities are well known from the Qiongdongnan Basin (Xie et al., 2006), and from other basins that are located more proximal. Future studies are necessary to analyze these unconformities, to define their age, and to see if they can be linked with unconformities in the more distal parts of the margin. This would, however, request a drilling campaign, which would also allow to determine the origin of these unconformities and to link them with the observed and restored tectonic processes.

2. From crustal separation to onset of seafloor spreading: how to define breakup?

What was done before?

In no other place on Earth so much effort has been spent to investigate the formation of a new plate boundary and the creation of first oceanic crust as in the SCS. Three IODP Legs have been dedicated to find answers to how continental plates break and seafloor spreading initiates. IODP Legs 1499, 1500, 1502, 1503 drilled the OCT and first oceanic crust and this area is the only one, apart from the Iberia-Newfoundland margins, where the OCT is so well calibrated. The results of the IODP campaigns, combined with an excellent seismic dataset, enabled to investigate and better understand the breakup processes and to get access to rocks of the OCT transition (for a review see Zhang et al., 2021). While the drilling proposals predicted exhumed mantle, inspired by the successful Iberia model, none of the IODP drill holes penetrated the expected serpentinized mantle but penetrated only basalts. Therefore, it was concluded that breakup was sharp and the OCT localized in a narrow transition zone, between unequivocal continental and oceanic crusts (Ding et al., 2019, Larsen et al., 2018, Nirregarten et al., 2020; Deng et al., 2020, Sun et al., 2019, Wang et al., 2019). However, these studies did not specify the crustal structure of the OCT and the related syn-breakup sedimentary evolution. More recently, Zhang et al. (2021) provided a detailed description of the nature of the OCT in the central N-SCS, located approximately 200 km east of my study site. These authors described the structural

architecture and discussed the mechanisms responsible for continental breakup. Their main conclusions were that breakup structures are complex, show a strong along strike variability, include core complex structures that are intimately associated with magmatic additions, and that the latter may be responsible for the final lithospheric breakup. Ding et al. (2019) proposed that magma triggers a sharp continental breakup following and superimposing a wide continental rift (Deng et al., 2020; Zhang et al., 2020). Luo et al. (2021), working in the SW SCS propagator, provided evidence for a very abrupt transition between detachment faulting and magma-induced breakup. All these recent studies show that there are some similarities and differences among the SCS OCTs, where the relative timing between magmatic activity and extension during breakup leads to lateral changes that can be in the order of tens of kilometers (Zhang et al., 2021).

Main results from this study

Previous studies in the SCS showed that the breakup process is complex and occurs within an OCT that separates unequivocal continental and oceanic crusts. In the second part of my PhD, I analyzed this transitional domain with the aim to describe the crustal architecture of this transition and the related syn-breakup sedimentary sequence, with the aim to better understand the nature of the processes operating between crustal and lithospheric breakup. Like for the rest of the PhD, I used the high-quality seismic data that image the OCT at the tip of the NW South China Sea (SCS) propagator. Three points make the study area exceptional: 1) the high quality and dense reflection seismic data set and the occurrence of refraction seismic sections at the tip of the oceanic propagator allow to image the conjugate system and characterize the nature of the crust; 2) the high sedimentation rates that provide an excellent record of the syn-breakup tectono-magmatic evolution; and 3) the vicinity to the IODP drill sites that enable to provide additional information on the observed sequences. To enable correlations with IODP drill sites, I extended my study area into the location where IODP drilled several sites. Following a similar workflow like in part 1 of my PhD, I defined nature of the crust (continental, hybrid or oceanic), the limits of the OCT, and their relationships with the overlying syn-breakup

sedimentary sequence (Fig. V.4). My aim was to reconstruct the tectono-magmatic and sedimentary evolution during the breakup phase, i.e. from the onset of crustal separation (crustal breakup) to the onset of seafloor spreading (lithospheric breakup) (Fig. V.5).

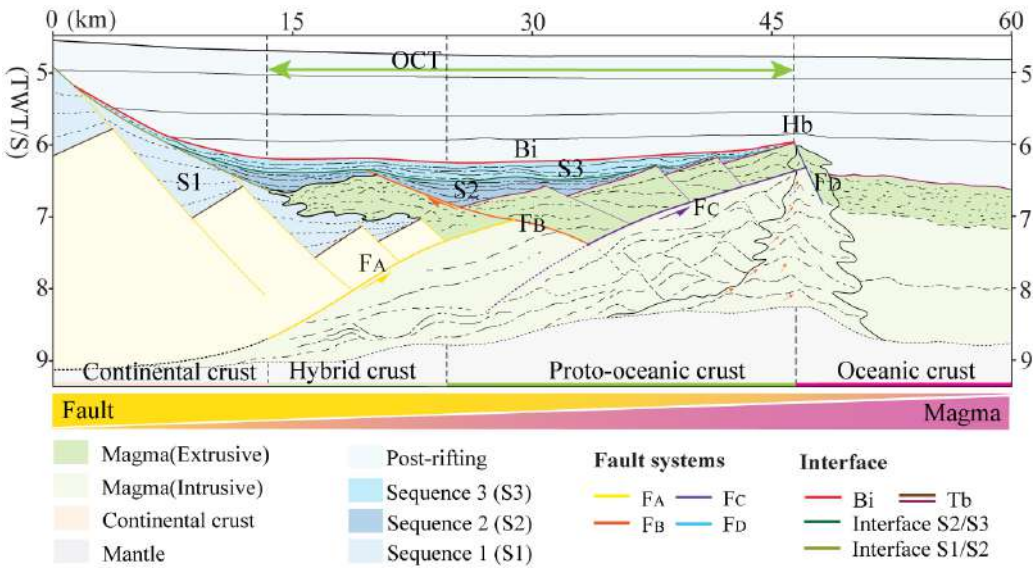

Figure V.4. *Cartoon showing a schematic representation of the nature and characteristic structures of the crust in the OCT and their link to the sedimentary sequences and magmatic additions. The section summarizes the main observations described from sections CGN-1,2,3 and 1555.*

The results of my study show that the NW SCS OCT displays a transition from fault-dominated rifting to magma-controlled seafloor spreading both in space (Fig. V.4) and time (Fig. V.5). On its continent-ward side, the OCT is made of hybrid crust where extensional thinning of the crust is compensated by syn-extensional magmatic addition. Oceanward, a fully magmatic but fault-dominated proto-oceanic crust can be identified and exhibits a sharp contact to a mature/Penrose-type oceanic crust. The fault systems in the OCT are difficult to identify based solely on seismic observations but can be deciphered based on their relationships with the syn-breakup sedimentary sequence and syn-tectonic magmatic additions, both of which display growth structures. Relying on this tectono-magmatic tape recorder where the sedimentary sequences (S1 to S3) are linked to the sequence of faults (F_A to F_D) and the emplacement of magmatic bodies, I propose a kinematic restoration of

the breakup phase (Fig. V.5). The transition from final rifting to seafloor spreading is best explained by out-of-sequence, flip-flop detachment faults showing a progressive decrease in fault heaves. According to the seismic observations and restoration of the OCT, the breakup process can be best explained as a transition from fault-dominated rifting to magma-controlled seafloor spreading. In this framework, the continent-ward side of the OCT is made of *hybrid crust*, while its oceanward side is made of fully magmatic but fault-dominated *proto-oceanic crust.* This proto-oceanic crust finally turns into a mature/*Penrose-type oceanic crust*, marking the start of the true oceanic domain. The results of my PhD show that breakup is not an event but a lasting phase that starts with crustal separation, referred to as crustal breakup, and ends with the onset of steady-state seafloor spreading, referred to as lithospheric breakup.

Remaining questions

In my study, I rely on the growth structures of the syn-breakup sedimentary and magmatic sequences to propose a kinematic restoration. However, the way the magmatic additions form and interact with faulting process remains interpretative and is not validated by drilling results in the SCS. The process of underplating shown in Fig. V.5 and its link to detachment faulting needs to be further investigated. So-called magmatic growth has been suggested by Zhang et al. (2021) from the N SCS. Based on field observations and petrological investigations in the Alps, Manatschal et al. (2011) and Tribuzio et al. (2020) proposed that gabbros were underplated in the footwall of an active detachment fault and were exhumed to the seafloor. IODP Hole U1309 recovered gabbroic material from the footwall of a detachment fault drilled at the Atlantis Massif oceanic core complex (Blackman et al., 2006), and the paleomagnetic data indicate that a back-rotation of the footwall may have occurred (Morris et al., 2009; Blackman et al., 2011), consistent with a rolling hinge model and flexural rotation (Buck, 1988) proposed in Fig. V.5. It would be interesting to drill deeper into the magmatic crust in order to test this concept.

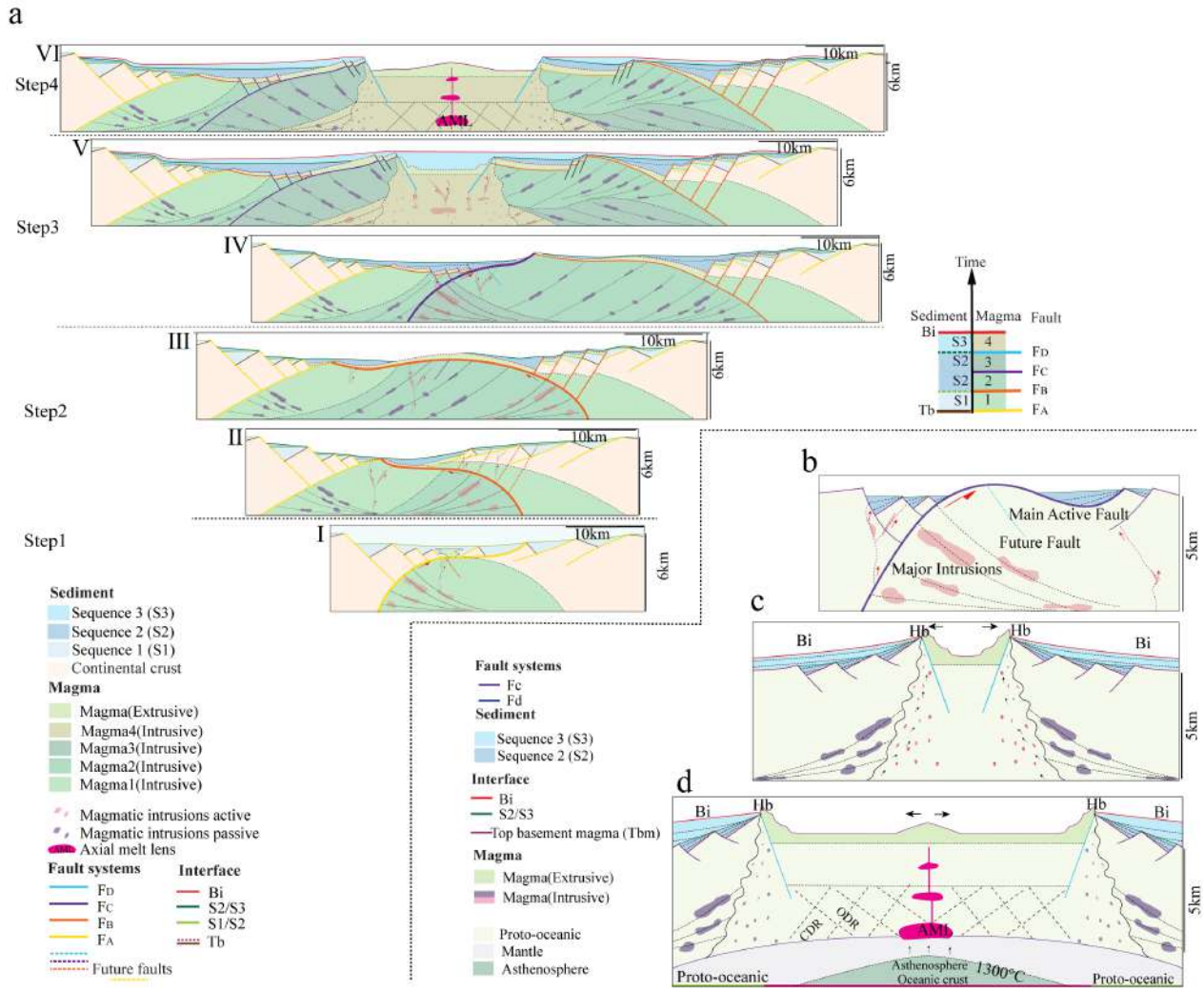

Figure V.5. *Kinematic restoration of the OCT crustal structure and sedimentary architecture from the moment of lithospheric breakup back to the moment of crustal separation (breakup). (a) Evolution steps of the system: I Steady-state seafloor spreading stage: section is based on the observed sections CGN-1 and CGN-3). II. Lithospheric breakup stage: lithospheric breakup is triggered at a pair of syn-magmatic conjugate normal faults FD, which break away at the outer high (Breakup High, Hb). III. OCT stage: FC is a northward-dipping detachment fault truncating the older FB. Both faults are syn-magmatic and form during deposition of the sedimentary sequences S2 and S3). IV. OCT stage: FB act as a long offset detachment fault creating new real estate simultaneous to the emplacement of extrusive and intrusive magma and deposition of S2. V. OCT stage: Onset of formation of FB offsetting FA and S1 and dipping southward. VI. Continental breakup stage: FA is a northwad-dipping detachment fault separating the two margins and controlling the S1 deposition and related magmatic additions. (b-d) The tectono-magmatic and sedimentary evolution during the breakup phase.*

The existence of an outer high, here called Breakup High (Hb) and its link to underplating has been also observed and drilled at the Newfoundland margin (Bronner et al., 2011) and described from the Australia-Antarctica conjugate margins (Gillard et al. 2016). However, it remains difficult to make further conclusions from seismic reflection data only and it remains unclear why and how underplating can produce such a basement high and what controls the abrupt switch from proto-oceanic to mature seafloor spreading observed in Fig. V.4.

Another process that merits further investigation is the evolution of fault systems when approaching breakup. From both seismic studies at present-day Australia–Antarctica rifted margins (Gillard et al. 2016) and field studies at remnants of the former Alpine Tethys rifted margins (Epin et al., 2019), it appears that faults develop from in- to out-of-sequence to short flip-flop detachment faulting. My observations are similar to those reported by these studies but it remains unclear what may drive this evolution. It would also be interesting to evaluate whether the decrease in fault heaves is compensated by the increasing importance of magmatic accretion. Another, more local question is linked to how the sedimentary section described in the continent (T5 of paper 1) can be correlated with the sequences S1 to S3 in the OCT.

3. Crustal breakup: how does it propagate?

What was done before?

Propagation of continental breakup and onset of seafloor spreading is a singular event that cannot be directly observed to occur at present. The best places to investigate breakup propagation are so-called *V-shaped basins* since they record a snapshot of the propagation. There are a handful of good examples, among which the best studied ones are the Woodlark basin (Taylor et al. 2009), the Gulf of California (Lizzaralde et al., 2007), the northern tip of the Red Sea (Ligi et al., 2018), and the Afar/western Gulf of Aden (Nonn et al., 2019). In contrast to these examples, the NW-SCS propagator has the major advantage that it benefits from an excellent dataset including reflection and refraction

seismic studies and nearby drill IODP hole data. A further advantage is that the volume of magmatic additions during breakup is limited (i.e., no occurrence of SDR sequences), there is no salt and sedimentation rates are high. Altogether these particularities make that the crustal structure and related syn-breakup sedimentary sequence are well imaged. However, even in excellent seismic images, the interpretation of OCT domains remains challenging. A main difficulty is that breakup is not a moment, and thus is not marked by a simple/sharp interface, but a lasting process that expresses throughout a transition zone. Thus, the many contradictory interpretations of the breakup location may also simply reflect the fact that breakup is not defined and mapped in a consistent way by the different authors.

A different but very powerful approach to investigate the propagation of breakup is the use of 3D modelling techniques (Le Pourhiet et al., 2018). The main advantage of such models it that they allow to test the physical parameters controlling the propagation. However, a major difficulty in such models is to define the initial conditions and to define breakup. The models for the SCS proposed by Le Pourhiet et al. (2018) show strong similarities with the map produced in our study, however, it appears that that the model rather predict crustal separation than lithospheric breakup and onset of seafloor spreading.

There are several examples where V-shaped propagators have been investigated. Vink (1982) was among the first to study propagators and to conclude that the tip of the oceanic propagator does not coincide with the Euler pole, which is the case in both the SCS (Le Pourhiet et al., 2018) and the Woodlark Basin (Taylor et al., 2009). Nirrengarten et al. (2018) investigated breakup in the southern North Atlantic. In this example, the ocean propagated into a domain that underwent mantle exhumation, and large amounts of continental extension occur ahead of the oceanic crust. This suggests that continental boundaries are not isochrons. Luo et al. (2021) discussed the nature of the propagator in the SW SCS and concluded that the partitioning of extension among different rift segments is the most convincing way to explain seismic observations (see their Fig. 12c). In their model, partitioning between different segmented basins occur simultaneous to propagation

of lithospheric breakup, which is also compatible with a far Euler pole and with the observed magnetic anomalies (Briais et al., 1993). Their model is also compatible with the study of Le Pourhiet et al. (2018) who showed that the SCS oceanic propagators cannot be explained by horizontal rotation around a Euler pole located at the tip of the oceanic propagator. It also may explain, in line with the numerical modelling study by Neuharth et al. (2021), that continental micro-blocks may form through the linkage of rift segments prior to breakup. However, there are, at present only few places where such models can be compared with observations. The NW SCS propagator is one of the few places where the quality of data may allow for such a comparison. Numerous studies, among which Li et al. (2021) Ding et al. (2012) and Wu et al. (2012) investigated the nature and structure of the crust using refraction seismic data that complements the reflection seismic interpretations of Cameselle et al. (2015, 2021) and Franke et al. (2014). These studies came to different interpretations and definitions of the limits of continental and oceanic crusts, the budget of magma during breakup and the relative role of extension vs magmatism in triggering breakup.

Main results from this study

In my study I analyzed and interpreted reflection seismic sections across and along the tip of the NW SCS propagator, compared them with refraction seismic data, mapped the OCT and its oceanward and continent-ward boundaries using reflection seismic, gravity and magnetic data, and described the tectonic structures and magmatic additions at the tip of the propagator. I focused on the description of the structures, magmatic additions and sediments formed during the breakup stage to deduce where, when and how breakup occurred and how it propagated.

A first result of this study was to produce a map showing the distribution of the extensional domains, i.e., the necking, hyperextension, OCT, and oceanic domains at the tip of the propagator. I also described the tectono-stratigraphic and magmatic evolution linked to breakup of the propagating system. I identified three sequences (S1, S2, S3): S1 was deposited during continental breakup and affected by faults, while S2 and S3 were

linked to the formation of the OCT and onlapp onto magmatic crust. Based on the mapping of top basement and Moho, I highlight the 3D architecture of the crust and I mapped the faults that are responsible for crustal thinning along strike. The results show that what is commonly referred to as the tip of the NW SCS is actually more complex and includes two frontal tips along which the crust is thinning and separating. A first tip is located in the north and propagates towards the Xisha Trough but terminates before reaching it. A second tip located further south points towards the SW. A small continental block is separating the two rift propagators (Fig. IV.10).

At a larger scale, it can be observed that necking and hyperextension are controlled by fault systems. Even when magma enters the system during hyperextension, faulting continues to partially control extension. It is only in more advanced stages of the OCT formation that magma begins to play a leading role and that major faults are not observed anymore, although they may still form and accommodate extension (see previous section). My observations show, however, that breakup propagation in the NW SCS is controlled by faulting and not, as proposed by Cameselle et al. (2017) by the abrupt propagation of the spreading center into continental crust.

Remaining questions

The main remaining questions are about what controls the propagation and what can explain the stalling of the breakup process in the NW SCS? Three possible explanations can be envisaged: (1) the far-field compression due to the west-to-east topographic gradient across the Indochinese Peninsula prevent continental breakup propagation, (2) the inherited arc-crust trending from SE China to Indochina in the SW was too strong and inhibited a successful breakup and forced the system to step southwards, or (3) the subduction system in the south and east controlled extensional settings in the NW SCS, and hence oceanic accretion and the propagation of the oceanic system. While hypothesis (1) has been demonstrated by numerical modelling (Le Pourhiet et al., 2018), the latter two, i.e, (2) the control of inheritance or (3) the large-scale geodynamic boundary conditions cannot be ruled out and a combination of the three may be possible as well. It

may be interesting to design experiments that enable to test independently each of the possible controlling factors to analyze to what extend they may control breakup processes.

Another open question relates to what extend existing structures may be used or ignored during the propagation of a rift/oceanic spreading system. It remains unclear what is the relationship between the NW SCS propagator and the Xisha Trough. Did they rift simultaneously or is the Xisha Trough an independent and earlier system? and if so, why did the propagator not follow this structure? Other open questions are how/why did rift propagation stop? How and when was the NW SCS propagator decoupled from the remaining SCS system? and how, where and why did this ridge jump occur?

References

Briais, A., Patriat, P., & Tapponnier, P. (1993). Updated interpretation of magnetic anomalies and seafloor spreading stages in the south China Sea: Implications for the Tertiary tectonics of Southeast Asia. *Journal of Geophysical Research: Solid Earth*, *98*(B4), 6299–6328. https://doi.org/10.1029/92JB02280

Bronner, A., Sauter, D., Manatschal, G., Péron-Pinvidic, G., & Munschy, M. (2011). Magmatic breakup as an explanation for magnetic anomalies at magma-poor rifted margins. *Nature Geoscience*, *4*(8), 549.

Buck, W. R. (1988). flexural rotation of normal faults. *Tectonics*, *7*(5), 959–973. https://doi.org/10.1029/TC007i005p00959

Cameselle, A. L., Ranero, C. R., Franke, D., & Barckhausen, U. (2017). The continent-ocean transition on the northwestern South China Sea. *Basin Research*, *29*, 73–95. https://doi.org/10.1111/bre.12137

Cameselle, A. L., Ranero, C. R., & Barckhausen, U. (2020). Understanding the 3D Formation of a Wide Rift: The Central South China Sea Rift System. *Tectonics*, *39*(12). https://doi.org/10.1029/2019TC006040

Chen, H., Stow, D. A. V., Xie, X., Ren, J., Mao, K., Gao, Y., et al. (2021). Depositional architecture and evolution of basin-floor fan systems since the Late Miocene in the Northwest Sub-Basin, South China Sea. *Marine and Petroleum Geology*, *126*, 104803. https://doi.org/10.1016/j.marpetgeo.2020.104803

Decarlis, A., Gillard, M., Tribuzio, R., Epin, M. E., & Manatschal, G. (2020). Reply to Discussion on 'Breakup continents at magma poor rifted margins: a seismic v. outcrop perspective'. *Journal of the Geological Society, London* , 175, 875-882. *Journal of the Geological Society*, *177*(3), 667–669. https://doi.org/10.1144/jgs2020-001

Deng, H., Ren, J., Pang, X., Rey, P. F., McClay, K. R., Watkinson, I. M., et al. (2020). South China Sea documents the transition from wide continental rift to continental break up. *Nature Communications*, *11*(1), 4583. https://doi.org/10.1038/s41467-020-18448-y

Ding, W., Li, M., Zhao, L., Ruan, A., & Wu, Z. (2011). Cenozoic tectono-sedimentary characteristics and extension model of the Northwest Sub-basin, South China Sea. *Geoscience Frontiers*, *2*(4), 509–517. https://doi.org/10.1016/j.gsf.2011.05.010

Ding, W., Sun, Z., Mohn, G., Nirrengarten, M., Tugend, J., Manatschal, G., & Li, J. (2019). Lateral evolution of the rift-to-drift transition in the South China Sea: Evidence from multi-channel seismic data and IODP Expeditions 367&368 drilling results. *Earth and Planetary Science Letters*, 115932. https://doi.org/10.1016/j.epsl.2019.115932

Epin, M.-E., Manatschal, G., Amman, M., Ribes, C., Clausse, A., Guffon, T., & Lescanne, M. (2019). Polyphase tectono-magmatic evolution during mantle exhumation in an ultra-distal, magma-poor rift domain: example of the fossil Platta ophiolite, SE Switzerland. *International Journal of Earth Sciences*. https://doi.org/10.1007/s00531-019-01772-0

Falvey, D. A. (1974). THE DEVELOPMENT OF CONTINENTAL MARGINS IN PLATE TECTONIC THEORY. *The APPEA Journal*, *14*(1), 95–106. https://doi.org/10.1071/aj73012

Franke, D., Savva, D., Pubellier, M., Steuer, S., Mouly, B., Auxietre, J.-L., et al. (2014). The final rifting evolution in the South China Sea. *Marine and Petroleum Geology*, *58*, 704–720. https://doi.org/10.1016/j.marpetgeo.2013.11.020

Gillard, M., Manatschal, G., & Autin, J. (2016). How can asymmetric detachment faults generate symmetric Ocean Continent Transitions? *Terra Nova*, *28*(1), 27–34. https://doi.org/10.1111/ter.12183

Haupert, I., Manatschal, G., Decarlis, A., & Unternehr, P. (2016). Upper-plate magma-poor rifted margins: Stratigraphic architecture and structural evolution. *Marine and Petroleum Geology*, *69*, 241–261. https://doi.org/10.1016/j.marpetgeo.2015.10.020

Hubbard, R. J. (1988). Age and Significance of Sequence Boundaries on Jurassic and Early Cretaceous Rifted Continental Margins1. *AAPG Bulletin*, *72*(1), 49–72. https://doi.org/10.1306/703C81C8-1707-11D7-8645000102C1865D

Larsen, H. C., Mohn, G., Nirrengarten, M., Sun, Z., Stock, J., Jian, Z., et al. (2018). Rapid transition from continental breakup to igneous oceanic crust in the South China Sea. *Nature Geoscience*, *11*(10), 782–789. https://doi.org/10.1038/s41561-018-0198-1

Le Pourhiet, L., Chamot-Rooke, N., Delescluse, M., May, D. A., Watremez, L., & Pubellier, M. (2018). Continental break-up of the South China Sea stalled by far-field compression. *Nature Geoscience*, *11*(8), 605–609. https://doi.org/10.1038/s41561-018-0178-5

Liang, C., Liu, C., Xie, X., Yu, X., He, Y., Chen, H., et al. (2020). The role of large-scale mass wasting processes in changing the sediment dispersal pattern in the deep-water Central Canyon of the northwestern South China Sea. *Marine and Petroleum Geology*, *122*, 104693. https://doi.org/10.1016/j.marpetgeo.2020.104693

Ligi, M., Bonatti, E., Bosworth, W., Cai, Y., Cipriani, A., Palmiotto, C., et al. (2018). Birth of an ocean in the Red Sea: Oceanic-type basaltic melt intrusions precede continental rupture. *Gondwana Research*, *54*, 150–160. https://doi.org/10.1016/j.gr.2017.11.002

Lizarralde, D., Axen, G. J., Brown, H. E., Fletcher, J. M., González-Fernández, A., Harding, A. J., et al. (2007). Variation in styles of rifting in the Gulf of California. *Nature*, *448*(7152), 466–469. https://doi.org/10.1038/nature06035

Luo, P., Manatschal, G., Ren, J., Zhao, Z., Wang, H., & Tong, D. (2021). Tectono - Magmatic and stratigraphic evolution of final rifting and breakup: Evidence from the tip of the southwestern propagator in the south China sea. *Marine and Petroleum Geology*, *129*, 105079. https://doi.org/10.1016/j.marpetgeo.2021.105079

Maffione, M., Morris, A., & Anderson, M. W. (2013). Recognizing detachment-mode seafloor spreading in the deep geological past. *Scientific Reports*, *3*(1), 2336. https://doi.org/10.1038/srep02336

Manatschal, G., Sutra, E., & Péron-Pinvidic, G. (2010). The lesson from the Iberia-Newfoundland rifted margins: how applicable is it to other rifted margins? *Undefined*. Retrieved from https://www.semanticscholar.org/paper/The-lesson-from-the-Iberia-Newfoundland-rifted-how-Manatschal-Sutra/7b7b4d93f8c8cde9ad078060c37d4e10516f793b

Neuharth, D., Brune, S., Glerum, A., Heine, C., & Welford, J. K. (2021). Formation of Continental Microplates Through Rift Linkage: Numerical Modeling and Its Application to the Flemish Cap and Sao Paulo Plateau. *Geochemistry, Geophysics, Geosystems*, *22*(4). https://doi.org/10.1029/2020GC009615

Nirrengarten, M., Mohn, G., Kusznir, N. J., Sapin, F., Despinois, F., Pubellier, M., et al. (2020). Extension modes and breakup processes of the southeast China-Northwest Palawan conjugate rifted margins. *Marine and Petroleum Geology*, *113*, 104123. https://doi.org/10.1016/j.marpetgeo.2019.104123

Nonn, C., Leroy, S., Lescanne, M., & Castilla, R. (2019). Central Gulf of Aden conjugate margins (Yemen-Somalia): Tectono-sedimentary and magmatism evolution in hybrid-type margins. *Marine and Petroleum Geology*, *105*, 100–123. https://doi.org/10.1016/j.marpetgeo.2018.11.053

Sun, Z., Ding, W., Zhao, X., Qiu, N., Lin, J., & Li, C. (2019). The Latest Spreading Periods of the South China Sea: New Constraints From Macrostructure Analysis of IODP Expedition 349 Cores and Geophysical Data. *Journal of Geophysical Research: Solid Earth*, *124*(10), 9980–9998. https://doi.org/10.1029/2019JB017584

Sun, Z., Lin, J., Qiu, N., Jian, Z., Wang, P., Pang, X., et al. (2019). The role of magmatism in the thinning and breakup of the South China Sea continental marginSpecial Topic: The South China Sea Ocean Drilling. *National Science Review*, *6*(5), 871–876. https://doi.org/10.1093/nsr/nwz116

Taylor, B., Goodliffe, A., & Martinez, F. (2009). Initiation of transform faults at rifted continental margins. *Comptes Rendus Geoscience*, *341*(5), 428–438. https://doi.org/10.1016/j.crte.2008.08.010

Wang, P. (2019). New insights into marine basin opening. *National Science Review*, *6*(5), 870–870. https://doi.org/10.1093/nsr/nwz099

Wang, Q., Zhao, M., Zhang, H., Zhang, J., He, E., Yuan, Y., & Qiu, X. (2020). Crustal velocity structure of the Northwest Sub-basin of the South China Sea based on seismic data reprocessing. *Science China Earth Sciences*. https://doi.org/10.1007/s11430-020-9654-4

Wu, Y., Ding, W., Clift, P. D., Li, J., Yin, S., Fang, Y., & Ding, H. (2019). Sedimentary budget of the Northwest Sub-basin, South China Sea: controlling factors and geological implications. *International Geology Review*, *0*(0), 1–18. https://doi.org/10.1080/00206814.2019.1597392

Xie, X., Ren, J., Pang, X., Lei, C., & Chen, H. (2019). Stratigraphic architectures and associated unconformities of Pearl River Mouth basin during rifting and lithospheric breakup of the South China Sea. *Marine Geophysical Research*. https://doi.org/10.1007/s11001-019-09378-6

Yang, L., Ren, J., McIntosh, K., Pang, X., Lei, C., & Zhao, Y. (2018). The structure and evolution of deepwater basins in the distal margin of the northern South China Sea and their implications for the formation of the continental margin. *Marine and Petroleum Geology*, *92*, 234–254. https://doi.org/10.1016/j.marpetgeo.2018.02.032

Zhang, C., Su, M., Pang, X., Zheng, J., Liu, B., Sun, Z., & Manatschal, G. (2019). Tectono-sedimentary analysis of the hyper-extended Liwan sag basin (mid-northern margin of the South China Sea). *Tectonics*. https://doi.org/10.1029/2018TC005063

Zhang, Cuimei, Sun, Z., Manatschal, G., Pang, X., Li, S., Sauter, D., et al. (2021). Ocean-continent transition architecture and breakup mechanism at the mid-northern South China Sea. *Earth-Science Reviews*, *217*, 103620. https://doi.org/10.1016/j.earscirev.2021.103620

Zhang, Cuimei, Sun, Z., Manatschal, G., Pang, X., Qiu, N., Su, M., et al. (2021). Syn-rift magmatic characteristics and evolution at a sediment-rich margin: Insights from high-resolution seismic data from the South China Sea. *Gondwana Research*, *91*, 81–96. https://doi.org/10.1016/j.gr.2020.11.012

CHAPTER VI

Conclusion

The aim of this PhD was to investigate: (1) The tectono-stratigraphic and magmatic evolution of the NW SCS, (2) the transition from continental to lithospheric breakup, and (3) the 3D spatio-temporal evolution of the breakup process at the tip of the SW SCS relying on the analysis from seismic sections. The main results of the thesis can be summarized as follows:

(1) The identification and characterization of total accommodation space, crust thickness and shape and top basement topology allowed me to identify four rift domains on the CGN-1 seismic section, which are: the proximal domain, the necking domain, the hyperextended domain, and the proto-oceanic domain. The sediments have been subdivided into a syn-rift mega-sequence and a post-rift mega-sequence. The syn-rift mega-sequence was subdivided in 5 tracts and 4 magma units. The use of simple correlative surfaces within the syn-rift mega-sequence is hampered by the fact that rifting is polyphase, rift activity migrates and is diachronous and the mode of rifting changes through time. Therefore, in each of the 5 tracts I distinguished between syn- and post-tectonic packages. This approach enabled me to decipher the sedimentary evolution associated with the different deformation phases at play during the syn-rift time interval.

(2) A Wheeler approach has been used to build a time/space frame to describe the different tectonic events that lead to the formation of the rifted margins imaged by the CGN-1 seismic line. Based on the analysis of seismic data, I identified two critical rifting events. A first one is the necking-hyperextension stage that occurred from 43 to 34 Ma and was responsible for the thinning of crust to less than 10 km during the deposition of tracts

1 to 4. A second event was the breakup that occurred from 34 to 28 Ma and was linked to the formation of proto-oceanic crust during deposition of tract 5.

(3) Based on a detailed kinematic restoration of the CGN-1 section, I quantified extension values and rates for the different rift events. The results show that extension rates generally increase from the onset rifting to seafloor spreading, except during hyperextension that displays lower extension rates.

(4) The restoration of the CGN-1 line enabled me to distinguish between three stages. A first stage during which necking faults localize on either side of a largely un-deformed keystone, resulting in the individualization of an H-block. During a following stage deformation localizes inside the H-block and results in its dismembering of the block during a so-called hyperextension phase. Finally, magmatic accretion becomes dominant event but extension is still associated with faulting.

(5) The crustal structure of the NW-SCS OCT is best described on its continent-ward side by a hybrid crust where extensional thinning of the crust is compensated by syn-extensional magmatic addition, which leads to a sandwich-type crust, and on its oceanward side by a fully magmatic but still tectonized proto-oceanic crust, dominated by fault-controlled magmatic additions and a complex, non- layered crustal structure.

(6) Relying on seismic interpretations and restoration of sections I propose that the breakup phase includes out-of-sequence, flip-flop detachment faults showing a progressive decrease in fault heaves and a transition to magmatic accretion. This evolution is likely to be controlled by the rise of the asthenosphere that may not only control the focusing of the syn-tectonic magma, but also the localization of deformation as nicely documented in the syn-breakup sedimentary sequences S1 to S3.

(7) A striking observation is the uplift and continent-ward tilting of the proto-oceanic crust during breakup, resulting in the formation of a diagnostic outer basement high (Hb) that bounds the mature oceanic crust. This evolution is documented in the syn-

breakup sedimentary sequence overlying the proto-oceanic crust. Indeed, oceanward migration of the syn-tectonic sedimentary sequence occurs simultaneous to uplift and continent-ward tilting of the proto-oceanic domain. The proto-oceanic crust affected by faults that are syn-magmatic, as documented by converging reflection bundles in the crust interpreted as magmatic growth structures, and underplated with magmatic bodies.

(8) Mapping of rift domains and syn-hyperextension and syn-breakup sequences provide the temporal and spatial constraints necessary to discuss the 3D structural and magmatic evolution during breakup in the NW SCS and to propose a kinematic model for it. The results of this study provide a well-documented example of the spatial and temporal evolution of a rift system during breakup and shows that the V-shaped NW SCS may not be the result of a stalling oceanic propagator, but may rather be explained the a retrogradation and reorganization of a rift system. A hypothesis to explain this evolution may be linked to the inherited arc setting and the related depleted mantle, which may have prevented a magmatic breakup.

CHAPTER VII

Outlook

An outlook commonly embraces results, ideas or questions originating from the thesis manuscript that merit further investigation. In the present outlook, I take the opportunity to list some ideas that took seed during my PhD but for which I lacked time/ was not able to further develop during my thesis. As may be the case for many PhDs, my research project changed, matured, and focused through time, and therefore not all ideas I developed during the PhD made it to the final manuscript. It took me a lot of time to develop and find my way to get where I'm today, due to three main reasons:

Project: The initial plan was to study crustal and lithospheric thinning in the SCS, i.e., the necking process, and to compare it with that of the Iberia-Newfoundland and Alpine Tethys rifted margins. The aim was to learn what has been done before in the Atlantic and former Alpine rift systems and to apply it to the SCS. It took me some time to understand the concepts developed for the Alps and the Atlantic and when I wanted to apply them to the SCS, I realized that there are major differences between them.

Data: In many PhD studies the problem is to access to data, but in my case, it was the opposite: there were too many data. I spent more than one year looking at data from the SCS and worldwide margins, and the more data I was looking at, the more questions I had.

Culture: There is not only the language, but also the scientific culture. I came to Strasbourg to be taught about rifted margins but my supervisor did not teach me "final knowledge" as I expected; conversely, he asked me even more questions that I did neither understand nor was I able to answer. It took me some time to understand that I should not

expect answers about ongoing research from my professors but that I was actively participating to the building of cutting edge knowledge, which I should dig out from the data I had.

Thus, trying to formulate the good questions, finding the appropriate data to answer them, being able to focus, discussing and finding the good answers is what I learned in my PhD. I certainly have lost a lot of time during my PhD because I spent too much time in trying to find my way and thinking about all what I saw. Thus, I ended up with far more questions and observations than what I was able to develop, write and document in the PhD manuscript presented here. Therefore, I take the opportunity to list in this outlook some of the ideas that germinated in my mind during my PhD and some of the problems that remain to be solved, which I did not integrate in my PhD manuscript due to the lack of time.

1. Time space correlations, unconformities and tectono-stratigraphic concepts

In my research I provided a detailed description of the crustal architecture, the tectono-sedimentary and magmatic evolution (Fig. VII.1a). As there are lots of sediments filling in the syn-rift accommodation space in the NW-SCS, the crustal thinning and crustal and lithospheric breakup are well recorded in the stratigraphic tape recorder. Based on a careful analysis of seismic data, I defined and characterized a necking unconformity and a breakup sequence, and I could observe how syn-tectonic sediments localized and migrated from the location of necking to the area of breakup (Figs. VII.1b and VII.1c). In chapter II I focused mainly on the necking domain, while in chapter III I focused on the crustal and lithospheric breakup, and in chapter IV I looked at the time propagation. But in none of the studies, I was able to put the sediment sequences in the perspective of an entire rift system evolution, i.e., I didn't make the connection between the proximal and the distal/ proto-oceanic part (Fig. VII.1d). Indeed, I defined in chapter II (paper 1) five system tracts (T1 to T5) that were limited by the rift onset unconformity (ROU) at the base and the

breakup interface (Bi) at the top. Within the syn-rift sequence, I defined a necking unconformity (NU) (Fig. VII.1). In chapter III (paper 2) I defined three syn-breakup sequences that I referred to as S1 to S3, and finally in chapter IV (paper 3) I defined two sequences that can be mapped across the tip of the propagator, that are SA and SB. However, I did not find the time to develop a more global description of the syn-rift and syn-breakup sequence, although this is possible as shown in Fig. VII.1. Between the NU and the Bi, in the proximal and necking part, there is a sediment sequence, which I defined as tract 5 (T5). T5 is characterized by parallel reflections, is not control by faults and shows post-tectonic structures. A key question that remains is whether T5 is the time equivalent of S2 to S3 sequence, and if this sequence can be defined as the breakup sequence. At present, I can define in the breakup sequence growth structures only in the distal part and interfingering and onlapping onto the magmatic crust of the OCT. However, I do not clearly understand neither what are the relationships between the unconformities in the necking zone and the unconformities in the OCT, nor what are the spatial and temporal relationships between the T5 and S2-S3. Another question is whether T4 that is post-necking corresponds to S1 that is syn-hyperextension. If this is the case, T1 to T3 that are syn-necking should be pre-hyperextension, and thus would be seen as pre-tectonic in the distal margin and should not be present in the OCT. Answering to this question is fundamental to understand the kinematic evolution and the processes that occur between necking and onset of breakup.

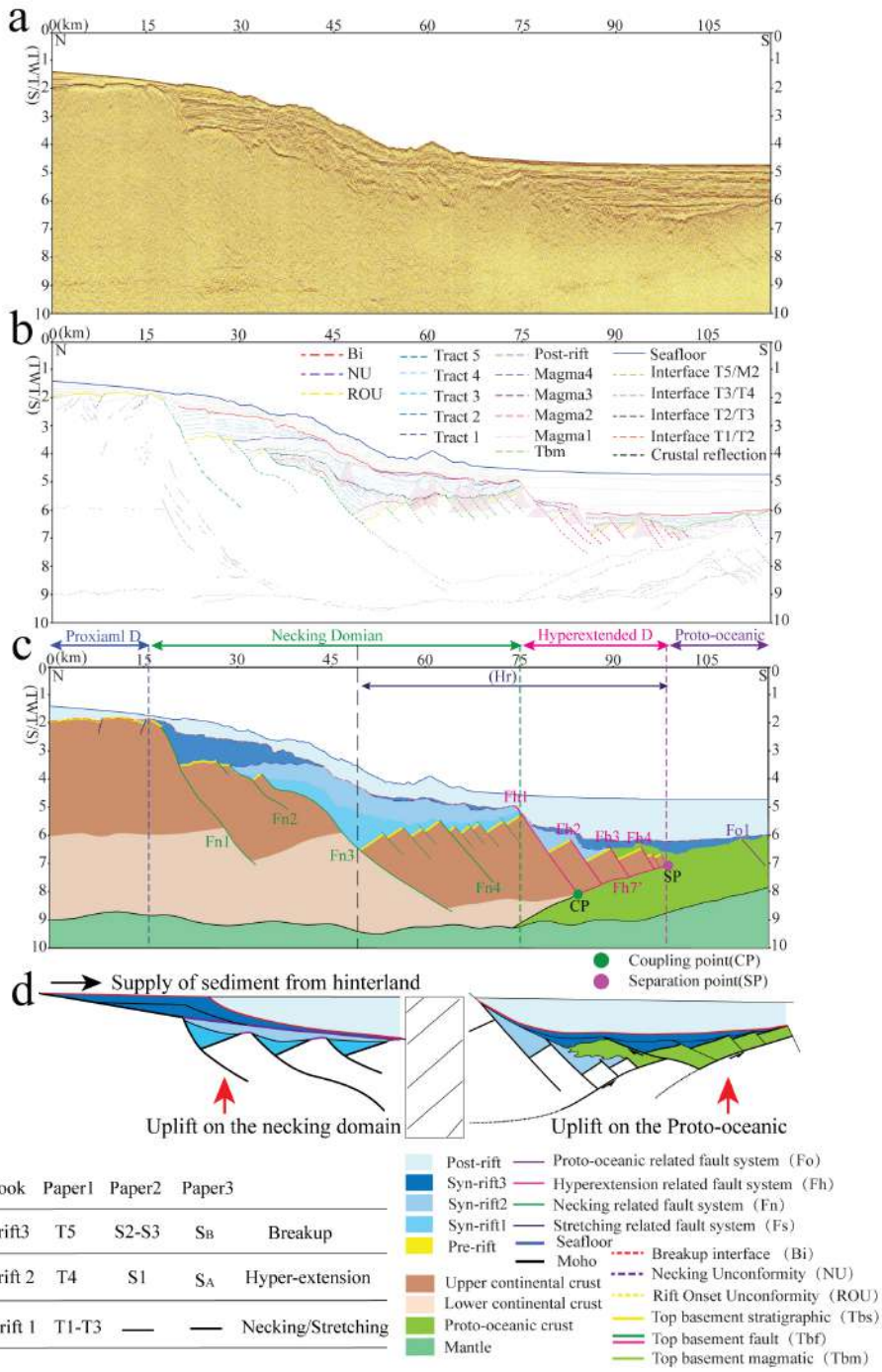

Figure VII.1*(a) Zoom on CGN-1 line showing the sedimentary architecture of the northern margin (for location see chapter II, Fig. II.2a). (b) Line drawing of the section shown in (a). (c) Interpretation of seismic section shown in (a). (d) Cartoon highlighting the question about the architecture of the transition between proximal and the distal/proto-oceanic part. Note that while the two domains are well described and understood, their transition is ill construed.*

Main pending questions are:

- How to validate and calibrate correlations between the proximal and distal parts of the syn-rift mega-sequence?
- How can the necking unconformity and breakup sequence be defined and what is their exact timing?
- Are the unconformities in the necking domain and proto-oceanic domain controlled by uplift, and if yes, what are the controlling processes?
- What is the architecture of the breakup sequence and how can it be identified in seismic data? What is its precise link to breakup? and how does it relate to the necking unconformity in the proximal and necking domain?
- Can information about crustal uplift and bathymetry be obtained from the breakup sequence?

Answering to these questions will ask to better define the necking unconformity and breakup sequence and to establish the evolution and processes occurring between crust necking and lithosphere breakup. Eventually it will be necessarily to drill, test and calibrate these geometrical relationships. Due to its efficient syn-rift sedimentary record, the NW SCS is certainly the best location to perform such drilling worldwide.

2. Evidence for a ridge jump in the NW SCS?

Based on detailed observations of high-quality seismic data, I separated an OCT from a Penrose-type oceanic crust in the NW SCS. This work provided a better understanding of the characteristics and extent of oceanic crust in the NW SCS. I analyzed spreading-parallel seismic transects (Figs. VII.2a to VII.2d) that image the oceanic crust in the NW SCS (Fig. VII.2e). This careful study enabled me to define two main oceanic sub-domains displaying distinct structural characteristics associated with different structures and thicknesses that may evidence a ridge jump in the NW SCS. However, in my study I did not have the time to further characterize this evolution and to confirm it.

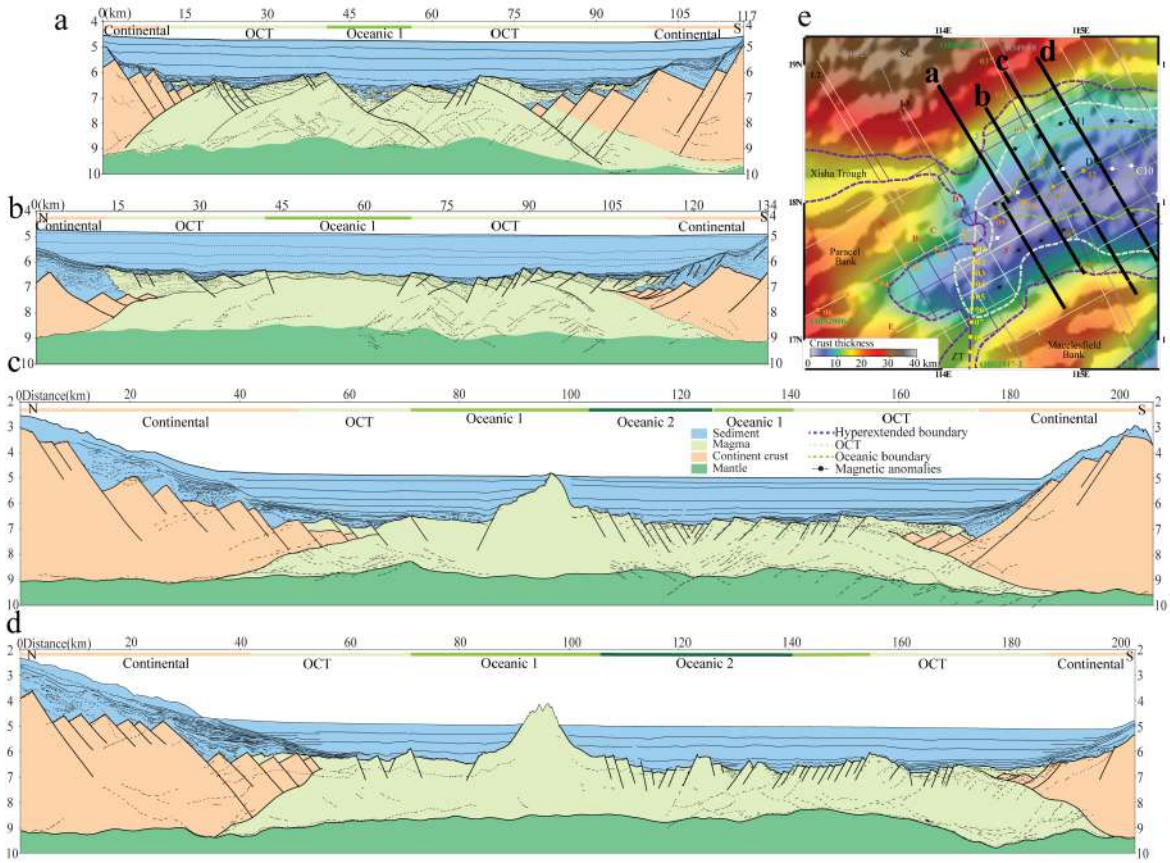

Figure VII.2. *The characteristics and extent of oceanic crust in the NW SCS. (a-d) The spreading-parallel seismic transects that image the oceanic crust in the NW SCS. Two main oceanic sub-domains displaying distinct structural characteristics associated with different structures and thickness. (e) Map showing the location of the seismic lines.*

Main questions that remain are:

- What are the structural and sedimentary architectures and magmatic characteristics of the two oceanic sub-domains?
- What is the geographical distribution of the two oceanic sub-domains in map view?
- When, how and why did the ridge jump occur?
- How is the ridge jump in the NW SCS linked to the reorganization of seafloor spreading in the SCS, i.e., what is the link between the local and regional reorganization?

Future work will need to better describe and map the two oceanic sub-domains in order to define the temporal and spatial evolution of this reorganization of the spreading system.

3. Sedimentation rates vs magmatic budget during rifting: towards a new classification

Based on seismic reflection and refraction data, the NW SCS was interpretated as an intermediary rifted margin, i.e., a margin that is neither magma-poor nor magma-rich. However, Zhang et al. (2020) and my study (chapter II) showed that there is evidence for magma emplacement during rifting. Indeed, significant amounts of both magma and sediments were emplaced during final rifting and breakup. However, there are no SDRs, which are the emblematic structures of magma-rich rifted margins, nor evidence for exhumed mantle, which is characteristic of magma-poor margins. Thus, by comparison with Atlantic rifted margins, the NW SCS shows evidence for a sediment-rich and magma-intermediate margin. It is unclear what is the effect of high sedimentation rates on the magmatic evolution and if magma-rich margins can form when sedimentation rates are high. The main question is how is accommodation space filled when sediments compete with magmatic additions? Therefore, rather than using Atlantic-type classifications (magma-rich vs magma-poor) or to try to oppose rifting in the SCS and in the Atlantic only based on the magmatic budget, I propose a classification in which both the sedimentation rates and magmatic budget are introduced (Fig. VII.3). In such a classification the NW SCS may be a type example for a magma-rich /sediment-rich margin (Type III; Zhang et al., 2020). Other endmember margins may be the Iberia margin that is a sediment- and magma-poor margin (Type I; Péron-Pinvidic et al., 2007); the East Greenland margin that is a magma-rich and sediment-poor margin (Type IV; Geoffroy et al. 2015), and the Gabon margin that can be classified as sediment-rich and magma-poor margin (Type II; Epin et al., 2021). Thus, margins cannot only be compared based on the magmatic budget alone but need to be analyzed based on the interaction between tectonics, sedimentation and

magmatism. However, such a classification requires to better define and describe magmatic and sedimentary systems, i.e., to understand the magmatic plumbing system and related structures in sediment-rich basins and to recognize them in high-quality multi-channel seismic data (see also the work of Zhang et al., 2020).

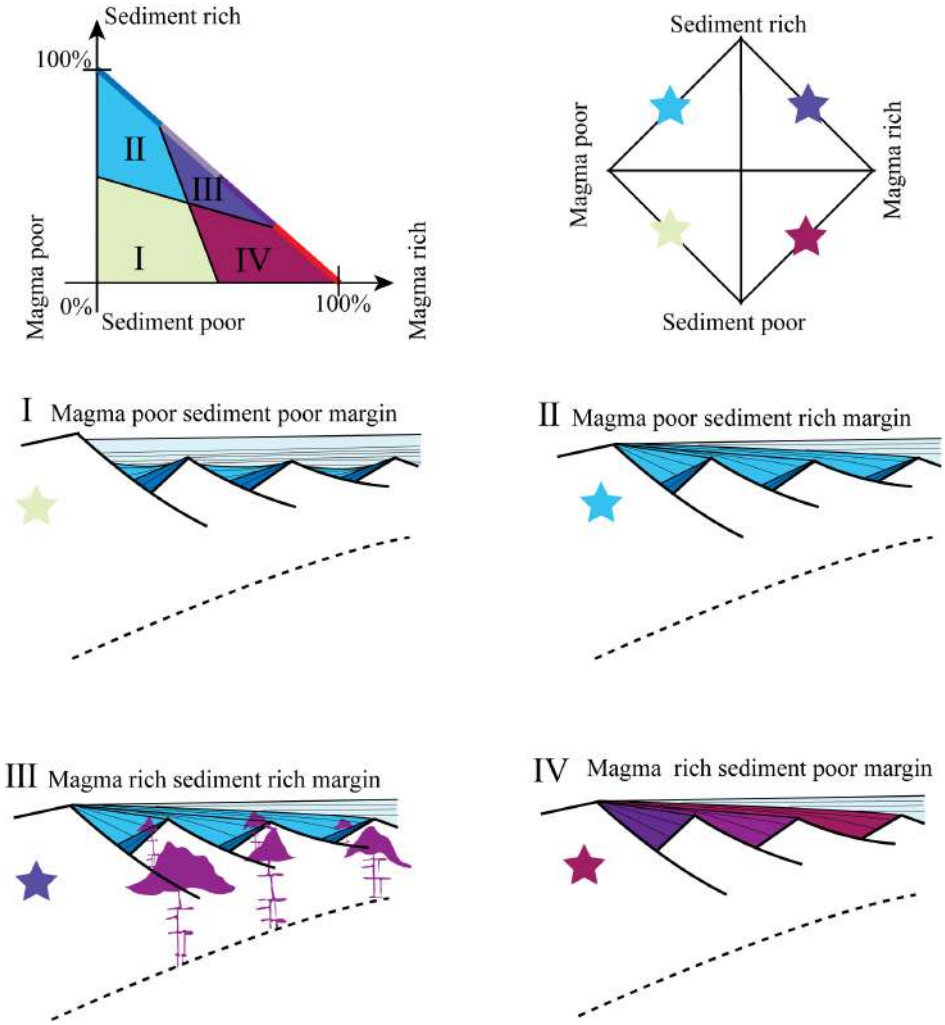

Figure VII.3. *The sedimentation rates and magmatic budget. Ⅰ. Cartoon showing a magma-poor and sediment poor-margin. Ⅱ. Cartoon showing a magma-poor and sediment-rich margin. Ⅲ. Cartoon showing a magma-rich and sediment-rich margin. Ⅳ. Cartoon showing a magma-rich and sediment-poor margin.*

4. Lower crustal flow during crust necking

Based on field work in the Campo-Grosina units of the fossil Alpine Tethys margin, Mohn et al. (2012) provided observational evidence for crustal thinning that result from the interplay between detachment faulting in brittle layers and decoupled thinning in ductile mid-crustal levels along localized ductile decollements. Ribes et al. (2020) described the syn-necking sedimentary evolution and Chenin et al. (2018, 2019 and 2020) presented numerical models to show the evolution of necking systems and discussed the controlling processes. Chenin et al. (2020; see their Fig. 14), proposed that crustal flow with little syn-necking subsidence occurs when both mantle and crustal strength are weak. While inspecting seismic reflection sections from extended basins in the N SCS, I observed evidence for detachment faults that I interpreted to be linked to crustal flow (Fig. VII.4). Fig. VII.4a shows that detachment faulting results in growth-type structures in its footwall, which can be explained as the result either from flow of the crust, or from magmatic addition. However, in such systems ductile flow prevents formation of narrow necking zones (Fig. VII.4c), conversely to what was proposed by Sutra and Manatschal (2012) for classical necking zones formed in stronger crustal/lithospheric rocks. It is interesting to mention that elsewhere in the SCS detachment faults can also form of narrow necking zones (see chapter II and the work of Luo et al. (2021)). One aim for future research would be to understand, in a more systematic way, the evolution and processes linked to necking and the formation of necking unconformities.

Main questions that need to be addressed are:

- What are the structures related to crustal necking?
- What are the relationship between the necking process, lower crustal flow and the necking unconformity?
- What is the architecture of syn-necking sediments and what is the relative accommodation space created during and after necking?

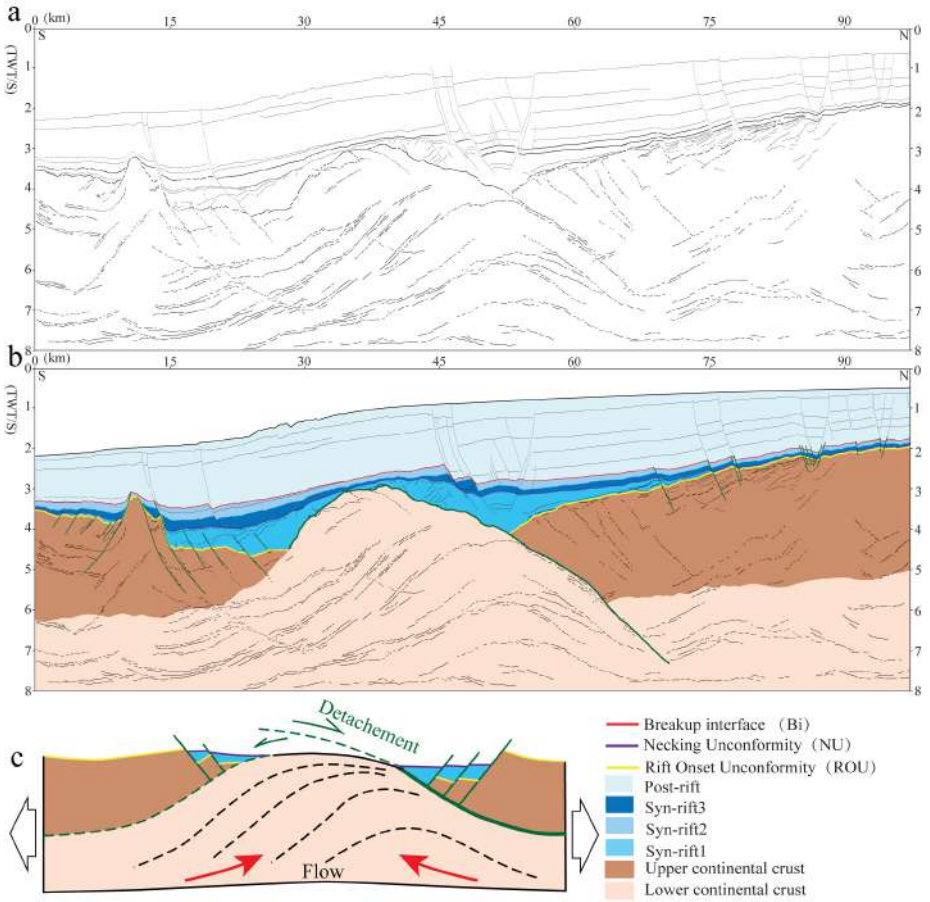

Figure VII.4. *The lower crustal flow during crust necking. (a) Line drawing of the seismic section come from Baiyun Sub-basin, North SCS. (b) Interpretation of the seismic section. (c) Cartoon model show the evolution and processes linked to necking and the formation of necking unconformites.*

Careful analysis of high-quality reflection seismic data imaging both the tectono-stratigraphic and lower crust architectures is necessary to gain further insights into the necking process and to answer these questions. In this perspective, the northern SCS margin is an ideal area to study these aspects at a regional scale.

5. Extensional tectonic and crustal accretion at oceanic transform faults

Oceanic transform faults are seismically and tectonically active plate boundaries that leave scars known as fracture zones on oceanic plates. Such transform faults/oceanic

fracture zones can crosscut entire oceanic basins (Oldenburg and Brune, 1972; Kanamori and Stewart, 1976). Current descriptions often consider transform faults as conservative two-dimensional strike-slip boundaries, at which lithosphere is neither created nor destroyed, and along which the lithosphere cools and deepens as function of its age (Igon et al., 2021). While I analysed reflection seismic data from the whole SCS, I identified between the E-SCS and the NW SCS a location where the crust is affected by structures that offset the top of oceanic crust and thin the crust (Fig. VII.5). From the gravity map I can observe the spatial extent and diamond-shape of this domain, which separates the E-SCS and NW-SCS. I also recognized three types of oceanic crust with different extensional structures and altitude on seismic lines (cf. the blue, green and orange domains in Fig. VII.5a to VII.5e). Based on all these observations I interpreted the green domain as belonging to an oceanic transform fault. If this interpretation is correct, this site would be an excellent location to understand how such zones form, what is the nature of the associated crust. Is it newly accreted crust or older crust that is fractured by transform faults?

Other questions are:

- What are the characteristics of the E-SCS oceanic, NW-SCS and possible new oceanic crust in between?
- What is the nature of the structure separating the E-SCS and NW-SCS (is it a transform fault?) and how can it be mapped?
- If the crust is new, how and when did it form and in what kinematic framework did accretion occur.
- Careful analysis of high-quality reflection seismic data imaging the crustal structure and tectono- sedimentary architecture of the limit between the NW- and E-SCS and their comparison with gravity and magnetic data is necessary to get more constraints on this potential oceanic transform system.

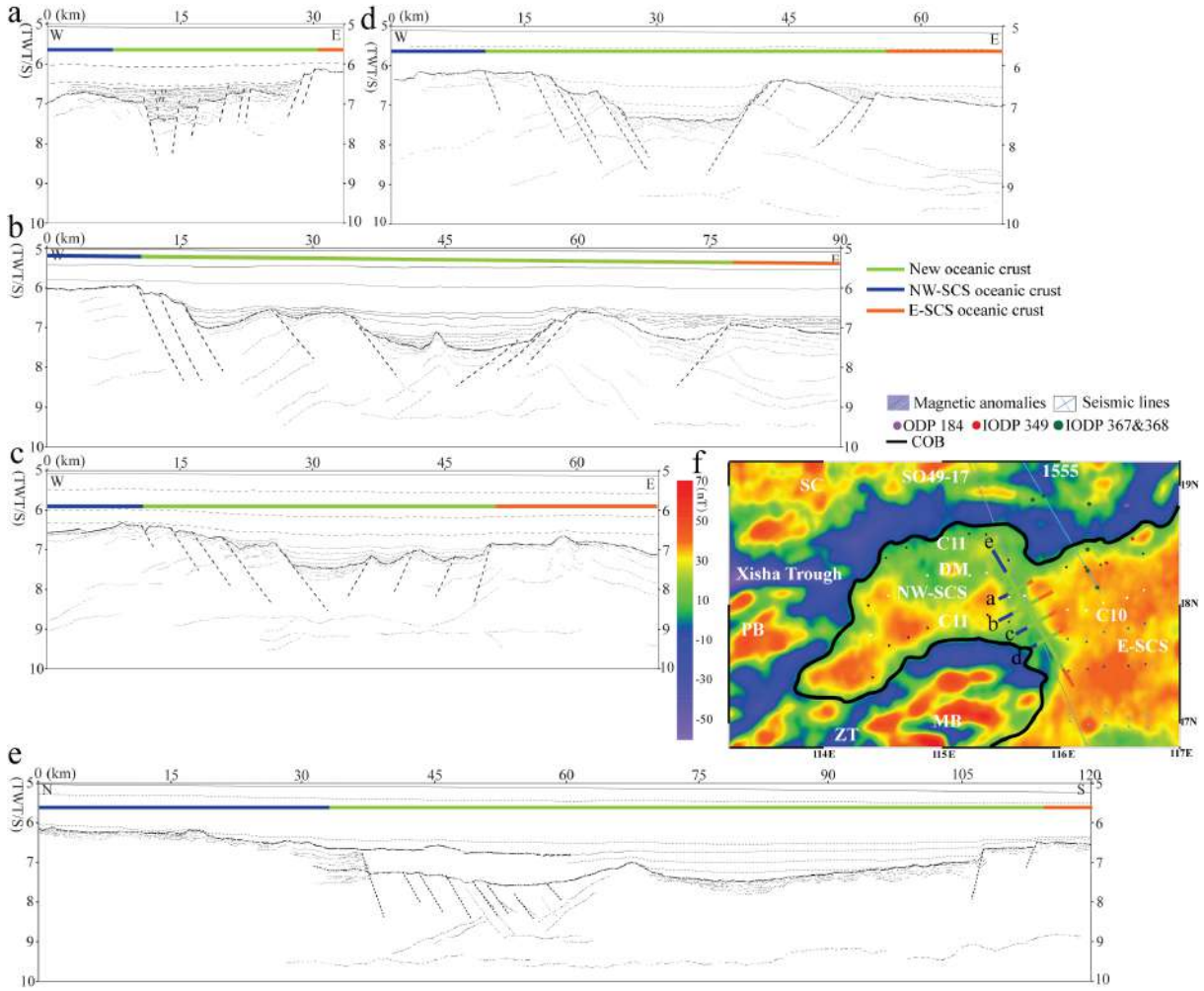

Figure VII.5. *Extensional tectonic and crustal accretion at oceanic transform faults. (a-d) Line drawing of seismic section across the transform fault. (e) Line drawing of seismic section parallel the transform fault. (f) Free-air gravity anomaly map with location of seismic sections.*

6. From foreland basins to rifted margins: an example from the NE SCS

While exploring potential sites for my research during the first year of my PhD, I investigated and interpreted the Jinhai and Chaoshan subbasins in the NE-SCS. The study of reflection seismic sections in this area is difficult due to the occurrence of thick Mesozoic sediment layers, that have been drilled (LF35-1-1(MZ-1-1); Yao et al., 2011; Huang et al., 2017; Fig. VII.6b, VII.6c, VII.6d) . It is important to note that rifting initiated in this area in a complex system made of convergent, foreland basins (Li et al., 2018; Huang et al., 2017) that are imaged in the Mesozoic sequences. In my interpretations, I observed

pre-rift thrust systems overprinted and/or reactivated by extensional fault systems. Although it is not clear to me how the SCS changed from convergence to extension/rifting and finally turned into a passive margin and what are the precise relationships between thrust faults and extensional faults, it is important to recognise this structural complexity and to integrate it in the structural interpretation of the evolution of the SCS. This evolution may be comparable to that shown in Fig. VII.6a illustrating the evolution of the Caledonian system in the North Atlantic realm during the Paleozoic and Mesozoic, although a major difference exists; the SCS rift evolution was much faster.

Related to this discovery, several questions arise, such as:

- How, when and where did the SCC evolved from an active orogenic system into a passive rifted margin?
- How was this evolution documented in the tectono-stratigraphic record?
- What were the implications of this orogenic inheritance on the subsequent rift evolution?

Future work will be necessary to answer some of these questions and the best location to do so is the NE-SCS rifted margin. In this area the structures documenting the evolution between the orogenic stage, its collapse and subsequent rifting can be best studied. One point that needs particular attention is distinguishing between compressional thrust structures and extensional low-angle detachment structures.

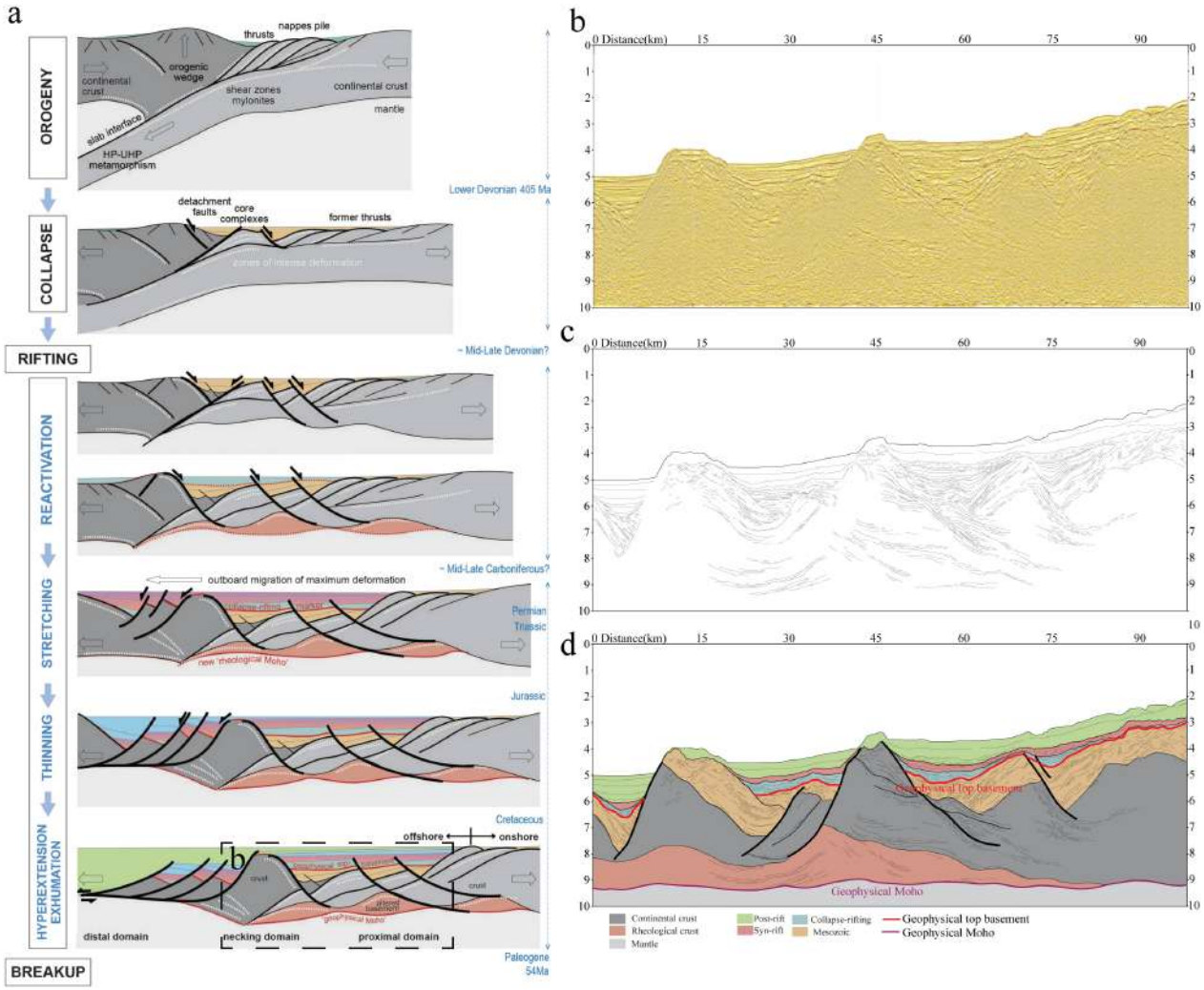

Figure VII.6. *(a) Schematic representation of the structural evolution of the crust from an orogenic context to a rift. Modified from Peron-Pinvidic et al. (2020). (b-d) An un-interpreted, line drawing and interpreted section of the time migrated reflection seismic section across the Jinghai Sub-basin, in the N SCS.*

References

Chenin, P., Schmalholz, S. M., Manatschal, G., & Karner, G. D. (2018). Necking of the Lithosphere: A Reappraisal of Basic Concepts With Thermo-Mechanical Numerical Modeling. *Journal of Geophysical Research: Solid Earth*, *123*(6), 5279–5299. https://doi.org/10.1029/2017JB014155

Chenin, P., Manatschal, G., Decarlis, A., Schmalholz, S. M., Duretz, T., & Beltrando, M. (2019). Emersion of Distal Domains in Advanced Stages of Continental Rifting Explained by Asynchronous Crust and Mantle Necking. *Geochemistry, Geophysics, Geosystems*, *20*(8), 3821–3840. https://doi.org/10.1029/2019GC008357

Chenin, P., Jammes, S., Lavier, L. L., Manatschal, G., Picazo, S., Müntener, O., et al. (2019). Impact of Mafic Underplating and Mantle Depletion on Subsequent Rifting: A Numerical Modeling Study. *Tectonics*, *38*(7), 2185–2207. https://doi.org/10.1029/2018TC005318

Epin, M.-E., Manatschal, G., Sapin, F., & Rowan, M. G. (2021). The tectono-magmatic and subsidence evolution during lithospheric breakup in a salt-rich rifted margin: insights from a 3D seismic survey from southern Gabon. *Marine and Petroleum Geology*, 105005. https://doi.org/10.1016/j.marpetgeo.2021.105005

Geoffroy, L., Burov, E. B., & Werner, P. (2015). Volcanic passive margins: another way to break up continents. *Scientific Reports*, *5*, 14828. https://doi.org/10.1038/srep14828

Huang, C.-D., Lee, T.-Y., Lo, C.-H., Chung, S.-L., Wu, J.-C., Tien, C.-L., et al. (2017). Structural inversion in the northern South China Sea continental margin and its tectonic implications. *Terrestrial, Atmospheric and Oceanic Sciences*, *28*(6), 891–922. https://doi.org/10.3319/TAO.2017.03.27.01

Kanamori, H., & Stewart, G. S. (1976). Mode of the strain release along the Gibbs fracture zone, Mid-Atlantic ridge. *Physics of the Earth and Planetary Interiors*, *11*(4), 312–332.

Li, F., Sun, Z., & Yang, H. (2018). Possible Spatial Distribution of the Mesozoic Volcanic Arc in the Present-Day South China Sea Continental Margin and Its Tectonic Implications. *Journal of Geophysical Research: Solid Earth*. https://doi.org/10.1029/2017JB014861

Luo, P., Manatschal, G., Ren, J., Zhao, Z., Wang, H., & Tong, D. (2021). Tectono - Magmatic and stratigraphic evolution of final rifting and breakup: Evidence from the tip of the southwestern propagator in the south China sea. *Marine and Petroleum Geology*, *129*, 105079. https://doi.org/10.1016/j.marpetgeo.2021.105079

Mohn, G., Manatschal, G., Beltrando, M., Masini, E., & Kusznir, N. (2012). Necking of continental crust in magma-poor rifted margins: Evidence from the fossil Alpine Tethys margins. *Tectonics*, *31*(1). https://doi.org/10.1029/2011TC002961

Oldenburg, D. W., & Brune, J. N. (1972). Ridge Transform Fault Spreading Pattern in Freezing Wax. *Science*, *178*(4058), 301–304. https://doi.org/10.1126/science.178.4058.301

Péron-Pinvidic, G., Manatschal, G., Minshull, T. A., & Sawyer, D. S. (2007). Tectonosedimentary evolution of the deep Iberia-Newfoundland margins: Evidence for a complex breakup history. *Tectonics*, *26*(2), TC2011.

Ribes, C., Petri, B., Ghienne, J.-F., Manatschal, G., Galster, F., Karner, G. D., et al. (2020). Tectono-sedimentary evolution of a fossil ocean-continent transition: Tasna nappe, central Alps (SE Switzerland). *GSA Bulletin*, *132*(7–8), 1427–1446. https://doi.org/10.1130/B35310.1

Sutra, E., & Manatschal, G. (2012). How does the continental crust thin in a hyperextended rifted margin? Insights from the Iberia margin. *Geology*, *40*(2), 139–142. https://doi.org/10.1130/G32786.1

Yao, B., Zhang, L., Wei, Z., Yi, H., Lin, Z., Wan, L., et al. (2011). THE MESOZOIC TECTONIC CHARACTERISTICS AND SEDIMENTARY BASINS IN THE EASTERN MARGIN OF SOUTH CHINA: THE MESOZOIC TECTONIC CHARACTERISTICS AND SEDIMENTARY BASINS IN THE EASTERN MARGIN OF SOUTH CHINA. *Marine Geology & Quaternary Geology*, *31*(3), 47–60. https://doi.org/10.3724/SP.J.1140.2011.03047

Zhang, C., Su, M., Pang, X., Zheng, J., Liu, B., Sun, Z., & Manatschal, G. (2019). Tectono-sedimentary analysis of the hyper-extended Liwan sag basin (mid-northern margin of the South China Sea). *Tectonics*. https://doi.org/10.1029/2018TC005063

Zhang, Cuimei, Sun, Z., Manatschal, G., Pang, X., Qiu, N., Su, M., et al. (2021). Syn-rift magmatic characteristics and evolution at a sediment-rich margin: Insights from high-resolution seismic data from the South China Sea. *Gondwana Research*, *91*, 81–96. https://doi.org/10.1016/j.gr.2020.11.012

ACKNOWLEDGMENTS

I thank Gwenn Péron-Pinvidic, Laetitia LePourhiet, Manuel Pubellier, Geoffroy Mohn, Daniel Sauter, Jianye Ren, Cuimei Zhang and Nick Kusznir for helpful discussions. This research was financed and supported by National Natural Science Foundation of China (No.41830537; NO.41772109), China Scholarship Council (No.201706410090) and supported by the M5/M6 consortium. The authors acknowledge CNOOC for the permission to publish seismic reflection lines.

Direction de la **recherche**
et de la **valorisation**
Collège **doctoral**
Université de Strasbourg

Déclaration sur l'honneur
Declaration of Honour

J'affirme être informé que le plagiat est une faute grave susceptible de mener à des sanctions administratives et disciplinaires pouvant aller jusqu'au renvoi de l'Université de Strasbourg et passible de poursuites devant les tribunaux de la République Française.

Je suis conscient(e) que l'absence de citation claire et transparente d'une source empruntée à un tiers (texte, idée, raisonnement ou autre création) est constitutive de plagiat.

Au vu de ce qui précède, **j'atteste sur l'honneur que le travail décrit dans mon manuscrit de thèse est un travail original et que je n'ai pas eu recours au plagiat ou à toute autre forme de fraude.**

I affirm that I am aware that plagiarism is a serious misconduct that may lead to administrative and disciplinary sanctions up to dismissal from the University of Strasbourg and liable to prosecution in the courts of the French Republic.

I am aware that the absence of a clear and transparent citation of a source borrowed from a third party (text, idea, reasoning or other creation) is constitutive of plagiarism.

In view of the foregoing, ***I hereby certify that the work described in my thesis manuscript is original work and that I have not resorted to plagiarism or any other form of fraud.***

Nom : Prénom : Chao Peng

Ecole doctorale : Ecole doctorale Sciences de la Terre et Environnement (ED413)

Laboratoire : Institut Terre & Environnement de Strasbourg - ITES

Date : 29/10/2021

Signature :